International Association of Hydrogeologists

Yasuo Sakura

Department of Earth Sciences
Faculty of Science
Chiba University
Chiba (Japan)

(Editor)

Selected Papers on Environmental Hydrogeology

from the
29th International Geological Congress (I. G. C.)
Kyoto (Japan)
August 24 – September 3, 1992

Volume 4
1993

Volume 4
1993

HEISE

HEISE

Volume 4, 1993
Hydrogeology, Selected Papers

International Association of Hydrogeologists

Yasuo Sakura
Department of Earth Sciences
Faculty of Science
Chiba University
Chiba (Japan)

(Editor)

Selected Papers on Environmental Hydrogeology

from the
29th International Geological Congress (I.G.C.)
Kyoto (Japan)
August 24 – September 3, 1992

Volume 4, 1993
Hydrogeology, Selected Papers
Verlag Heinz Heise

Die Deutsche Bibliothek – CIP-Einheitsaufnahme

International Geological Congress <29, 1992, Kyôto>:
Selected papers on environmental hydrogeology from the 29th International Geological Congress (I.G.C.): Kyoto (Japan), August 24 – September 3, 1992 / International Association of Hydrogeologists. Yasuo Sakura (ed.). – Hannover: Heise, 1993
(Hydrogeology; Vol. 4)
ISBN 3-922705-63-4
NE: Sakura, Yasuo [Hrsg.]; International Association of Hydrogeologists; HST; GT

Volume 4, 1993
Hydrogeology, Selected Papers
Yasuo Sakura (Editor)
ISSN 0938-6378
ISBN 3-922705-63-4
Printed by R. van Acken GmbH, Josefstraße 35, D-49809 Lingen

P.O.B. 61 04 07, D-30604 Hannover

TABLE OF CONTENTS

TABLE OF CONTENTS (continued)

TABLE OF CONTENTS (continued)

Page

ACKNOWLEDGEMENTS

The Editor expresses his appreciation to the Scientific Referees for this Volume, viz: C.A.J. Appelo (The Netherlands), W. Back (USA), A.H. Bath (U. Kingdom), Jens-Olaf Englund (Norway), R.W. Gillham (Canada), J.D. Mather (U. Kingdom), A. Monjoie (Belgium) and A. Parriaux (Switzerland) for their excellent and conscientious efforts.

Thanks are also extended to the Convenors of the 29th I.G.C. for inviting the papers and to K. Fujinawa, Y. Yoshioka, A Kamata, S. Shindo, J. Shimada, Y. Momikura, F.L. Peterson and T. Yokoyama.

Yasuo Sakura
(Editor)

Section 1 :

CONTAMINANT TRANSPORT :

MODELLING AND CASE STUDIES

PORE-SCALE VARIATION IN RETARDATION FACTOR AS A SOURCE OF NON-IDEAL REACTIVE BREAKTHROUGH CURVES

F. SUGITA
National Institute for Earth Sciences and Disaster Prevention
Tsukuba, Ibaraki 305 Japan
R.W. GILLHAM
Waterloo Centre for Groundwater Research
University of Waterloo
Waterloo, Ontario, CANADA N2L 3G1

ABSTRACT. Non-reactive solute transport in a homogeneous medium can be described successfully by the classical advection-dispersion equation (ADE). However, the results of field and column experiments almost always give breakthrough curves (BTCs) for reactive solutes that seriously deviate from the local equilibrium assumption based ADE. Although this non-ideality of reactive BTCs is often attributed to physical or chemical kinetics, some evidence indicates that kinetic mechanisms are not sufficient. This paper presents a mechanism which accounts for non-ideality only for reactive solutes in a homogeneous medium under equilibrium sorption conditions. The proposed mechanism is based on pore-scale variation in the retardation factor *(R)*. The effect of the mechanism on BTCs was assessed by mathematical experimentation using a stochastically derived macro-dispersivity equation which accounts for retardation factor variation in the medium. In the examples presented, the stochastic dispersivities calculated for reactive solutes, which account for pore-scale variation in R, are significantly larger than those for non-reactive solutes. The BTCs predicted with the stochastic dispersivities showed better agreement with the experimental reactive BTCs by showing typical non-ideality, than the ones predicted with conventional dispersivities. Although this model is based on a highly hypothetical porous medium, it is concluded that pore-size variation in R contributes to non-ideality observed in reactive BTCs even in a homogeneously packed column under conditions of equilibrium sorption.

INTRODUCTION

Most existing models that represent solute transport in a porous medium are based on the advection-dispersion equation (ADE). Non-reactive breakthrough curves obtained in homogeneous media are known to be well described by the ADE. When instantaneous equilibrium with a singular and linear isotherm can be assumed for the adsorption reaction, the reactive solute transport should be described by the local equilibrium assumption (LEA) based ADE. However, the results of field and column experiments almost always give BTCs for reactive solutes that seriously deviate from the LEA based ADE prediction by showing greater spreading accompanied with earlier appearance and longer tailing (e.g. Davidson et al., 1968, Reynolds et al., 1982). Curves which deviate from the LEA based ADE are often called non-ideal BTCs.

Non-ideality of reactive BTCs is often attributed to violation of the LEA (i.e. presence of kinetic mechanism), and a number of models which account for a kinetic mechanism or mechanisms have been proposed. However, some inconsistencies have been reported in the application of the kinetic models. Persistent deviation of reactive curves from ideal curves implies that the mechanism which

causes non- ideality observed in reactive BTCs exists in most porous media. This paper presents a mechanism which would contribute large spreading of reactive BTCs even in a homogeneous medium under equilibrium conditions. The effect of the mechanism on BTCs was assessed by mathematical experimentation using a stochastically-derived macro-dispersivity equation.

THEORY

An ideal BTC for a reactive solute is described by the LEA based ADE

$$R\frac{\partial C}{\partial t}=D\frac{\partial^2 C}{\partial X^2}-V\frac{\partial C}{\partial X} \qquad (1)$$

where

$$R=1+\frac{\rho_b}{n}K_d \qquad (2)$$

R is the retardation factor, C is the concentration, t is time, D is the dispersion coefficient, X is the distance, V is the average linear velocity, ρ_b is the bulk density of the medium, n is the porosity and K_d is the distribution coefficient. On the scale of an REV, the retardation factor, with its value averaged over several pores, is uniform everywhere in a homogeneous medium. At the pore-scale, however, the R value would vary depending on pore size, even though the distribution coefficient is uniform everywhere. A large pore has a smaller R value because it has a smaller adsorbing surface area per unit volume of solution, provided that the reaction is a surface process (Helfferich, 1962). Similarly, a small pore has a large R value because it provides a large adsorbing surface area per unit volume of solution. Thus, at the pore-scale, the retardation factor varies from pore to pore depending on the ratio of solution volume to surface area contacted by the solution.

Micro-scale (pore-scale) variation in solute velocity and molecular diffusion are known to cause spreading (hydrodynamic dispersion) in the BTCs. Reactive solute velocity is expressed as non-reactive solute (water) velocity divided by retardation factor, R. If R values are applied at the pore-scale, the pore-scale velocity variation of a reactive solute could be considerably different from that of a non-reactive solute and the degree of variation may be larger. This may lead to large spreading commonly observed in reactive BTCs. The effect of the proposed mechanism was assessed by mathematical experimentation using a stochastically derived macro-dispersivity equation.

MACRO-DISPERSIVITY CALCULATION

Macro-dispersivity equation

It is generally accepted that the dispersion coefficient *(D)* can be expressed as

$$D=AV+D_0\tau \qquad (3)$$

where A is the dispersivity and D_0 is the molecular diffusion coefficient in free solution and τ is the tortuosity. The dispersivity, D, has been considered to depend only on properties of the porous medium. Using stochastic theory, however, recent works that consider the field scale have shown that a reactive solute could have a dispersivity value that differs from that of a non-reactive solute, even in the same porous medium, when heterogeneity of distribution coefficient in the aquifer is accounted for. Several macro-scale theoretical studies (e.g. van der Zee and van Riemsdijk, 1987,

Cvetkovic and Shapiro, 1990) reported that a negative correlation between pore-water velocity and retardation factor enhances reactive solute dispersion.

Garabedian (1987) derived an equation for reactive solute dispersivity accounting for retardation factor variation at the field scale. The final equation he obtained as the asymptotic longitudinal macroscopic dispersivity for a reactive solute with linear adsorption in a statistically isotropic 3D medium, is

$$A_{11}=\frac{(\sigma_g^2\lambda_g+\sigma_e^2\lambda_e)}{R_n^2}+\frac{\sigma_f^2\lambda_f}{\gamma^2}\left[1-\frac{\gamma(b_1+b_2)}{R_n}\right]^2 \qquad (4)$$

where

$$\gamma=\frac{q}{K_1 J_1} \qquad (5)$$

A_{11} is the longitudinal macrodispersivity for a reactive solute; R_n is the mean of retardation factor times porosity; σ_e, σ_f and σ_g are standard deviations of ρK_d , log transformed hydraulic conductivity *(f)*, and *n*, respectively; λ_e, λ_f and λ_g are correlation lengths of ρK_d , *f*, and *n*, respectively; b_1 and b_2 are constants; γ is the flow factor; *q* is the volumetric flux; K_1 is the hydraulic conductivity in the x-direction; J_1 is the mean hydraulic gradient in the x-direction.

The main underlying assumptions are:1) *f*, n and K_d can be described as the sum of stationary means and perturbations 2) The expected value of each perturbation is zero 3) Linear relation between *n* and *f*, and between ρK_d and *f*, with a random variation around the linear relationships existing such that

$$n=a_1+b_1 f+g \qquad (6)$$

$$\rho K_d=a_2+b_2 f+e \qquad (7)$$

where a_1 a_2 b_1 b_2 are constants and *g* and *e* are perturbation part of n and ρK_d respectively.

In order to redefine all the parameters in equation (4) at the pore-scale, additional assumptions were made: 4) Porosity is uniform because it has no meaning at the pore scale 5) Correlation length of hydraulic conductivity and distribution coefficient is the same because both parameters are only functions of pore radius at the pore-scale 6) Perfect pipe flow is occurring in the pores 7) Every pore has the same distribution coefficient value. Then, equation (4) at the pore scale can be expressed as

$$A_r=\lambda\left[\frac{\sigma_e^2}{R_n^2}+\frac{\sigma_f^2}{\gamma^2}\left(1-\frac{\gamma b_2}{R_n}\right)^2\right] \qquad (8)$$

where A_r is the longitudinal dispersivity for reactive solute and λ is the correlation length of hydraulic conductivity and distribution coefficient.

Evaluation of the parameters

All parameters on the right-hand-side of equation (8) were evaluated for three different glass bead media and a sand medium to obtain macro-dispersivities which account for pore-scale variation in *R*. Since R_n is a mean value, it was measured in the laboratory. Pore-size *(2r)* distribution of the porous media were also measured in the laboratory by the mercury intrusion. The remaining five parameters on the right-hand-side of equation (8) were evaluated based on the pore-size distribution as follows.

As perfect pipe flow was assumed, f which is the log-transformed hydraulic conductivity is expressed as

$$f=\ln\left[\frac{\rho_w g r^2}{8\mu_w}\right] \qquad (9)$$

where ρ_w is the density of water, μ_w is the viscosity of water, r is the pore radius and g is the gravitational acceleration. Since all the term on the right-hand-side of equation (9) except r are constants, f is the only function of r. Thus, the distribution of f could be evaluated based on the distribution of r, then standard deviation of f (σ_f) was obtained.

The flow factor γ in 3D is defined by Gelhar and Axness (1983) as

$$\gamma=1+\frac{\sigma_f^2}{6} \qquad (10)$$

Thus it was obtained by substituting the value of σ_f.

Dispersivity for non-reactive solute (A_n) can be expressed as

$$A_n=\lambda\left[\frac{\sigma_f^2}{\gamma^2}\right] \qquad (11)$$

A_n can be obtained by fitting an ADE solution to the experimental BTC. Thus λ was calculated by substituting the obtained values of σ_f, γ and A_n into equation (11).

ρK_d on the REV scale is equivalent to $2K_d/r$ at the pore scale. Thus it is also only a function of r. The standard deviation of ρK_d was obtained based on the distribution of r.

The mean part of equation (7) is

$$\overline{\rho K_d}=a_2+b_2\bar{f} \qquad (12)$$

where overline denotes mean values. The mean value of ρK_d was plotted against the mean value of f, and b_2 was evaluated from the slopes of the fitted lines.

All six parameters in the dispersivity equation (4) were evaluated for four porous media and stochastic dispersivities which account for pore-scale variation in R were calculated.

APPLICATION OF THE MACRO-DISPERSIVITIES

The stochastic dispersivity values obtained are listed in Table 1 together with non-reactive dispersivities and pore-size distributions obtained experimentally. Although non-reactive and reactive dispersivities should be the same in the same porous medium according to the conventional ADE theory, the reactive dispersivities are found to be approximately four to nine times larger than the non-reactive ones when pore-scale variation in R is accounted for.

Figure 1 shows BTCs predicted using stochastic and conventional dispersivities, and experimental BTCs. The difference between the experimental curve and the predicted curve with the conventional dispersivity indicates non-ideality. It is found that the pore-size variation in R contributes to approximately half of the non-ideality observed in these cases. Figure 2 shows

Table 1: Non-reactive (A_n) and stochastic reactive (A_r) dispersivities and pore-size distributions for the four porous media.

		Small Glass Bead	Medium Glass Bead	Large Glass Bead	Medium Sand
Pore	Size Distribution				
	Mean Diameter (μm)	30.90	48.19	60.20	33.49
	Standard Deviation	6.16	14.12	14.88	12.17
A_n	(cm)	0.012	0.011	0.008	0.035
A_r	(cm)	0.047	0.080	0.057	0.312

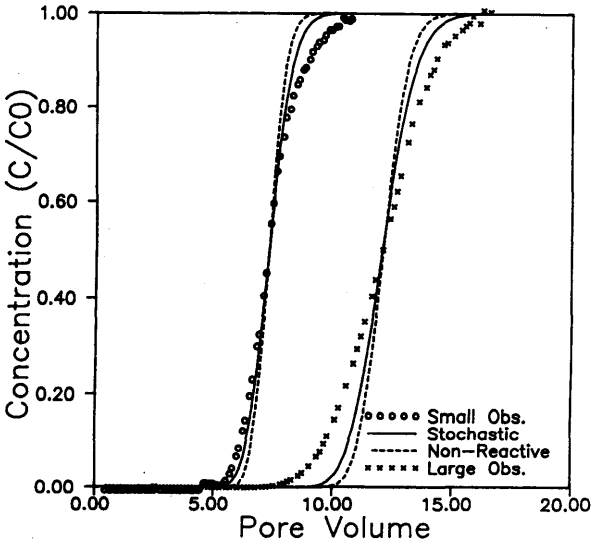

Figure 1: Observed and predicted BTCs using non-reactive and stochastic dispersivities for small and large glass bead media.

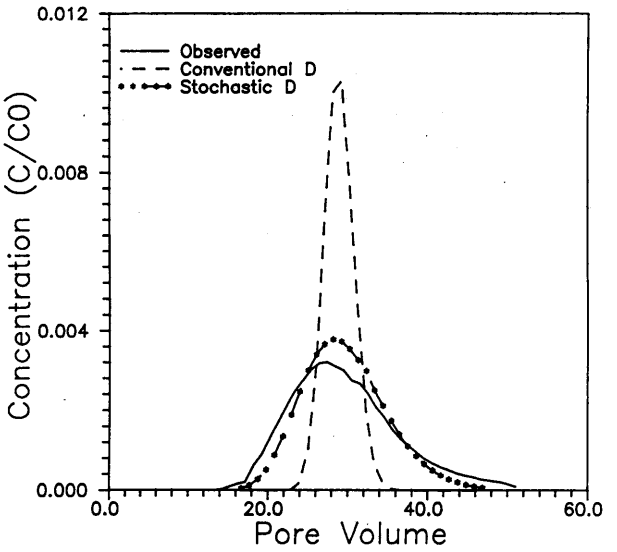

Figure 2: Observed and predicted BTCs using non-reactive and stochastic dispersivities for the sand material.

BTCs for a homogeneous medium sand material. The tracer which was strontium was injected as pulses rather than as a continuous source. In this case, the pore- scale variation in R accounts for almost all non-ideality observed.

Although the calculation conducted in this paper is based on a number of assumptions and is valid only for some ideal media, it is shown that pore-scale variation in R significantly contributes to the non-ideality of reactive BTCs. It is obvious that pore-scale variation in R due to pore-size variation does exist in real porous media, though its degree of importance may vary. Therefor, it is concluded that pore-scale variation in R is at least partially responsible for the non-ideality observed in reactive BTCs.

REFERENCES

Cvetkovic, J.T. and Shapiro, A.M. 1990. Mass arrival of sorptive solute on heterogeneous porous media. *Water Resour.Res.*, 26; 2057-2067.

Davidson, J.M., Rieck, C.E. and Santelmann, P.W. 1968. Influence of water flux and porous material on the movement of selected herbicides. *Soil Sci. Soc. Am. Pro.*, 32; 629-633.

Garabedian, S.P. 1987. *Large-scale Dispersive Transport in Aquifers:Field Experiments and Reactive Transport Theory.* Ph.D. thesis, Department of Civil Engineering Massachusetts Institute of Technology, Cambridge, Massachusetts.

Gelhar, L.W. and Axness, C.L. 1983. Three-dimensional stochastic analysis of macrodispersion in aquifers. *Water Resour. Res.*, 19; 161-180.

Helfferich, F. 1962. *Ion Exchange.* McGraw-Hill, New York.

Reynolds, W.D., Gillham, R.W. and Cherry J.A. 1982. Evaluation of distribution coefficients for the prediction of strontium and cesium migration in a uniform sand. *Canadian Geotch. J.* 19; 92-103.

van der Zee, S.E.A.T.M. and Riemsdijk, W.H. 1987. Transport of reactive solute in spatially variable soil systems. *Water Resour. Res.*, 23; 2059-2069.

SORPTION OF ORGANIC POLLUTANTS ONTO NATURAL SOLIDS: IONIZABLE ORGANICS IN A SATURATED SYSTEM AND VOLATILE ORGANICS IN AN UNSATURATED SYSTEM

Y.SHIMIZU, N.TAKEI, S.YAMAZAKI & Y.TERASHIMA
Department of Environmental & Sanitary Engineering
Kyoto University, Kyoto 606, Japan

ABSTRACT. The sorption of pentachlorophenol (PCP, pK_a = 4.75) and trichloroethylene (TCE) onto natural solids, respectively in a saturated and an unsaturated systems, were evaluated by batch sorption experiments. Experimental results of PCP in a saturated system indicated that the sorption decreased with increasing pH of the aqueous phase. The sorption of PCP is dependent upon the degree of dissociation. The ionized species has smaller sorption coefficients than the non-ionized species. The dependence of the natural solid characteristics on pH is also considered to have an influence on the sorption of PCP. The sorption coefficients of TCE from vapor-phase (K_d') were about one to four orders of magnitude greater than those from the aqueous phase. The K_d' values correlate well with the cation exchange capacity (CEC) and swelling clay content of natural solids. The K_d' values decreased with increasing the moisture content of natural solids. The water on natural solid surface interferes with the vapor-phase sorption of TCE. Neither the sorption of ionizable PCP nor TCE vapor were controlled by hydrophobic sorption.

INTRODUCTION

The pollution of subsurface environments including groundwater by organic compounds has been of growing concern due to their widespread utilization by industrial, agricultural, and domestic users. Evaluating the transport, potential biological effects, and ultimate fate of organic pollutants requires knowledge of the sorption behavior of the organic compounds, *i.e.* of their distribution between the natural solids (*e.g.* aquifer materials, soils, and sediments) and aqueous- or vapor-phases.

Much effort has been put toward understanding the sorption of a variety of hydrophobic organic compounds onto natural solids from the aqueous phase. The vast majority of the organic compounds investigated were non-ionizable hydrophobic organic compounds of limited water solubility ($< 10^{-3}$ M) (Karickhoff [1981 & 1984]). For those non-ionizable organic compounds, the sorption to natural solids from aqueous phase is dominated by "hydrophobic sorption". Sorption isotherms are linear if the equilibrium aqueous phase organic compound concentration is below 10^{-5} M or below one half of the aqueous phase solubility (whichever is lower) (Karickhoff [1981 & 1984], McCarty *et al.* [1981]). For natural solids, the organic matter constituent dominates the sorption of non-ionizable organic compounds. Sorption coefficients normalized to organic carbon content of natural solids (K_{oc}), are relatively independent of other natural solid and aqueous phase characteristics. The sorption onto the organic matter can be *a priori* estimated from the hydrophobicity of organic compounds based on the Linear Free Energy Relationships (Chiou *et al.* [1981, 1982 & 1983],

Karickhoff [1981 & 1984], Leo *et al.* [1971], Miller *et al.* [1985], Schwarzenbach & Westall [1981]), as indicated by the 1-octanol/water partition coefficient (K_{ow}) (Figure 1).

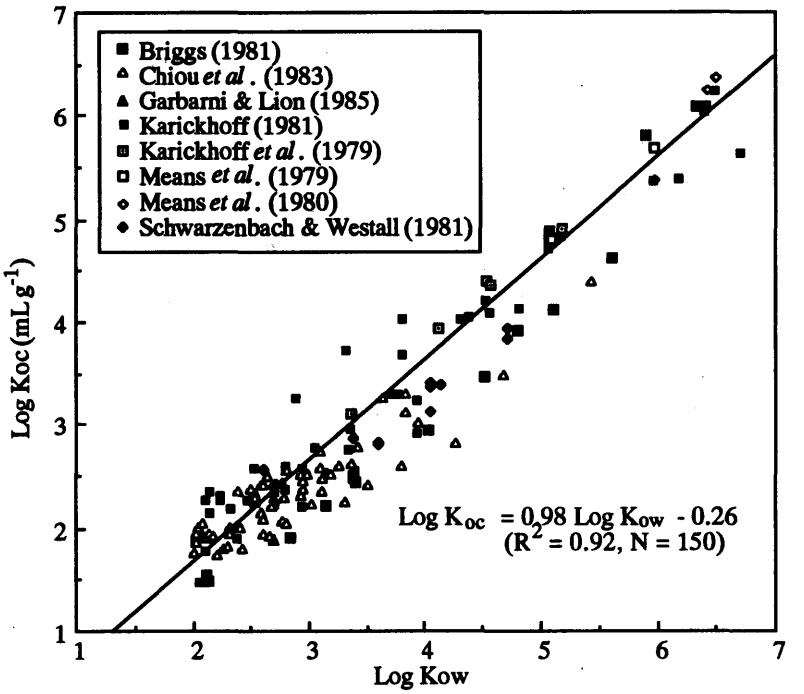

Figure 1: Correlation Between observed sorption coefficients (K_{oc}) and 1-octanol/water partition coefficients (K_{ow}).

The mechanisms of sorption of organic compounds—including neutral (non-ionic and non-polar), ionic, and polar species—onto natural solids from the aqueous phase have been summarized by several investigators (Fuerstenau [1971], Hamaker & Thompson [1972], Harter [1977], Khan [1972], Mortland [1970 & 1985], Stevenson [1972], Voice & Weber [1983]). An organic compound may be sorbed by the various sorptive mechanisms:

(a) Interactions between an organic ion and the electrical double layer
(b) Ion exchange
(c) Coordination by surface metal cations
(d) Ion-dipole interaction
(e) Hydrogen bonding
(f) Van der Waals-London forces
(g) Hydrophobic interaction

Due to the heterogeneous nature of natural solids, it is difficult to evaluate the relative importance of the various sorption mechanisms. Actual sorption processes probably involve

varying degrees of several types of interactions, but often one type predominates (Hamaker & Thompson [1972], Voice & Weber [1983]).

The sorption mechanisms (a) and (b) are not important for the non-ionic organic compounds. Coordination by exchanged metal cations is important when the organic compound is an electron donor (Lewis base) relative to water, such as amines (Mortland [1970 & 1985], Stevenson [1972]). The ion-dipole interaction between charged surface and the uncharged non-ionic organic compound is also expected to be negligible in aqueous solution. Finally, hydrogen bonding is considered to be an insignificant contribution to the sorption (Mortland [1970 & 1985]).

These arguments lead to the conclusion that the sorption of non-ionic organic compounds results primarily from van der Waals-London forces reinforced by the hydrophobic interaction. The combined effect of these two mechanisms is often referred to as "hydrophobic sorption" (Hamaker & Thompson [1972], Voice & Weber [1983]). The thermodynamic driving force for the hydrophobic sorption is the increase in entropy which occurs upon dehydration of the organic molecules. In the aqueous phase, the non-ionic organic molecule is surrounded by an envelope of structured water molecules. As the organic molecule is transferred from the aqueous phase to the non-aqueous solid phase, the structural envelope of water molecules breaks down and the entropy of the system increases (Chiou *et al.* [1979], Hamaker & Thompson [1972], Horvath *et al.* [1977 & 1978], Schwarzenbach & Westall [1981], Voice & Weber [1983]).

The organic carbon referenced hydrophobic sorption is, however, applicable only to a limited degree to organic compounds which are fully or partially ionized at natural pH values, such as amines, carboxylic acids, and chlorinated phenols (Means *et al.* [1982], Schellenberg *et al.* [1984]). The pH of the aqueous phase may affect the sorption of ionizable organic compounds, since the pH affects not only the speciation of ionizable organic compounds but also the surface characteristics of natural solids (*e.g.* surface charge and potential).

Many hydrophobic chlorinated organic compounds, such as TCE, tetrachloroethylene (PCE), and trichloroethane (TCET), volatilize when they are released to the environment due to their low boiling points. For these volatile organic compounds, the sorption in an unsaturated system must be considered. The investigations on the vapor-phase sorption onto natural solids are, however, generally lacking. Under oven-dried conditions, vapor-phase sorption coefficients have been shown to be highly correlated with specific surface area (Ong & Lion [1991]). The sorption is greatly affected by the amount of moisture present in the system (Ong & Lion [1991]).

Given these limited data, the effect of pH on the sorption of ionizable organic compounds in a saturated system and the relative importance of natural solid characteristics and moisture content on the sorption of volatile organic compounds in an unsaturated system are not clear. Additional information would enhance the present ability to predict the fate of such organic compounds in subsurface environments.

EXPERIMENTAL METHODOLOGY

This research consists of two major subjects in the sorption of organic compounds onto natural solids: the pH effect on ionizable organic compounds in a saturated system and the influence of natural solid characteristics and moisture content in an unsaturated system. For batch sorption experiments, different experimental methodologies were applied to these two subjects. Each procedure is described in this section separately.

Measurement of the pH effect

Materials: The PCP was chosen as an ionizable organic compound. The pK_a value of PCP in the aqueous phase is 4.75 (Schellenberg *et al.* [1984]), which is the smallest among chlorinated phenols. Therefore, at typical ambient pH values, PCP is present in the water predominantly as ionized phenolate anion. As internal standard for the quantitative determination of PCP in the aqueous phase by High Performance Liquid Chromatography (HPLC), 2,4,5-trichlorophenol (TCP) was used. These chlorinated phenols were purchased from Nacalai Tesque (> 99%), and used without further purification. High purity distilled deionized water from a Milli-Q system was used throughout the research. The methanol and acetic acid for HPLC mobile phases were of special quality. All other chemicals (*e.g.* acids, bases, and salts) were of the highest available purity.

Natural solids consist of a heterogeneous mixture of various solid components (*e.g.* organic matter, clay minerals, and metal oxides), all of which have the possibility of involving the sorption of ionizable organic compounds. In this research, six natural solids collected by US.EPA (*i.e.* EPA-6, -9, -14, -15, -22, and -23) were selected. They provide a wide range of characteristics that have been shown to affect the degree of sorption of organic compounds (Table 1). Two of the most important characteristics for the selection were organic carbon and swelling clay contents, which range from 0.11 to 2.38wt% and 10.1 to 60.8wt%, respectively.

Table 1: Characteristics of the US.EPA natural solids.

Solid	pH (1:1)	CEC (meq/100 g)	Organic carbon (wt%)	Swelling clay (wt%)	Specific gravity
EPA-6	7.83	33.01	0.72	60.8	2.6992
EPA-9	8.34	12.40	0.11	16.3	2.7217
EPA-14	4.54	18.86	0.48	13.8	2.7536
EPA-15	7.79	11.30	0.95	10.1	2.6927
EPA-22	7.55	8.53	1.67	14.8	2.6995
EPA-23	6.70	31.15	2.38	57.6	2.6520

Batch sorption experiments: The experimental aqueous phase was prepared for set values of pH and ionic strength. The pH (2 to 12) was adjusted by addition of 12 N HCl or 10 N NaOH. Ionic strength was adjusted to 0.01 M by $CaCl_2$. Concentrated stock solutions of PCP were made up in methanol. The experimental aqueous phase was spiked with the stock PCP solutions. The concentrations of PCP in the spiked test solutions were less than 1 mg L^{-1} (3.8×10^{-6} M). The resulting spiked test solutions contained 500 mg L^{-1} of methanol, which does not affect the aqueous activities of PCP enough to cause observable effects on the sorption of PCP by natural solids (Backhus and Gschwend [1990]).

The batch sorption experiments were carried out in 50 mL (nominal volume) borosilicate glass centrifuge tubes with Teflon-lined septum screw caps. The natural solids were weighed into the tubes, and the spiked test solutions were introduced. The mass of natural solids used was less than 1 g. The tubes were closed immediately with the cap, leaving a minimum head space

to avoid loss of PCP to the gaseous phase. The amount of spiked test solutions were determined by weight. The samples were equilibrated in the dark at 20°C for 24 hours. A rotating tumbler (30 rpm.) was used for the mixing, because it has better reproducibility than other mixing systems (Clunie & Giles [1957], Diamondstone *et al.* [1982], Roy *et al.* [1985]).

Sorption is generally regarded as a rapid process (times to reach equilibrium of minutes to a few hours) and equilibration times of 24 hours are frequently used because of its convenience. Karickhoff (1980 & 1984), however, reported that true sorption equilibrium may require weeks (to months) to achieve. In this research, no attempt was made to measure the sorption kinetics. The PCP may disappear from the system due to adsorption on the glass walls of the tubes, escape to the gaseous phase, or chemical and biological degradations. In order to minimize these losses of PCP, the equilibration time of 24 hours was adopted. Therefore, the sorption coefficient obtained in this research is a conditional sorption (or distribution) coefficient after 24 hour equilibration.

After equilibration, the aqueous phase was separated from the solids by centrifugation (700 g for 30 min), and the pH was measured immediately. Then, the internal standard (TCP) was added to the aqueous phase. After adjusting the pH to 2.0 by 12 N HCl, the aqueous phase was passed through cellulose nitrate filter (pore-size 0.45 μm) and the PCP concentration in the filtrate was analyzed by HPLC.

A Yanako HPLC system (L-5000 pump and M-315 UV/vis detector) was used together with C-18 reversed phase columns, a pre-column (30 x 4.6 mm, YANAPAK ODS-A, 7 μm particle size) and a main column (250 x 4.6 mm, YANAPAK ODS-A, 7 μm particle size). A 100 μL sampling loop was used. The mobile phase was methanol/water/acetic acid, 800/200/1 (by volume), and its flow rate was adjusted to 1.5 mL min^{-1}. The detector wavelength was set at 210 nm.

Measurement of the vapor-phase sorption

Materials: TCE was selected as the subject for the investigation because it is one of the most common volatile organic pollutants. The TCE was purchased from Nacalai Tesque (99.5%), and used without further purification. The six US.EPA natural solids were also used.

Batch sorption experiments: The headspace technique developed by Peterson *et al.* (1988) was employed to measure the TCE vapor phase sorption coefficients. The batch sorption experiments were carried out in 50 mL (nominal volume) borosilicate glass bottles. The natural solids were weighed into the bottles, and the bottles were immediately sealed with Teflon-lined rubber septa and aluminum crimp caps. A 0.05 mL of TCE vapor taken from the headspace over pure liquid TCE at 20°C was injected to each bottle with a 0.5 mL gas-tight syringe. The initial relative vapor pressure of TCE was 0.073%. The natural solids and vapor were equilibrated in the dark at 20°C for 24 hours by the rotating tumbler (30 rpm.).

The equilibration time in batch sorption experiments should be the time interval in which the system reaches chemical equilibrium and the concentrations of the products and reactants cease to change with respect to time. In this subject, an operational definition of equilibrium suggested by US.EPA (1982) was adopted, that is, the equilibrium time should be the minimum amount of time needed to establish a rate of change equal to or less than 5% per 24 hour interval. The kinetic investigation indicated that this operational definition was satisfied within 24 hours.

After the equilibration, 0.5 mL of the gaseous headspace was withdrawn with a 1 mL gas-tight syringe and analyzed by a mass fragmentgram method with a gas chromatography/mass

spectroscopy (GCMS) (Shimadzu QP-1000) equipped with a column of Shimadzu CBP20-S50-050 (0.50 μm film, 50 m x 0.33 mm ID). The column temperature was held at 50°C for the first 1 min, then increased to 100°C at 20 °C min^{-1}. The flow rate of He carrier gas was set at 30 mL min^{-1}.

Four different moisture content values, which ranged from 0 to 11.1wt%, were used. First, the natural solids were dried at 105°C for 24 hours. Then, water was added and mixed for 24 hours with the rotating tumbler (30 rpm.).

Sorption coefficients (K_d') are determined by the slope of the following relationship:

$$\frac{C_{G1} \cdot V_{G1}}{C_{G2} \cdot V_{G2}} = K_d' \frac{M}{V_{G2}} + 1 \qquad (1)$$

Equation (1) can be obtained by equating the mass balance relationships for bottles with natural solids to control bottles without natural solids (Peterson *et al.* [1988]). In Equation (1), M is the oven-dried mass of the natural solids (masses used ranged from 0.05 to 4 g depending on the moisture content of natural solids), C_{G1} and C_{G2} are the headspace concentrations or equivalently the GCMS signals for a control bottle and a sample bottle, respectively, and V_{G1} and V_{G2} are the volumes (mL) of the control bottle (measured as 68.55 mL) and the available gas volume (*i.e.* total volume less volume of natural solids) of a sample bottle, respectively.

RESULTS AND DISCUSSION

Effect of pH on the sorption of PCP

Figure 2 shows the effect of pH on PCP sorption for the natural solid EPA-6.

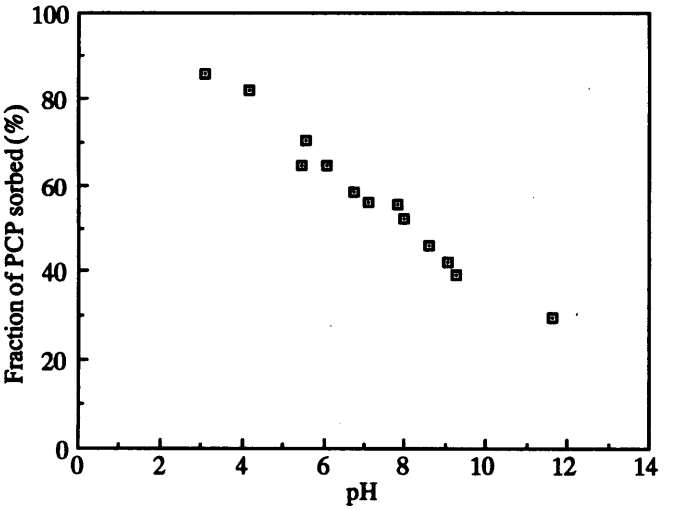

Figure 2: Effect of pH on the sorption of PCP onto EPA-6.

In this experiment, the initial PCP concentration in the spiked test solution and natural solids added to the centrifuge tubes were set at 1 mg L^{-1} and 1 g, respectively. The same tendency, decrease in sorption with increasing pH over the entire pH range tested (2 to 12), was observed for the other three natural solids (EPA-15, -22, and -23). For EPA-9, no appreciable amount of sorption was obtained with the experimental condition used in this research. This may resulted from the fact that the organic carbon and swelling clay contents of this natural solid were simultaneously low (0.11 and 16.3wt%, respectively). For EPA-14, the pH adjustment greater than 5 could not be achieved, since the original pH of this natural solid was low (4.54, which was measured on a solid/water, 1/1 suspension).

Schellenberg *et al.* (1984) investigated the sorption of several chlorinated phenols onto natural solids. They considered the sorption of non-ionized phenols, but the sorption of phenolate anions was not included in their analysis. For highly chlorinated phenols (*i.e.* tetra- and penta-chlorophenols), it was suggested that the phenolate sorption could not be neglected, since these compounds are present predominantly in the ionized form at ambient pH range.

In this research, a simple mathematical model was developed including the sorption of phenolate anion. The ionization of PCP is expressed by the acidity constant (K_a').

$$K_a' = \frac{[A^-]\{H^+\}}{[AH]} \tag{2}$$

In Equation (2), A^- and AH are ionized and non-ionized PCP species, respectively. The brackets, [ ] and { }, represent the concentration and activity in the aqueous phase, respectively. If the ionized and non-ionized PCP species have different sorption coefficients (K_d^0 and K_d', respectively), the overall sorption coefficients (K_d) can be given by

$$K_d = \frac{K_d^0[AH] + K_d'[A^-]}{[AH] + [A^-]} \tag{3}$$

Combining Equations (2) and (3) yields

$$K_d\left(1 + \frac{K_a'}{\{H^+\}}\right) = K_d^0 + K_d' \frac{K_a'}{\{H^+\}} \tag{4}$$

In the pH range between 6 to 8, the plot of Equation (4) for the natural solid EPA-6 is presented in Figure 3. From the linear relationship (correlation coefficient, R = 1.00) in Figure 3, K_d' = 55.5 mL g^{-1} and K_d^0 = 2061.6 mL g^{-1} are obtained as the slope and intercept, respectively.

For the other three natural solids (EPA-15, -22, and -23), K_d' and K_d^0 were also obtained by the linear relationship (Table 2). The values of K_d' are more than one order of magnitude smaller than those of K_d^0. The contributions of the non-ionized and ionized PCP to the sorption are estimated based on the sorption coefficients in Table 2. The estimation for the natural solid EPA-6 is presented in Figure 4. The sorption not only of the non-ionized PCP but also of its ionized PCP can occur. When the pH was greater than 7, more than 90% of the sorption resulted from the sorption of ionized PCP. The agreement between measured and estimated values for the sorption also indicates that the pH has only negligible effect on the characteristics of the natural solids in this pH range (6 to 8). However, when the data analysis was expanded to the pH ranges below 6 or above 8, the simple mathematical model could not describe the pH effect on the sorption of PCP. In order to develop the mathematical model

which can be applicable to the data of broader pH range, the pH effect on natural solid characteristics must be included. Similar results were obtained for the other three natural solids.

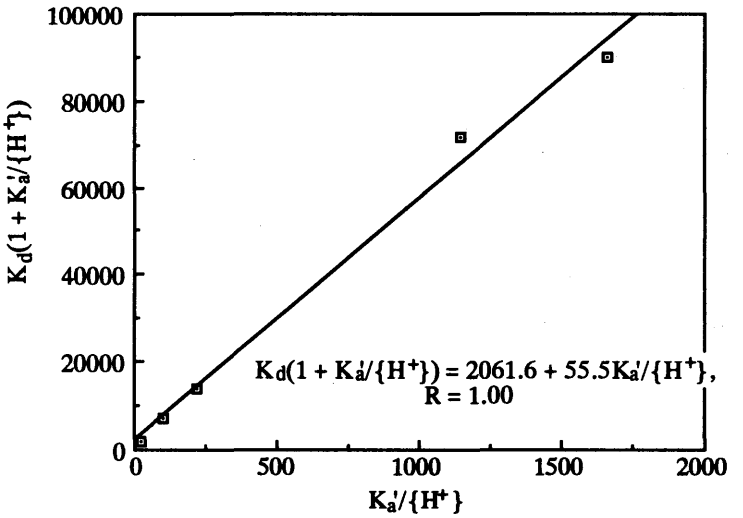

Figure 3: Estimation of K_d for non-ionized and ionized species of PCP for EPA-6.

Table 2: Estimated sorption coefficients of PCP for the US.EPA natural solids.

Solid	Sorption coefficient ($mL\ g^{-1}$)	
	Non-ionized PCP	Ionized PCP
EPA-6	2,061.6	55.5
EPA-15	1,192.8	20.0
EPA-22	901.3	16.3
EPA-23	1,765.0	57.2

Correlation coefficients of the natural solid characteristics to the sorption coefficients of non-ionized and ionized species were calculated (Table 3). The organic carbon content of the natural solids had a poor correlation. On the other hand, CEC and swelling clay content were highly correlated. These results indicate that mechanisms other than hydrophobic sorption to the organic matter of natural solids must be considered when dealing with the sorption of hydrophobic organic compounds containing ionizable functional group(s) which may strongly interact with the various organic and inorganic constituents of natural solids.

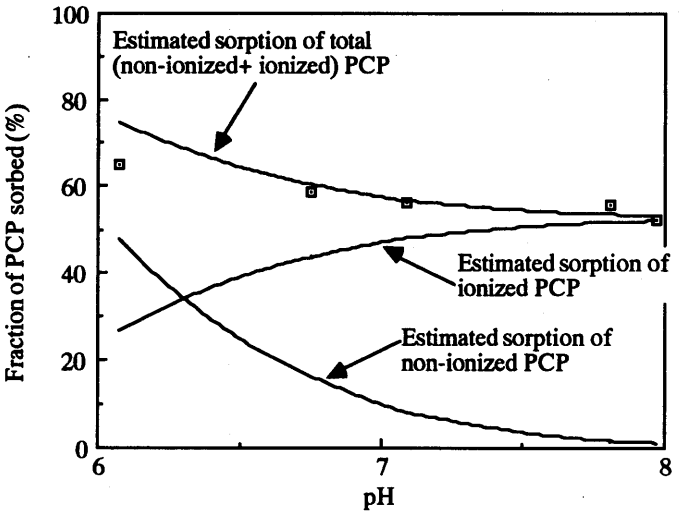

Figure 4: Sorption of PCP onto EPA-6. Symbols represent experimental data and lines are estimated.

Table 3: Correlation matrix (R) for sorption coefficients of non-ionized (K_d^o) and ionized (K_d^-) PCP at 6 < pH <8.

Solid characteristics	Correlation coefficient K_d^o	K_d^-
pH (1:1)	0.18	0.46
CEC (meq/100g)	0.97	1.00
Organic carbon (wt%)	0.12	0.19
Swelling clay (wt%)	0.94	0.99

Influence of natural solid characteristics and moisture content on the sorption of TCE vapor

Table 4 summarizes the vapor phase sorption coefficients of TCE (K_d') under various moisture contents. The sorption coefficients under saturated conditions (K_d), which are estimated from the Equation shown in Figure 1 with K_{ow} of TCE ($\log K_{ow}$ = 2.29), are also given in Table 4. The values of K_d' are about one to four orders of magnitude greater than those of K_d for all six natural solids under the moisture contents tested in this research. The organic carbon content of natural solids cannot be used as a predictor of K_d'.

Table 4: TCE vapor phase sorption coefficients under different moisture content (K_d') and estimated aqueous phase sorption coefficients (K_d).

Solid	Sorption coefficient K_d' (mL g^{-1})				K_d (mL g^{-1})
EPA-6	2,196.9 (0)	989.0 (1.0)	25.3 (5.9)	7.2 (10.6)	0.69
EPA-9	410.2 (0)	249.0 (0.6)	6.3 (1.7)	1.0 (5.0)	0.11
EPA-14	888.7 (0)	328.2 (1.1)	12.3 (3.8)	2.3 (8.2)	0.46
EPA-15	450.0 (0)	248.5 (0.5)	36.0 (1.6)	14.3 (4.7)	0.92
EPA-22	200.7 (0)	51.3 (0.5)	23.7 (1.3)	8.2 (4.7)	1.61
EPA-23	1,713.3 (0)	1,877.6 (1.5)	44.2 (5.2)	10.9 (11.1)	2.30

Values in the parenthesis represent moisture content (%) of natural solids.

Table 5 provides the correlation coefficients of K_d' at oven-dried conditions to the natural solid characteristics. The CEC and swelling clay content were highly correlated. Ong & Lion (1990) observed the highest correlation between the sorption of TCE vapor and specific surface area of natural solids under oven-dried conditions. Specific surface area measurements were not available during the course of this research. The specific surface area, in general, has high correlation to CEC and swelling clay content in natural solids. Therefore, the mineral surfaces of natural solids play an important role in the sorption of TCE.

Table 5: Correlation matrix (R) for TCE vapor phase sorption coefficients under oven-dried conditions.

Solid characteristics	Correlation coefficient
pH (1:1)	0.11
CEC (meq/100 g)	0.99
Organic carbon (wt%)	0.22
Swelling clay (wt%)	0.94

The influence of moisture content for the six natural solids is shown in Figure 5. On Figure 5, the ordinate is the K_d' values at various moisture contents normalized with respect to K_d' at oven-dried condition of each natural solid. The sorption is decreased with increasing moisture content for all six natural solids. A possible reason is that sorption of water onto natural solids results in a decrease in sorption sites available for TCE vapor. It is, however, interesting to note that the decrease in the sorption is not necessarily consistent for all natural solids. For EPA-9 and -23, which respectively have the lowest and highest organic carbon contents among the six natural solids, show rapid and slow decreases, respectively. Although water is sorbed

both by organic and mineral constituents of natural solids, the water sorbed by the organic matter may give less interference in the sorption of TCE vapor than that by the minerals.

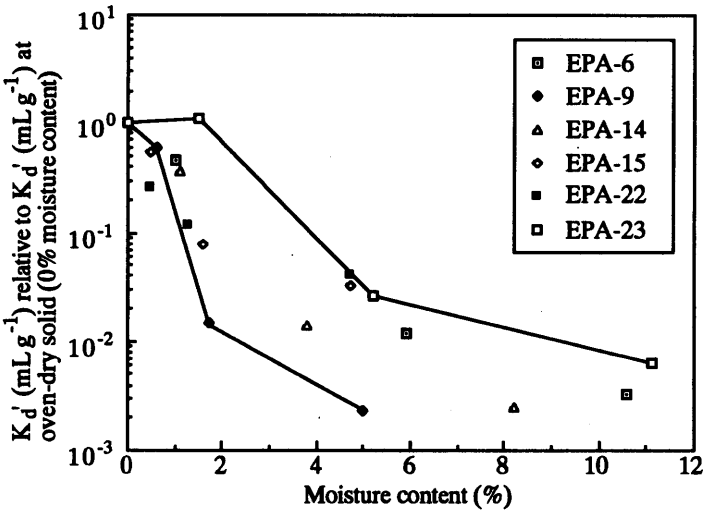

Figure 5: Effect of moisture content on TCE vapor phase sorption.

CONCLUSIONS

The predominance of organic carbon in "controlling" the sorption of non-ionic hydrophobic organic compounds from the aqueous phase to natural solids of very different origins has been extensively documented. The generalized experimental observations have suggested that the sorption of those organic compounds results primarily from "hydrophobic sorption," and those compounds are sorbed predominantly by the organic matter of natural solids. The sorption coefficient for a natural solid consisting of multiple components can be reduced to a form containing only sorption to organic matter as the controlling phase.

This research indicates that the sorption of ionizable hydrophobic organic compound (*i.e.* PCP) depends upon the pH of the aqueous phase, because the non-ionized and ionized species have different sorption coefficients, and the natural solid characteristics are dependent upon the pH. The sorption cannot be predicted by the hydrophobic sorption. Moreover, the use of saturated sorption coefficients for TCE onto natural solids as an approximation for vapor phase sorption is not valid. The water sorbed by natural solids reduces the sorption of TCE vapor. The sorption of ionizable PCP and TCE vapor are controlled primarily by mineral constituents of natural solids, which is indicated by the high correlations of the sorption coefficients of these organic compounds to CEC and swelling clay content.

Overall, this research provides additional insights on the sorption of organic compounds onto natural solids. The practice of assuming the hydrophobic sorption for ionizable organic compounds and organic vapor should be avoided to obtain accurate predictions. Various natural solid characteristics (organic carbon content, particle size distribution, clay mineral

composition [amount and type], pH, CEC, and specific surface area) are considered to affect the sorption of these organic compounds. Among them, CEC and swelling clay content may be the most important characteristics to the prediction. Further investigation is, however, required to make a final conclusion, since the combination of only two organic compounds and six natural solids was used in this research.

ACKNOWLEDGEMENT

We are grateful to Dr.H.M.Liljestrand of the University of Texas and Dr.W.L.Banwart of the University of Illinois for providing the U.S.EPA natural solids.

REFERENCES

Backhus, D.A. & Gschwend, P.M. 1990. Fluorescent polycyclic aromatic hydrocarbons as probes for studying the impact of colloids on pollutant transport in groundwater. *ES & T*, 24; 1214-1223.

Briggs, G. G. 1981. Theoretical and experimental relationships between soil adsorption, octanol-water partition coefficients, water solubilities, bioconcentration factors, and the parachor. *Journal of Agricultural & Food Chemistry*, 29; 1050-1059.

Chiou, C.T., Peters, L.J. & Freed, V.H. 1979. A physical concept of soil-water equilibria for nonionic organic compounds. *Science*, 206; 831-832.

Chiou, C.T., Peters, L.J., & Freed, V.H. 1981. Soil-water equilibria for nonionic organic compounds. *Science*, 213; 683-684.

Chiou, C.T., Schmedding, D.W. & Manes, M. 1982. Partitioning of organic compounds in octanol-water systems. *ES & T*, 16; 4-10.

Chiou, C.T., Porter, P.E. & Schmedding, D.W. 1983. Partition equilibria of nonionic organic compounds between soil organic matter and water. *ES & T*, 17; 227-231.

Clunie, A. & Giles, C.H. 1957. Thumbling apparatus for liquid-phase adsorption experiment. *Chemistry & Industry*; 481-482.

Diamondstone, B.I., Burke, R.W. & Garner, E.L. 1982. Improved leach measurements on solid wastes. *ASTM Standardization News*, June; 28-33.

Fuerstenau, D.W. 1971. *The Chemistry of Biosurfaces Vol.1*. M.L. Hair (ed). Mercel Dekker, New York; 143-176.

Garbarini, D.R. & Lion, L.W. 1985. Evaluation of sorptive partitioning of nonionic pollutants in closed systems by headspace analysis. *ES & T*, 19; 1122-1128.

Hamaker, J.W. & Thompson, J.M. 1972. Adsorption. In: *Organic Chemicals in the Soil Environment*, C.A.I. Goring & J.W. Hamaker (eds), Marcel Dekker, New York; 49-143.

Harter, R.D. 1977. Reactions of minerals with organic compounds in the soil. In: *Minerals in Soil Environments*, J.B. Dixon & S.B. Weed (eds), Soil Science Society of America, Madison, Wis.; 709-739.

Horvath, C., Melander, W. & Molnar, I. 1977. Liquid chromatography of ionogenic substances with nonpolar stationary phases. *Analytical Chemistry*, 49; 142-154.

Horvath, C. & Melander, W. 1978. Reversed-phase chromatography and the hydrophobic effect. *American Laboratory*, 10; 17-36.

Karickhoff, S.W., Brown, D.S. & Scott, T.A. 1979. Sorption of hydrophobic pollutants on natural sediments. *Water Research*, 13; 241-248.

Karickhoff, S.W. 1980. Sorption kinetics of hydrophobic pollutants in natural sediments. In: *Contaminants & Sediments Vol.2*, R.A. Baker (ed), Ann Arbor Science, Ann Arbor, Mich.; 193-205.

Karickhoff, S.W. 1981. Semi-empirical estimation of sorption of hydrophobic pollutants on natural sediments and soils. *Chemosphere*, 10; 833-846.
Karickhoff, S.W. 1984. Organic pollutant sorption in aquatic systems. *Journal of Hydraulic Engineering*, 110; 707-735.
Khan, S.U. 1972. Adsorption of pesticide by humic substances, a review. *Environmental Letters*, 3; 1-12.
Leo, A.J., Hansch, C. & Elkins, D. 1971. Partition coefficients and their uses. *Chemical Reviews*, 71, 525-616.
McCarty, P.L., Reinhard, M. & Rittmann, B.E. 1981. Trace organics in groundwater. *ES & T*, 15; 40-51.
Means, J.C., Hassett, J.J., Wood, S.G. & Banwart, W.L. 1979. Sorption properties of energy-related pollutants and sediments. In: *Polynuclear Aromatic Hydrocarbons*,.P.W. Jones & P. Leber (eds), Ann Arbor Science, Ann Arbor, Mich.; 327-340.
Means, J.C., Wood, S.G., Hassett, J.J. & Banwart, W.L. 1980. Sorption of polynuclear aromatic hydrocarbons by sediments and soils. *ES & T*, 14; 1524-1528.
Means, J.C., Wood, S.G., Hassett, J.J. & Banwart, W.L. 1982. Sorption of amino- and carboxy-substituted polynuclear aromatic hydrocarbons by sediments and soils. *ES & T*, 16; 93-98.
Miller, M.M., Wasik, S.P., Huang, G., Shiu, W. & Mackay, D. 1985. Relationships between octanol-water partition coefficient and aqueous solubility. *ES & T*, 19; 522-529.
Mortland, M.M. 1970. Clay-organic complexes and interactions. *Advances in Agronomy*, 22; 75-117.
Mortland, M.M. 1985. Interaction between organic molecules and mineral surfaces. In: *Ground Water Quality*, C.H. Ward, W. Giger & P.L. McCarty (eds), John Wiley & Sons, New York; 370-386.
Ong, S.K & Lion, L.W. 1991. Effects of soil properties and moisture on the sorption of trichloroethylene vapor. *Water Research*, 25; 29-36.
Peterson, M.S., Lion, L.W. & Shoemaker, C.A. 1988. Influence of vapor-phase sorption and diffusion of the fate of trichloroethylene in an unsaturated aquifer system. *ES & T*, 22; 571-578.
Roy, W.R., Krapac, I.G., Chou, S.F.J. & Griffin, R.A. 1985. *Batch-Type Adsorption Procedures for Estimating Soil Attenuation of Chemicals (EPA/530-SW-85)*. Office of Solid Waste & Emergency Response, US. EPA, Washington, DC.
Schellenberg, K., Leuenberger, C. & Schwarzenbach, R.P. 1984. Sorption of chlorinated phenols by natural sediments and aquifer materials. *ES & T*, 18; 652-657.
Schwarzenbach, R.P. & Westall, J. 1981. Transport of non polar organic compounds from surface water to groundwater, laboratory sorption studies. *ES & T*, 15; 1360-1367.
Stevenson, F.J. 1972. Organic matter reactions involving herbicides in soil. *Journal of Environmental Quality*, 1; 333-343.
US. EPA. 1982. *Test Guidelines: Chemical Fate (EPA-560/6-82-003)*. Office of Pesticides & Toxic Substances, Washington, DC.
Voice, T.C. & Weber, W.J.Jr. 1983. Sorption of hydrophobic compounds by sediments, soils and suspended solids-I. *Water Research*, 17; 1433-1441.

THE DISTRIBUTION OF CONTAMINANTS CONTRIBUTED FROM MULTIPLE POLLUTANT SOURCES IN GROUNDWATER FLOW SYSTEM

D. SANGER & Y. SAKURA
Department of Earth Sciences, Chiba University
Chiba City 263, Japan

ABSTRACT. This research was to study about the pollution plumes spreading process in groundwater flow system caused by the organic chemical waste product from multiple pollutant sources as consequence of industrial activities at the study site, which locates in the Shimosa Upland covered by Kanto loam. First, we gathered all the important data, these were the hydrogeological and industrial data of the study site and the field observation result of contamination in boreholes and wells. Then we applied the U.S. Geological Survey modular 3-dimensional finite difference groundwater flow model and a modular 3-dimensional transport model to simulate the groundwater flow and the pollution plumes spreading process and estimate the extent of the plumes. The mass transport here involved the processes of advection, dispersion, linear sorption, and sinks and sources, and the investigated contaminants mass was halogenated organic compounds. On the basis of the results of pollution measurement at the observed aquifer and the simulation of mass transport process, we could trace the pollution plumes and confirm the location of their sources. We could also estimate the extent of the plumes at present, characterize their size, shape, and movement, and predict their moving plume in groundwater flow system in the future.

INTRODUCTION

The intensive exploitation of natural resources and the large production of wastes in modern lifestyle often threaten to be worse groundwater quality and already have resulted in many incidents of groundwater contamination(Fusillo et al.,1985; Guerrera, 1981; Reinhard & Goodman, 1984; Seraglitz & Miller, 1978). The vast subsurface reservoir of fresh water, which was relatively unblemished by man's activities a few decades ago, is gradually becoming degraded. Extensive evidence from laboratories across many countries in the last few years indicates that misuses, mishandling, or improper disposal of a group of chlorinated organics has caused widespread groundwater contamination(Petura, 1981). Since the maximum allowable concentration of these substances in drinking water is often on the order of a few parts per billion, it is obvious that even very slight leakage from industrial wastewater can lead to serious incidents of groundwater contamination. Organic compounds reach the unsaturated and saturated zones as the result of natural processes or are added by man in his effort to control the ecosystem or to dispose of his wastes. The sources of this kind of groundwater contamination are many and the contaminants numerous, and its appearance looms over industrialized, suburban, and rural areas. It has created a dilemma that requires the attention of public health officials and professional specialist in chemistry, hydrogeology, and environmental sciences and engineering(Dunlap, 1981; Fetter, 1988).

The objectives of this study were (a) to study about pollution plumes spreading process in groundwater flow system caused by the organic chemical waste product from multiple pollutant sources as consequence of industrial activities at the study site; (b) to carry out a number of experiments by using a model in order (i) to estimate the extent of the plumes; (ii) to confirm the

source of contaminant as suggested by a soil organic vapor survey and wells observation in the study site; and (iii) to make prediction about future distribution of the plumes. This study focused on four particular chlorinated organic compounds as contaminants detected at study site, these were trichloroethylene, tetrachloroethylene, trichloroethane, and carbon tetrachloride. They are volatile, weakly hydrophobic, slightly degradable, and toxic(Petura, 1981; Fetter, 1988; Domenico & Schwartz, 1990). These compounds do not naturally exist in groundwater resources. If spill onto the ground and allowed to contact water, they will have only lighted solubility, and sink to the bottom of the water phase(Schwille, 1984).

STUDY SITE

Location of the study site

The study site is located on the Shimosa Upland in the north of the Boso Peninsula as shown in Fig. 1. Administratively, it is a part of Chiba City in Chiba Prefecture, Japan. The length and width of this study site is 2 km and 1.5 km, respectively. Fig. 2 shows the topographic map of study site with 2 m contour interval, the location of factories, and a number of factory's pumping wells which have a screen layer depth between 13 and 70 m below the ground surface. Municipal's pumping wells were not drawn here because it is assumed that the water quantity pumped from these wells is less enough to be neglected compare to the drawn pumping wells. The actual areas of each factory is wider than the factory mark on this figure. Beside the drawn factories in Fig. 2, there are some industrial activity locations that have a possibility to be a chlorinated organic pollutant source, but they were not observed and recorded by the survey team.

Geological structure

Geologically, the study site and area surrounding study site is composed of the quarternary system

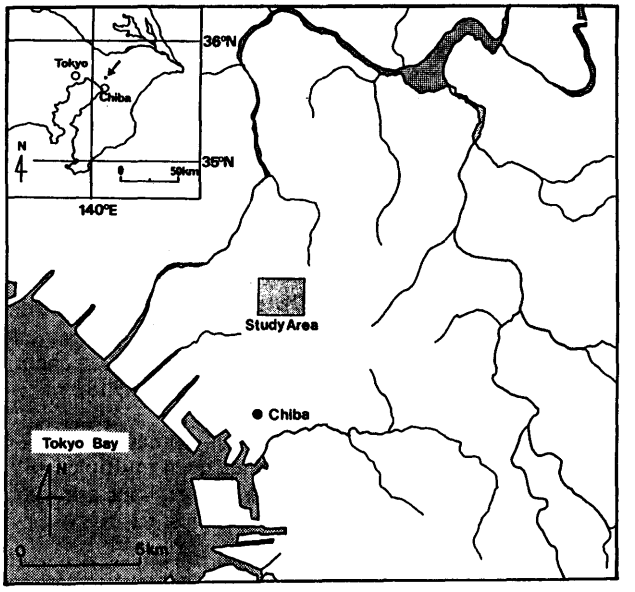

Fig. 1 Location of the study site.

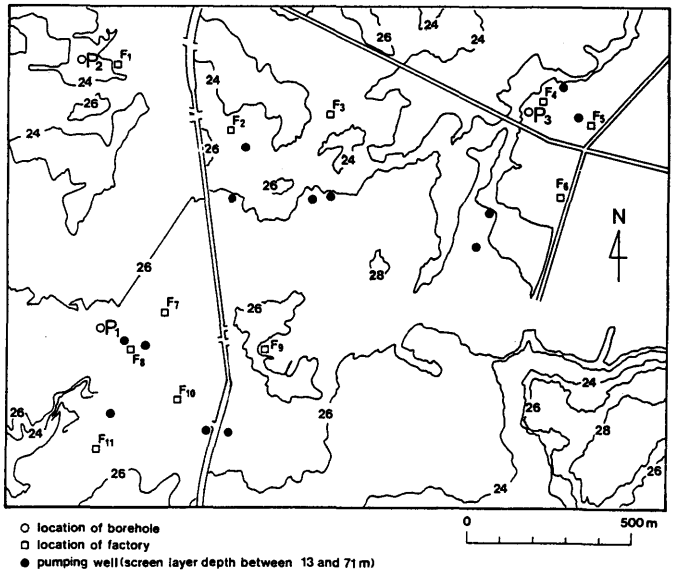

Fig. 2 Topography of the study site and location of factories and pumping wells.

with the Shimosa Group and the Kanto Loam formation in the upland regions and the alluvium sediment distributed along the rivers. The Shimosa Group is composed of shallow marine sands and fresh or brackish water mud(Omori et al., 1986). The mud beds interbedded by the sandy beds are mainly composed of silt and/or clay, and are locally accompanied by gravel beds of fresh water sediment forming channels. The geological structure of the study site at three boreholes is shown in Fig. 3. Its subsurface consists of interbedded gravels, sands, silts, and clays with some hardpan layers. Subsurface is dominantly composed of sand, and it has three aquifers separated by silt-clay layers. The first aquifer is separated by a thin discontinuous silt-clay sediment layer to be the upper and lower aquifers. The thickness of each aquifer and each silt-clay layer is varied in space. This figure also shows the hydraulic head for each borehole for three different depths.

RESULTS OF FIELD SURVEY

Aquifer system

The subsurface of study site could be illustrated as Fig. 4. Three main producing aquifers, separated by significant thicknesses of silt-clayey sediments that form semi-confined aquifer at first aquifer and confined aquifers at second and third aquifers, have been identified beneath the study site area. In this report, these aquifers are referred as first, second, and third aquifers, respectively. First aquifer is separated by a thin silt-clay to be the first-upper and first-lower aquifers. The hydraulic heads of the first upper aquifer and the first lower aquifer are not so different at the same observation point of study site as shown in Fig. 3. The hydraulic head difference between the first-lower aquifer and second aquifer is quite large compare to the hydraulic head difference between the first-upper and first-lower aquifers. Fig. 5 shows the distribution of the hydraulic head of the first upper, first lower, and second aquifers reported in March 1991 by the field survey team.

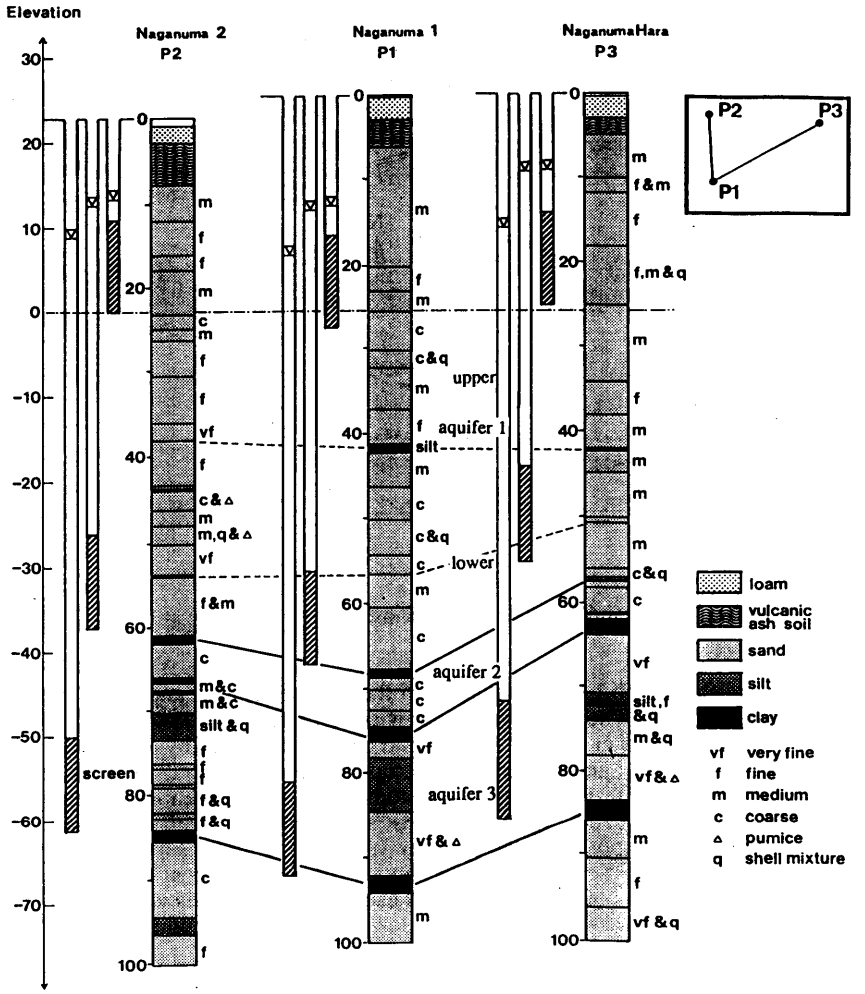

Fig. 3 Geological structure and hydraulic heads of the study site surveyed at three boreholes.

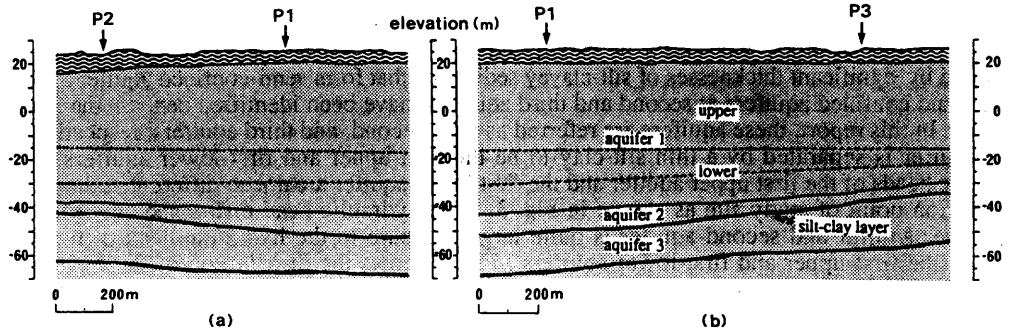

Fig. 4 Cross section of subsurface showing the three aquifers and the silt-clay layers.

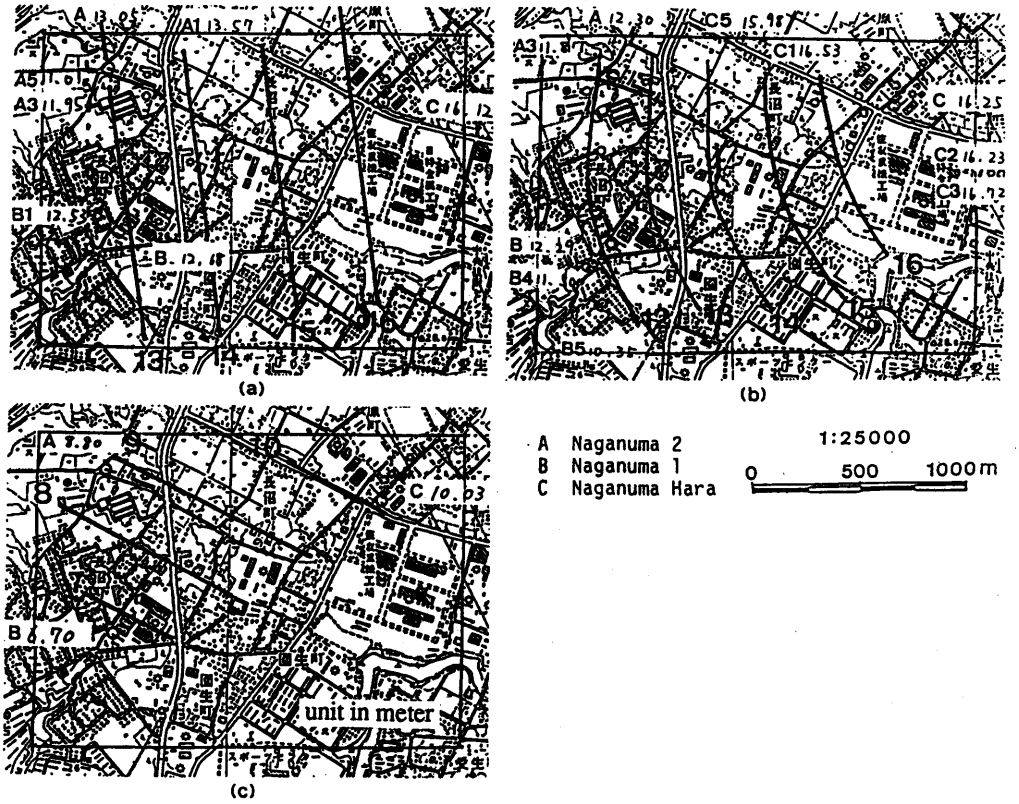

Fig. 5 Distribution of hydraulic heads at (a) first upper, (b) first lower, and (c) second aquifers.

The average porosity of aquifer sampled from the boreholes was 0.25, and hydraulic conductivity of the first-upper, first-lower, and second aquifers surveyed by the pumping test were 3.53×10^{-4}, 3.46×10^{-4}, and 1.33×10^{-4} m s^{-1}, respectively. The precipitation on the surface of study site is about 1300 mm $year^{-1}$. About 600 mm $year^{-1}$ from this amount recharges into the subsurface and the remain is removed by the evapotranspiration and surface flow processes.

Contaminated wells

The observation result of contaminated wells at study site is shown in Fig. 6. The wells observed by the survey team were only the shallow wells. Most of the observed wells have a screen layer less than 60 m deep below the ground surface. At some areas, we have got only a few data of observed wells, for example at the upper left hand side of Fig. 6. At some other sub-areas we have got enough data of observed wells, for example at the sub area surrounding the center-left hand side(west side) of Fig. 6. The east-south side of this area was not interested because it belongs to the other watershed and there was no enough data to be studied. A black dot(•) mark represents an uncontaminated well. In the following sub sections, *sub area* is defined as a part of study site area which locates near or surrounding the factory as shown in Fig. 2.

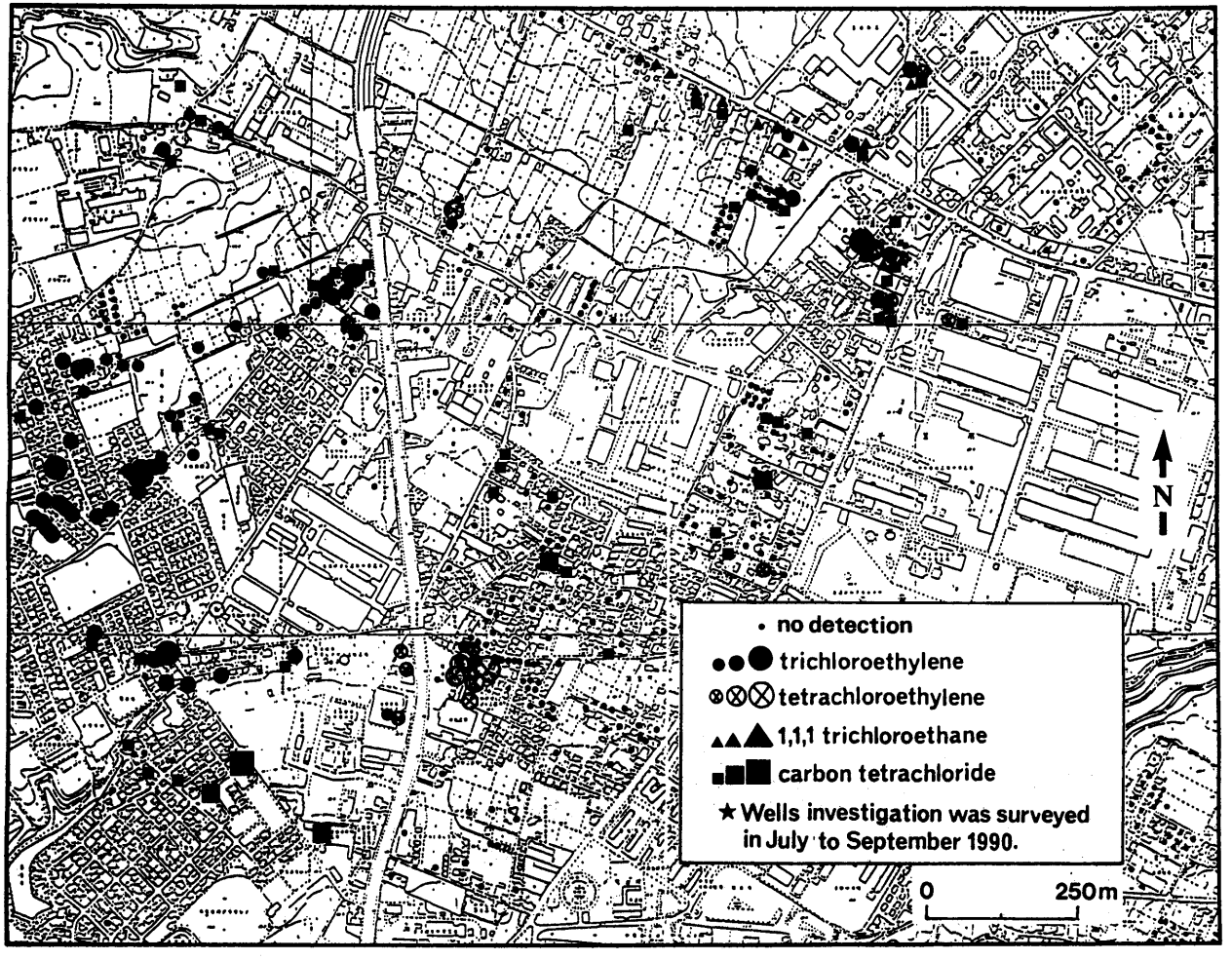

Fig. 6 Observed result of contamination in the wells at study site.

Trichloroethylene: Trichloroethylene(TCE = C_2HCl_3) contaminants were found in many and wide sub areas and one of the most frequently detected in the observed wells. At least we could recognized that there were five contaminated sub aquifers. In Fig. 6, each red circle represents the location of well where TCE pollutant was detected. A small, medium, and big circle(●) marks show the pollutant concentration(C) ≤ 0.001, $0.001 < C \leq 0.01$, and $C > 0.01$ ppm, respectively.

Tetrachloroethylene: In Fig. 6, each circle(⊗) shows the contaminated well by tetrachloroethylene (PCE = perchloroethylene = C_2Cl_4) pollutant. A small, medium, and big circle marks show the pollutant concentration ≤ 0.01, $0.01 < C \leq 0.1$, and $C > 0.1$ ppm, respectively. Wells near location of factory F9(in Fig. 2) seem to be the most polluted wells by PCE. This is because of cleaning service industry at factory F9. The contamination of groundwater near the PCE pollutant source is higher than that of the farther one. At location near P3, some wells have been detected contaminated by PCE, but their distributions had no specific pattern plume, so that it is difficult to recognize their pollutant sources.

Trichloroethane: In Fig. 6 each trichloroethane(TCA = $C_2H_3Cl_3$) contaminated well is represented by a triangle(▲) mark. A big, medium, and small marks represent the pollutant concentration ≤ 0.01, $0.01 < C \leq 0.1$, and $C > 0.1$ ppm, respectively. These contaminated wells were found near area along the road at the northeast area of Fig. 6. There is possibility that the TCA pollutants were first transported by the surface flow of waste water at the drain parallel to the road. Then the wastewater infiltrated downward and spread to the sub aquifer under its drain. The data of TCA consumption for each factory near the TCA contaminated wells were not known, and as a consequence their pollutant sources cannot be identified.

Carbon tetrachloride: Like TCE contaminant, this pollutant was also frequently detected at the observation wells in study site, and its distributions cover many sub areas. Each contaminated well by carbon tetrachloride(CTET = CCl_4) is shown by a green rectangular(■) mark in Fig. 6. A small, medium, and big circle mark shows the pollutant concentration ≤ 0.001, $0.001 < C \leq 0.01$, and $C > 0.01$ ppm, respectively. At the center part of Fig. 6 there are some CTET contaminated wells but they are surrounded by the uncontaminated wells. This condition was probably caused by a pulse pollutant source type or local sources of CTET.

METHOD

Basic principles

Based on the observation result of hydrogeology, distribution of contaminated wells, and industrial activities in this study site, the possible sources of pollutants and the distribution of pollutants were studied and analyzed. The data of factories that recorded the beginning year of use and kinds of chlorinated organic compound for each factory identified to be a pollutant source were used as information to estimate the beginning year of aquifer contamination. This step was followed by an aquifer modeling and the simulations of groundwater flow and contaminant transport processes using MODFLOW(McDonald & Harbaugh, 1988) and MT3D(Zheng, 1991) models, respectively. The estimated simulation time of contaminant transport process is counted since the first time contaminants reached the saturated zone, i.e. the top of aquifer. A time approximating contaminants transport through the unsaturated zone to the saturated zone was not kind of this study concern. Adding or subtracting 0.5 year to the estimated simulation time sometimes would give a better matching between the observation result and simulation result of pollution plumes, but in this study only the integer number of years of the estimated simulation time was chosen. From the comparison of the simulated distribution of pollution and actual one, we can find the appropriate simulated distribution of pollution for the future prediction of moving plumes.

The simulation was carried out with assumptions:
(a) A geology characteristic of aquifer is homogeneous and isotropic; (b) Hydraulic head at any point in aquifer system is constant along the year, i.e. steady state condition; (c) The mass pollutant transport process does not influence the movement and velocity of water flow; (d) Pollutants entered aquifer system have a low concentration, so that they are dissolved in water and the mass transport equation is valid for this condition; (e) Pollutant sources are continuous pollutant types; and (f) No biological process of degradation and no mass chemical transport process except linear-sorption process.

Aquifer modeling

In order to simulate the groundwater flow and mass transport processes in the study site, the first and second aquifers were modeled as grid modeling of aquifer shown in Fig. 7. It has 2 km long, 1.6 km wide, and 56.25 m high. The aquifer is divided to be six layers and the thickness of each layer is shown in Fig. 7. Each layer consists of 40 X 32 cells, and each cell has 50m X 50m size. The first layer is above sea level and the other layers are below sea level. This modeled aquifer covers the first and second aquifers of the study site. In this modeled aquifer, layer 1,2,3 and 4 represent the semi-confined first aquifer, layer 6 represent the confined second aquifer, and layer 5 which is sliced by layer 4 and 6 locates between the semi-confined first aquifer and the confined second aquifer separated by a silt-clay sediment layer. This model will be used for water flow and mass transport processes simulation three-dimensionally, regarding calculation of each process from one cell to the other cells for both horizontal and vertical components.

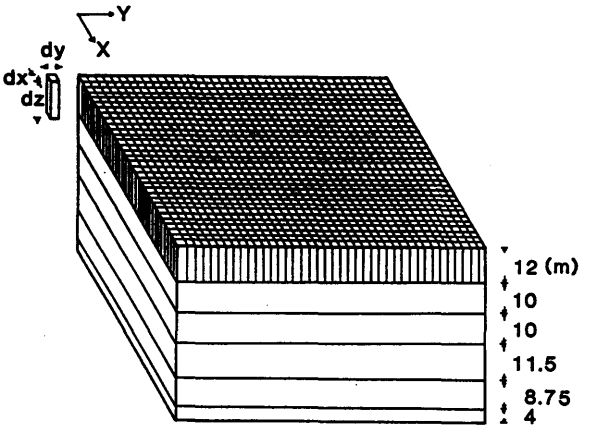

Fig. 7 Grid modeling of aquifer.

Parameters of simulation

From the observation results and previous studies, the parameters of simulation were selected as followings,

porosity(θ) = 0.25; bulk density(ρ_b) = 1.5 g cm^{-3}; hydraulic conductivity(K) first-upper aquifer = 3.53×10^{-4} m s^{-1}; K first-lower aquifer = 3.46×10^{-4} m s^{-1}; K second aquifer = 1.33×10^{-4} m s^{-1}; K silt-clay between 10^{-7} to 10^{-8} m s^{-1}; ratio of horizontal to vertical hydraulic conductivity = 100; longitudinal dispersivity = 20 m; ratio of horizontal transverse to longitudinal dispersivity = 0.3;

ratio of vertical transverse to longitudinal dispersivity = 0.1; precipitation = 1300 mm $year^{-1}$; recharge = 600 mm $year^{-1}$.

The values of K parameter were observed and determined by the field survey team using pumping test method. Kinzelbach(1986) and Domenico and Schwartz(1990) reviewed the reported studies on longitudinal dispersivity values in numerous locations at various scale of observation. On the basis of their reports of scale of observation versus longitudinal dispersivity, we estimated the longitudinal dispersivity as shown value above. For a linear isotherm adsorption process, the retardation factor(R) can be calculated by an equation $R = 1 + K_d(\rho_b/\theta)$ (Freeze & Cherry, 1976; Javandel et al., 1984). Avon and Bredehoeft(1989) made a safe assumption for f_{oc}(fraction of organic carbon) between 0.01 and 1.0 %, and used f_{oc} = 0.1 % as an intermediate value in their model. Based on this approach, the same f_{oc} parameter value of 0.1 % was applied in this study. Table 1 shows the organic compounds, distribution coefficient(K_d) from the previous studies of the sorption process in the field or laboratory(Curtis et al.,1986; Fetter, 1988; Goltz & Roberts, 1986; Mackay et al., 1986) in their observed site, and calculated result of R for linear sorption process.

Table 1: K_d and R of the simulated organic compounds.

Organic compounds	$K_d(cm^3/g)$	R
trichloroethylene(TCE)	0.20	2.28
tetrachloroethylene(PCE)	0.46	3.94
carbon tetrachloride(CTET)	0.17	2.09

RESULTS AND DISCUSSION

Groundwater flow

The distribution of the groundwater hydraulic heads simulated for the layer 1, 3 and 5 are shown in Fig. 8a, d, and e. The hydraulic heads observed from field survey are also shown for layer 1 and 5. This shows that the simulation results resemble to the hydraulic heads observed by the field survey. From this result, it can be seen clearly that activity of pumping wells does not significantly influence the hydraulic heads of the groundwater. The vertical hydraulic head profile of the cross section of aquifer system along AA' and BB' lines are shown in Fig. 8b and c, respectively. At the depth between 30 and 40 m below the top of the modeled aquifer the isopotential curve bends drastically. Vector of groundwater flow is perpendicular to the isopotential plane of hydraulic head. Based on the Fig. 8b and Fig. 8c, we can say in general that the groundwater flows 3-dimensionally downward and south-west ward of the aquifer system. The hydraulic head of groundwater flow system is not constant throughout the year. Because the lack of the detail data of this problem in this study the hydraulic head was assumed constant through the years of simulation(steady state condition).

Distribution of TCE

The simulation result of TCE is shown in Fig. 9 for layer 1, 3, and 5. The data of the depth of contaminated wells were not available. In consequence of this limitation, we plotted on the layer 1, 3, and 5, the same data of the contaminated wells observation results, represented by the marks that show wells being contaminated by a particular pollutant and their concentration levels. Pollutants

entered to groundwater flow system in the saturated aquifer tend to form plumes of polluted water and extend to downstream from the pollutant source until they are attenuated to a minimum quality level. The extent of pollution in groundwater from a point source decreases as pollutants move

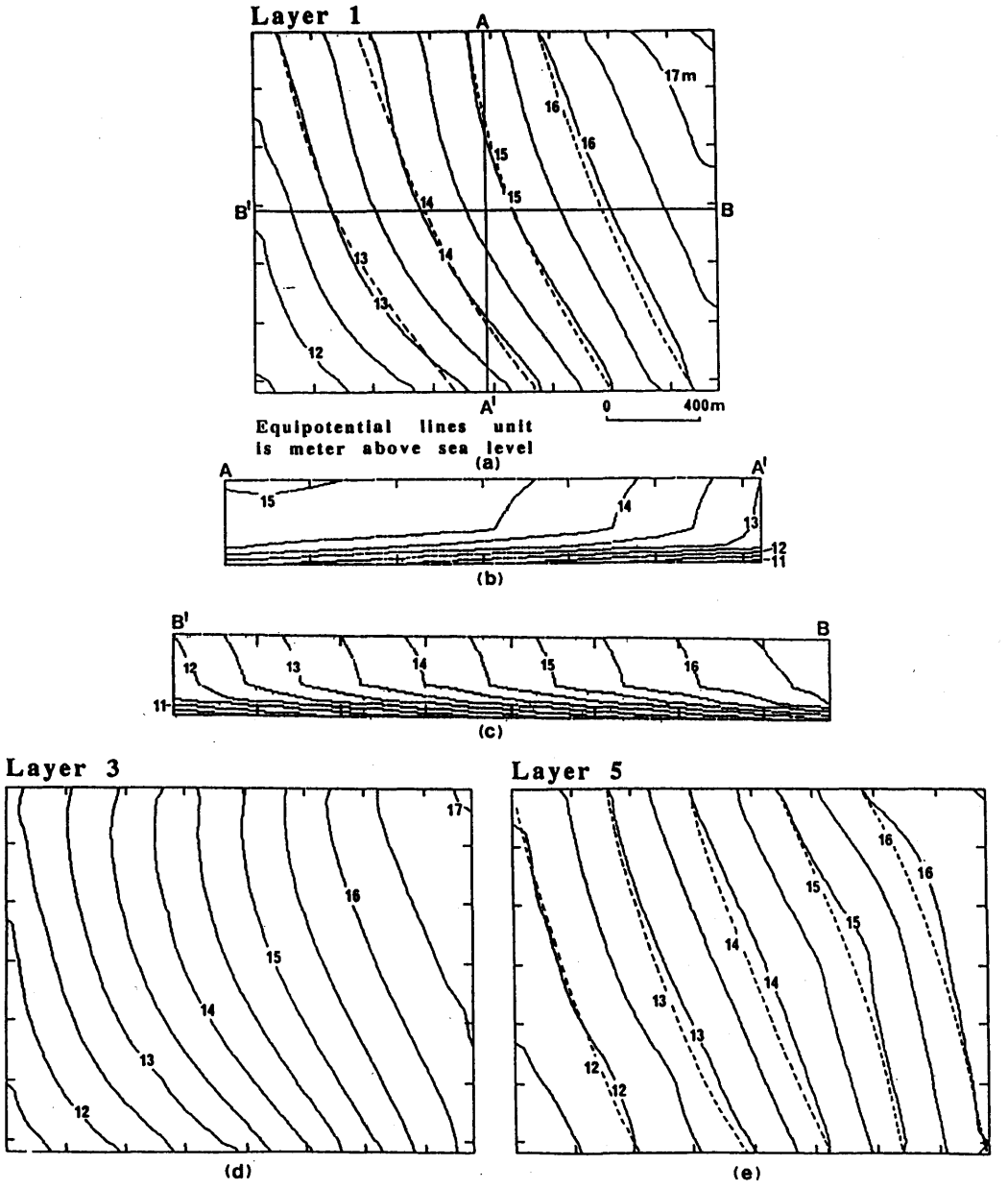

Fig. 8 Distribution of groundwater hydraulic heads (---- observed; — simulated).

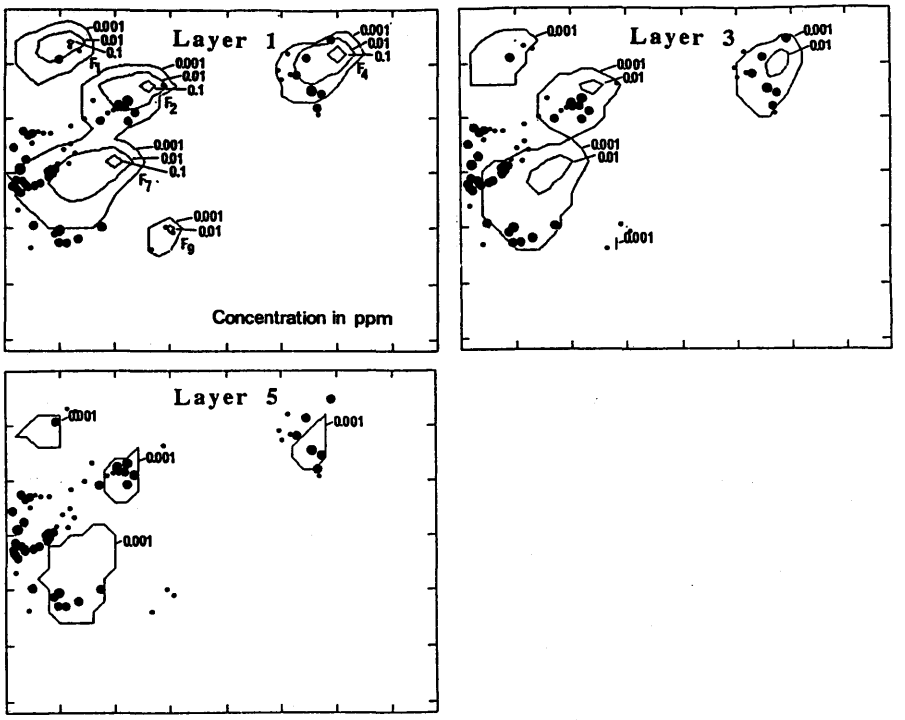

Fig. 9 Distribution of TCE pollution plumes.

away from the source until its concentration exceeds the limit of detection. Here, for each plume caused by any pollutant source, the plume of TCE pollution is represented by a region separated by isoconcentration lines of 0.001, 0.01, and 0.1 ppm. In simulation, we just concerned about aquifer pollution with concentration level > 0.001 ppm. Each plume pattern looks like an unsymmetry and oval shape, especially at the upper layers.

The pollutants are dominantly transported by advection process(Domenico & Schwartz, 1990), and they are spread by dispersion process in the direction of groundwater movement. From Fig. 9 it is clear that the pollutants were transported and dispersed in the aquifer system along the direction of groundwater flow line. This spreading of pollutants is attenuated by linear-adsorption process which tends to localize groundwater pollution near their sources. The simulation result of pollution plumes from each pollutant source will be discussed as followings. The F_1, F_2, etc. indexes are the same as shown in Fig. 2.

Pollutant source F_1: A number of the observed contaminated wells in sub area near or surrounding F_1 was just a few so that it causes a difficulty to confirm simulation result accurately. Unavailability of enough data made it impossible to estimate where the front of the actual pollution plume was. From this simulation result, we can only predict the tendency of pollution plume movement in the aquifer. This pollution plume was simulated for 3 years since the aquifer contamination started.

Pollutant source F_2: The simulation result gave a good representation of the actual aquifer contamination. The contaminated wells near the source have the observed concentration higher than

the far one. At the north part of pollution plume there were no data of the observed contaminated wells. Based on this simulation result, we can estimate the size and shape of pollution plume caused by the pollutant source F_2 and its spreading movement. Simulation time was 3 years.

Pollutant source F_4: The simulation result covers the dot marks of TCE contaminated wells. The contaminated wells near the pollutants source has a higher concentration than the outer one. The pollutant concentration decreases along the movement path of pollutants transport as shown by the simulation result. It agrees with the observation result of contaminated wells. The front zone of pollution plume reached the deeper layers, but the back zone did not reach it. Simulation time was 5 years, but a little more simulation time(less than 0.5 year) is required to get a better result.

Pollutant source F_7: In comparison with the other contaminated sub aquifers, the sub aquifer near this factory is the most and widest contaminated. The contaminated wells were distributed at the left hand side and south-west side of this factory. Most of these contaminated wells had the TCE pollutant concentration > 0.01 ppm. Unavailability of the data of source position inside or near the factory made it difficult to determine the best fitting point source of pollutants in simulation. Except for the north-west area, the simulation result of pollution plume covers almost all the contaminated wells in the sub aquifer of study side near location F_7. Simulation time was 4 years. The contaminated wells at the north-west area may be due to the following reasons, (a) The actual local hydraulic heads around this area did not agree with the simulation result of groundwater flow around this sub aquifer. It was caused by the lack of the detail data of hydraulic head used for the flow transport simulation; (b) The waste water which solute the pollutants flowed to the north-west sub area through the drain and infiltrated from this drain to the unsaturated zone. The concentration of simulated pollution plume has one order lower than the pollutant concentration measured in the field observation. The possible reasons of this difference are as follows, (a) the actual pollutant source had a concentration higher than that of the simulated point source; (b) there were more than one point pollutant source inside or near the factory.

Pollutant source F_9: In this sub area, the observation result of contaminated wells just gave 3 data of contaminated wells. Simulation time was 2 years. The simulation result of pollution plume covers the TCE contaminated wells, but a number of the observed wells covered by this plume were not contaminated. It is possibly because this pollution plume caused by a TCE pollutant source that could not be classified to be a continuous pollutant source type and it had caused no detection of pollutant at some wells.

Distribution of PCE

The simulated distribution of PCE, 2 years after the beginning of contamination is shown in Fig. 10. The same observation result data of the contaminated wells were also plotted for each layer, because we cannot classify the layer or the depth of each well. The contaminated wells are marked by a circle mark which has a big, medium, and small size for pollutant concentration ≤ 0.01, $0.01 < C \leq 0.1$, and $C > 0.1$ ppm, respectively. Even though the concentration 0.001 ppm of observation result of contaminated wells was not detected, here the simulated isoconcentration line of 0.001 ppm is shown in Fig. 10. The observation result showed two wells contaminated by PCE near factory F_2, some wells near F_4, and almost all wells near F_9. The contaminated wells near F_4 had no specific distribution pattern. Consequently, it is difficult to determine their pollutants source. These contaminated wells may be due to the unsteady concentration of PCE pollutant released by their pollutant sources.

The simulated distribution of pollution plume caused by source F_9 agreed with the observational result of contamination. In the upper layers, the contaminated wells with pollutant concentration > 0.1 ppm is surrounded by the simulated isoconcentration line of 0.1 ppm, and the contaminated wells with concentration between 0.01 and 0.1 ppm lay down between the simulated

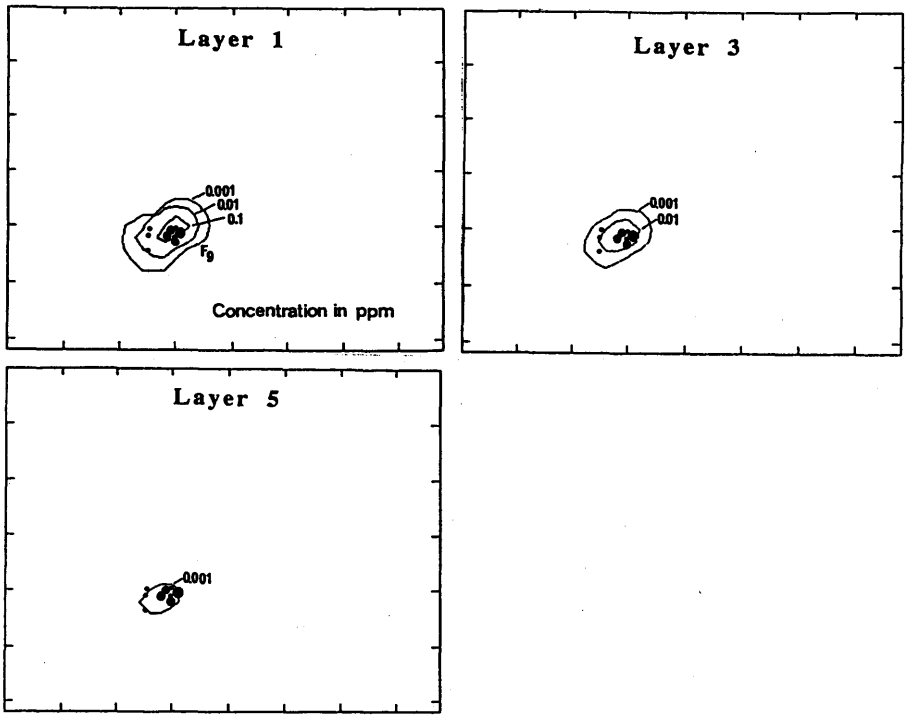

Fig. 10 Distribution of PCE pollution plumes.

isoconcentration lines of 0.01 and 0.1 ppm. The actual size and shape of pollution plume caused by pollutant source at F9 is represented by the simulation result.

Distribution of CTET

The simulation result of CTET pollution plumes is shown in Fig. 11. For each layer in Fig. 11 the same observation result data of the contaminated wells were also plotted and marked by a big, medium, and small size of circle mark that represents pollutant concentration ≤ 0.001, $0.001 < C \leq 0.01$, and $C > 0.01$ ppm, respectively. Observational result showed that most of the CTET contaminated wells have the pollutant concentration ≤ 0.001 ppm. Only the contamination wells caused by the pollutant source F_{10} had a high concentration at wells near the source and its concentration decreased as the function of distance. At the center of Fig. 11 there are some contaminated wells surrounded by the CTET uncontaminated wells. Some possibilities that caused the contamination around this area were as followings, (a) local sources of CTET pollutant in this area; ((b) CTET pollutants were released by a non-continuous source contaminated for a certain short time. Because it is difficult to confirm their pollutant sources, the pollution plume in this area was not simulated.

Pollutant source F_1: As mentioned before, the number of the observed wells data in this sub area were too few. Therefore, it is difficult to compare the observational result with the simulated one of the aquifer and to estimate the front zone of the simulated pollution plume. Here, the simulated result could give only the information about the flow direction of pollution plume and its shape. Simulation time was 4 years.

Pollutant source F_2: In this sub area only four wells were detected contaminated by CTET pollutants and had a concentration < 0.001 ppm. The other wells did not show any CTET contamination, and their number was more than the number of contaminated wells. It means the pollutant source was not a continuous type. Here, the simulated result can give only the information about the movement tendency of CTET pollutant. Simulation time was 5 years.

Pollutant source F_4: All the CTET contaminated wells are covered by the simulated pollution plumes as shown in Fig. 11, except for one well located at the most northern part of the simulated pollution plume. An exceptional well was possibly contaminated by a local pollution source. The contaminated wells all had the pollutant concentration ≤ 0.001 ppm, and this value agreed with the simulated one. At the front zone of pollution plume, pollutants reached the lower layers. Simulation time was 6 years, and CTET compound was not consumed anymore since 1990.

Pollutant source F_8: The data of CTET contaminated wells caused by this pollutant source were only three wells and all had the pollutant concentration ≤ 0.001 ppm. Simulation time was 3 years. Simulated result suggested that the layer 5 has not been contaminated.

Pollutant source F_{10}: The contaminated wells in this sub area seem to have the expected concentration. The wells near the pollutant source had a higher concentration comparing to the far ones. The simulated result shows the possible size and shape, and possible flow direction of pollutants. Simulation time was 4 years. In 1989 this CTET compound was not consumed anymore in this factory.

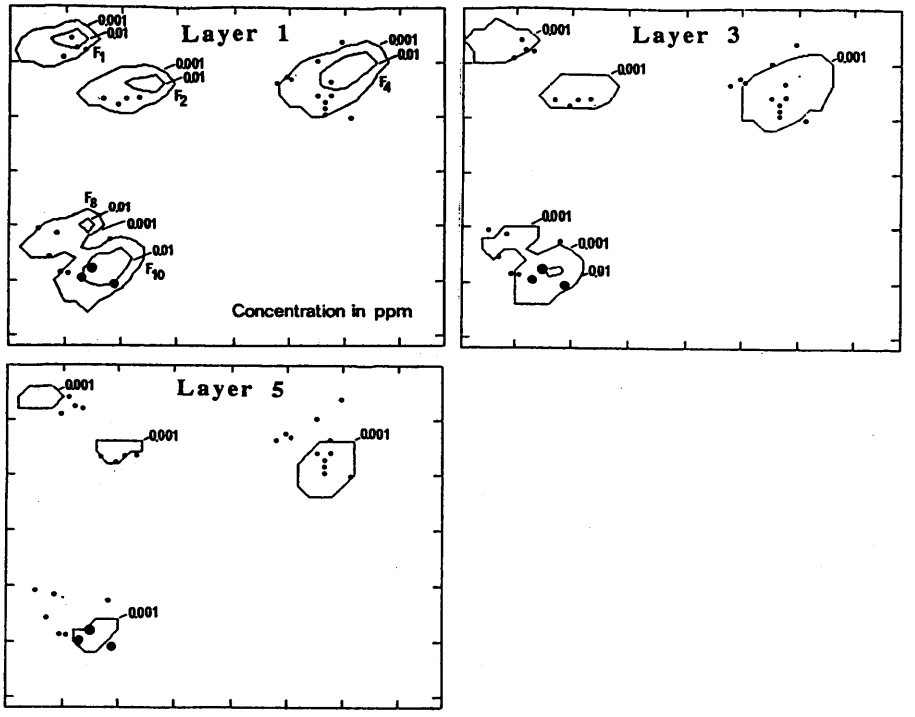

Fig. 11 Distribution of CTET pollution plumes.

The differences in concentration between the observed and simulated results may be due to the following reasons, (a) geologic heterogeneities, which affect flow dynamics; (b) multiple point sources at one location with different intensities; (c) temporal releases of contaminants at source locations; (d) contaminants released by pollutant source, which is an instantaneous source; (e) spatial variability in either the physical process sampling problems which are not representative of local groundwater conditions; (g) incorrect preserve of samples or laboratory analysis; and (h) difference between the actual pollutants quantity entered the studied aquifer and the simulated

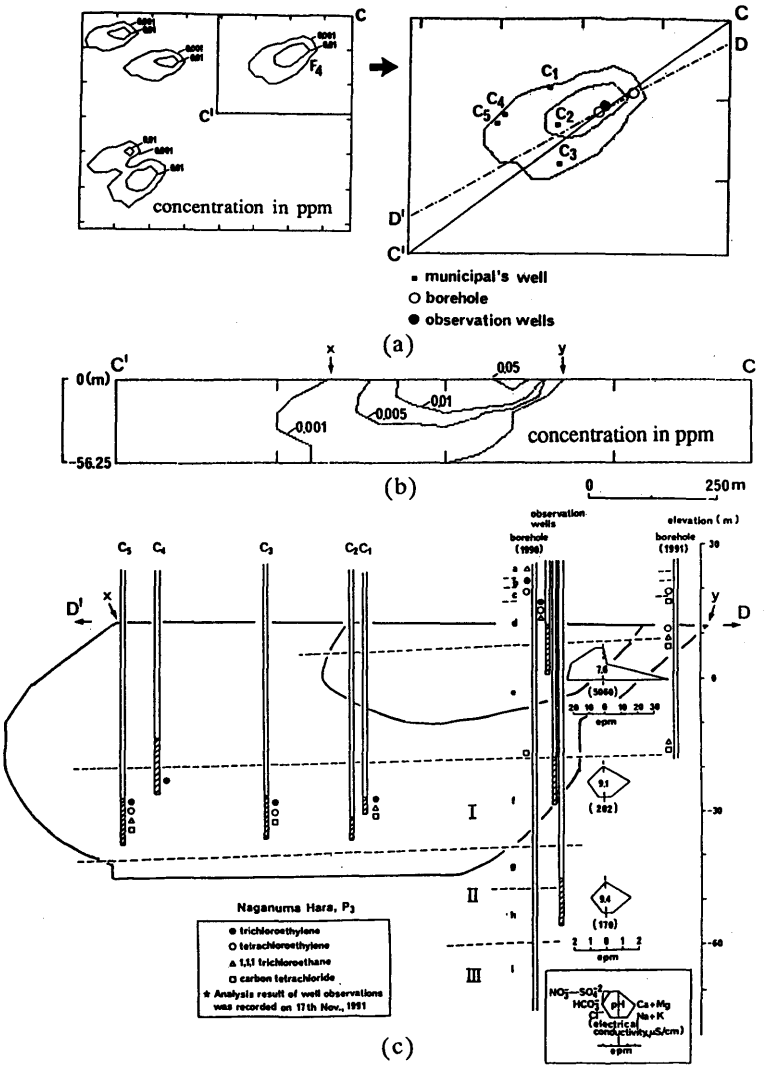

Fig. 12 Cross section distribution of CTET pollution: (a) location of observation, (b) cross section of CTET pollution plumes, (c) field observation and simulation results.

pollutants quantity. And time difference of elapsed time between the actual contamination and the simulation of aquifer. Avon and Bredehoeft(1989) in their study also have reported a number of reasons of differences in concentration that are same as some reasons mentioned above.

Vertical distribution of pollutants

The simulation results of pollution plume discussed above can be represented by a cross-sectional distribution of pollution plume caused by each of their pollutant sources. For example, one of them is presented as shown in Fig. 12. The upper-left hand side of Fig. 12 is the simulated result of the CTET pollution plume at layer 1. We only considered about the pollution plume caused by the pollutant source F_4 and it was drawn once again at the upper right hand side of Fig. 1a. A CC' is the line at the top of the cross section of the simulated aquifer and a DD' is a projection line for each observed contaminated well. The vertical distribution of pollution plume caused by a pollutant source F_4 is shown in Fig. 12b. Here, we can see the size and shape of the simulated pollution plume in the cross section. In Fig. 12c, the observed distribution of contaminated wells is shown. We can see the contaminated wells were covered by the simulated pollution plume. From Fig. 12c, it seem to us that this pollution plume reached the deeper aquifer which locates at the bottom of the modeled aquifer. This is because we only simulated the modeled aquifer of 56.25 thick, so that a simulated pollution plume of 0.001 ppm at the deeper aquifer is not presented here. This cross section of simulated result showed the possible size, shape, and movement direction of pollution plume as a representative model of the actual vertical contamination in this aquifer.

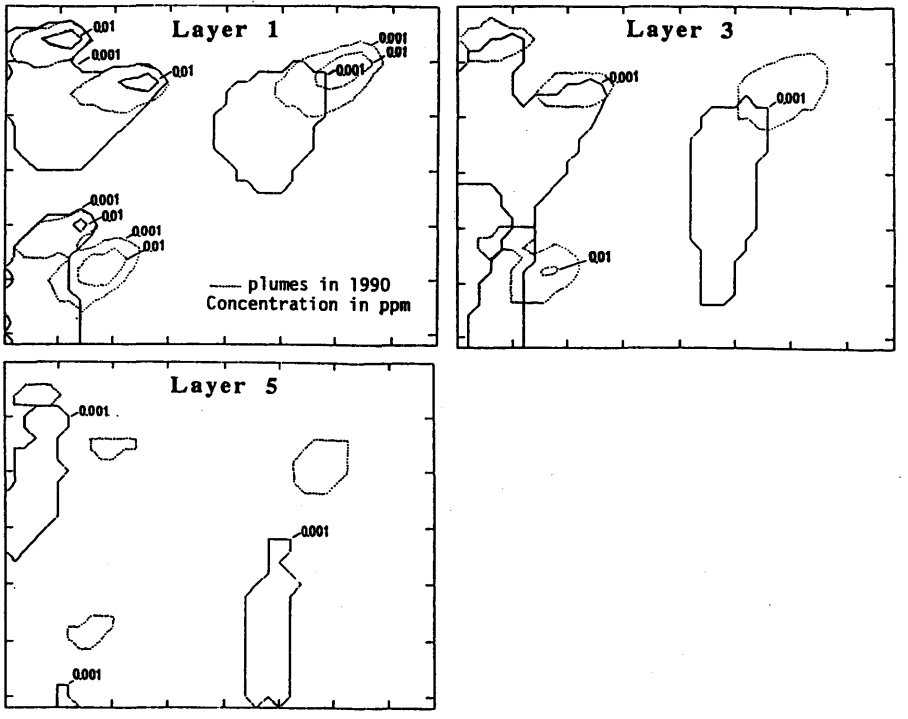

Fig. 13 Simulated result of CTET pollution plumes in the future (1996).

Distribution of pollutants in the future

The distribution of pollution plumes in the future will be shown only for CTET contaminant, because the other pollution plumes have the same characteristics of transport process as CTET in this study site. The future condition of the simulated pollution plume after 6 years of time elapses(condition in 1996) is shown in Fig. 13. By comparing this result to the simulated result in 1990(Fig. 8), we can trace the movement direction and the distribution tendency of pollutants in this observed aquifer. In first layer, each continuous pollutant source has a constant concentration plume near each point source, but the outer isoconcentration line is spreading with time. The pollutants caused by the past consumption of CTET released by pollutant source F_4 and F_{10} still remain and spread in this aquifer. In each layer, its size and shape become wider and wider. This is because except by the pumping well activities there is no other mechanism to pull out the pollutants that have entered to this studied aquifer, and pollutants amount extracted by these pumping well activities is only a really small proportion of the pollutants in the aquifer. The front zone of pollution plume caused by the past pollutant source reached a longer distance at the lower layers compare to the distance at the upper layers. This phenomenon could be explained by a cross section pattern of pollution plume as discussed before. This result gave the information about the pollution plume size, shape, and movement direction in this aquifer system.

CONCLUSION

From this study we concluded as following,
(a) Management and control of organic chemical waste products from industrial activities in study area need to be evaluated and improved, because it threatens aquifer system and groundwater quality;
(b) Contaminants entered the aquifer system remain for a long time as contaminants dissolved and transported in groundwater and contaminants adsorbed on solid; There is no mechanism to pull out it except for a negligible proportion which is withdrawn by pumping well activities;
(c) Because the lack of data about points number and location of observation wells, hydraulic heads in detail, the actual quantity and time function of pollutants entered the aquifer, and the beginning time of aquifer contamination, this study emphasized the research to understand the movement direction, movement mechanism, size and shape, and future tendency of pollution plumes rather than to understand the quantity of contamination;
(d) The remediation of aquifer system in this area is a difficult task to be carried out and it takes a long time, because the groundwater moves slowly to transport contaminants downward, furthermore the pollution plumes were distributed in many and wide sub aquifers of sub areas;
(e) On the basis of the appropriate simulation of groundwater flow and mass transport processes, it is possible (i) to estimate the extent of the plumes covering the contaminated wells that surrounded by the uncontaminated wells; (ii) to characterize the size and shape of the plume; (iii) to confirm the likely source of contaminants as suggested by a soil organic vapor survey and wells observation; and (iv) to estimate or make prediction about future distribution of the plumes.

REFERENCES

Avon, L. & Bredehoeft, J.D.1989. An analysis of trichloroethylene movement in groundwater at Castle Air Force Base, California. *J. of Hydrol.*, 110; 23-50.

Curtis, G.P., Roberts, P.V. & Reinhard, M.1986. A natural gradient experiment on solute transport in a sand aquifer 4. Sorption of organic solutes and its influence on mobility. *Water Resour. Res.*, 22(13); 2059-2067.

Domenico, P.A. & Schwartz, F.W. 1990. *Physical and Chemical Hydrogeology* (1st edn). John Wiley & Sons, New York.

Dunlap, W. 1981. Organic pollution of groundwater: Its prevalence, implication and control. *Environ. Sci.*, 17; 575-580.

Fetter, C.W. 1988. *Applied Hydrogeology* (2nd edn). Merril Publishing Co., Columbus, Ohio.

Freeze, R.A. & Cherry, J.A.1979. *Groundwater* (1st edn). Prentice-Hall, Englewood Cliffs, N.J..

Fusillo, T.V., Hochreiter Jr., , J.J. & Lord, D.G.1985. Distribution of volatile organic compounds in a New Jersey coastal plain aquifer system. *Groundwater*, 23; 354-360.

Goltz, M.N. & Roberts, P.V. 1986. Interpreting organic solute transport data from a field experiment using physical non equilibrium models. *J. of Contaminant Hydrol.*, 1(1/2); 77-93.

Guerrera, A.A. 1981. Chemical contamination of aquifers on Long Island, New York. *J. Am. Water Works Assoc.*, 190-199.

Javandel, I., Doughty, C. & Tsang, C.F.1984. Groundwater transport: Handbook of mathematical models. *Water Resources Monograph* (no. 10) Amer. Geophy. Union, Washington, D.C..

Kinzelbach, W. 1986. *Groundwater Modeling* (1st edn.). Elsevier Science Publishers B.V., Amsterdam, Netherlands.

Mackay, D.M., Ball, W.P. & Durant, M.G.1986. Variability of aquifer sorption properties in a field experiment on groundwater transport of organic solutes: Methods and preliminary results. *J. of Contaminant Hydrol.*, 1; 119-132.

McDonald, J.M. & Harbaugh, A.W.1988. A modular three-dimensional finite-difference groundwater flow model. In: *Techniques of Water Resources Investigations of the U.S. Geological Survey* (no. 6).

Omori, M., Hayama, Y. & Horiguchi, M. 1986. *Regional Geology of Japan: Part 3 Kanto* (1st edn.). Kyoritsu Shuppan Co., Tokyo, Japan.

Petura, J.C. 1981. Trichloroethylene and methyl chloroform in groundwater: A problem assessment. *J. Am. Water Works Assoc.*, 200-205.

Reinhard, M. 1984. Molecular weight distribution of dissolved organic carbon and dissolved organic halogen in advanced treated wastewaters. *Environ. Sci. Technol.*, 18(6); 410-415.

Reinhard, M. & Goodman, N.L.1984. Occurrence and distribution of organic chemicals in two landfill leachate plumes. *Environ. Sci. Tech.*, 18(12); 953-961.

Schwille, F. 1984. Migration of organic fluids immiscible with water in the unsaturated zone. In : *Pollutants in Porous media*, B. Yaron et al., Springer-Verlag Berlin Heidelberg, Germany; 27-48.

Seraglitz, J.J. & Miller, D.W.1978. Status of groundwater contamination in the United States. *J. Am. Water Works Assoc.*, 70; 162-166.

Zheng, C. 1991. A modular three-dimensional transport model for simulation of advection, dispersion and chemical reactions of contaminants in groundwater systems(1st edn). S.S. Papadopulos & Associates Inc., Maryland.

SURFACE SOIL GAS SURVEY FOR IDENTIFYING POLLUTANT SOURCE AND EXISTING FORM OF ORGANOCHLORINES IN SUBSURFACE ENVIRONMENT

T. HIRATA & O. NAKASUGI
National Institute for Environmental Studies
16-2 Onogawa, Tsukuba, Ibaraki 305, Japan

ABSTRACT. 2 through 5 percent of the groundwater samples taken across the nation every year have overshot the drinkable limits of trichloroethylene and tetrachloroethylene of Japan. Such pollutants should be removed to match the pollution level with regional groundwater usages, however, the remedial operation is basically so costly. The success of the remediation totally depends on picking up the suitable technique to repair the subsurface pollution, corresponding to contaminant existing form in subsurface environment. In this context, soil-gas survey as an option of remote geochemical reconnaissances to identify the contaminant source and to determine the sites for making boreholes was employed, reducing the cost of site investigation. Then, four boreholes were installed for soil vapor extraction and groundwater extraction, and a pilot-scale subsurface remediation has been undertaken to evaluate the effectiveness of both remediation techniques. The paper describes the results of remediation to find a way for optimizing the remediation scheme.

INTRODUCTION

The groundwater pollution due to volatile organochlorine like trichloroethylene and tetrachloroethylene has been becoming a great environmental issue in Japan as well in US and many developed nations. The nation-wide groundwater pollution survey as to organochlorines started in 1982(Hirata et al., 1992), and so far 2 through 5 percent of groundwater samples every year cannot meet the standards for drinking water of trichloroethylene and tetrachloroethylene. Consequently, several legislations were compelled to be changed and modified to prevent and conserve the subsurface environment from being polluted, and at present any water containing trichloroethylene, tetrachloroethylene and carbontetrachloride is not allowed to be injected and recharged into subsurface environment.

The organochlorines have several insidious features to be little soluble in water (Hunt & Sitar, 1988) and to be strongly resistant to biodegradation in subsurface environment (Vogel & McCarty, 1985). Such physico-chemical properties prolong the groundwater pollution once the undiluted liquids intrude into soil and groundwater zones. In addition, the groundwater pollution incidents involve difficulties to be solved, for example, not easy to identify the contaminant source and existing form in subsurface environment because of various usages in many industries, insufficient number of wells in existence to delineate the contaminant plume boundary in regional groundwater, etc. Distributing many observation wells over the contaminated region is the most reliable method to monitor the pollution state in groundwater, however, making boreholes is so costly. In this context, soil gas survey, which includes activated carbon fixation, n-Hexane extraction, gas-detector tube and combination of these methods, etc., is much useful as a preliminary reconnaissance to determine the sites for making boreholes. This is because from cost-beneficial and hydrogeological point of view, the remediation will be the more effective, the closer the remediation wells to contaminant source are constructed. The surface soil-gas techniques

were applied to several pollution sites, and areal distributions of volatile organochlorine concentrations in surface soil-gas were obtained. Then, borings were carried out to elucidate the pollution extent and existing form of organochlorines in soil and groundwater aquifer, considering the areal distribution of gaseous organochlorines in surface soil. The boreholes for soil vapor extraction and groundwater extraction were also installed in one of study sites to evaluate the effectiveness of both remediation techniques and to optimize the remediation scheme for subsurface contamination. The paper describes the role of the surface soil-gas survey playing in site investigation from identifying the contaminant source to determining the suitable remediation techniques. In addition to this, a pilot-scale subsurface remediation using soil vapor extraction and groundwater extraction is introduced as one of case studies.

SURFACE SOIL-GAS EXPLORATION

Existing form of organochlorines

Many years passed from the time when contaminants had touched the ground to the discovery of groundwater pollution to reach the domestic or public water supply wells, therefore, in general the exact solution of pollution mechanisms remains indefinite. In case that fortunately the pollution mechanisms were unveiled, almost all of pollution incidents were caused by solvent spill and accidental leakage from cracks on the storage tank and faults of supply pipe joints, and unacceptable disposal and casual treatment during cleansing processes. Thereby the undiluted solvents like trichloroethylene and tetrachloroethylene are presumed to infiltrate into the subsurface zone. The organochlorines are basically little soluble in water, so that the large scale pollution incidents which exhibit wide-range spreading of contaminants and continuance of pollution plume in aquifers are undoubtedly thought to still keep the contaminants of being undiluted original forms in soil/aquifer.

The undiluted liquids of organochlorines possess the specific physico-chemical properties to be less in viscosity and surface tension and much higher in density than water. Such far different properties compared to water allow the undiluted solution to readily migrate in the unsaturated porous media rather than water. In addition the column tests packing the glass beads characterized the migration behavior of undiluted organochlorines that in case of the test using fine particles, the whole liquid of trichloroethylene coming down smoothly from the unsaturated zone tended to stagnate on the table of the aqueous layer saturated with water, while in case of coarse particles it moved easily into the saturated zone without stagnating on the water table (Hirata & Muraoka, 1988). In particular the test liquid reached to the bottom of the column, being left in the pore space of the aqueous layer in the test of the coarse particles.

Nearly the same migration behavior of organochlorines as the column test results mentioned above is confirmed to take place in the pollution incidents in the real field. Table 1 listed the maximum concentrations of soil and groundwater, obtained from the undisturbed boring cores taken in the various pollution sites in Japan. The depth at which the soil concentration takes the maximum differs among the pollution sites, however, the contaminants tend to raise their soil concentrations at locations between gravel and clay layers, which correspond to the bottom of the groundwater aquifer.

Surface soil-gas survey as remote geochemical monitoring

In order to reduce the cost for remediation, it is inevitable for remediation to be carried out with the minimum of extracted soil-gas and pumped groundwater volumes. In this context, highly contaminated parts as arranged in Table 1 should be discovered around the contaminant source. The all-core borings and subsequent chemical analyses are the most reliable procedure, however, covering the whole area is much costly. The volatile organochlorines staying in the vadose and

Table 1: The maximum concentrations of organochlorines in soil and groundwater in pollution incidents of Japan with their soil features.

Locations	Solvent	Depth (m)	Soil feature	Soil conc. ($mg\ kg^{-1}$)	Groundwater conc. ($mg\ l^{-1}$)
TK-A	TCE	7	Clay	64	11
	cis-DCE	7		39	19.2
TK-B	TCE	11.5	Silt	0.2	1.9
	cis-DCE	6.3		3.43	5.5
T1	TCE	2	-	6,600	42
	TCE	37	Silty sand	5.4	103
KT-U	TCE	25-27	Silt	40	360,000
KT-K	TCE	0.7	Surface soil	10	>10
KM-K	PCE	5.5	Silt	360	80
KM-T	TCE	46	Silty sand	138	294
SZ-A	PCE	2.1	Coarse sand	8,100	8.6
SZ-B	PCE	0.8	Clay	25,000	22
IT-S	TCE	3	Coarse sand	232	1,390
IT-M	TCE	7-8	Silty sand	210,000	40

Solvents are: TCE - trichloroethylene, PCE - tetrachloroethylene, and cis-DCE - cis-1,2-dichloroethylene.

groundwater zones tend to become vapored into the pore space in soil and to migrate upward to the groundsurface. The surface soil-gas monitoring is expected as quick and less-expensive technology to delineate the pollution boundary in aquifer and to determine the sites for making boreholes, utilizing the areal distribution of organochlorine vapor.

The organochlorine in the vadose zone is basically well partitioned among air(soil-gas), liquid and solid phases. In order to apply the soil-gas monitoring to pollution sites under the various conditions, the interrelations among them should be examined in advance. The site investigation for soil-gas monitoring was designed in several study sites. First, Fig. 1 displays the relationship between tetrachloroethylene concentrations in soil and soil-gas. The geological profile of the study site is described as the site is covered by the gravel of 5m deep, overlying the bedrock, and the groundwater table appears at 4m depth. The contaminated soil for chemical analysis was taken from the bottom of a small hole of 2cm in diameter and 2m in depth, and the soil-gas was collected from the same hole through a diaphragm pump to keep in a bag. The organochlorines in the soil were extracted using n-Hexane, and the chemical determination for soil and soil-gas concentrations was made with a gaschromatography-ECD. On the basis of the nineteen samples, it results in a nearly linear correlation between them on a full-log scale. A similar correlation

between the concentrations of soil-gas and groundwater was also obtained by Yoshioka et al. (1992), indicating slight scattering compared to Fig. 1. In addition to this, the areal distribution of the tetrachloroethylene vapor in soil-gas was drawn as Fig. 2. There can be recognized a distinct extension pattern of the vapor like concentric circles around a suspicious contaminant source to be a laundry firm.

Another result for the surface soil-gas monitoring is illustrated in Fig. 3. The site investigation confirmed that the sandy soil extends until 3m depth with groundwater table being at 1.5m depth, overlying the clay layer. The tetrachloroethylene concentration in the surface soil-gas was determined with the gaschromatography-ECD, fixing the volatile constituents of soil-gas into the n-Hexane liquid. The significant high values of tetrachloroethylene concentrations in this site ensure the existence of the devastating soil and groundwater pollution. The maximum vapor concentration of tetrachloroethylene in air calculated from the vapor pressure takes approximately 18400ppmv, hence, the vapor concentrations overshooting 10^4ppmv nearby the dry-cleaning machines are enough high to imagine the undiluted tetrachloroethylene residue in soil and groundwater. In fact the undiluted liquid of up to eight liters was recovered from the soil around the sludge wastes sites illustrated in Fig. 3. As a result, the soil-gas monitoring is confirmed to be an effective technique as a remote geochemical exploration for delineating the pollution plume and identifying the contaminant source in subsurface environment.

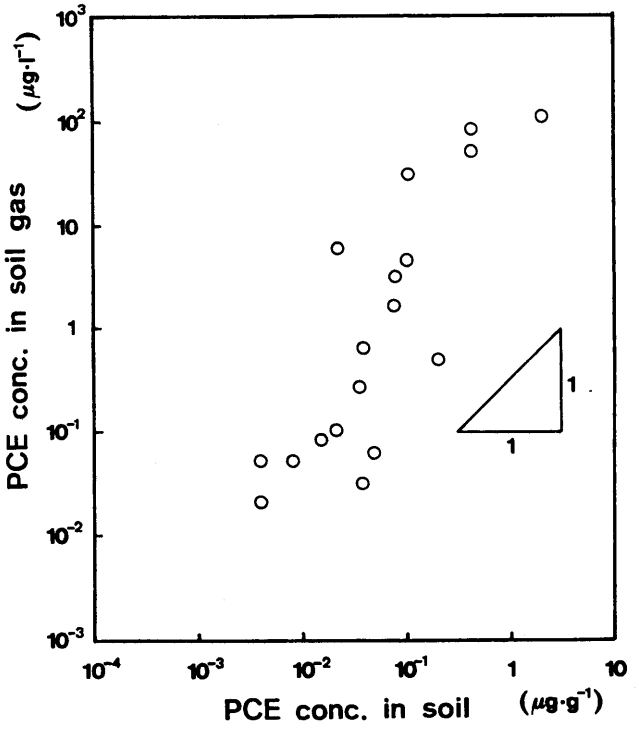

Fig. 1: Relationship between tetrachloroethylene (PCE) concentrations in soil and soil-gas collected in a shallow groundwater region.

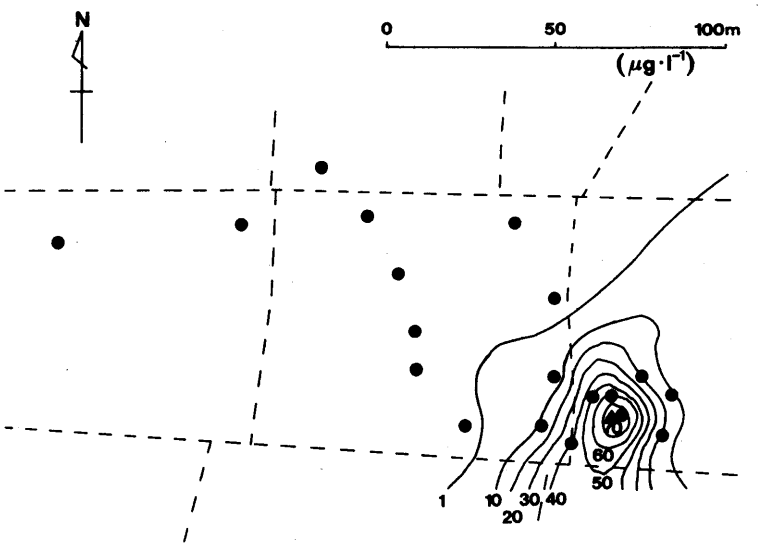

Fig. 2: A plume of tetrachloroethylene vapor in surface soil-gas in a shallow groundwater region. The closed circles denote the locations for soil and soil-gas collections and a triangle does for a laundry firm.

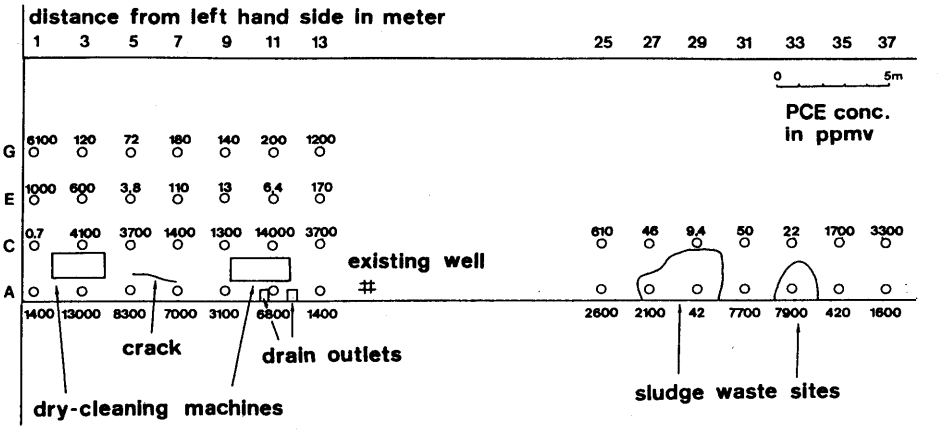

Fig. 3: Tetrachloroethylene concentration in surface soil-gas. The soil-gas was collected after the building and floor concrete had been evacuated.

REMEDIATION USING SOIL VENTING AND GROUNDWATER EXTRACTION

Site investigation and pollution extent

The study site is covered by volcano ash over 60m, overlying the impermeable clay layer. The groundwater pollution due to trichloroethylene was discovered from the domestic water supply wells. At the first stage, the surface soil-gas survey using the gas tube method and the Finger Print method developed by NERI-Petrex was provided to identify the contaminant source. Taking account of the areal distribution of vaporized trichloroethylene obtained in a firm, which had utilized trichloroethylene as solvent for many years, fourteen borings of B-1 through B-14 were achieved as shown in Fig. 4 to investigate the existing form and pollution extent of trichloroethylene (Hirata & Nakasugi, 1993). The borings revealed the trichloroethylene concentration in soil as displayed in Fig. 5, which is in the cross-section along the boring sites through B-7, B-5, B-6, B-1 to B-9. The maximum concentration in soil reaches 138mgkg^{-1} at 46.1m depth at B-6 site, and that in groundwater is raised to 131mgl^{-1} at the same site. It is clearly recognized that with respect to the soil concentration, the heavily contaminated part, the concentration of which takes around/more than 100mgkg^{-1}, remains within approximately 20m, even when the contaminant infiltrates over 50m. Such migration behavior indicates that the organochlorine in vadose zone flows down in the form of a narrow band with little spreading in the lateral direction, being consistent with the result of the column test.

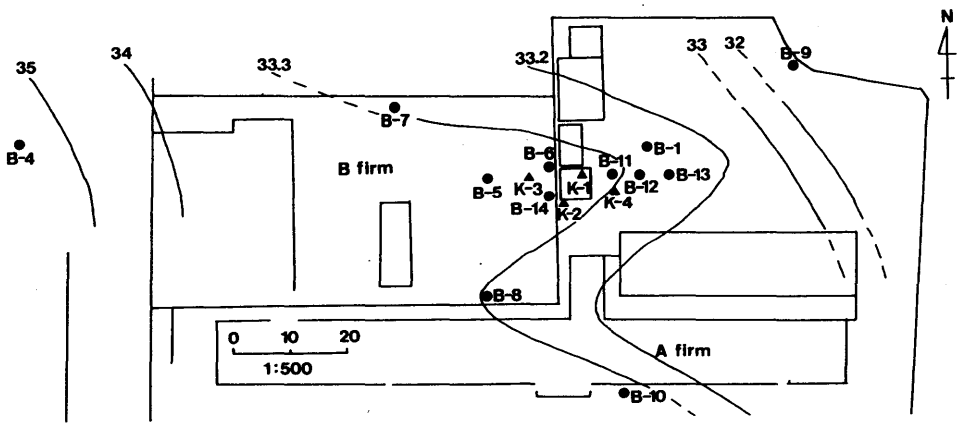

Fig. 4: Locations of borings and boreholes for remediation. The lines in the figure denote the altitude of the groundwater table from sea level. The closed circles are the locations for borings, and the triangles for the dual extraction wells.

Pilot scale remediation

The highly residual part of trichloroethylene is standing over both sides of the groundwater table, and hence the soil vapor extraction method was employed for the vadose zone remediation with pumping the groundwater up. In order to evaluate the effectiveness of both techniques four dual extraction wells K-1 through K-4, which means to remove soil-gas and groundwater at the same time, were configurated at the locations in Fig. 4. The dimensions of the wells are; the diameter is 10cm in K-1 well and 20cm in other wells, and the depth is 60m in all wells. The screen to

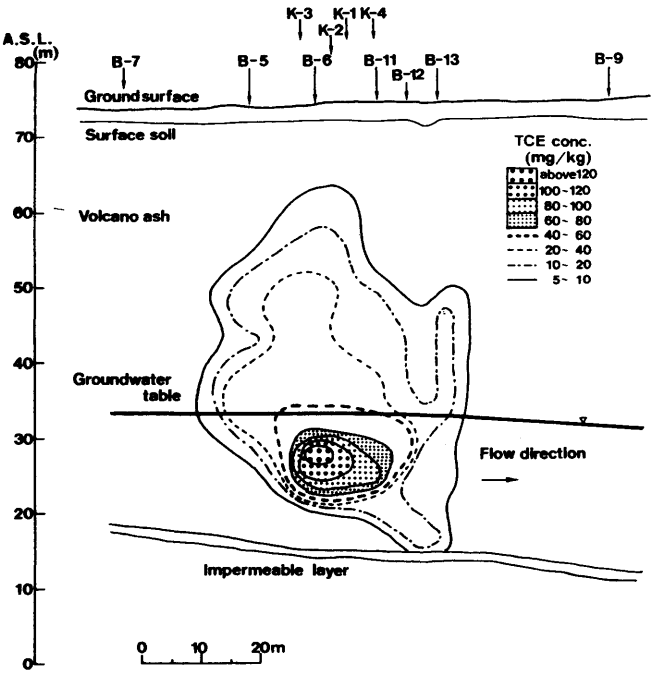

Fig. 5: Soil concentration and existing form of trichloroethylene in case of relatively deep soil/groundwater pollution incident.

take the soil-gas and groundwater was installed between GL-30m and GL-60m in each well. Since the groundwater table appears at GL-42m, the soil-gas from the vadose zone is collected from the vertical span of 12m.

The soil-gas extracted by a vacuum unit inflows first into a gas-liquid separator, and then the contaminant in the soil-gas is adsorbed to the activated carbon in two canisters. The groundwater abstracted is treated with an air stripping system, and also in this case the contaminant in the air is recovered with the carbon canister prior to the emission into atmosphere. After that the treated groundwater is discharged into the surface water or sewage system, because at present in Japan, any water containing trichloroethylene, even below the drinkable limit, is not allowed to be reinfiltrated into the subsurface environment.

In order for the soil venting to sufficiently work, the vadose pollution should be within the withdrawal reach of soil-gas migration. Then the radius of influence due to the soil vapor extraction was checked using the K-2 well and surrounding investigation wells. Fig. 6 illustrates the time-dependent changes of the depressions of the soil-gas pressure at the K-3 and B-14 wells, when the soil vapor extraction was set into motion at the K-2 well at the extraction pressure of 0.6atm. The calculation using the extraction and soil-gas depression pressures at two wells with their distances provided the radius of influence to be 10.1m between the K-2 and K-3 wells and 10.9m between the K-2 and B-14 wells, following the method presented by Johnson et al. (1990). In addition the soil-gas flowrate extracted from the well is already confirmed by Hirata & Nakasugi (1993) to rise exponentially with increasing the extraction pressure.

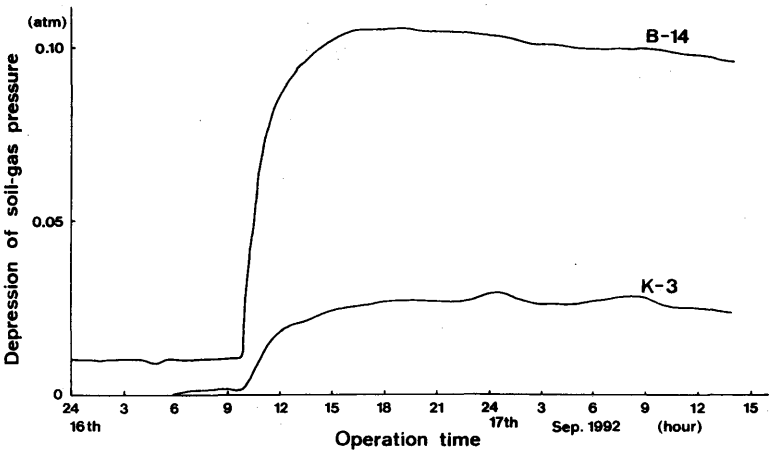

Fig. 6: Time-varied changes of the soil-gas pressure at the K-3 and B-14 wells due to the soil-gas extraction at the K-2 well. The pressure depression in the vertical coordinate is expressed as positive. The distances between the wells of K-2 and B-14 and between K-2 and K-3 are 2.82m and 6.8m respectively. The soil vapor extraction began at the time of 0855 on 17th September, setting the extraction pressure at 0.6atm.

Fig. 7 shows the time-dependent changes of the trichloroethylene concentration in the soil-gas extracted. Since the K-2 well was constructed nearly at the central part of the subsurface pollution, its vapor concentration takes the highest value among the extraction wells. All of the trichloroethylene vapor concentrations are clearly recognized to be linearly reduced with the passage of the operation time on a full-log scale. With respect to the removal rates of trichloroethylene estimated by multiplying the flowrate by the vapor concentration, they are expected to exhibit the results similar to the vapor concentrations, as illustrated in Fig. 8. This is because the soil-gas flowrate at each extraction well tends to be unchangeable through the remediation except a couple of days just after the extraction pressure is exerted. During the beginning of the remediation, the extraction pressure is propagating into the surrounding vadose zone with reducing the soil-gas flowrate, and reaches a quasi-steady state in a couple of days. In this remediation, the soil-gas flowrate at the quasi-steady state is 90 at K-1, 160 at K-2, 55 at K-3 and 330 at K-4 in the unit of liter per minute per well.

The groundwater was also pumped up to recover the contaminant from the aquifer and to offset the rise of the groundwater table due to the depression of the soil-gas pressure. The time-dependent change of the removal rate by the groundwater extraction is arranged in Fig. 9 with the total removal rate of the soil vapor extraction. The groundwater volume pumped up is subject to the capacity of the stripping treatment system, and the total volume of $2m^3hr^{-1}$ was extracted from the K-1 well at $0.5m^3hr^{-1}$and the K-4 well at $1.5m^3hr^{-1}$. At the beginning of the remediation, the removal rate of the soil vapor extraction amounts to $1.0kghr^{-1}$, which is approximately ten times as high as the groundwater extraction. The time passage for the remediation is reducing the removal rates exponentially in both techniques. In particular, the reduction of the removal rate of the soil vapor extraction nearly doubles the groundwater extraction, comparing the exponents on the full-log scale. The removal rate behavior of the groundwater extraction totally depends on the physico-chemical property of trichloroethylene to be little soluble in water (Hunt & Sitar, 1988). Such remediation characteristic results in meeting both removal rates in 15400 hours after the onset of the remediation. After that time, the groundwater extraction will be more effective technique in removing the contaminant than the soil vapor extraction.

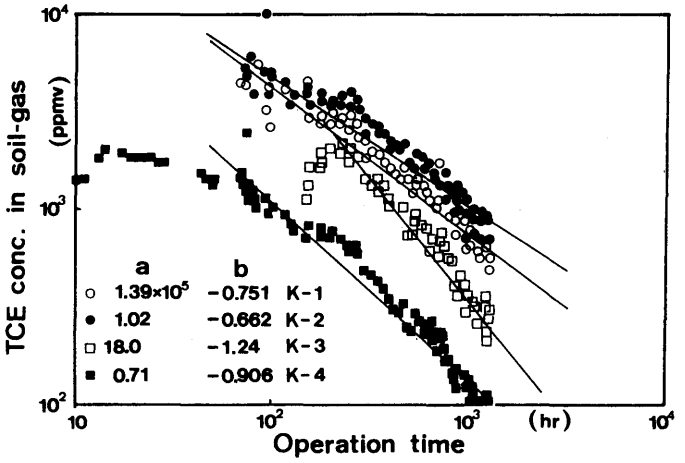

Fig. 7: Time-varied changes of the trichloroethylene (TCE) concentrations in the soil-gas extracted. The numerals of a and b in the figure are the constants, when the concentration (C) and the operation time (t) are expressed in the form of $C = at^b$.

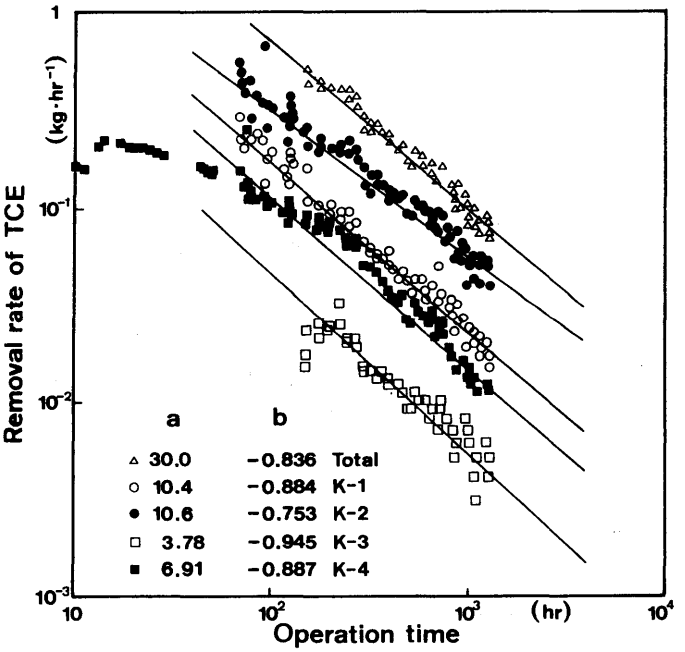

Fig. 8: Time-varied changes of the removal rates due to the soil vapor extraction. The total removal rate means the summation of four extraction wells, and the numerals of a and b are the same as in Fig. 7.

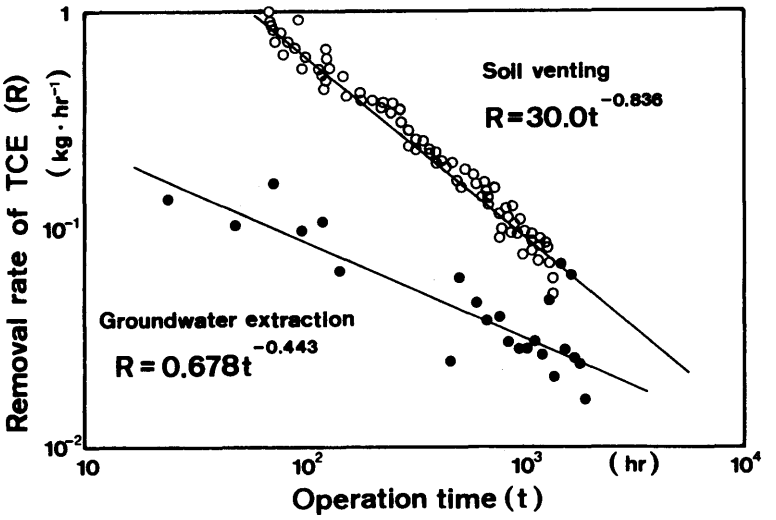

Fig. 9: Comparison of the removal rates of soil venting and groundwater extraction. The removal rate of the soil vapor extraction comprises the summation of the four dual extraction wells.

CONCLUDING REMARKS

The subsurface remediation including the site investigation is much costly, hence, the final goal is to optimize the remediation scheme and to establish the comprehensive remediation system in order to repair the subsurface environment in many sites contaminated with organochlorines. In this context the surface soil-gas survey was applied as a quick and less-expensive technology, and was substantiated to be an option of remote geochemical explorations to identify the contaminant source.

In addition, a pilot scale remediation utilizing soil vapor extraction and groundwater extraction has been undertaken in one of the study sites to evaluate the effectiveness of the technologies applied. The result indicates that at the beginning of the remediation, the soil vapor extraction is much prominent in the removal rate of contaminant at one order as high as the groundwater extraction, however, the time passage in the remediation is going to reverse the removal rates of the soil vapor extraction and the groundwater extraction. This is because the existing form and concentration of contaminant have changed in the subsurface environment with progressing the remediation. Moreover, the application of a single technique to the contaminated site is limited to reach the final goal, in which the subsurface contamination is repaired to meet the regional groundwater usages. From the cost-beneficial point of view, it is of great significance to pick the suitable techniques up or combination of techniques, and in particular to keep the flexible operation in changing remediation techniques, corresponding to the existing form of contaminant in the subsurface environment.

REFERENCES

Hirata, T. and Muraoka, K. 1988. Vertical migration of chlorinated organic compounds in porous

media. *Wat. Res.*, 22(4); 481-484.
Hirata, T., Nakasugi, O., Yoshioka, M. and Sumi, K. 1992. Groundwater pollution by volatile organochlorines in Japan and related phenomena in subsurface environment. *Wat. Sci. Tech.*, 25(7); 9-16.
Hirata, T. and Nakasugi, O. 1993. Remedial operation for subsurface pollution due to volatile organochlorine using soil ventilation and groundwater extraction. *Contaminated Soil '93*, Kluwer Academic Publisher; 1019-1028.
Hunt, J.R. and Sitar, N. 1988. Nonaqueous phase liquid transport and cleanup. 1. Analysis of mechanisms. *Wat. Resour. Res.*, 24(8); 1247-1258.
Johnson, P.C., Kemblowski, M.W. and Colthart, J.D. 1990. Quantitative analysis for the cleanup of hydrocarbon-contaminated soils by in-situ soil venting. *Ground Water*, 28(3); 413-429.
Vogel, T. M. and McCarty, P. L. 1985. Biotransformation of tetrachloroethylene to trichloroethylene, dichloroethylene, vinyl chloride, and carbon dioxide under methanogenic conditions, *Appl. Environ. Microbiol.*, 49; 1080-1083.
Yoshioka, M.,Yamasaki, T., Okuno, T., Hirata, T. and Nakasugi, O. 1992. Soil gas monitoring for survey on groundwater pollution due to volatile halogenated hydrocarbons. *J. Jpn. Soc. Wat. Environ.* 15(10); 719-725 (in Japanese).

Section 2 :

ENVIRONMENTAL GEOCHEMISTRY OF GROUNDWATER, SOIL AND SEDIMENTS

GROUNDWATER POLLUTION BY NITRATE ORGINATING FROM FERTILIZER IN KAKAMIGAHARA HEIGHTS, CENTRAL JAPAN

H. TERAO
Gifu Prefectural Institute of Public Health
6–3, Noishiki–4, Gifu 500, Japan
R. YOSHIOKA
Disaster Prev. Research Institute, Kyoto Univ.
Gokasho, Uji, Kyoto 611, Japan
K. KATO
Water Research Institute, Nagoya Univ.
Furo–cho, Chikusa, Nagoya 464–01, Japan

ABSTRACT. Kakamigahara Heights located in the central Japan is composed of low hills of 20–60m a.s.l. Under the surface soil there are virtually no clay layers in evidence, so typical unconfined aquifers are spread throughout the Heights. A nitrate increase in the groundwater was observed in the east area at the beginning of the 1970's. In 1984, from the investigation of an area in the Heights, it was elucidated that pollution was due to fertilizer scattered over vegetable fields. Six years later, in 1990 and 1991, we investigated the same area in the Heights again. A total of 282 samples of groundwater was collected from 141 locations, and their concentration of NO_3^- and other main components were measured. The results were as follows. The high concentration area of NO_3^- above $100mgl^{-1}$ still persists, and the components derived from fertilizer have spread farther toward the central area during the past 6 years. The influence of this spread on the wells for water supply in the west area has become a serious problem, and so countermeasures against pollution have started, in particular, by decreasing the amount of fertilizer used.

INTRODUCTION

High nitrate concentration in groundwater has been encountered at many locations around the world. Moody(1990) and Bel *et al.* (1989) summarized respectively the pollution cases by nitrate in the United States and in Western Europe. Kato & Ogura (1992) reported the gradual increase in nitrate in neighboring districts in Tokyo. There have been many articles on nitrate increase. Its causes are from various sources, but mainly from agricultural activities such as seepage of stock raising drainage and scattering of fertilizer.

In the east area of Kakamigahara Heights, central Japan, nitrate increase in the groundwater was observed at the beginning of the 1970's. At that time, it was thought that the pollution,

which occurred in a small limited area, would not spread further. But, in 1984, the major components of groundwater were investigated throughout the entire area in the Heights, and it was found that not only nitrate but also sulfate, calcium and magnesium ions were high, especially at several sampling locations with nitrate at above $100mgl^{-1}$. From the distribution of the fertilized area, chemical composition and pesticide detection of the groundwater, Terao *et al.* (1985) clarified that the pollution was caused by nitrogen fertilizer used on the vegetable fields in the east area.

Kakamigahara Heights has a population of over 130,000 and all the drinking water in these areas depends upon the groundwater. Therefore, the elucidation for distribution, future forecast, and pollution reduction is very important and has been investigated by researchers in different disciplines.

Water samples were collected twice in 1990 and 1991 in the Heights and nitrate and the other major components were analyzed to elucidate the present circumstances by nitrate pollution. By comparing the concentration contour maps for nitrate and the other components of July, 1990 with those of July, 1984, the variations in concentration over the 6 year period were clearly shown. These results should be very important for forecast and countermeasures against pollution in this area, and should provide various information for other cases of groundwater pollution all over the world.

METHOD

Study site

Kakamigahara Heights, located along the north border of the Nobi Plains, is composed of low hills of 20–60 m a.s.l. as shown in Figures 1 and 2. Along the south edge of the Heights, the Kiso River, a representative large river in Japan, flows from east to west and runs toward the plains. Mountainous regions, forming basement rocks under the Heights, extend in the northward and eastward directions. Under the surface soil of the Heights, stratified, thick gravel and sand layers, having a thickness of 20–80m, lie on basement rocks, with very few clay layers in evidence. Geologically, therefore, typical unconfined aquifers are spread throughout the Heights (Yokoyama & Makinouchi, 1991).

Sample collection and Measurement

Groundwater samples were collected from 141 locations in the Heights, ranging from 12km in the east–west and 6km in the north–south directions. Sampling was carried out in July, 1990 (upper water level) and January, 1991 (lower water level). Samples were collected from the wells pumped daily, whose depths ranged from 10–80m, mainly 20–40m. Collected samples were measured for major components, namely Na^+, K^+, Ca^{2+}, Mg^{2+} ions as cations, NO_3^-, Cl^-, SO_4^{2-}, HCO_3^- ions as anions, silica (SiO_2), and electric conductivity (EC). As mentioned above, the Heights is formed by thick gravel and sand layers under the surface soil, and with hardly any clay layers intercepting downward flow. Also the wide screen of the well is equipped because of thick aquifers. For these reasons, it is thought that the

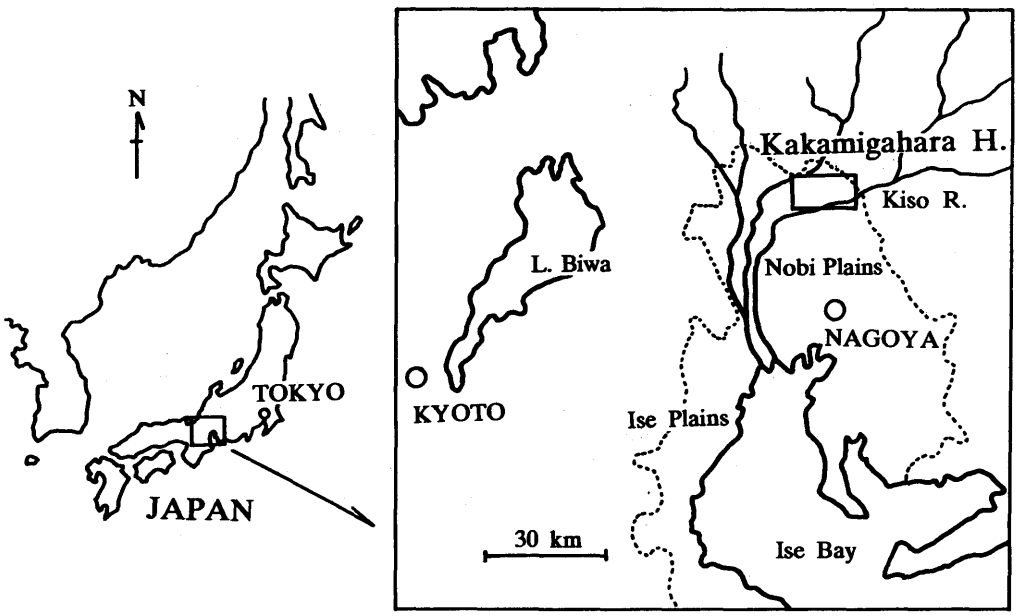

Figure 1: Map showing the Nobi Plains and location of Kakamigahara Heights.

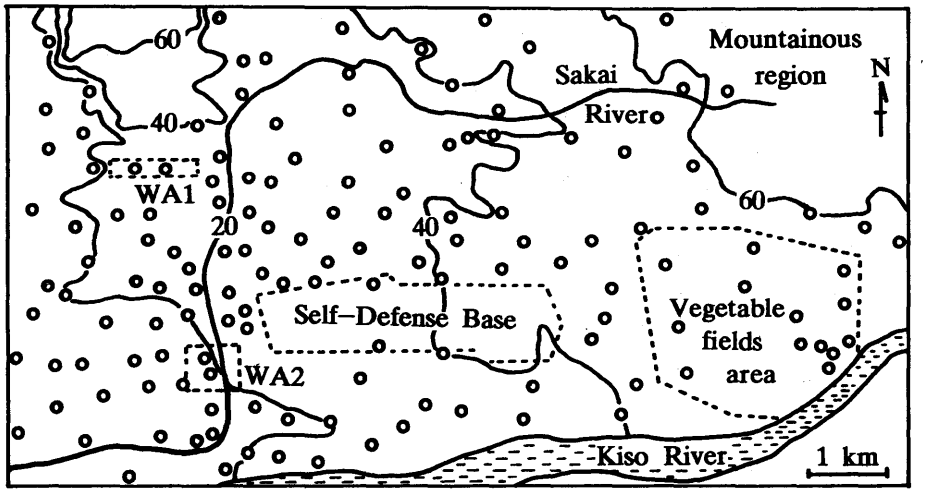

Figure 2: Map showing 141 sampling locations.
(WA1 and WA2: Well areas for water supply. Omitted contour line more than 80m a.s.l.)

difference of components in depth is not so large, and that the depth of collected wells was not a necessary consideration to discuss the results.

Concentration contour maps for NO_3^- and other major components were drawn by computer aid, based on the data of July, 1984 and July, 1991 samplings, and the changes in pollution circumstances during the 6 year period were discussed.

RESULTS AND DISCUSSION

Concentrations of major component

Table 1 shows the analytical results of major components, expressed by mean values and ranges, for samples collected from 141 locations. Compared with mean values, the difference between those in summer and those in winter were relatively small. Na^+, K^+, Mg^{2+}, NO_3^- and HCO_3^- ions and EC, indicating the sum of ionic components, were a little higher in winter; Ca^{2+}, Cl^- and SO_4^{2-} ions were lower; and nonionic component, SiO_2, had the same values. Concerning EC and NO_3^-, the ratios of the values in winter to those in summer against the individual location were calculated.

Table 1: Analytical results of the major components in groundwater samples collected from 141 locations.

		July, 1990		Jan., 1991	
		Mean	Range	Mean	Range
Na^+	($mg\,l^{-1}$)	11.8	1.5 - 24.1	13.1	1.5 - 27.4
K^+	($mg\,l^{-1}$)	3.7	1.0 - 10.4	4.0	0.8 - 11.2
Ca^{2+}	($mg\,l^{-1}$)	18.8	0.3 - 73.5	18.7	0.4 - 76.7
Mg^{2+}	($mg\,l^{-1}$)	4.1	0.4 - 15.4	4.4	0.9 - 15.0
Cl^-	($mg\,l^{-1}$)	12.4	2.1 - 36.0	12.3	2.1 - 35.6
NO_3^-	($mg\,l^{-1}$)	28.9	0.7 - 132.0	29.4	0.0 - 139.8
SO_4^{2-}	($mg\,l^{-1}$)	24.1	1.3 - 157.2	22.4	0.4 - 135.5
HCO_3^-	($mg\,l^{-1}$)	34.8	2.4 - 85.6	36.0	2.7 - 82.1
SiO_2	($mg\,l^{-1}$)	33.4	7.7 - 70.0	33.4	4.4 - 59.4
EC	($\mu S\,cm^{-1}$)	196.6	24 - 554	203.1	24 - 582

As a result, locations which showed the ratios ranging from 0.9–1.1 amounted to 86.5% for EC and 55.3% for NO_3^-. Consequently, it is thought that seasonal variations in major components were not so large. In the Heights, the routine observation for groundwater level and NO_3^- concentration at several locations has been done by the municipal office, but little seasonal variation in concentration was observed except for shallow wells less than 10m in depth. The cause of the low percentage in NO_3^- than EC was owing to the wide variations

of low concentration wells such as those below $10mgl^{-1}$.

Key diagram

Figure 3 shows the key diagram for representing characteristics of the major components. The key diagram was drawn based on the results of groundwater samples collected from 141 locations in July, 1990. Many of the locations belonged to the section in which both $Ca^{2+}+Mg^{2+}$ as cation and $NO_3^-+Cl^-+SO_4^{2-}$ as anion were above 50%. This result indicates that the polluted groundwater, differing from the common composition represented by Na–HCO_3 or Ca–HCO_3 type, had spread over the Heights, and that the influence of fertilizer extended far beyond the east area.

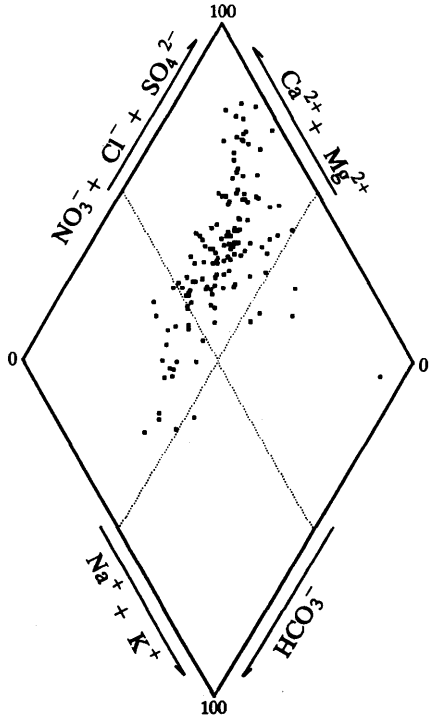

Figure 3: Key Diagram of the major components drawn from 141 samples in July, 1990.

Correlationship

Table 2 is the correlation matrix table of major components was prepared from the results of the July, 1990 sampling. The components that correlated highly with NO_3^- were Ca^{2+} and Mg^{2+} ions, and their correlation coefficient were 0.76 in both cases. This would suggest that magnesia–lime fertilizer for soil improvement was scattered together with nitrogen fertilizer

in the same area.

There was lower correlation between NO_3^- and SO_4^{2-} (0.58), though the main component in nitrogen fertilizer is ammonium sulfate, $(NH_4)_2SO_4$ as chemical form. NH_4^+ transforms into NO_3^- in the surface soil easily, and transfers from soil to aquifer together with SO_4^{2-}. The ratio of S/N in ammonium sulfate is 1.14, but that in the groundwater of vegetable fields ranged widely from 0.5–2.6 because of the differences in nitrogen absorption by plants depending on the location.

Correlation coefficients of Ca^{2+}, and Mg^{2+} with SO_4^{2-} were 0.88 and 0.83, respectively. On the other hand, those with HCO_3^- were 0.23 and 0.10, respectively. These results suggest that Ca^{2+} and Mg^{2+} in the groundwater is not dissolved out from soil or rock by CO_2, but were the effects of scattered fertilizer.

Table 2: Correlation matrix table of the major components calculated from 141 samples obtained in July, 1990.

Na^+	*									
K^+	0.35	*								
Ca^{2+}	0.50	0.22	*							
Mg^{2+}	0.42	0.22	0.87	*						
Cl^-	0.78	0.48	0.58	0.56	*					
NO_3^-	0.40	0.37	0.76	0.76	0.62	*				
SO_4^{2-}	0.46	0.16	0.88	0.83	0.46	0.58	*			
HCO_3^-	0.24	-0.15	0.23	0.10	-0.05	-0.30	0.08	*		
SiO_2	0.16	0.13	0.16	0.16	0.08	0.12	-0.08	0.42	*	
EC	0.65	0.34	0.97	0.90	0.72	0.83	0.86	0.14	0.16	*
	Na^+	K^+	Ca^{2+}	Mg^{2+}	Cl^-	NO_3^-	SO_4^{2-}	HCO_3^-	SiO_2	EC

Comparison of concentration contour maps

Nitrate: During the 6 year period, the mean NO_3^- concentration increased from 25.4 to 28.9mgl^{-1}, and the pollution showed a tendency to expand over the Heights. Compared

individually with 106 locations sampled twice, the concentration decreased in only 22 locations. The 12 locations above 50mgl^{-1} in 1984 exceeded that level again after 6 years, and 5 more locations were newly above 50mgl^{-1}.

Concentration contour maps of NO_3^- are shown in Figure 4. In the east area where fertilizer was scattered repeatedly, the area above 80mgl^{-1} did not change distinctly. On the contrary, in the central and west areas, the total area above 20mgl^{-1} expanded. This result suggests that the groundwater having a long-residence time in the east area, the one with highest

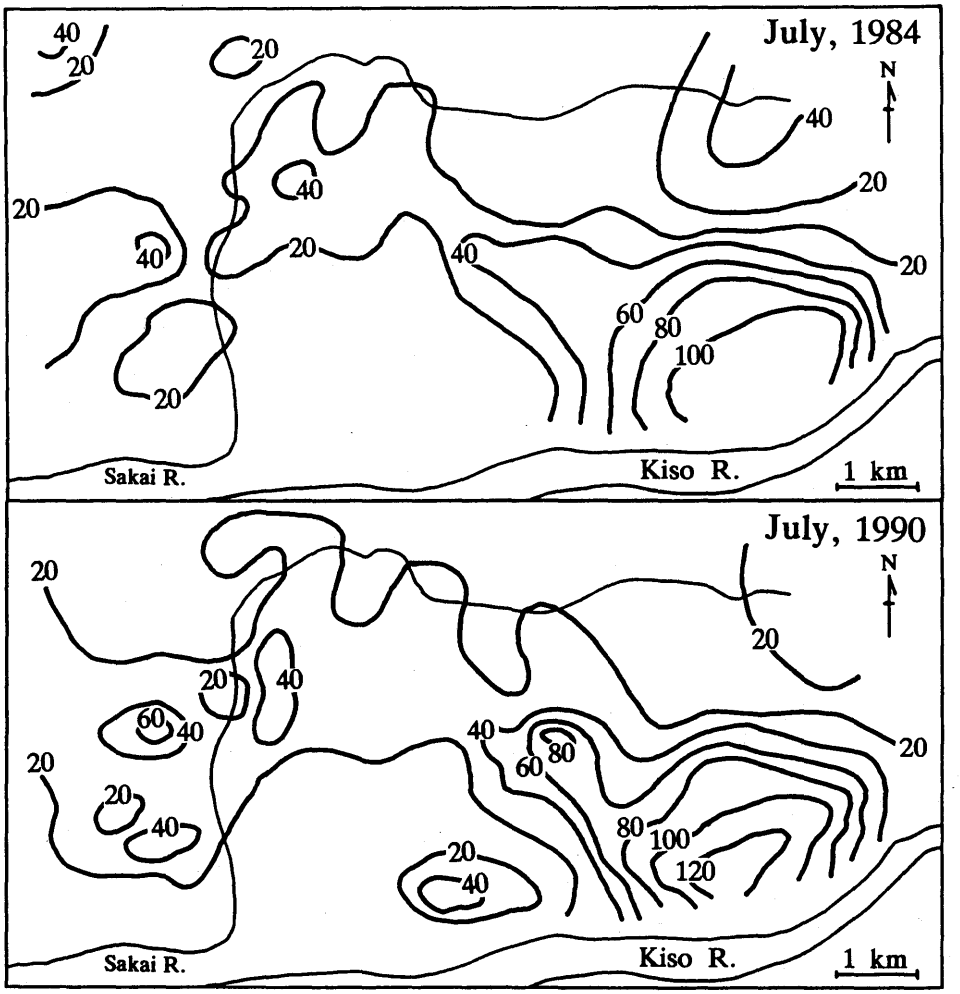

Figure 4: Comparison of NO_3^- concentration contour maps. (unit: mgl^{-1})

concentration, flows downward toward the direction of the west-northwest and west-southwest. This finding also is consistent with the investigation of the underground structure, groundwater level and recharge source.

The field area for carrot cultivation in the Heights has hardly changed for 10 years, and it was elucidated that the groundwater had not been recharged from the Kiso River by means of stable isotopic compositions. From these reasons, it was concluded that the pollution has continued for a long term and has had a stronger effect toward the central and west areas.

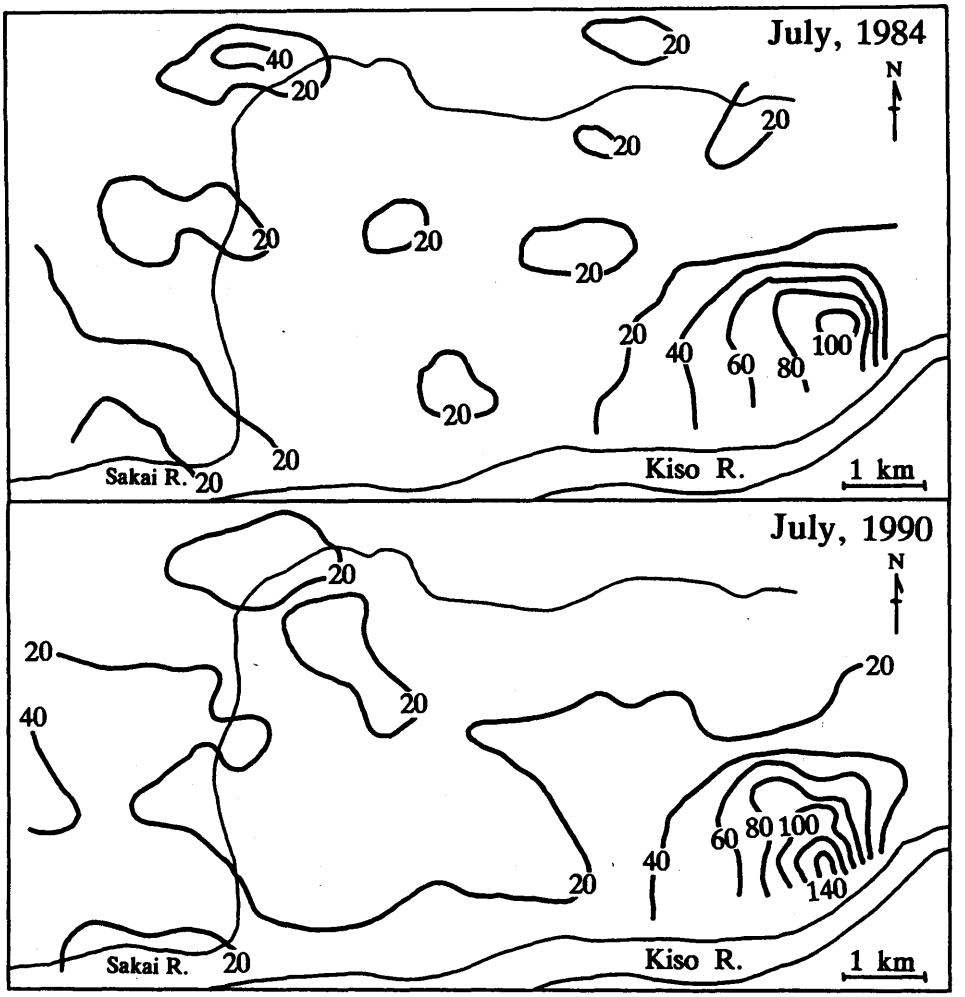

Figure 5: Comparison of SO_4^{2-} concentration contour maps. (unit: mgl^{-1})

Sulfate: Concentration contour maps of SO_4^{2-} are shown in Figure 5. SO_4^{2-} had as high a concentration as NO_3^- in the east area because it is one of the major components in fertilizer, and areas above $100mgl^{-1}$ were observed in both 1984 and 1990. In 1990, the $20mgl^{-1}$ line extended toward the central area, and the area above $20mgl^{-1}$ expanded during the 6 year period. This result was similar to that of NO_3^-.

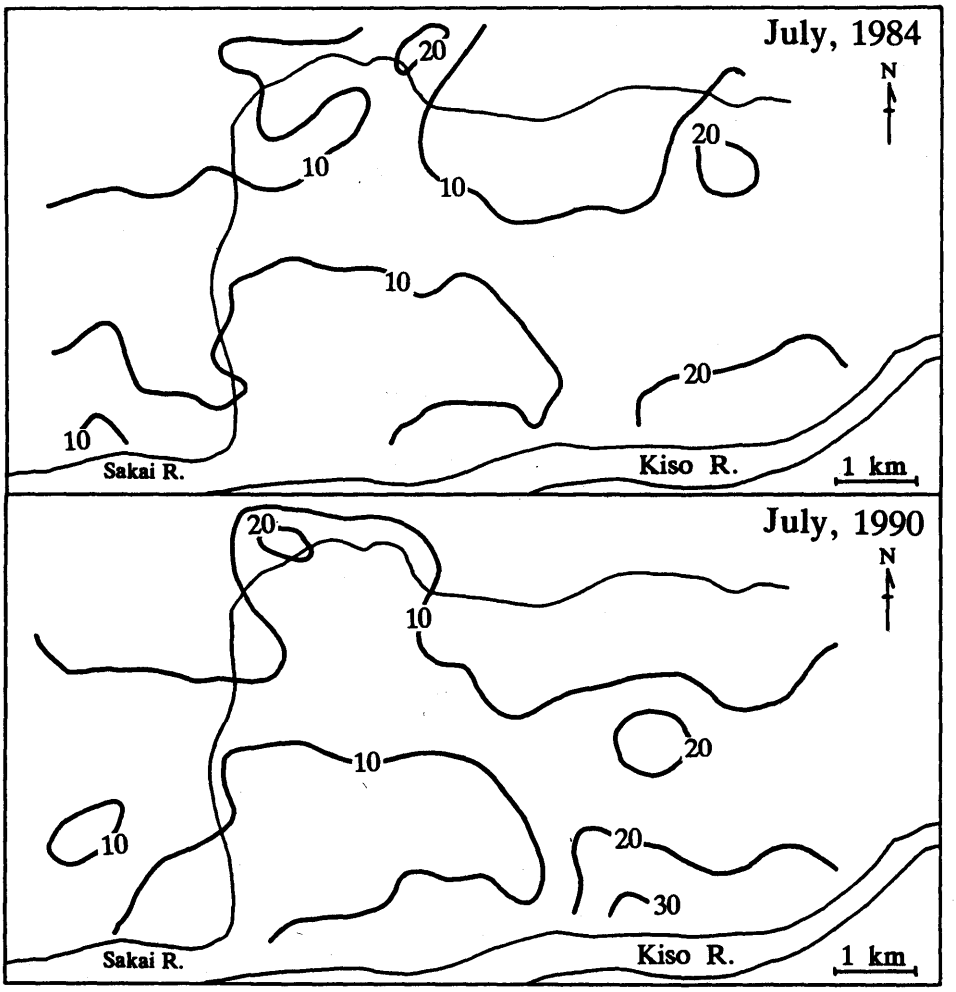

Figure 6: Comparison of Cl^- concentration contour maps. (unit: mgl^{-1})

Ca^{2+} and Mg^{2+} are also the main components in fertilizer, so that maps of these ions were closely similar to those of SO_4^{2-} and NO_3^-.

Chloride: Concentration contour maps of Cl^- are shown in Figure 6. Different from NO_3^- and SO_4^{2-}, the concentration elevation of Cl^- in the east area was barely observed, and only 10 locations were above $20mgl^{-1}$ in July, 1990. These results agree with the fact that Cl^- is hardly scattered as fertilizer. Also it is suggested that domestic waste water hardly affects the groundwater over the Heights.

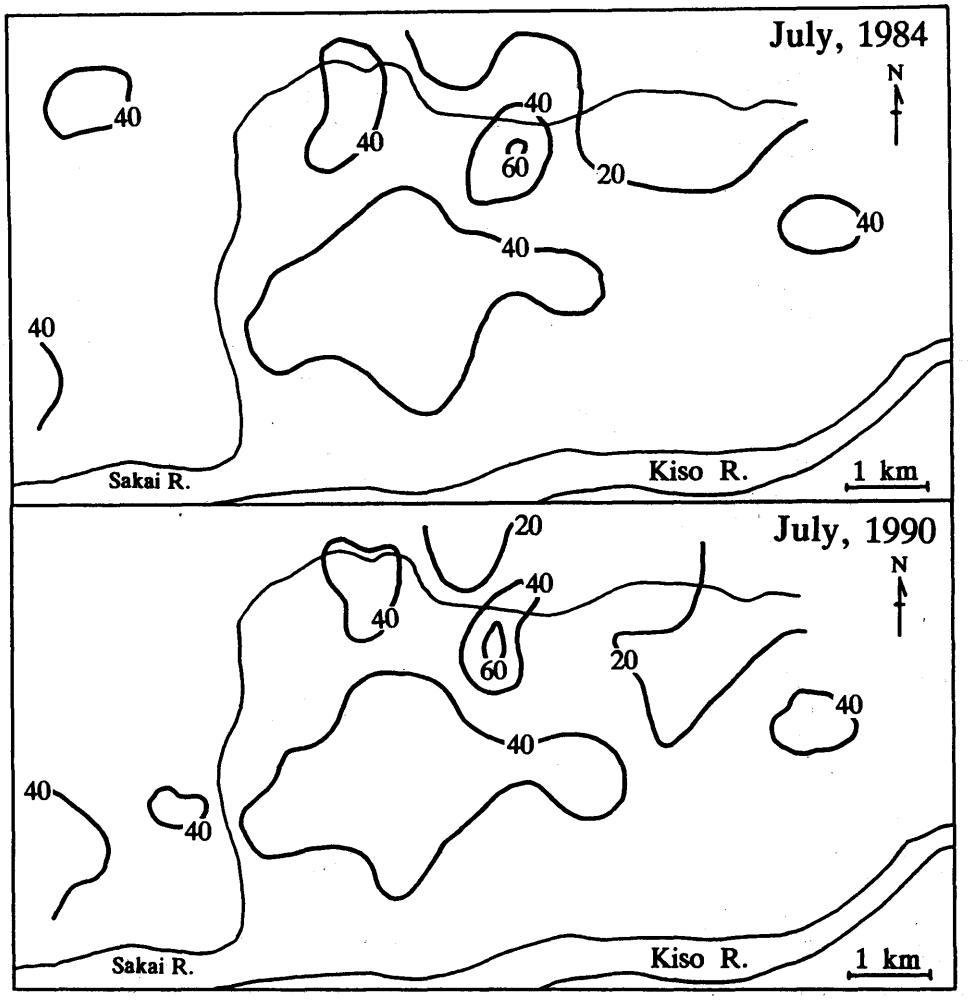

Figure 7: Comparison of SiO_2 concentration contour maps. (unit: mgl^{-1})

Na^+ showed closely similar patterns to Cl^-, with only 3 locations being above $20mgl^{-1}$ over the Heights in July, 1990.

Silica: With regard to SiO_2, as shown in Figure 7, there was hardly any change during the 6 year period except for the locations near the north mountainous region. SiO_2 in groundwater should be supplied by the interaction between water and soil, and not generally affected by human activities. This result suggests that during period examined the groundwater quality was essentially unchanged except for pollutants.

It is characteristic that the concentrations of SiO_2 as well as Cl^- show different patterns from results of pollution-derived components such as NO_3^- and SO_4^{2-}. This confirms that almost all of NO_3^- and SO_4^{2-} were derived from fertilizer.

Countermeasures and forecast

In Kakamigahara Heights, investigations on agriculture discipline such as gradual decrease of fertilizer have been done by agricultural scientists together with chemists and geologists.

By means of investigations using experimental vegetable fields, it should be possible to decrease considerably the amount of fertilizer scattered without decrease in carrot yield or deterioration of quality. The amount of fertilizer for carrot cultivation in this area was above $300kgha^{-1}year^{-1}$ as nitrogen before 1978, and a deterioration by its excess use was observed. Later, recommended amounts decreased to about $220kgha^{-1}year^{-1}$ from 1979, and further to $170kgha^{-1}year^{-1}$ in 1990.

Removal of pollutants which have permeated and are diffused in the aquifer will be accomplished only with difficulty and over an extremely long period of time. So the decrease of the quantity of fertilizer scattered would be unavoidable to reduce groundwater pollution. The effect of fertilizer decrease had not yet appeared as of 1991 in Kakamigahara Heights, but any reduction of pollution would show gradual improvement if observed over a long period of time. As mentioned above, all of the drinking water in Kakamigahara Heights depends on groundwater. Before the wells for water supply in the west area are affected, further acceleration of pollution should be prevented.

ACKNOWLEDGEMENT

We thank the members of Kakamigahara Groundwater Research Group for their helpful suggestions.

REFERENCES

Bel, O., Duynisveld, W. H. M. & Boettcher, J. 1989. Nitrate pollution of groundwater in Western Europe. *Agri. Ecosyst. Environ.*, 26; 189–214.

Kato, H. & Ogura, N. 1992. Nitrate nitrogen in ground waters in the Kitatama area of Tokyo. *Japan J. Limnol.*, 53; 265–272.

Moody, D.W. 1990. Groundwater contamination in the United States. *J. Soil and Water Conservation*, 42; 243–248.

Terao, H., Kajikawa, M., Morishita, Y. & Kato, K. 1985. Influence of pesticide and fertilizer on the ground water in vegetable field zone. *Chikyukagaku (Geochemistry)*, 19; 31–38.

Yokoyama, T. & Makinouchi, T. 1991. Geology of the Kakamigahara Terrace and underlying groundwater basin, Gifu Prefecture, central Japan. *J. Geol. Soc. Japan*, 97; 887–901.

SULFUR ISOTOPES IN A ROOF COVERED FORESTED CATCHMENT AT LAKE GÅRDSJÖN, WESTERN SWEDEN

C-M. MÖRTH & P. TORSSANDER
Dept. of Geology and Geochemistry, Stockholm University,
S-106 91 Stockholm, Sweden

ABSTRACT. The reversibility in acidification is investigated in a whole catchment manipulation experiment at Lake Gårdsjön on the Swedish west coast. A roof has been built over a forested catchment and water of pristine composition is sprinkled under the roof. Sulfur isotope ratios have been determined in bulk deposition, throughfall, runoff, groundwater and lysimeter water during one year before and one year during the roof experiment. The $\delta^{34}S$ values of the deposition are almost identical for bulk deposition (+7.4‰) and throughfall (+8.0‰) and higher than $\delta^{34}S$ in runoff (+5.4‰). Two sources of sulfur in the atmospheric deposition are identified: anthropogenic sulfur and sea water spray. Sea water sulfur is added in the sprinkler water and the sprinkler water has a $\delta^{34}S$ value of +19.5‰. Measured $\delta^{34}S$ values in the area the year before the sprinkling started suggest that the old sulfur sulfate pool has a $\delta^{34}S$ value of +5.4‰. The change the first year of sprinkling in the $\delta^{34}S$ values in the runoff is a small increase, only 0.4‰. Simultaneously the sulfate concentration has gone down by 15%. Mass balance calculations suggest that the sulfate in runoff consist of a mix of about 25% sprinkler water and 75% old sulfur coming from within the area. This is contradicted by the sulfur isotope composition in sulfates that suggest that all sulfur that is coming out from the area is old sulfur. Retention times for sulfur in this soil is therefore suggested to be longer than mass balance calculations suggest.

INTRODUCTION

Large areas in Europe and North America are affected by acid atmospheric deposition. Sulfate is the predominant anion associated with acid rain. Emissions of sulfur have decreased by 20 - 30% in Europe and 65% in Sweden during the last ten-year period. No change in sulfate concentration and deposition over Sweden is recorded during the same period. At Lake Gårdsjön in western Sweden (Fig. 1) has a whole scale catchment manipulation experiment been undertaken to investigate the effects of the decrease in atmospheric deposition of sulfur, nitrogen and mercury. This is made by building a roof that covers the catchment. A major question has been if the decrease in acid deposition will result in recovery of the ecosystems and reversibility concerning water chemistry in acidification. If so, how long will it take before recovery is seen in the runoff water, i.e., normal pH values and a balance in input and output for sulfate and other ions. To compensate for anions that have an anthropogenic origin in runoff, excess base cations are released and the recovery is therefore dependent on a reduction in sulfate release down to a level were weathering alone can contribute the base cations.

The Lake Gårdsjön became chronically acidified in the late 60´s, lake monitoring started in 1970,

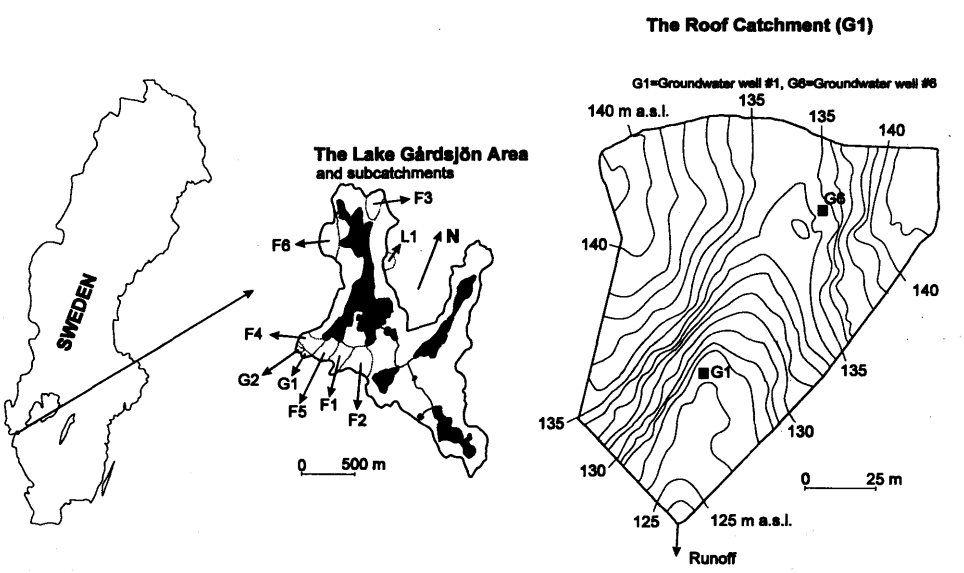

Figure 1: Maps showing the location of Lake Gårdsjön, the Lake Gårdsjön area and the roof catchment, G1.

catchment investigations started in 1979 and whole catchment manipulation experiments in 1984 (Andersson & Olsson, 1985; Hultberg & Grennfelt, 1992). One catchment, F1, has been used as a reference catchment since 1979 for more than 10 sub catchments, which are and have been dealing with different investigations and experiments (Hultberg & Grennfelt, 1992). Several of these experiments have dealt with sulfur flux dynamics. The results from these experiments have suggested that the retention time for sulfur in Lake Gårdsjön soils is short. Sodium sulfate was spread in one area in 1985 and after three years almost all sulfur added (95%) could be accounted for in runoff by mass balance calculations. Other evidence for short retention times is clearfelling of a catchment that immediately gave a response in sulfate in runoff corresponding to open field collector deposition.

Many sulfur isotope investigations of natural and anthropogenic sulfur in the environment have been published (Krouse & Grinenko, 1991). Most of these studies have applied sulfur isotope ratios to fingerprint natural and anthropogenic derived sulfur or to trace geochemical processes in the atmosphere, hydrosphere and biosphere (Caron et al., 1986; Castleman et al., 1973; Krouse and Van Everdingen, 1984; Mitzutani & Rafter, 1969; Nriagu & Coker, 1983; Saltzman et al., 1983; Trembaczowski, 1991; Winner et al., 1978). Relatively few sulfur isotope studies have been made concerning sulfur dynamics in soils (Fuller et al., 1986; Krouse & Case, 1981; Krouse & Tabatabai, 1986; Van Stempoort et al., 1990; 1992). No attempt has so far been made to apply stable sulfur isotope ratios in a whole catchment manipulation experiment using sulfur with a known isotopic composition as a tracer apart from this work. The aim of this study is to determine the source of sulfur in the deposition and to investigate the sulfur flux and retention time within

the catchment. This paper reports the results obtained from the first year of the experiment as well as a one pre experimental year cycle of bulk deposition, throughfall, runoff, groundwater and lysimeter water in the catchment.

SITE DESCRIPTION

The roof catchment, G1, covers a well-defined drainage area that is situated around 110 - 170m above sea level (Hultberg et al., in press). Highest coast line has been determined to be 130m above recent sea level. Granite and gneiss are the bedrock found in the area (Olsson et al., 1985). Soil depth in G1 is on average 40cm and consists of till of local origin. Peat areas can be found in the lower regions of the Lake Gårdsjön area but is lacking in G1. Due to the closeness to the coast a maritime climate prevails and small variations in monthly mean temperatures are measured. Snow never covers the area for longer periods. Maximum precipitation is seen in late autumn and winter. Annual precipitation is 1198mm, annual throughfall 730mm, annual evapotranspiration 596mm and annual runoff 602mm. These are mean values for the period 1979 - 1990. In the Lake Gårdsjön area mature Norway spruce is the dominating tree.

The roof has an area of 6300m^2, about 2 - 4m above the ground. Holes have been made in the roof to fit approximately 370 tree trunks. Small v-shaped dams have been placed around the holes so that runoff water from the roof is not included in stemflow. Small amounts of stemflow still reach the ground but mass balance measurements have shown that this is at very low levels for all elements (F. Moldan, pers. comm.). Throughfall water that reaches the roof is collected and analyzed. Needles that fall on the roof are collected and dried and are spread over the area by hand.

A small amount of sea water and KCl is added to deionized lake water from Lake Gårdsjön. This water is spread under the roof with the aid of a sprinkler system (275 sprinklers) that has a capacity of three mm/h. Chemically the water that is now added to G1 is very different from the present throughfall water. No N-compounds are found in the sprinkler water and of course it has much lower concentrations of sulfur. The reduction in sulfur deposition under the roof is about 50%.

METHODS

Sampling

The sampling in the Lake Gårdsjön area started 14 months (February 1990) before the sprinkling started under the roof in April 1991. Two catchments are sampled in the area: the roof catchment G1 and for comparison the reference catchment F1. Samples have been taken from runoff, groundwater, lysimeter waters, throughfall and bulk deposition (open field collectors). Sampling has been performed very intensively, sometimes on a weekly basis, during a two and a half year period. Runoff water has been collected in two ways; At first a specific volume collected at some predetermined intervals; Nowadays there is an automatic sampling during a certain period (for the moment two weeks) that is proportional to the runoff. Lysimeter water is collected on a monthly basis at different depths, 20cm, 40cm and 70cm, by under pressure lysimeters. All the

waters are sampled and stored in 2L polyethylene bottles and filtered with 0.45 µm membrane filters before processing.

Analytical techniques

Chemical analyses Analyses have been made for sodium, chloride and sulfate concentrations. Sodium analyses have been performed with ICP-AES and cation chromatography. Chloride and sulfate have been analyzed with anion chromatography.

Isotopic analyses Sulfate in water is converted to $BaSO_4$ for the isotopic analyses. An ion exchange system modified from Nearing et al. (1977) and Hesslein et al.(1988) have been used to pre concentrate sulfate and to ensure purely precipitates of $BaSO_4$. The setup is described in Andersson et al. (1992). Sulfate in water is ion exchanged with a strong basic anion exchange resin (Dowex 1-X8), 20 - 50 mesh, and is eluated with 200ml 0.5M NaCl. HCl is then added to adjust the pH to about two. Samples are boiled for one minute and after that $BaCl_2$ is added to precipitate the sulfate as $BaSO_4$. Precipitates are heated on a water bath, approximately 90°C, for 2h. The $BaSO_4$ is collected on a 0.4µm membrane filter and washed with distilled water. This is followed with drying of the filter at 75°C for 24h. Filters with the precipitated $BaSO_4$ are then weighted and scraped to collect the $BaSO_4$. If less than 20mg of $BaSO_4$ is weighted, the filter is burned at 600°C to collect all the $BaSO_4$. Ten mg of $BaSO_4$ is mixed with 200 mg of V_2O_5 and SiO_2

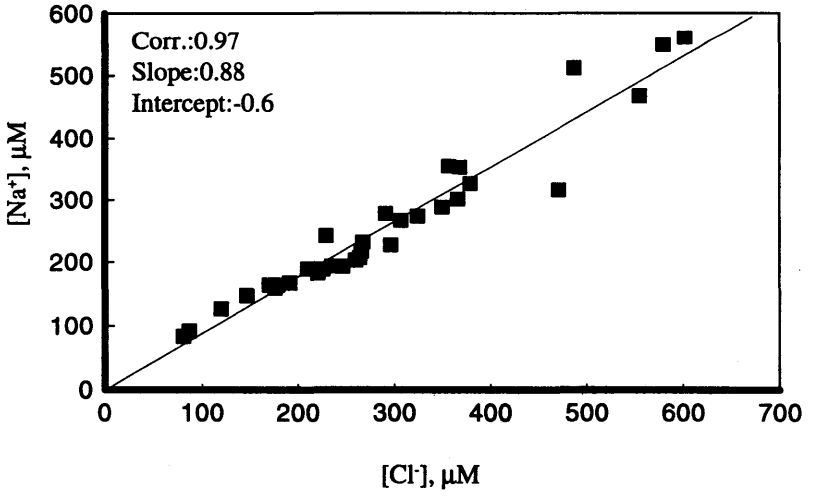

Figure 2: Sodium concentration versus chloride concentration in bulk deposition and throughfall.

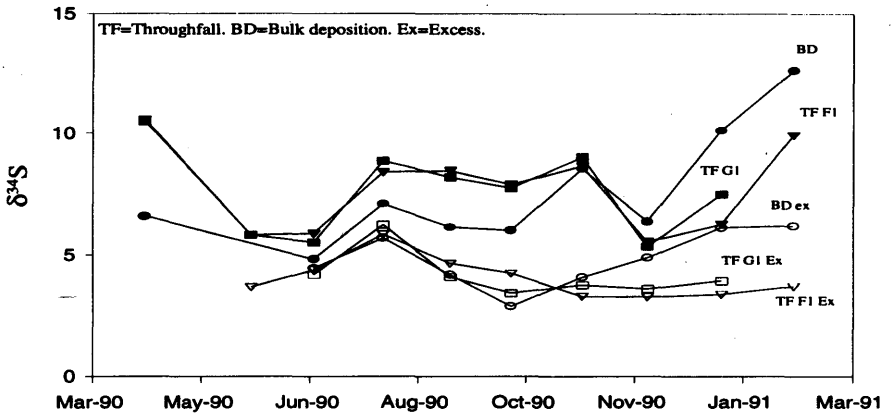

Figure 3: The sulfur isotope composition of sulfate in bulk deposition in catchments G1 and F1 through time. Ex=Excess and refers to the antrophogenic sulfur isotope composition.

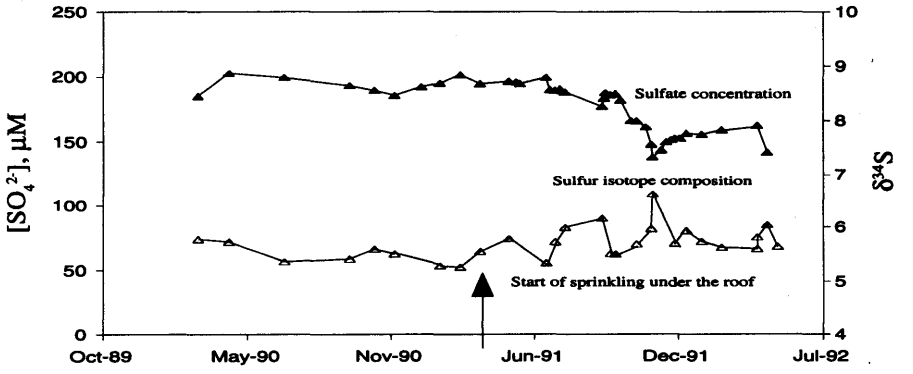

Figure 4: Sulfate concentration, chloride concentration and the sulfur isotope composition in sulfate in runoff through time.

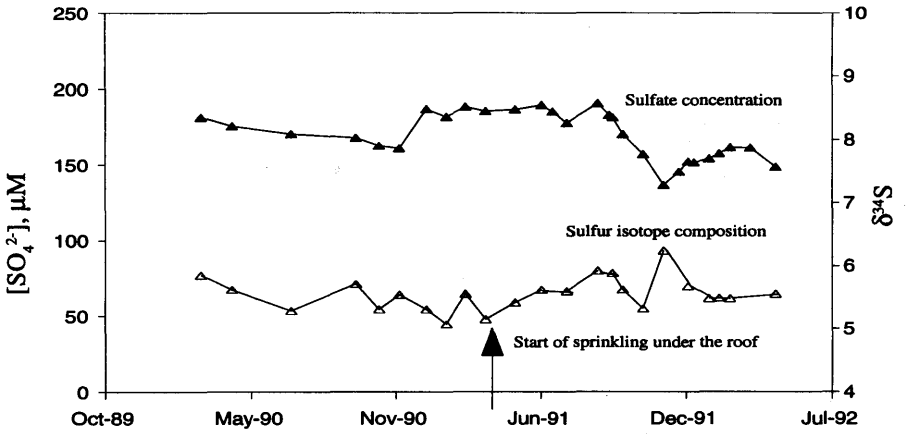

Figure 5: Sulfate concentration, chloride concentration and the sulfur isotope composition in sulfate in groundwater well #1 through time.

and burned at 950°C in a vacuum line (Yanagisawa & Sakai, 1983). The formed SO_2 is collected in small glass ampoules and later analyzed for its sulfur isotope composition with a modernized and rebuilt Micromass 602 mass spectrometer at the Laboratory of Isotope Geology of the Naturhistoriska riksmuseet in Stockholm.

The sulfur isotope composition is defined as a deviation in ‰ of the ratio $^{34}S/^{32}S$ between a sample and a standard, expressed in the conventional $\delta^{34}S$ notation relative to Cañon Diablo Troilite (CDT). The accuracy in the measurements is for all samples better than ± 0.2‰ but generally around ± 0.1‰.

RESULTS

Deposition

The sodium and chloride concentration in bulk deposition and throughfall varies from 80 - 500µM and from 80-600µM respectively. Fig 2 shows how well the Na and Cl concentrations correlate (r=0.97), with a slope of 0.89 very close to the Na/Cl ratio in sea water of 0.86 (based on Berner, 1971, Cl=550mM and Na=475mM).

Sulfur isotope composition of bulk deposition and throughfall is plotted in Fig 3, where some co-

Table 1: Mean values for $\delta^{34}S$ of sulfate and the sulfate concentration in G1. (pre=before roof, post=after roof). Concentrations in µM.

Type of sample	Pre $\delta^{34}S$	Post $\delta^{34}S$	% change	Pre Conc.	Post Conc.	% change
Runoff	5.4	5.8	+7	195	165	-15
Groundwater:						
well #1	5.4	5.6	+4	176	167	-5
well #6	5.9	5.9	0	218	171	-22
Lysimeter:						
20 cm	6.1	5.9	-3	169	182	+8
40 cm	6.0	5.9	-2	206	195	-5
70 cm	5.7	5.9	+3	218	200	-8
Throughfall	8.0			60		
Bulk deposition	7.4			26		
Sprinkler water		19.5			29	

variation can be seen. If weighted mean values are calculated for the period the $\delta^{34}S$ values are very similar between bulk deposition and throughfall, +7.4‰ and +8.0‰ respectively.

Calculated anthropogenic $\delta^{34}S$ values by calculating excess sulfur using Na as a conservative element and then assign the marine sulfur a $\delta^{34}S$ of +20.3‰ (from measurement of Kattegatte water, which is preferentially used instead of Rees et al.'s (1978) global average $\delta^{34}S$ = +20.99‰) is very similar for bulk deposition and throughfall: The weighted mean average $\delta^{34}S$ is +4.9‰ and +4.7‰ respectively. A close resemblance can be seen between throughfall data in the G1 and the F1 area (Fig 3). It can be concluded that the F1 area is good reference catchment area when it comes to $\delta^{34}S$ values in throughfall. Seasonal variation in the $\delta^{34}S$ values in bulk deposition has been reported from other investigations (Andersson et al., 1992; Caron et al. 1986; Nriagu & Coker, 1978) but cannot be seen at lake Gårdsjön, whether the marine input is subtracted from $\delta^{34}S$ by excess sulfate calculation.

Runoff and groundwater

Sulfate concentration and sulfur isotope composition in runoff (Fig. 4) and groundwater well #1 (Fig. 5) show close resemblance both before (pre roof) and after the roof was built (post roof). The pre roof weighted mean average $\delta^{34}S$ of 5.4‰ in runoff is also identical to the pre roof mean $\delta^{34}S$ of well #1 (Table 1). The results from the first post roof year are of course influenced by the composition of the sprinkler water. It has a sulfate concentration of 29µM and a $\delta^{34}S$ value of +19.5‰ (a small amount of Kattegatte sea water with $\delta^{34}S$ = +20.3‰ is mixed with deionized lake

water). For the first year of sprinkling only a minor change in the $\delta^{34}S$ values (increase +0.4‰) has been seen in runoff but the sulfate concentration has decreased by 15%. This value is a weighted mean for the first year of sprinkling. Single runoff events at the end of the first year show 30% decreases, corresponding to small increases in the $\delta^{34}S$ values (Fig. 4). In the groundwater the same trend is seen, small changes in the $\delta^{34}S$ values and a decrease in the sulfate concentration. Groundwater well #6 has slightly higher $\delta^{34}S$ values than groundwater well #1 and the runoff (Table 1). Lysimeter $\delta^{34}S$ values are also higher and upon comparison with the other waters they show some conflicting results, but the measurements are relatively few.

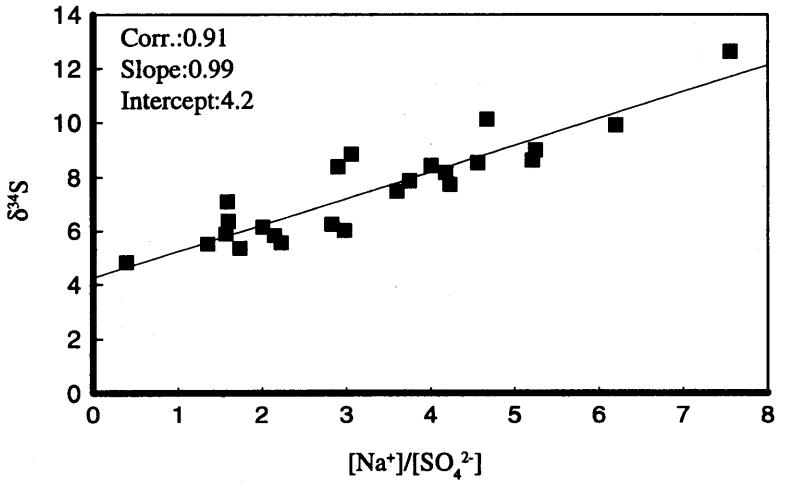

Figure 6: Plot between the sulfur isotope composition in sulfate and the sodium/sulfate ratio in throughfall and bulk deposition.

DISCUSSION

Deposition

The correlation between sodium and chloride concentration suggests the origin of Na and Cl are from sea spray. In fact, Na and Cl are the dominant ions in the runoff from the catchments in the area due to the location close to the sea (Hultberg & Grennfelt, 1992). It is implicated that Na and Cl will give very similar excess sulfur values.

Sulfur deposition to the Lake Gårdsjön area is best described as a mixing between a sea water source and anthropogenic sources. This is clearly seen in Fig. 6, $\delta^{34}S$ vs. the Na/SO_4 ratio. The regression line gives a $\delta^{34}S$ value of +20.6‰ for the sea water Na/SO_4 ratio (16.57). The anthropogenic end member is at the intercept with a $\delta^{34}S$ value around +4.2‰ in relatively good agreement with the mean excess $\delta^{34}S$ values (Table 1).

If it is assumed that the $\delta^{34}S$ values in wet and dry deposition is different; Then the very similar $\delta^{34}S$ values in bulk deposition and throughfall could suggest that the proportion between dry deposition and wet deposition is almost the same in bulk deposition and throughfall. The mass of sulfur deposited differs. These results also suggest that the internal circulation of sulfur in trees is small, previously suggested in the Lake Mjösjön study in Sweden (Andersson et al., 1992) and shown with sulfur-35 studies in throughfall. Less than 10% of the sulfur in these sulfur-35 studies was internally circulated sulfur (Lindberg & Garten, 1988). The field results at Lake Gårdsjön also imply that internally circulated sulfur is a quick process, a short time between uptake and exudation. This was also shown with the sulfur-35 study by Lindberg & Garten, 1988, which was made during three months period. A close resemblance can be seen between throughfall data in the G1 catchment and the F1 catchment (Fig 2). It can be concluded that the F1 area is good reference catchment area when it comes to $\delta^{34}S$ values in throughfall.

It has been suggested that the seasonal variation is a result of different reaction pathways in the atmosphere during winter and summer. The homogeneous gas phase reaction will dominate during summer giving a kinetic isotope effect (Saltzman et al., 1983) and lower $\delta^{34}S$ values. The heterogeneous reaction will dominate during winter and give a temperature dependent equilibrium fractionation (Eriksen, 1972), α=1.0109 at 25°C, when dissolving SO_2 in water and a small kinetic isotope effect (Saltzman et al. 1983), α=0.996, when oxidizing sulfite to sulfate in water and higher $\delta^{34}S$ values. An explanation to the lack of a seasonal variation at Lake Gårdsjön is that a reservoir effect is seen, a large proportion of the sulfur is oxidized before it is deposited. If the fraction between homogeneous and heterogeneous oxidation is the same over the year a small variation in temperature will give a small variation in the fractionation factor. The observed then are a small variation in the $\delta^{34}S$ values in the formed sulfate. In the Lake Mjösjön study the local temperature showed a correlation with the $\delta^{34}S$ values in the bulk deposition (Andersson et al., 1992). However, in the Lake Mjösjön area in central Sweden wet deposition dominates (dry deposition could account for some 10-20% of the total deposition) while estimates for dry deposition in Lake Gårdsjön is around 50%.

Runoff and groundwater

Hultberg & Grennfelt (1992) has shown that Na, Cl and S have been in balance at reference catchment F1 at Lake Gårdsjön for the past ten years. Therefore, we need first to examine if sulfur isotope fractionation in the soil could explain the difference in $\delta^{34}S$ of deposition, input of heavy sulfur to the catchment, and runoff, output of lighter sulfur from the catchment. Several investigations have suggested that there is no sulfur isotope fractionation when adsorbing/ desorbing sulfate (Fuller et al., 1986; Van Stempvoort et al. 1990), although the lysimeter $\delta^{34}S$ values are higher than the runoff $\delta^{34}S$. Lysimeter water sampling in the study in the Hubbard

Brook by Fuller et al., 1986, showed a similar trend, higher $\delta^{34}S$ values in the lysimeter samples than in the adsorbed sulfate in the soil. This could be an effect of the sampling of water through capillaries as in this study, but the lysimeter waters were in the Hubbard Brook study sampled with tension free lysimeters. The change in $\delta^{34}S$ of the pre and post periods at 20cm depths suggests that mineralization of organic sulfur to sulfate occurs but could be an artifact as only a few samples have been measured.

Stable isotope research in forest soils in Ontario have led to the conclusion that the only processes that fractionate isotopes in sulfate at Earth-surface conditions are microbial processes (Van Stempvoort et al., 1990). Peat areas fractionate the sulfur isotope composition highly by bacterial sulfate reduction. We have seen this in F1 from groundwater well #5. This reduction leads to higher $\delta^{34}S$ values of sulfate and low concentrations in sulfate. Bacterial sulfate reduction is commonly observed under stagnant periods, i.e., low discharge or dry periods as in the Lake Mjösjön study (Andersson et al., 1992). In G1 none of this has been seen and as the $\delta^{34}S$ of runoff is lower than the $\delta^{34}S$ of the deposition this difference cannot be explained by bacterial sulfate reduction. We can thus point out that F1 is not a good reference catchment to G1. Further more, it is suggested that fractionation of the sulfur isotope composition within G1 is not significant.

Cl concentrations show first signs of the sprinkler water input in September, after five months and the whole water reservoir have been exchanged after one year (L. Nyberg, oral comm.). The sulfur decrease occurred after nine months (Fig 4, 5) suggesting that sulfate is not as conservative as chloride although many whole catchment experiments have suggested otherwise.

During the first year about 721mm water has been sprinkled under the roof and about 450mm of water has been measured in runoff. 110 moles of sea water sulfur have been added to the area but 468 moles of sulfur have left the roof catchment in the runoff. This means, according to mass balance calculations that about 25% of the runoff can be accounted to the sulfur inputs from the sprinkler water. A composition of 25% sprinkler water and 75% old sulfur, found from mass balance calculations, in runoff corresponds to a $\delta^{34}S$ value of +8.9‰, measured value is +5.8‰. Thus, if the runoff can be seen as a total mix between sprinkler water and old sulfur within the area, similar to the assumption in mass balance calculations, almost all sulfur in runoff is old sulfur according to the isotope data.

All this data implies that the retention time for sulfur is long and that the sulfate in runoff is a mixing between deposited sulfur during several years. Thus, the observed $\delta^{34}S$ values in runoff are average values for the retention time period. A quick equilibration between sulfate in solution and adsorbed sulfate has been shown with small amounts of sulfate-35 added to soil equilibrated with water (Karltun, pers. comm.). This was shown on many different soils with an equilibration time of only two hours. In this way the deposited sulfate will be mixed with the adsorbed sulfate soil pool and as the sulfate content in the soil is much larger than the sulfate content of the input and output, the change in $\delta^{34}S$ values in runoff from year to year will then be small. The slightly higher $\delta^{34}S$ values found at groundwater well #6 is also in accord with this process because of hydrological reasons. Groundwater exists only at certain times at well #6 and the surrounding area is mostly an inflow area for the groundwater in the catchment.

Table 2: Antrophogenic sulfur in runoff. The amount of antrophogenic sulfur is calculated by comparing total sulfur in throughfall and excess sulfur in runoff the same year. Excess sulfur is calculated by using the excess sulfur definition. $\delta^{34}S$ in runoff is calculated by using the formula; % antrophogenic sulfur/100 x 4.2 + % sea water sulfur/100 x 20.3 ($\delta^{34}S$ value in sea water in Kattegatt). Data from Hultberg & Grennfelt (1992).

Year	% antrop. sulfur	% sea water	Calculated $\delta^{34}S$
80/81	100	0	4.2
81/82	100	0	4.2
82/83	100	0	4.2
83/84	61	39	10.5
84/85	90	10	5.8
85/86	100	0	4.2
86/87	100	0	4.2
87/88	80	20	7.4
88/89	46	54	12.9
89/90	85	15	6.6
mean	88	12	6.1
+/-	12	12	2

The mixing between anthropogenic sulfur and sea water sulfur according to the model presented for the throughfall during the first year of sampling is 76% and 24% respectively. The mixing model can be used also backwards in time; 17% decrease in sea water derived sulfur is needed to explain the +5.4‰ measured in runoff. Mixing would then be 93% anthropogenic sulfur and 7% sea water sulfur. An average for the mixing for sulfur in runoff during the period 1980 - 1990, table 2, according to the excess sulfate calculation is 88% anthropogenic sulfur and 12% sea water sulfur (Hultberg & Grennfelt, 1992), which gives a calculated $\delta^{34}S$ value during the period of +6.1‰, using a $\delta^{34}S$ of anthropogenic S of +4.2‰. According to Table 2 the variation from year to year has been large and the calculated $\delta^{34}S$ value in runoff has varied. It can be concluded, also from table 2, that the error in measurements for the mass balance approach to calculate the $\delta^{34}S$ value average in runoff for the period 1980 - 1990 is well within what is measured in runoff today. A historical record of lake sediments in Ontario showed different anthropogenic $\delta^{34}S$ values in North America with respect to time (Nriagu & Coker, 1983). It is likely that the sulfur isotope composition of anthropogenic sulfur has changed during the 20th century in Europe due to different emissions of sulfur in that period.

CONCLUSIONS

The origin of sodium and chloride is through sea spray. Addition of chloride into the area from pollution is negligible if any. The atmospheric deposition of sulfur in the Lake Gårdsjön area is from two sources. It is dominated by anthropogenic sources (in the year of investigation it amounts to about 75%), the remaining part is sulfur of marine origin by sea water spray.

The lack of a proportional change in the sulfur isotope composition in the sulfate in runoff to the decreased sulfate deposition suggests that added sulfate to the catchment is quickly equilibrated with the adsorbed pool of sulfate. Since the pool of inorganic sulfur in the roof catchment and also in soils in general is much larger than the deposition a dilution effect is seen which then explain the small change in $\delta^{34}S$ values in this study. This implies that an acidification reversal concerning water chemistry will take much longer time than mass balance calculations suggest. Retention time for the sulfur in the Lake Gårdsjön soils has in this investigation been shown to be much longer than previously suggested from mass balance calculations.

ACKNOWLEDGEMENTS

This project is funded by the Swedish Natural Science Research Council. Sampling has been performed in cooperation with the Swedish Environmental Research Institute (IVL) in Gothenburg, H. Hultberg, I.B. Andersson and F. Moldan. Runoff discharge, precipitation and throughfall volumes have been provided from IVL, F. Moldan and U. Nyström. Lysimeter water has been provided from Norwegian Forest Research Institute (NISK), A. Stuanes and J. Kjönaas. K. Hajnal is thanked for help with the isotopic preparation of the samples and M. Hedberg is thanked for technical assistance with the mass spectrometer.

REFERENCES

Andersson, F. & Olsson, B. (eds.) 1985. *Lake Gårdsjön An acid forest lake and its catchment. Ecological Bulletins 37.* Publishing House of the Swedish Research Counsils, Stockholm.

Andersson P., Torssander P. and Ingri J. 1992. Sulphur isotope ratios and oxygen isotopes in water from a small watershed in Central Sweden. *Hydrobiol.*, 235/236; 205-217.

Berner, R.A. 1971. *Principles of sedimentology*, McGraw-Hill, New York

Caron F., Tessier A., Kramer J.R., Schwarcz H.P. and Rees C.E. 1986. Sulfur and oxygen isotopes of sulfate in precipitation and lake water, Quebec, Canada. *Appl. Geochem.*,1; 601-606.

Castleman Jr, A.W., Munkelwitz, H.R. & Manowitz B. 1973. Contribution of volcanic sulphur compounds to the stratospheric aerosol layer. *Nature* 244; 345-346.

Eriksen T.E. 1972. Sulfur isotope effects. I. The isotopic exchange coefficient for the sulfur isotopes ^{34}S - ^{32}S in the system $SO_2(g)$ - $HSO_3^-(aq)$ at 25, 35 and 45°C. *Acta Chem. Scand.* 26; 573-580.

Fuller R.D., Mitchell M.J., Krouse H.R., Wyskowski B.J. and Driscoll C.T. 1986. Stable sulfur isotope ratios as a tool for interpreting ecosystem sulfur dynamics. *Water, Air Soil Pollut.* 28; 163-171.

Hesslein, R.H., Capel, M.J. & Fox, D.E. 1988. Sulfur isotopes in sulfate in the inputs and outputs of a Canadian shield watershed. *Biogeochem.* 5; 263-273.

Hultberg H., Andersson B. I. & Moldan F. in press. The covered catchment - an experimental approach to reversal of acidification in a forest ecosystem. *Proc. EXMAN-conf.*, Copenhagen, May 1992.

Hultberg H. & Grennfelt P. 1992. Sulphur and sea salt deposition as reflected by throughfall and runoff chemistry in forested catchments. *Environ. Pollut.* 75; 215-222

Krouse, H.R. & Case, J.W. 1981. Sulphur isotope ratios in water, air, soil and vegetation near Teepee creek gas plant, Alberta. *Water, Air, Soil Pollut.* 15; 11-28.

Krouse, H.R. & Grinenko, V.A. (eds) 1991. *Stable isotopes Natural and anthropogenic sulphur in the environment. Scope 43.* John Wiley & sons, Chichester, UK.

Krouse, H.R. & Tabatabai, M.A. 1986. Stable sulfur isotopes. In: *Sulfur in agriculture.* M.A. Tabatabai (ed). Amer. Soc. Agron. - Crop Sci. Soc. Amer. - Soil Sci. Soc. Amer., Madison, Wisconsin.

Krouse, H.R. & Van Everdingen, R.O. 1984. ^{34}S variations in vegetation and soil exposed to intense sulphide emissions near Paige Mountain, N. W. T., Canada. *Water, Air Soil Pollut.* 23; 61-67.

Lindberg S.E. & Garten Jr C.T. 1988. Sources of sulfur in forest canopy throughfall. Nature, 336; 148-151

Mitzutani, Y. & Rafter, T.A. 1969. Isotopic composition of rain water, Gracefield, New Zealand. *N.Z.J. Sci.* 12; 69-80.

Nehreing, N.L., Bowen, P.A. & Thrusdell, A.T. 1977. Techniques for the conversion to carbon dioxide of oxygen from dissolved sulfate in thermal waters. *Geothermics* 5; 63-66.

Nriagu, J.O. & Coker, R.D. 1978. Isotopic composition of sulfur in precipitation within the Great Lakes Basin. *Tellus* 30; 365-375.

Nriagu, J.O. & Coker, R.D. 1983. Sulphur in sediments chronicles past changes in lake acidification. *Nature* 303; 692-694..

Olsson, B., Hallbäcken, L., Johansson, S., Melkerud, P-A., Nilsson, S.I. and Nilsson T. 1985. The lake Gårdsjön area - physiographical and biological features. In: *Ecological Bulletins 37: Lake Gårdsjön An acid forest lake and its catchment*, F. Andersson & B.Olsson, (eds.) Publishing House of the Swedish Research Counsils, Stockholm; 10-28.

Rees, C.E., Jenkins, W.J. & Monster, J. 1978. The sulphur isotope composition of ocean water sulphate. *Geochim. Cosmochim. Acta.*, 42; 377-381.

Saltzman E.S., Brass G.W. and Price D.A. 1983. The mechanism of sulfate aerosol formation; Chemical and sulfur isotopic evidence. *Geophys. Res. Lett.* 10; 513-516.

Trembaczowski A. 1991. Sulphur and oxygen isotopes behaviour in sulphates of atmospheric groundwater system observations and model. *Nordic Hydrol.* 22; 49-66.

Van Stempvoort D.R., Reardon E.J. and Fritz P. 1990. Fractionation of sulfur and oxygen isotopes in sulfate by soil sorption. *Geochim. Cosmochim. Acta* 54; 2817-2826.

Van Stempvoort D.R., Fritz P. and Reardon E.J. 1992. Sulfate dynamics in upland forest soils, central and southern Ontario, Canada; stable isotope evidence. *Appl. Geochem.* 7; 159-175.

Winner, W.E., Bewley, J.D., Krouse, H.R. & Brown, H.M. 1978. Stable sulphur isotope analysis of SO_2 pollution impact on vegetation. *Ocelogica* 36; 351-361.

Yanagisawa, F. & Sakai, H. 1983. Thermal decomposition of barium sulfate - vanadium pentoxide - silica glass mixtures for preparation of sulfur dioxide in sulfur isotope ratio measurements. *Anal. Chem.* 55; 985-987.

ANNUAL RATES OF SULPHUR REMOVAL FROM SUBSURFACE LAYERS OF FRESHWATER PEATS: A MINIMUM ESTIMATE USING ^{210}Pb CHRONOLOGY

M. NOVÁK & T. PAČES
Czech Geological Survey, Malostranské námesti 19, 118 21 Prague 1,
The Czech Republic
R.K. WIEDER
Department of Biology, Villanova University, Villanova, PA 19085, U.S.A.
W.R. SCHELL
Department of Radiation Health, University of Pittsburgh,
Pittsburgh, PA 15261, U.S.A.

ABSTRACT. Apparent sulphur accumulation rates in selected freshwater *Sphagnum*-derived peat deposits in the United States and the Czech Republic are used for an estimate of sulphur loss during early peat diagenesis. At two relatively unpolluted sites, Marcell Bog, Minnesota, and Jezerni slat', South Bohemia depth x is identified below which ^{210}Pb-dated 2 cm thick peat layers start to show a steady decrease in apparent sulphur accumulation rates. The estimate is based on a comparison between apparent sulphur accumulation rates in peat layers deeper than x and that for depth x, assuming that at various points of time in the past each deeper peat layer exhibited apparent sulphur accumulation rate equal to the present value at depth x.

INTRODUCTION

Freshwater *Sphagnum*-dominated wetlands have consistently been identified as net sinks for atmospheric sulphur rather than net sources (Brown 1985, Bayley *et al.* 1986, Urban *et al.* 1989, Giblin & Wieder 1989). Fluxes of gaseous sulphur compounds, predominantly H_2S, dimethylsulphide, carbonylsulphide, carbon disulphide, methane thiol and dimethyl-disulphide from peat surface into the atmosphere are difficult to measure directly and their estimates vary considerably (Bremner & Steele 1978, Adams *et al.* 1981, Aneja *et al.* 1982, Freney *et al.* 1983, Steudler & Peterson 1984, Wieder & Cichowski 1988). Bulk sulphur emissions from wetlands are generally believed to be at least two orders of magnitude lower compared to anthropogenic sources (Castro & Dierberg 1987). Nriagu *et al.* (1987) were the first to suggest that up to 30 percent of sulphur annually deposited in peatland areas in Canada may be revolatilized and redeposited on the earth as acid precipitation. Few attempts have been made to evaluate the degree of openness of peat deposits toward buried sulphur based on the geochemical record in peat.

Most sulphur in freshwater peats is typically present as organic rather than inorganic S, with carbon bonded S much more abundant than ester bonded S (Casagrande *et al.* 1977, Casagrande *et al.* 1980, Behr 1985, Lowe 1986, Spratt *et al.* 1987). While the concentration of free sulphate is progresively depleted with depth, the rates of bacterially mediated sulphate reduction often exhibit a subsurface maximum (Howarth & Teal 1979, Brown & MacQueen 1985, Wieder *et al.* 1980). Radiolabelling experiments using ^{35}S have documented dynamic interconversions between individual sulphur species, including iron monosulphide S and pyrite S (Brown 1985, Skyring 1987, Wieder & Lang 1988). In our previous paper (Novák & Wieder 1992) we reported systematic presence of subsurface maxima in the concentration of total S, carbon bonded S and pyrite S in seven peat bogs with contrasting sulphur inputs. Here we propose a simple method of estimating the amount of sulphur released during diagenesis from peat layers located deeper than these concentration maxima. We combine S concentration data with radiogenic ages of 2 cm peat layers determined using ^{210}Pb chronology (Novák 1992).

SAMPLES AND TECHNIQUES

Two study sites are situated in relatively pristine continental settings, one in the United States, and one in the Czech Republic, with no local sources of atmospheric pollution. The third study site is located in a heavily polluted part of West Virginia in the eastern United States.

The first unpolluted site, Marcell Bog, is located in the Marcell Experimental Watershed S-2 (Verry & Timmons 1982) in north-central Minnesota, U.S.A. (47°32' N, 93°28' W; elevation 420 m a.s.l.). The 3.2-ha *Sphagnum*-derived peat deposit, surrounded by 6.5 ha of mineral soil upland, fills a kettle hole 4-8 m deep. Fine-grained lacustrine sediments seal the basin and allow the existence of perched water table within the bog. The bog is forested with black spruce and an understory of ericaceous shrubs. The surface water pH fluctuates around 3.6, water sulphate concentration averages 4.6 mg . l^{-1}. Mean annual precipitation reaches 550 mm, the average annual temperature is +4°C. The atmospheric pollution level is negligible, with bulk atmospheric sulphur deposition rates of approximately 12.4 kg S . ha^{-1}. $year^{-1}$ (cf. Novák & Wieder 1992, Lindberg & Lovett 1992).

The second relatively unpolluted site, Jezerni slat', is located in the Sumava Mts. Natural Preserve in South Bohemia, the Czech Republic (49°03' N, 13°36' E; elevation 1070 m a.s.l.). The sparsely forested wetland (*Pinus mugo*) covers an area of 156 ha with a total depth of the peat deposit 7.5 m (Dohnal *et al.* 1965). The bedrock is biotite-muscovite granite of the Moldanubian Pluton. Surface water pH is 3.4 and sulphate concentrations in surface bog water do not exceed 5.0 mg . l^{-1}. Annual precipitation averages 760 mm and the average annual temperature is +4.9°C. The bulk atmospheric deposition of sulphur, calculated as twice the value of wet S deposition at a nearby catchment, is approximately 26 kg S . ha^{-1}. $year^{-1}$ (cf. Hlavaty 1992, Fottová 1992, Cerny 1993).

The heavily polluted Big Run Bog is an open 15-ha *Sphagnum*-derived wetland surrounded by 276 ha of forested catchment in the Appalachian Mts. of West Virginia, U.S.A. (39°07' N, 79°35'W; elevation 980 m a.s.l.). The catchment is underlain by sandstones of the

Pottsville Group. Peat depth averages 0.4 m and reaches a maximum of 2.30 m (Wieder & Lang 1984). The pH of bog stream water is roughly 4.0, while sulphate concentrations in the water fluctuate about 10 mg . l^{-1}. Annual precipitation is as high as 1560 mm, mean annual temperature is +7.9°C, and the bulk atmospheric deposition of sulphur slightly exceeds 91 kg S . ha^{-1} $year^{-1}$. All three study sites are physiographically minerotrophic, receiving water inputs by precipitation and by runoff from the upland portions of their catchments. Based on vegetation and water chemistry, however, these sites are similar to ombrotrophic bogs. Water table fluctuates between 2 and 10 cm below bog surface at all three sites.

One peat core was collected from each site using a 10 cm diameter, 50 cm long PVC pipe with a sharpened bottom edge. Cores were sliced into 2 cm thick sections, freeze dried and homogenized. Total S was determined on a subsample from each depth using a LECO SC-132 Sulphur Analyzer. The analytical error was lower than 1 % of S concentration. Organic sulphur was calculated by subtracting free sulphate S, acid volatile S and Cr^{2+} reducible S from total S. Detailed description of analytical procedures used for the sequential extraction of the individual sulphur species from peat is given in Novák & Wieder (1992). Sulphur for stable isotope determinations was extracted by combustion with Eschka's mixture (Chakrabarti 1978) and converted to sulphur dioxide according to Yanagisawa & Sakai (1983). Isotopic composition of total sulfur was determined on a Finnigan MAT 251 mass spectrometer with reproducibility within 0.3 per mil on the CDT scale. Peat profiles were dated by means of ^{210}Pb activity measurements using the digestion procedure of Tobin & Schell (1988) and the constant rate of supply model of Appleby & Oldfield (1978). A 3 g subsample was spiked with 15 dpm ^{208}Po as a chemical yield tracer and a slurry was made in 25 ml of distilled deionized water. Five ml of concentrated HCl and 5 ml of concentrated HNO_3 were added and the mixture was heated overnight. Then 1 ml of 30 % H_2O_2 was added and the samples were heated to dryness. Five ml of concentrated HCl with 50 ml of distilled deionized water were added, the samples were boiled for 5 minutes, filtered, and the filtrate evaporated to dryness. Three times 2 ml of concentrated HCl were added and the samples repeatedly evaporated to dryness. Then 150 ml of 0.3 M HCl were added along with 0.5 g of ascorbic acid to complex iron. The solution was stirred at 60°C for 1 hour. One silver disc (4 cm^2), covered on one side with an insulating varnish, was suspended in each beaker and both ^{210}Po and ^{208}Po were left to plate out on the unprotected side at 60°C overnight. The activity measurements were carried out on an Alpha spectrometer ORTEC 576.

RESULTS AND DISCUSSION

All three sites show similar changes in sulphur concentration with increasing depth (Fig. 1 a). At Marcell Bog, the subsurface maximum was found at a depth of 13 cm, at Jezerni slat' at a depth of 7 cm, and at Big Run Bog at a depth of 17 cm. Throughout the profiles, organic, mostly carbon bonded S is the dominant S species, making up 80 - 95 percent of total S. Isotopic composition of total sulphur (Fig. 1 b) exhibits two subsequent shifts along the vertical profile. In a paper reporting $\delta^{34}S$ values of total sulphur at a variety of peat bogs in the United States and the Czech Republic (Novák & Wieder *in review*) we interpret

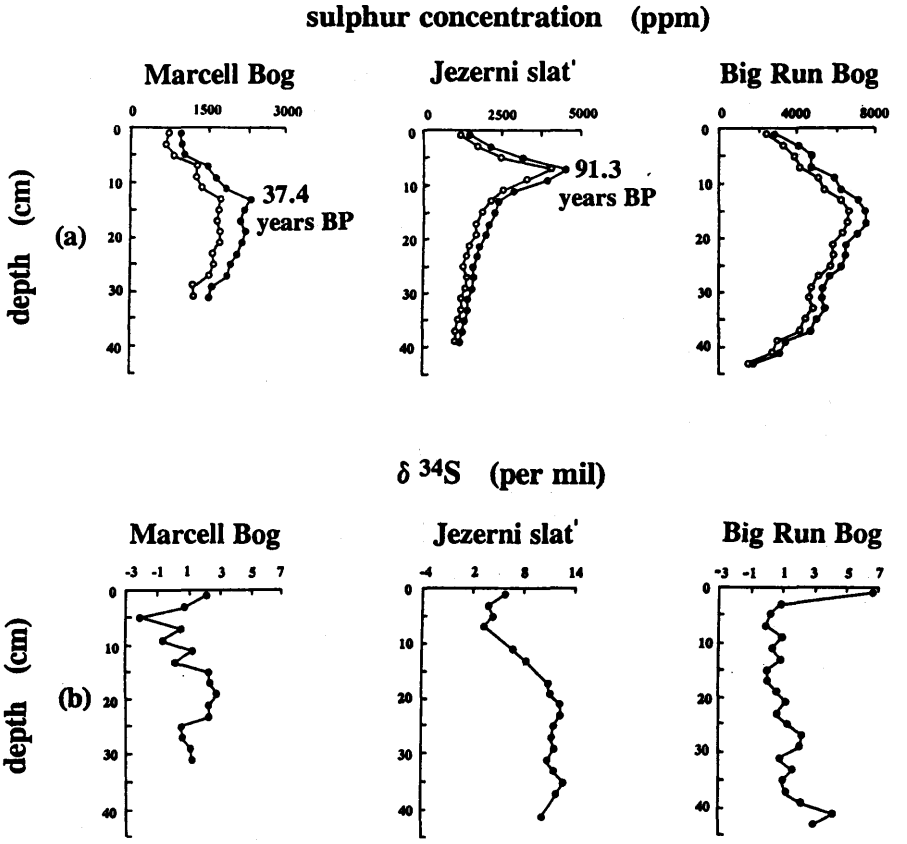

Figure 1 : Concentration and isotopic composition of sulphur in peat. Full circles - total S, open circles - organic S.

the near surface negative isotopic shift as resulting from dissimilatory sulphate reduction, and the deeper positive isotopic shift as resulting from diagenetic processes. Higher $\delta^{34}S$ values in deeper sections of the positive S isotopic shift may reflect preferential revolatilization of the lighter isotope ^{32}S during peat maturation. Both vertical isotopic signals demonstrate mobility of originally fixed sulphur along the profile: in a closed system no changes in $\delta^{34}S$ values of total sulphur can be expected, even though instantaneous fractionation between individual S species may still occur (Jorgensen 1979, Krouse 1986). The apparent vertical mobility of sulphur makes it difficult, if not impossible, to reconstruct historical records of *actual* S accumulation in peat deposits by combining peat dating techniques with S concentration data. In the following paragraphs, however, we attempt to combine a peat dating technique with S concentration data for a "reversed" purpose: to estimate sulphur losses from deeper peat layers based on *apparent* S accumulation rates which resulted from diagenetic processes.

Fig. 2 (a) gives the time spans for deposition of the individual 2 cm peat increments at Marcell Bog, Jezerni slat', and Big Run Bog. As of 1989, the history of peat accumulation could be followed for the past 143 years at Marcell Bog, 277 years at Jezerni slat', and 201 years at Big Run Bog. The number of years per section increases in a rather smooth, non-linear fashion at Marcell Bog and Big Run Bog, a similar compaction tendency is less clear-cut at Jezerni slat'. The error bars in Fig. 2 (a) represent 1 standard deviation propagated from the uncertainty of activity counting. These error bars become notably large for dates older than 100 - 120 years (i.e., 5 ^{210}Pb half-lives).

Vertical changes in bulk sedimentation rates in Fig. 2 (b) are a result of two superimposed phenomena: changes in the net primary production, and removal of decomposition endproducts, especially CO_2, CH_4, and dissoved organic molecules. At Marcell Bog bulk sedimentation rates decrease with increasing depth, possibly reflecting a cummulative effect: with increasing age more mobile macroelements are removed. The uppermost 2 cm at Jezerni slat' show a rather low bulk sedimentation rate (5 mg . cm^{-2} . $year^{-1}$) which is in agreement with field observation: no living *Sphagnum* was found at the sampling site, peat accumulation at Jezerni slat' has been discontinued. Big Run Bog is characterized by relatively fast peat accumulation with the deepest datable layer (38 - 40 cm below current bog surface) found nearly twice deeper than the deepest datable layer at the remaining two sites.

Our estimate of the amount of sulphur released from buried peat horizons is based on apparent sulphur accumulation rates in Fig 2 (c). Apparent sulphur accumulation rates were calculated as the product of bulk deposition rates and sulphur concentration at a particular depth:

$$A\ (\mu g\ S\ .\ cm^{-2}\ .\ year^{-1}) = B\ .\ [c]\ , \qquad (1)$$

where A denotes apparent sulphur accumulation rate, B is bulk sedimentation rate, and [c] sulphur concentration. If apparent sulphur accumulation rates (Fig. 2 c) are compared with sulphur concentrations (Fig. 1 a), two points bear mention. First, at the relatively unpolluted sites, Marcell Bog and Jezerni slat', vertical trends in both variables remain similar: a subsurface maximum in sulphur concentration is reflected in a subsurface maximum in apparent sulphur accumulation rates. Second, the depth (and age) of these maxima is not identical at either of the two sites. At Marcell Bog sulphur concentration peaks at the depth of 13 cm (37.4 years BP), while the apparent sulphur accumulation rate reaches a maximum 17 cm below current bog surface (53.4 years BP). At Jezerni slat', sulphur concentration increases to the depth of 7 cm (91.3 years BP), while the apparent sulphur accumulation rate peaks as shallow as 3 cm below surface (38.4 years BP).

For the development of the estimate of sulphur removal rate several assumptions are made:

(a) The presence of a sulphur concentration maximum in vertical freshwater peat profiles is a wide-spread phenomenon related to the proximity of bog surface, the level of fluctuating water table and, hence, the level of anaerobic environment, the intensity of near surface bacterial sulphate reduction, assimilatory uptake of sulphur, and the overall low degree of necromass maturation. (Novák & Wieder 1992). The presence of a near-surface maximum in S concentration is not a result of changing local pollution

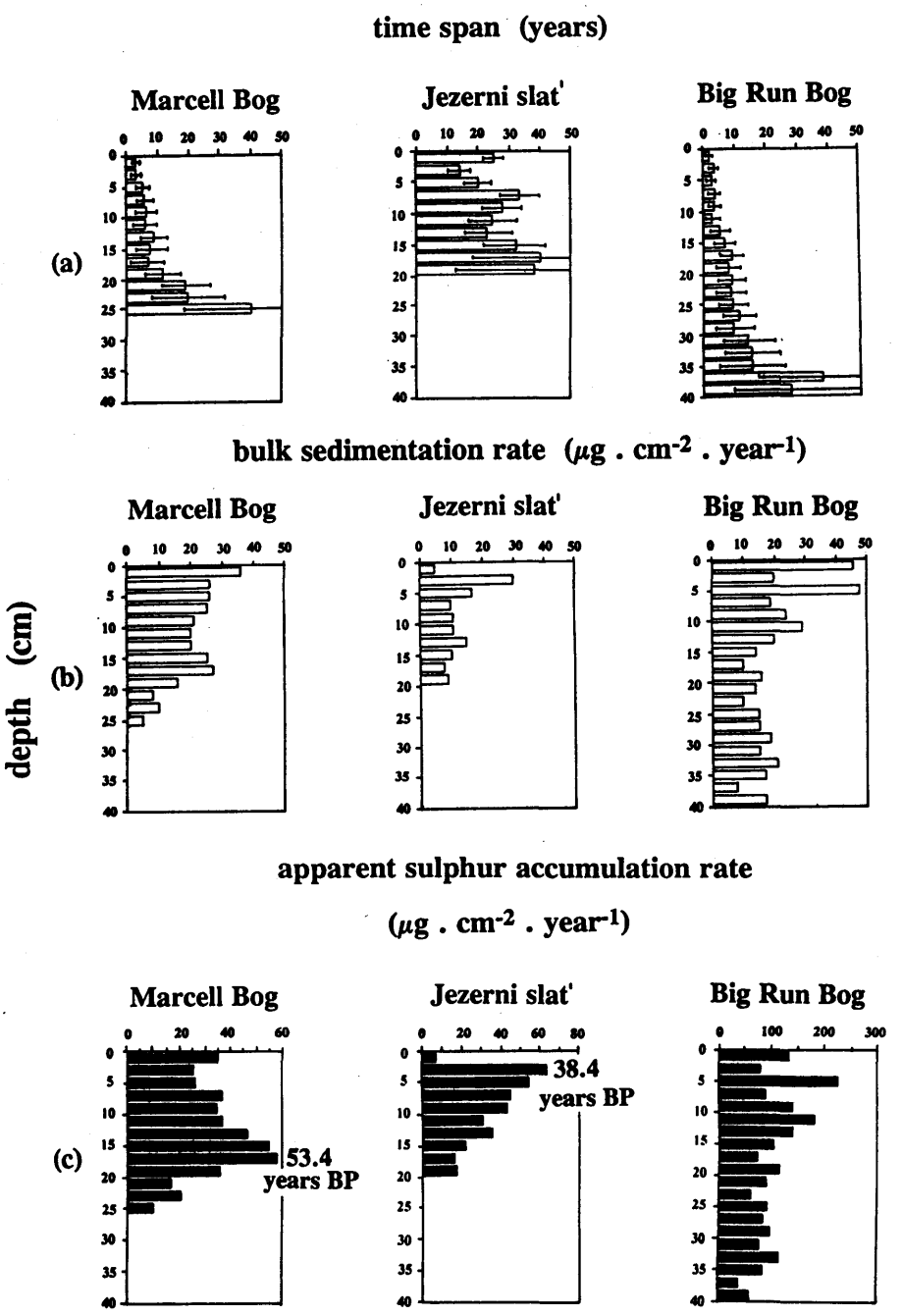

Figure 2: Bog characteristics based on ^{210}Pb chronology. Error bars in (a) represent one standard deviation. Similar errors in (b) and (c) not shown.

levels; intensity of pollution effects only its magnitude. It is important to note that at neither site in Figs. 1 and 2 near surface maxima in S concentration and apparent S accumulation rates correspond to maximum levels of local pollution: regional atmospheric sulphur burden on the northern hemisphere had been steadily increasing at least until 1970 - 1985 while these maxima are found in older layers.

(b) Due to vertical redistribution of sulphur deposited on bog surface and its transport toward the concentration maximum, only relatively unpolluted sites are suitable for the proposed evaluation. Elsewhere enhanced S inputs overprint the burial history of "background" sulphur.

(c) At a certain depth in relatively unpolluted peat bogs, apparent S accumulation rates begin to decrease steadily with increasing depth (as at Marcell Bog and Jezerni slat' in Fig. 2 c).

(d) In an unpolluted bog each newly grown moss layer, after a certain time, assumes the position of the older layer currently showing the maximum value of apparent sulphur accumulation rate.

(e) Secular changes in net primary production are assumed to be minor.

(f) Removal of sulphur by advection from peat layers deeper than 10-20 cm can be neglected.

Tab. 1 illustrates three steps of the calculation of a vertical upward flux of sulphur for Marcell Bog and Jezerni slat'.

1. Depth x (cm) with maximum apparent S accumulation rate is identified (first line in Tab. 1). Two centimeter thick layers situated deeper than x are denoted x-i, where i is the number of centimeters below level x (i = 2, 4, 6, 8, etc.).

2. At the time when any one-year peat increment was located at depth x its apparent sulphur accumulation rate was equal to present apparent sulphur accumulation rate at depth x (fourth column in Tab. 1). Time which passed since individual sulphur atoms now found in layer x - i were found at depth x is given in the fifth column of Tab. 1. Since then apparent sulphur accumulation rate decreased. Because both the initial apparent sulphur accumulation rate (A_x) and present apparent sulphur accumulation rate (A_{x-i}) are expressed on annual basis, their difference quantifies annual flux of sulphur being removed from depth x - i (column 7 in Tab. 1). Note that each peat layer is treated as an isolated system. The prevailing mechanism of sulphur removal is assumed to be ebullition of sulphur containing gasses. Below depth x, sulphur removed from a deeper layer is not fixed in shallower layers but penetrates further upward.

3. The total amount of sulphur released annually from the ^{210}Pb-datable segment of peat

Table 1: Minimum estimate of upward sulphur flux at depth x. A denotes apparent sulphur accumulation rate in peat.

depth (cm)		age of the layer (years BP)	initial A (μg S . cm^{-2} . yr^{-1})	time since depth x was passed (years)	present A in the layer x - i (μg S . cm^{-2} . yr^{-1})	$A_x - A_{x-i}$ (μg S . cm^{-2} . yr^{-1})
MARCELL BOG						
x	17	53.4	57.7	0.0	57.7	0.0
x-2	19	65.4	57.7	12.0	35.6	22.1
x-4	21	84.3	57.7	30.9	17.2	40.6
x-6	23	103.6	57.7	50.2	20.6	37.2
x-8	25	143.8	57.7	90.4	9.7	48.0
Total upward sulphur flux						U = 147.9
JEZERNI SLAT						
x	3	38.4	63.6	0.0	63.6	0
x-2	5	58.2	63.6	19.8	54.2	9.4
x-4	7	91.3	63.6	52.9	44.9	18.7
x-6	9	119.3	63.6	80.9	43.3	20.3
x-8	11	143.3	63.6	104.9	31.4	32.2
x-10	13	166.3	63.6	127.9	36.0	27.6
x-12	15	198.7	63.6	160.3	22.7	40.9
x-14	17	238.4	63.6	200.0	16.8	46.8
x-16	19	276.7	63.6	238.3	17.8	45.8
Total upward sulphur flux						U = 241.7

deeper than x is

$$U\ (\mu g\ S\ .\ cm^{-2}\ .\ year^{-1}) = \Sigma\ (A_x - A_{x-i}), \qquad (2)$$

where U is the upward flux of sulphur at depth x, A_x is apparent sulphur accumulation rate at depth x, and A_{x-i} is apparent sulphur accumulation rate at depth x - i.

As seen in Tab. 1, sulphur flux from peat layers deposited between 16 and 26 cm below current surface at Marcell Bog is approximately 147.9 $\mu g\ .\ cm^{-2}\ .\ year^{-1}$, or 14.8 $kg\ .\ ha^{-1}\ .\ year^{-1}$, and that from peat layers deposited between 2 and 20 cm below the surface at Jezerni slat' is roughly 241.7 $\mu g\ .\ cm^{-2}\ .\ year^{-1}$, or 24.2 $kg\ .\ ha^{-1}\ .\ year^{-1}$.

An obvious limitation to our approach is the lack of knowledge of apparent sulphur accumulation rates in peat layers positioned below the deepest ^{210}Pb-datable layer. Therefore the calculated values are a minimum estimate of the sulphur flux. There are indices, however, that around 30 - 50 cm below current surface sulphur concentrations flatten out and deeper may increase as pyrite accumulates first at the expense of labile organic S fractions and later at the expense of the relatively recalcitrant S fractions (cf. Altschuler et al. 1983, Novák 1992). For discussion of the fate of sulphur during later peat diagenesis and coalification see Price & Casagrande (1991).

Importantly, we do not suggest that the above calculated upward fluxes of sulphur actually reach bog surface and sulphur is thus revolatilized into the atmosphere. Rather, reduced sulphur forms which passed though depth x become partly oxidized and recycled, i.e., fixed, in the aerobic zone, or flushed horizontally downstream. The calculated intra-bog upward S fluxes for Marcell Bog and Jezerni slat' agree in the order of magnitude with local atmospheric S inputs. At Jezerni slat' the upward sulphur flux at depth x (24.2 $kg\ .\ ha^{-1}\ .\ year^{-1}$) is by 1.8 $kg\ .\ ha^{-1}\ .\ year^{-1}$ lower than the estimated atmospheric deposition of sulphur (26 $kg\ .\ ha^{-1}\ .\ year^{-1}$). At Marcell Bog the calculated upward sulphur flux (14.8 $kg\ .\ ha^{-1}\ .\ year^{-1}$) exceeds the estimated atmospheric deposition of sulphur by 2.4 $kg\ .\ ha^{-1}\ .\ year^{-1}$. Since both studied sites are runoff water fed, i.e., no sulphate S is being supplied from below by groundwater, the upward sulphur flux U principally cannot be greater compared to atmospheric sulphur inputs. Urban *et al.* (1989) estimated sulphur inputs into Marcell Bog even lower than 12.4 $kg\ .\ ha^{-1}\ .\ year^{-1}$, on the other hand, Baker *et al.* (1992) give for remote northern Wisconsin bordering on Minnesota atmospheric deposition of 15 $kg\ .\ ha^{-1}\ .\ year^{-1}$. If the latter value is used for the comparison, we arrive at an upward sulphur flux U lower by 0.2 $kg\ .\ ha^{-1}\ .\ year^{-1}$ than the atmospheric S input.

Due to vertical redistribution of sulphur in near-surface horizons in heavily polluted Big Run Bog, flux U for this site is difficult to estimate. Selection of the depth x (the right graph in Fig. 2 c) is hampered also by relatively low compaction, characteristic for Big Run Bog where substantial loss of labile organic S may not have been triggered off in the studied segment of peat column.

Note: In this paper, in the calculation of S deposition rates average ^{210}Pb dates for the whole 2-cm section were used. An alternative calculation approach would be to use dates corresponding to the top and the bottom of the section.

CONCLUSIONS

We propose a rough estimate of annual sulphur loss from subsurface layers of freshwater *Sphagnum*-derived peats. The method is based on empirical identification of depth x within the vertical peat profile, defined by (i) maximum apparent sulphur accumulation rate, and (ii) by a sequence of steadily decreasing apparent sulphur accumulation rates below this depth. Existence of a subsurface maximum in total S concentration not corresponding to maximum local pollution levels at a number of peat bogs (Novák & Wieder 1992) indicates partial transport of newly deposited S downward and/or carbon mineralization faster compared to sulphur mineralization at depths above x. At unpolluted bogs we postulate that each one-year peat increment at a certain time assumes the position of peat layer currently found at depth x. At this point each peat increment exhibits the same (maximum) value of apparent S accumulation rate. By ongoing diagenesis apparent S accumulation rates become smaller and the total loss is greater or equal to the sum of differences $(A_x - A_{x-i})$, where A_x is apparent sulphur accumulation rate at depth x, and A_{x-i} is apparent S accumulation rate in 2 cm thick peat layers below x datable by ^{210}Pb. The procedure can be applied only to relatively unpolluted bogs. For Marcell Bog, Minnesota (USA) annual sulphur flux through depth x was estimated as 14.8 kg . ha^{-1} . $year^{-1}$, that for Jezerni slat' in south Bohemia (the Czech Republic) as 24.2 kg . ha^{-1} . $year^{-1}$. Actual sulphur flux from bog surface into the atmosphere is controlled by the residence time of S-containing gases in peat above depth x and by internal cycling in the top peat layers and is believed to be lower than the estimated upward sulphur flux at depth x.

REFERENCES

Adams, D.F., Farwell, S.O., Robinson, E. & Pack, M.R. 1981. Biogenic sulfur source strengths. *Envir. Sci. Tech.*, 15; 1493-1498.

Aneja, V.P., Aneja, A.P. & Adams D.F. 1982. Biogenic sulfur compounds and the global sulfur cycle. *J. Air Pol. Control. Assoc.*, 32; 803-807.

Altschuler, Z.S., Schnepfe, M.M., Silber, C.C. & Simon, F.O. 1983. Sulfur diagenesis in Everglades peat and the origin in coal. *Science*, 221; 221-227.

Appleby, P.G. & Oldfield, F. 1978. The calculation of ^{210}Pb dates assuming a constant rate of supply of unsupported ^{210}Pb to the sediment. *Catena*, 5; 1-8.

Baker, L.A., Engstrom, D.R. & Brezonik, P.L. 1992. Recent sulfur enrichment in the sediments of Little Rock Lake, Wisconsin. *Limnol. Oceanogr.*, 37; 4, 689-702.

Bayley, S.E., Behr, R.S. & Kelly, C.A. 1986. Retention and release of S from a freshwater wetland. *Water Air Soil Poll.*, 31; 101-114.

Behr, R.S. 1985. *Sulfur Dynamics in an experimentally acidified mire in northwestern Ontario.* M.S., Masters thesis. Univ. of Manitoba.

Bremner, J.M. & Steele C.G. 1978. Role of microorganism in the atmospheric sulfur cycle. *Adv. Microbiol. Ecol.*, 2; 155-201.

Brown, K.A. 1985. Sulphur distribution and metabolism in waterlogged peat. *Soil Biol. Biochem.*, 17; 39-45.

Brown, K.A. & MacQueen, J.F. 1985. Sulphate uptake from surface water by peat. *Soil Biol. Biochem.*, 17; 4, 411-420.

Casagrande, D.J., Gronli, K. & Sutton, N. 1980. The distribution of sulfur and organic matter in various fractions of peat: Origins of sulfur in coal. *Geochim. Cosmochim. Acta*, 44; 25-32.

Casagrande, D.J., Seifert, K., Berschinski, G. & Sutton, N. 1977. Sulfur in peat-forming systems in the Okefenokee Swamp and Florida Everglades: Origins of sulfur in coal. *Geochim. Cosmochim. Acta*, 41; 161-167.

Castro, M.S. & Dierberg, F.E. 1987. Biogenic hydrogen sulfide emissions from selected Florida wetlands. *Water Air Soil Poll.*, 33; 1-13.

Chakrabarti, J.N. 1978. Analytical procedures for sulfur in coal desulfurization products. In: *Analytical methods for coal and coal products*, C.J. Karr (ed), Academic Press, New York.

Cerny, J. 1993. Atmospheric deposition in the Krusné hory Mts.: Preliminary results of throughfall measurements. *Acta Universitatis Carolinae*. In press.

Dohnal, Z., Kunst, M., Mejstrík, V., Raucina, S. & Vydra, V. 1965. *Czechoslovak peat bogs*. Publishing House of the Czechoslovak Academy of Sciences, Prague. In Czech.

Fottová, D. 1992. *Monitoring of small catchments in the system GEOMON*. M.S., Final Report No. 73/1992, Czech Geological Survey, Prague. In Czech.

Freney, J.R., Ivanov, M.V. & Rodhe, H. 1983. The sulphur cycle. In: *The major biogeochemical cycles and their interactions*, Bolin, B. & Cook, R.B.(eds), SCOPE Report No. 22, John Wiley, New York; 55-61.

Giblin, A. & Wieder, R.K. 1989. Sulfur cycling in saline and freshwater wetlands. - A review. In: *Sulfur cycling in terrestrial systems and wetlands*, Howarth, W.R. & Stewart, J.W.(eds), Proc. of SCOPE 1989 Trent Meeting, John Wiley, New York.

Hlavaty, T. 1992. *Determination of total atmospheric deposition of ecologically significant elements into the catchment of the Certovo lake*. M.S., Masters thesis, Univ. of Chemical Technology, Prague. In Czech.

Howarth, H.W. & Teal, J.M. 1979. Sulfate reduction in a New England salt marsh. *Limnol. Oceanogr.*, 24; 999-1013.

Jorgensen, B.B. 1979. A theoretical model of the stable sulfur isotope distribution in marine sediments. *Geochim. Cosmochim. Acta*, 43; 363-374.

Krouse, H.R. 1986. Sulphur isotopes in our environment. In: *Handbook of environmental isotope geochemistry*, P.Fritz, J.Ch.Fontes (eds), Elsevier, New York.

Lindberg, S.E. & Lovett, G.M. 1992. Deposition and forest canopy interactions of airborne sulfur: Results from the Integrated Forest Study. *Atm. Environ.*, 26A(8); 1477-1492.

Lowe, L.E. 1986. Application of sequential extraction procedure to the determination of the distribution of sulfur forms in selected peat materials. *Can. J. Soil*, 66; 337-345.

Novák, M. 1992. *Metabolism of sulphur in freshwater peat bogs*. M.S., Ph.D.thesis, Czech Geological Survey, Prague. In Czech.

Novák, M. & Wieder, R.K. 1992. Inorganic and organic sulfur profiles in nine Sphagnum peat bogs in the United States and Czechoslovakia. *Water Air Soil Poll.*, 65; 353-369.

Novák, M. & Wieder, R.K. Mobility of sulfur during early diagenesis in Sphagnum peat: Evidence from stable sulfur isotopes. In review.

Nriagu, J.O., Holdway, D.A. & Coker, R.D. 1987. Biogenic sulfur and the acidity of rainfall in remote areas of Canada. *Science*, 237; 1189-1192.

Price, F.T. & Casagrande, D.J. 1991. Sulfur distribution and isotopic composition in peats from the Okefenokee Swamp, Georgia and the Everglades, Florida, *Int. J. Coal Geol.*, 17; 1-20.

Skyring, G.W. 1987. Sulfate reduction in coastal ecosystems. *Geomicrobiol.*, 5; 295-374.

Spratt, G.H., Morgan, M.D. & Good, R.E. 1987. Sulfate reduction in peat from a New Jersey Pinelands Cedar Swamp. *Appl. Environ. Micro.*, 53; 1406-1411.

Steudler, P.A. & Peterson, B.J. 1984. Contribution of gaseous sulphur from salt marshes to the global sulphur cycle. *Nature*, 311; 455-457.

Tobin, M.J. & Schell, W.R. 1988. *Deposition history of atmospheric chemicals at terrestrial sites in New York State*. M.S., Progress Report, Grant No. 008/87B/018, Univ. of Pittsburg.

Urban, N.R., Eisenreich S.R. & Grigal, D.F. 1989. Sulfur cycling in a forested *Sphagnum* bog in Minnesota. *Biogeochem.*, 7; 81-109.
Verry, E.S. & Timmons D.R. 1983. Water-borne nutrient flow through an upland peatland watershed in Minnesota. *Ecology*, 63; 1456-1467.
Wieder, R.K. & Cichowski, K.M. 1988. Hydrogen sulfide emission from Big Run Bog, West Virginia. *Proc. 39th AIBC Annual Meeting*, Univ. of California.
Wieder, R.K. & Lang, G.E. 1984. Influence of wetlands and coal mining on stream water chemistry. *Water Air Soil Poll.*, 23; 381-396.
Wieder, R.K. & Lang, G.E. 1988. Cycling of inorganic sulfur in peat from Big Run Bog, West Virginia. *Biogeochem.*, 5; 221-242.
Wieder, R.K., Yavitt, J.B. & Lang, G.E. 1990. Methane production and sulfate reduction in two Appalachian peatlands. *Biogeochem.*, 10; 81-104.
Yanagisawa, F. & Sakai, H. 1983. Precipitation of SO_2 for sulphur isotope ratio measurements by the thermal decomposition of $BaSO_4$ - V_2O_5 - SiO_2 mixtures. *Anal. Chem.*, 55; 985-987.

THE INFLUENCE OF OKCHON BLACK SHALES ON THE CONCENTRATIONS OF Cd, Mo AND Se IN SOILS AND CROP PLANTS IN KOREA

K.W. KIM & I. THORNTON
Environmental Geochemistry Research Group
Centre for Environmental Technology
Imperial College
London SW7 2BP
England, U.K.

ABSTRACT. High contents of potentially toxic elements of concern to animal and human health are present in some natural geological materials. The Okchon uraniferous black shale in Korea provides an important example of this. Cadmium, molybdenum, selenium and uranium are enriched in the uraniferous black shale in the Deog-Pyoung area. Soils developed on these materials tend to reflect their extreme geochemical composition. The trace element concentrations in these soils have been shown to be higher than the worldwide average concentrations in non-polluted soils. The Cd concentrations in soils in early summer are higher than those in autumn ; Se concentrations in residual soils are positively related to soil organic matter content.

High Cd and Mo concentrations in some crop plants are related to those in soils. The total Mo and Se concentrations in soils are major factors affecting concentrations in plants. The availability of these elements for plant uptake has been shown to be relatively low in these mainly acid soils and increases with increasing soil pH. Cadmium uptake by plants is not simply linearly related to any one soil factor but is influenced by the total concentrations of Cd in soil, pH, organic matter content and clay content. The speciation of elements and other interacting elements in soils have been considered. Molybdenum and Se concentrations in paddy rice decline with maturity, and decrease in order young shoot > stalk > grain. Unlike Mo and Se, Cd concentrations are higher in rice grain than in rice shoot.

INTRODUCTION

The contents of trace elements in crop plants consumed everyday are related to plant and soil factors (Gissel-Nielsen *et al.*, 1984 ; Friberg *et al.*, 1974 ; Gupta & Lipsett, 1981) and those of soils are influenced by the parent material and the processes of soil formation (FitzPatrick, 1971). Where trace element concentrations are high in the parent rocks, this is likely to influence the composition of the corresponding soils and plants (Thornton, 1983). This paper investigates soil forming factors determining trace element concentrations in soils developed from black shales, and examines soil and plant factors which influence trace element uptake

from these soils into plants. The principal pathways and factors of transfer of trace elements in the rock-soil-plant-human system are shown in Figure 1.

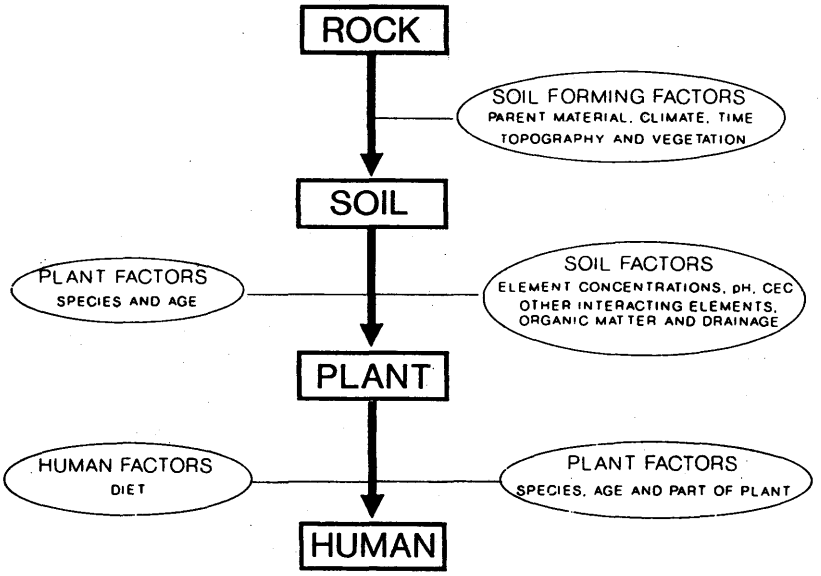

Figure 1: The principal pathways and factors of transfer of trace elements in the rock-soil-plant-human system.

MATERIALS AND METHODS

Sampling of rocks, soils and plants in the Deog-Pyoung area was carried out on transect lines crossing the alluvium lying along tributary drainage valleys (Kim, 1993). Rock samples comprising uraniferous black shales and black slates/grey chlorite schists (> 1 kg) were taken at random from available outcrops. Surface (0 - 15 cm depth) and subsurface (15 - 30 cm depth) soils, and plants were sampled along transect lines. Each surface soil sample comprised a composite of nine subsamples taken from a 2 X 2 metre square. Subsurface soils were composed of at least three subsamples. Rice, tobacco, red pepper and lettuce were sampled where possible on each transect line or from selected gardens in the village of the Deog-Pyoung area. Sample preparation, analytical techniques including acid digestion methods and determination of other parameters are described in detail by Kim (1993). Analytical data were assessed for accuracy and precision using a quality control system integral to the analytical procedure (Ramsey *et al.*, 1987).

SOIL FORMING FACTORS INFLUENCING TRACE ELEMENT CONCENTRATIONS IN SOILS

Parent material

Parent material is defined as the initial state of the soil system (Jenny, 1941). A significant correlation exists between the nature of rocks and their related soils, but the same type of rock can give rise to very different soils depending upon the nature of other soil forming factors, particularly climate (FitzPatrick, 1986).

Comparison of trace element concentrations in rocks and soils: Some beds of black shale are known to contain trace elements in concentrations more than a hundred times their average crustal abundances (Krauskopf, 1956). Soils tend to reflect the extreme geochemical composition of some bedrock types, and trace element concentrations in the soils derived from the black shales are expected to be high (Kim, 1993).
The trace element contents of parent rocks dominate those of soils derived from these (West, 1981). Cadmium, Mo and Se concentrations in uraniferous black shales in Korea (average 6.3 μg Cd g^{-1}, 136 μg Mo g^{-1} and 8.6 μg Se g^{-1}) are higher than those in nearby black slates/grey chlorite schists (0.8 μg Cd g^{-1}, 2.1 μg Mo g^{-1} and 1.1 μg Se g^{-1}) (Kim & Thornton, 1993). This is directly reflected in the trace element concentrations in surface soils (Figure 2), and the trace element concentrations in alluvial soils from the uraniferous black shale area (average 1.2 μg Cd g^{-1}, 63 μg Mo g^{-1} and 1.6 μg Se g^{-1}) are higher than the worldwide average concentrations in non-polluted soils (0.4 μg Cd g^{-1}, 1.5 μg Mo g^{-1} and 0.4 μg Se g^{-1}) (Berrow & Reaves, 1984).

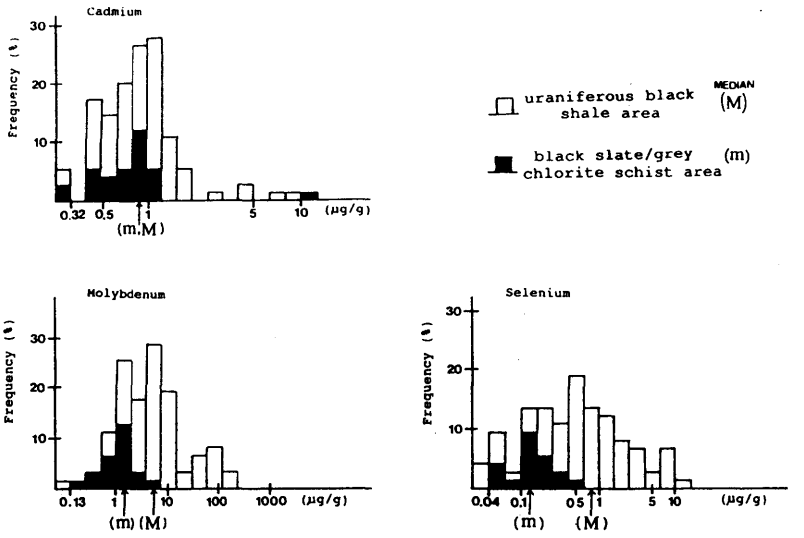

Figure 2: Frequency distribution histogram of Cd, Mo and Se concentrations in surface soils (0 - 15 cm depth) in the Deog-Pyoung area.

Analysis of Variance (ANOVA): The one way analysis of variance (ANOVA) is appropriate to test the hypothesis that the trace element concentrations in alluvial soils derived from different bedrock areas are similar (Davies, 1973). Analysis of variance includes a wide variety of potent statistical procedures dependent on the fact that the total variability in a data set can be divided into parts that arise from different sources. Individual sources of variability can then be assessed relatively to each other (Howarth, 1983). Therefore, variability of trace element concentrations between different bedrock areas can be compared to those within an area.

The hypothesis tested is that trace element concentrations in alluvial soils developed from uraniferous black shales are similar to those from black slates/grey chlorite schists. If the F probability is bigger than 0.05, then the hypothesis is accepted with a 95 % of confidence level, otherwise it is rejected with the same confidence level. From Table 1, the F probabilities for Cd, Mo and Se concentrations are smaller than 0.05, and this suggests that the Cd, Mo and Se concentrations in alluvial soils derived from uraniferous black shales are significantly different to those derived from black slates/grey chlorite schists. The SD ratio is the ratio of the standard deviation for trace element concentrations within one bedrock area to that between two different bedrock areas. The values for Cd and Mo are smaller than that of Se, and this suggests that the influence of different bedrock on the variability of Se concentrations is smaller than that for Cd and Mo concentrations.

Table 1: Analysis of variance (ANOVA) on trace element in surface alluvial soils.

		DF	SS	MS	F (F_{prob})	SD	SD ratio
Cd	Between different bedrock areas	1	1.2	1.2	19.1	0.77	0.33
	Within one bedrock areas	141	9.2	0 07	(0.00*)	0.26	
	Total	142	10.4	0.37			
Mo	Between different bedrock areas	1	6.2	6.2	19.6	1.71	0.33
	Within one bedrock areas	106	33.4	0.32	(0.00*)	0.56	
	Total	107	39.6	0.37			
Se	Between different bedrock areas	1	3.1	3.1	9.8	1.18	0.47
	Within one bedrock areas	119	37.8	0.32	(0.00*)	0.56	
	Total	120	40.9	0.34			

* Significant at P = 0.05

Other soil forming factors

Climate: Climate is the principal factor governing the type and rate of soil formation, as well as being the main agent determining the distribution of vegetation. The climate of an area is a description of the prevailing atmospheric conditions, and for simplicity it is defined in terms of the averages of its components, the two most important being temperature and precipitation (FitzPatrick, 1986).

Climate affects the dispersion of trace elements mainly through its control of the moisture regime. Humid temperature climates provide optimum conditions for chemical dispersion (Rose *et al.*, 1979). In the study areas, trace element concentrations in soils in the summer are highly correlated to those in autumn. In order to avoid sampling and analytical inaccuracies, analytical precision and bias are fully determined using real test materials and

four types of quality control materials over the completed analytical period (Kim, 1993). The Cd and, to a lesser degree, Mo concentrations in soils in early summer are higher than those in autumn (Figure 3). These trends are also found in other black shale areas (Kim, 1993), and concordant with the results that there is a large reduction in Cd contents of topsoils after the monsoon rain in Korea (Moon, 1991). It is hypothesized that during the heavy rainfall in summer, Mo remains relatively mobile as potentially soluble molybdate whilst Cd solubility increases with a low soil pH. Where rainfall exceeds evaporation, readily soluble salts are dissolved by downward percolating water, and over a long period of time, sparingly soluble materials are removed from soils in humid regions. Thus a major effect of leaching is gradually to make the soil more acid leading to the development of a weathered B horizon (Bridges, 1988). In dry season, water movement is upward, so that soluble salts, colloids and small mineral particles tend to be transported into the surface layers (Greensmith, 1988). However, Se concentrations in soils do not change before and after the rainy season because the lowest solubility occurs when the soil is slightly acid (Adriano, 1986).

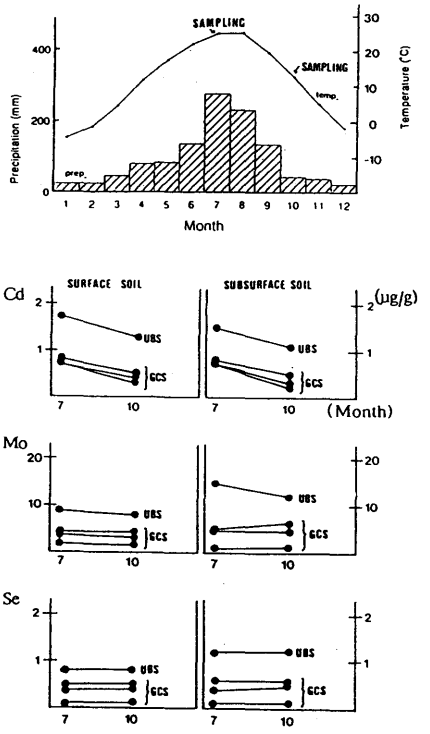

UBS : Uraniferous black shale area
GCS : Black slate/grey chlorite schist area

Figure 3: Seasonal variation of average Cd, Mo and Se concentrations in paddy fields. (Korea Meterological Office, 1991)

Topography: The topography of the region includes the dramatic mountain ranges and the flat featureless plains, both of which gives the impression of considerable stability and seem to be timeless. Topography influences the soil in many ways. For example, the thickness of the soil is often determined by the nature of the relief (FitzPatrick, 1986). It is apparent that relatively high trace element concentrations in rocks are found in the mountainous areas where uraniferous black shale outcrops. However, the trace element concentrations in soils tend to be higher on flat or gently sloping receiving sites as a result of removal of finer grained materials down slope. Lower trace element concentrations are found in strongly sloping ground (Kim, 1993).

Generally, the B horizon gives the best contrast of trace element concentrations (Levinson, 1974). When the trace element concentrations in soils from the uraniferous black shale area are compared with those from the black slate/grey chlorite schist area, the contrasting ratio for both Mo and Se is bigger in subsurface soils than in surface soils (Figure 4). However, this difference is not found for Cd perhaps because of the highly mobile nature of this element in these soils.

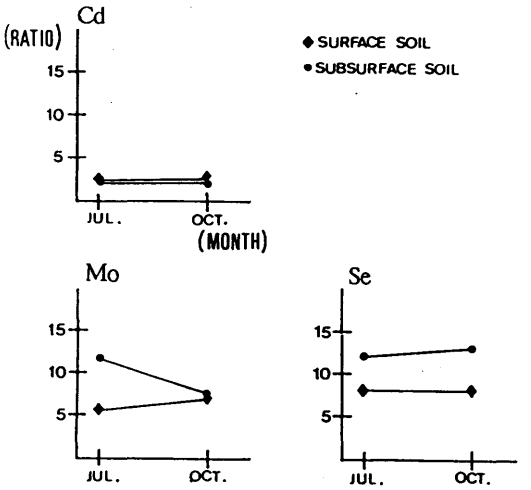

Figure 4: Ratio of trace element concentration in soils from the uraniferous black shale area to those from the black slate/grey chlorite schist area.

Vegetation: Nearly every organism living on the surface of the earth or in the soil affects the development of soils in one way or another (FitzPatrick, 1986). In addition, organic matter content is associated with the distribution and availability of trace elements in soils (Hodgson, 1963). It is evident that organic matter is associated with Se concentrations in residual soils developed from uraniferous black shales. The Se concentrations in soils increase as organic matter contents increase (Figure 5). Selenium is associated with the organic matter in soils via the cycling of the element through decay of plant material (Levesque, 1974). Elevated concentrations of Se in black shales may be attributed to deposition under reducing conditions, induced by the presence of organic matter at the time of formation (Krauskopf, 1979).

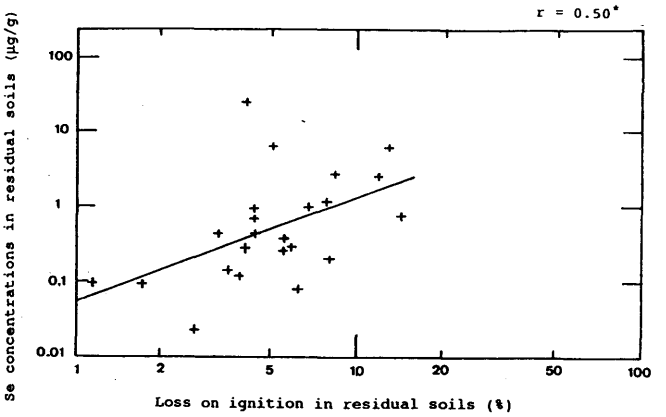

Figure 5: Relationship between Se concentrations and loss on ignition in residual soils.

Time: Time can not be considered in this study because soil formation is a very long and slow process requiring thousands and even millions of years (FitzPatrick, 1986). Generally the accumulation of parent material by weathering of bedrock takes longer than its differentiation into soil horizons (Rose *et al.*, 1979). In the Deog-Pyoung area, most soils have a clearly defined A horizon due to the weathering of the underlying parent material. In some cases there is no distinct B horizon as the soils are relatively young.

THE INFLUENCE OF SOIL AND PLANT FACTORS ON TRACE ELEMENT UPTAKE INTO PLANTS

The role of soil factors in determining trace element concentrations in plants

Factors reported to influence the availability and plant uptake of trace elements in the soil include the trace element concentration, soil pH, organic matter content, cation exchange capacity, speciation of the element, soil redox potential, soil texture and other interacting elements (Street *et al.*, 1978 ; Adriano, 1986 ; Alloway, 1990 ; Lakin, 1972).

Trace element concentrations in soils: Although various soil factors can affect availability, the total amount of the element present in the soil is one of the major factors affecting the trace element contents in plants (Alloway, 1990). Trace element concentrations in plants are generally high where those in soils are high. Selenium concentrations in rice (and tobacco) increase as those in soil increase (Figure 6), whilst Cd and Mo concentrations do not show a significant relationship. When the log transformed data are compared concentrations of Mo in rice are seen to be significantly related to those in soils (Figure 6). There is however no significant correlation between Cd concentrations in plants and soils.
The extractable trace element content in soils is generally a better indicator of trace element phytoavailability than the total content. For example, Browne *et al.* (1984) demonstrated that Cd accumulations in plants grown under greenhouse and aerobic conditions could generally be described by the linear equation of log transformed data. In this present study, the EDTA

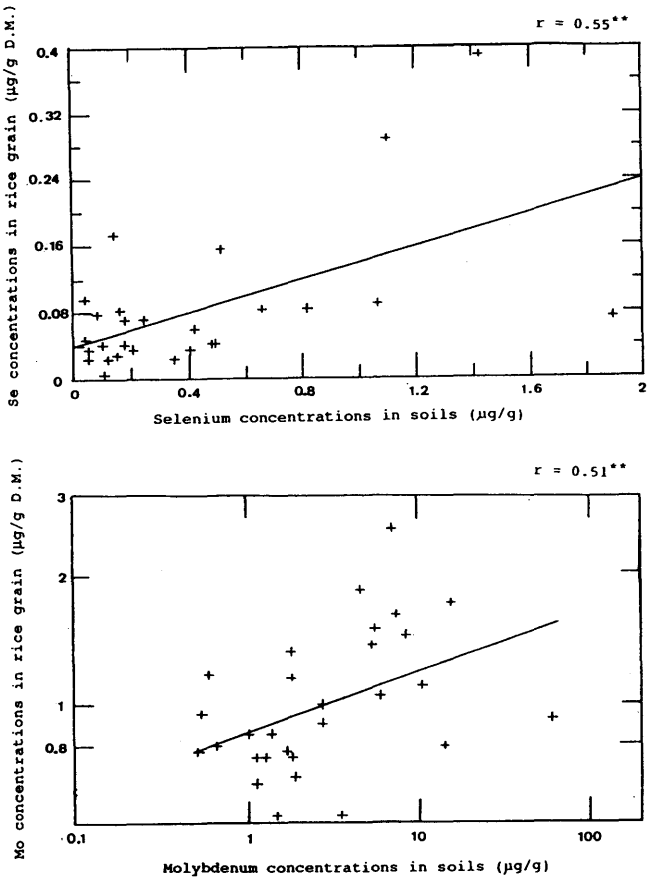

Figure 6: Relationship between trace element concentrations in rice and in soils.

extraction method is used to estimate plant available Cd. The Cd concentration extracted by the EDTA shows a positive relationship with the total Cd concentration in soils. However, no significant relationships are found between Cd concentrations in plants and total or EDTA extractable Cd concentrations in soils possibly because of the limited number of samples examined. The water soluble Cd in soils is also measured for selected soil samples, but most of the measured values are lower than the detection limit of 0.1 µg Cd g^{-1}. Plants were not growing in these soils in which the water soluble Cd contents are higher than the detection limit.

Soil pH: Soil pH appears to be the most important single soil property that determines trace element availability to plants in this study. Soils range from acidic (pH 2.8) to neutral (pH 7.1) with the majority < pH 6.0. Under these conditions the availability of Mo and Se is relatively low. Unlike most other micronutrients, the availability of these two elements in

soils is greatest under alkaline conditions and less under acidic conditions (Adriano, 1986). Although these acidic soils contain high Mo concentrations, the levels of Mo in plants growing in them are not markedly different from those of plants in soils with normal levels of Mo.

Cary & Allaway (1969) measured the Se uptake in alfalfa grown on soils ranging from a pH of 5.4 to 7.8 and found the highest Se concentrations in plants from the high pH soils. Similar results were found for cereals by Linberg and Bingefors (1970). Although it is shown that the rice plant does not reflect an increase in trace elements in the soil to a great extent, the ratio of Se concentrations in rice grain to those in soils increases as soil pH increases. Uptake of trace elements by red pepper is more sensitive to concentration in the soil than rice, and a significant relationship is also found between both Mo and Se concentrations in red pepper and soil pH (Figure 7).

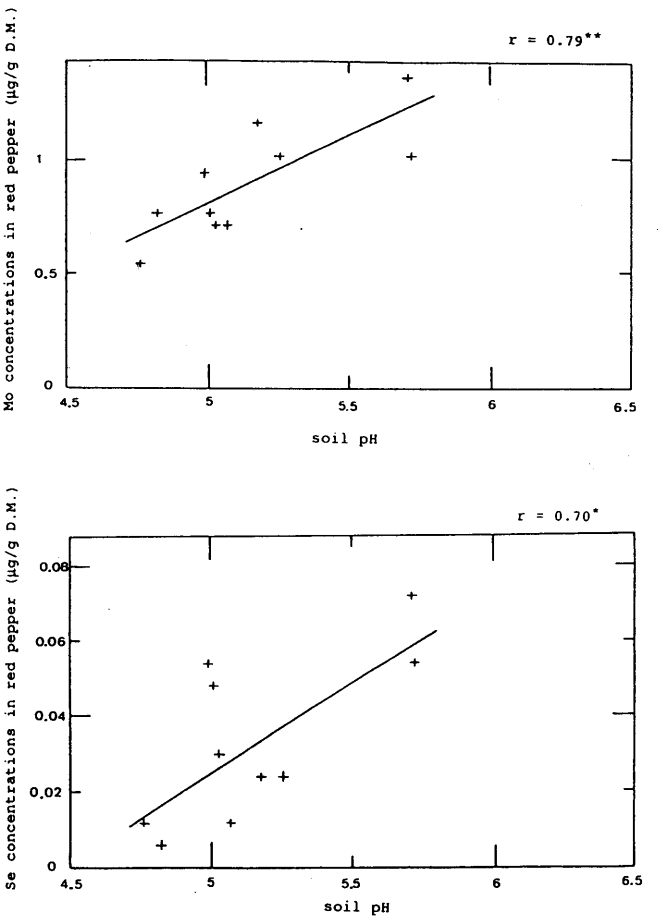

Figure 7: Relationship between trace element concentrations in red pepper and soil pH .

In general, Cd uptake by plants is usually higher in acidic than in alkaline soils (Mahler *et al.*, 1978). However, in this study with few exceptions no relationship is found between Cd concentrations in plants and those in soils. This suggests that the availability of trace elements is also related to other soil factors, and multiple linear regression using soil factors is needed to predict trace element uptake by plants.

Soil type: A higher sorption capacity or bonding energy is associated with fine textured soils or soils with a high organic matter or clay content (John, 1972 ; Andersson, 1977). Soil organic matter is known to adsorb considerable amounts of inorganic cations, including toxic metal ions, by an ion exchange mechanism (Adriano, 1986 ; Alloway, 1990).
The study soils give rise to low Mo contents in plants, because they are generally dry, well drained, acidic and low in organic matter. As the organic matter content of soils increases, Mo concentrations in rice shoots increase (Figure 8). High organic matter apparently increases the soluble Mo content due to its effect on the redox potential and the more rapid reduction of Fe rather than through formation of soluble organic forms of Mo (Adriano, 1986).

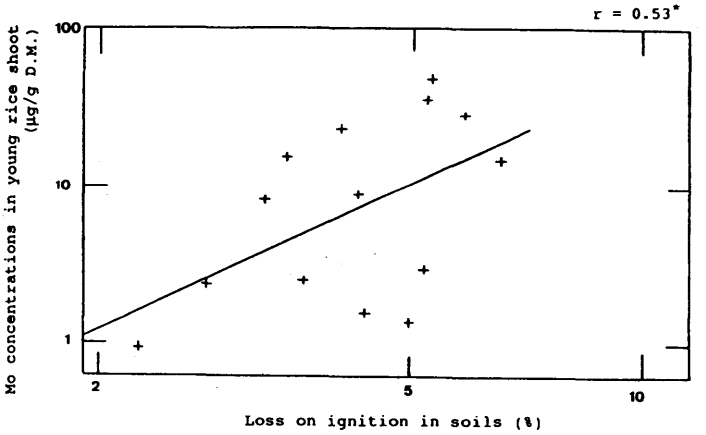

Figure 8: Relationship between Mo concentrations in young rice shoot and loss on ignition in soils.

Selenium uptake by plants is closely related to soil texture (Gissel-Nielsen *et al.*, 1984). In this present study, Se concentrations in tobacco increase where loss on ignition values in soils increase. From the soil textural analysis, most soils in the study areas are sandy loams (Kim, 1993). These are classified as well drained soils (Korea Soil Survey, 1971), and it is possible that some of the Se may be leached from soils under oxidising conditions if it is present as selenate (Adriano, 1986).

Speciation: As indicated above, most of the soils studied are acidic with pH ranging from 4 to 6. Under these conditions in systems exposed to the atmosphere, redox potential may be calculated as to being between 0.3 and 0.53 (V) (Garrels & Christ, 1965).
Cadmium is always divalent and the free ion Cd^{2+} predominates (Brookins, 1988). The free ion Cd^{2+} is more likely to be adsorbed on the surface of the soil solids than other species, such as the neutral or anionic species (Alloway, 1990). Ca^{2+}, Zn^{2+} and H^{+} are present in the soil or can significantly desorb Cd from the soil (Christensen, 1984), resulting in Cd being more mobile in soils and therefore more available to plants than many other heavy metals, including Pb and Cu (Alloway, 1990).
The species of Mo comprising soluble Mo in soils are anionic, with MoO_4^{2-} as the predominant ion (Lindsay, 1972), and MoO_4^{2-}, $HMoO_4^{-}$ and H_2MoO_4 predominating in soils over a pH range of 3 - 7 (Lindsay, 1979), covering the range of soils in the study areas. Molybdate is sorbed strongly by Fe and Al oxides and Mo sorption increases with a decreasing pH of 7.75 to 4.45 (Reisenauer *et al.*, 1962). This sorption mechanism reduces the availability of Mo to plants.
Selenium in these soils would be expected to exist either as selenite (SeO_3^{2-}) or biselenite ($HSeO_3^{-}$) depending on the pH, with $HSeO_3^{-}$ predominant in the soil at pH values of 2.8 - 7.1 (Brookins, 1988). Selenite is fixed in soil to a much greater extent than selenate, therefore, the uptake rate of selenite by plants in the field is much lower than that of selenate (Ganje & Whitehead, 1958). The low solubility of Se in acid soils can be attributed to its presence as selenite in combination with ferric iron or as basic ferric selenite (Adriano, 1986).

Interactions with other elements: In the present study, Cu in soil is found to reduce the uptake of Cd by rice grain and stalk (Kim, 1993). Soil Zn has been found to have an antagonistic effect on the Cd uptake by rice grain between the biological absorption coefficient (Brooks, 1983) of 0 and 2, but no effect in tobacco or red pepper. Lead is shown to have a synergistic effect on Cd uptake by rice grains or stalks (Figure 9) probably due to it being preferentially adsorbed, thus leaving more Cd in solution (Adriano, 1986). Iron in soils inhibits rice grains or stalks taking up Cd from soils.
Bingham & Garber (1960) found a synergistic effect of P fertilization on Mo uptake by orange seedlings in acid soils. In this study, Mo uptake by rice shoot is enhanced with increasing P concentrations in soils (Figure 9). However, Zn in the soil is found to depress Mo uptake by plants ; this may be explained by the influence of Zn ion on the translocation of Mo in plants (Singh and Steenberg, 1975).
The interaction between Se and P in plants has been inconsistent (Carter *et al.*, 1972 ; Levesque, 1974), although in this study the effect of P in soils has a negative effect on the uptake of Se by red pepper.

The role of plant factors in determining the trace element concentrations in plants

Plant species: The concentrations of trace elements in plants vary with the plant species. Many researchers have found lettuce to be one of the greatest accumulators of Cd among food crops (Adriano, 1986). Plant samples may be divided into several groups. Lettuce and tobacco are classified as leafy plants, and paddy rice as grain and cereal products.
Generally leafy plants contain higher levels of trace elements than grain and cereal products (Bosque *et al.*, 1990). Pettersson (1977) found that Cd concentrations are lowest in the grain or cereal products. However, absolute trace element concentrations in plants are not enough

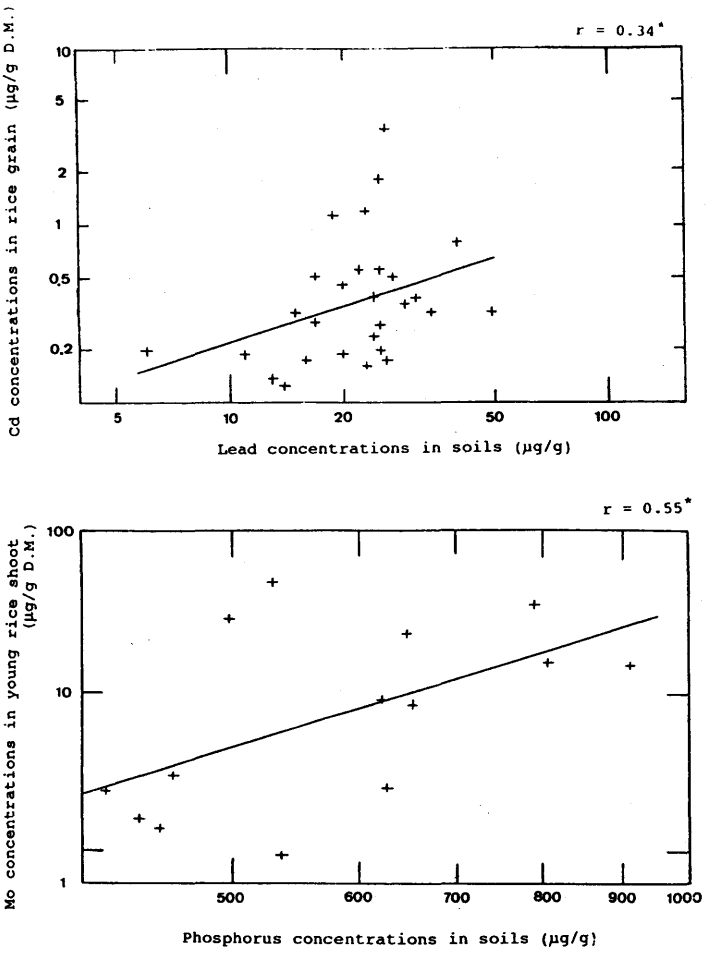

Figure 9: Relationship between Mo concentrations in plants and other interacting elements in soils.

to explain the trace element uptake by plant species. In order to consider the influence of trace element levels in soils on uptake by plants, the biological absorption coefficient (BAC) is used. The BAC is the ratio of trace element contents in plants to those in soils (Brooks, 1983 ; Kabata-Pendias & Pendias, 1984). The relative trace element ratios are found for various plants to be in the order tobacco > rice stalk > lettuce > red pepper > rice grain (Kim, 1993). This indicates that leafy plants such as tobacco and lettuce accumulate trace elements from soil to a greater degree than red peppers and rice grain. Rice shoots show different trends in the BAC compared to other plant species. For example, the average BAC of Mo in rice shoots is exceptionally high, being up to 3.5. Molybdenum is freely taken up by plants and apparently normal plants may exhibit a considerable range of contents. In general,

the greatest concentration of Mo is found in actively growing plant parts (Barshad, 1948) ; the rice shoot is one example (1.4 - 48 μg g^{-1} D.M.). This high concentration in plants may be explained by two possibilities. One is that the requirement for Mo by plants is related to the N supply, because the most important function of Mo in plants is NO_3 reduction (Hagstrom, 1977). High levels may also occur following the application of fertilizers containing Mo or the addition of lime to high Mo acid soils. Soils naturally high in available Mo, or contaminated by appropriate organic residues may also produce forage with unacceptably high Mo content (Gupta & Lipsett, 1981).
Some plant species including rice shoots are known to accumulate high levels of Mo. Symptoms of toxicity in plants under field conditions are very rare (Allaway, 1977 ; Gupta *et al.*, 1978), whereas toxicities in ruminant animals feeding on forage high in this element are well known (Miltimore & Mason, 1971).

Plant parts: Because of genetic variation among cultivars within a plant species, differences in Cd uptake and accumulation in various plant parts have been observed for rice and lettuce (Kitagishi & Yamane, 1981 ; John & VanLaerhoven, 1976)
The Mo content of leaves is found to decrease with maturity, and the Mo concentrations in paddy rice shown to decrease in the order shoot > stalk > grain (Figure 10). Selenium

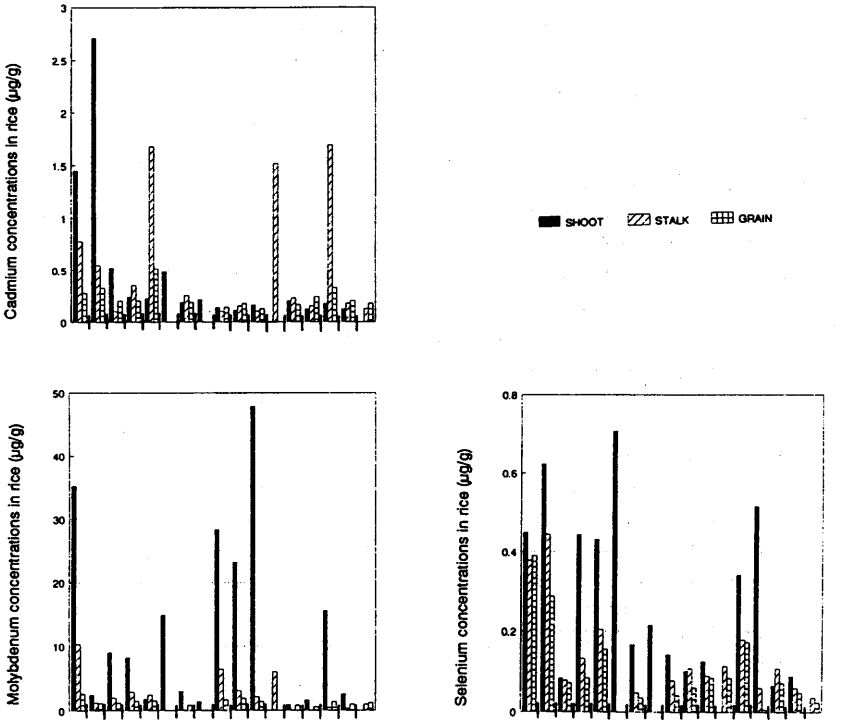

Figure 10: Variation of Cd, Mo and Se concentrations in rice parts (No. of rice: 17).

concentrations in plant tissues usually decline with maturity (Rosenfeld & Beath, 1964), and the Se concentration in paddy rice indicates that Se levels are highest in young rice shoots (Figure 10).

Cadmium concentrations are lower in seeds relative to the concentrations in other plant parts such as leafy tissues (Adriano, 1986). Unlike Mo and Se concentrations in paddy rice, Cd concentrations increase with plant maturity. As a major component of the Korean diet, rice grain is of paramount importance in determining the Cd accumulation in the human body (Kim, 1993).

CONCLUSIONS

(a) Cadmium, Mo and Se concentrations in the Okchon uraniferous black shales are significantly higher than in other rocks studied ; soils derived from these parent materials in general reflect their extreme geochemical composition. Cadmium and Mo concentrations in soils in summer are higher than those in autumn. Selenium concentrations in residual soils are positively related to soil organic matter content.

(b) Although various soil factors affect the availability of the trace element in these areas, it has been shown that the total Mo and Se concentrations in soil are the major factors affecting concentrations in plants. However, no significant correlation is found between total Cd concentrations in soils and plants. Cadmium extracted by EDTA shows a positive relationship to total Cd concentrations in soil, whilst most of the water soluble Cd concentrations are below the detection limit of 0.1 $\mu g\ g^{-1}$.

(c) Levels of Mo and Se in plants growing in these soils are not different from those of normal plants because the availability of Mo and Se is relatively low in the mainly acid soils over the pH range of 2.8 to 7.1. The uptake of these elements in plants increases with increasing soil pH. However, Cd uptake by plants is higher in acidic conditions and also relates to other soil factors.

(d) When values for loss on ignition in soil increase, Mo and Se concentrations in some plants also increase indicating a positive effect of soil organic matter on the availability of these two elements. Cadmium uptake by plants is not simply related to the organic matter content.

(e) Soil Cu, Zn and Fe inhibit uptake of Cd into rice stalk and grain, though Zn has no effect on the Cd content of tobacco and red pepper. Lead has a synergistic effect on the Cd uptake by rice grain and stalk. Molybdenum uptake by young rice shoot is enhanced with increasing P concentrations in soil but the effect of P in soil has a negative effect on the uptake of Se by red pepper.

(f) Trace element concentrations in plants also vary depending on plant species or parts. Leafy plants such as tobacco and lettuce accumulate Cd, Mo and Se. The greatest concentrations of Mo are found in actively growing plants such as the young rice shoot. Molybdenum and Se concentrations in paddy rice decline with maturity, and decrease in the order young shoot > stalk > grain. Unlike Mo and Se, Cd concentrations are higher in rice grain than in rice shoot.

ACKNOWLEDGEMENTS

I am grateful to the staff of the Environmental Geochemistry Research Group particularly Dr. Mike Ramsey, Barry Coles and Alban Doyle. I also wish to express my gratitude to Professor Hyo-Taek Chon and all members of the Applied Geochemistry Group at Seoul National University for their valuable support during the field and laboratory work in Korea.

REFERENCES

Adriano, D.C. 1986. *Trace Elements in the Terrestrial Environment.* Springer-Verlag, New York.

Allaway, W.H. 1977. Perspectives on molybdenum in soils and plants. In: *Molybdenum in the Environment, vol.2*, W.R. Chappell & K.K. Petersen (eds.), Dekker Inc., New York; 317-339.

Alloway, B.J. 1990. *Heavy Metals in Soils.* Blackie & Son, Glasgow.

Andersson, A. 1977. Heavy metals in Swedish soils ; on their retention, distribution and amounts. *Swedish J. Agric. Res.*, 7; 7-20.

Barshad, I. 1948. Molybdenum content of pasture plants in relation to toxicity to cattle. *Soil Sci.*, 66; 187-195.

Berrow, M.L. & Reaves, G.A. 1984. Background levels of trace elements in soils. In: *Proc. Int. Conf. Environ. Contamination*, R. Perry (ed.), CEP Consultants Ltd., Edinburgh; 333-340.

Bingham, F.T. & Garber, M.J. 1960. Solubility and availability of micronutrients in relation to phosphorus fertilization. *Soil Sci. Soc. Am. Proc.*, 24; 209-213.

Bosque, M.A., Schuhmacher, M., Domingo, J.L. & Llobet, J.M. (1990) Concentrations of lead and cadmium in edible vegetables from terragona province, Spain. *Sci. Total Environ.*, 95; 61-67.

Bridges, E.M. 1988. *World Soils (2nd ed.).* Cambridge University Press, Cambridge.

Brookins, D.G. 1988. *Eh-pH Diagrams for Geochemistry.* Springer-verlag, Heidelberg.

Brooks, R.R. 1983. *Biological Methods of Prospecting for Minerals.* John Wiley & Sons, New York.

Browne, C.L., Wong, Y.M. & Buhler, D.R. 1984. A predictive model for the accumulation of cadmium by container-grown plants. *J. Environ. Qual.*, 13; 184-188.

Carter, D.L., Robbins, C.W. & Brown, M.J. 1972. Effect of phosphorus fertilization on the selenium concentration in alfalfa. *Soil Sci. Soc. Am. Proc.*, 36; 624-628.

Cary, E.E. & Allaway, W.H. 1969. The stability of different forms of selenium applied to low-selenium soils. *Soil Sci. Soc. Am. Proc.*, 33; 571-574.

Christensen, T.H. 1984. Cadmium soil sorption at low concentrations ; I. Effect of time, cadmium load, pH and calcium. *Water, Air, Soil Pollut.*, 21; 105-114.

Davies, J.C. 1973. *Statistics and Data Analysis in Geology.* John Wiley & Sons, New York.

FitzPatrick, E.A. 1971. *Pedology.* Oliver & Boyd, Edinburgh.

FitzPatrick, E.A. 1986. *An Introduction to Soil Science (2nd ed.).* Longman Scientific & Technical, New York.

Friberg, L., Piscator, M., Nordberg, G.F. & Kjellstrom, T. 1974. *Cadmium in the Environment (2nd ed.).* CRC Press, Ohio.

Ganje, T.J. & Whitehead, E.I. 1958. Selenium uptake by plants as affected by the forms of selenium in the soil. *Proc. South Dakoda Acad. Sci.*, 37; 85-88.

Garrels, R.M. & Christ, C.L. 1965. *Solutions, Minerals and Equilibria*. Harper & Row, New York.

Gissel-Nielsen, G., Gupta, U.C., Lamand, M. & Westermarck, T. 1984. Selenium in soils and plants and its importance in livestock and human nutrition. *Adv. Agron.*, 37; 397-460.

Greensmith, J.T. 1988. *Petrology of the Sedimentary Rocks (7th ed.)*. Unwin Human Ltd., London.

Gupta, U.C., Chipman, E.W. & Macky, D.C. 1978. Effects of molybdenum and lime on the yield and molybdenum concentrations of crops grown on acid sphagnum peat soil. *Can. J. Plant Sci.*, 57; 983-992.

Gupta, U.C. & Lipsett, J. 1981. Molybdenum in soils, plants and animals. *Adv Agron.*, 34; 73-115.

Hagstrom, G.R. 1977. A closer look at molybdenum. *Fert. Solutions*, 21/4; 18-28.

Hodgson, J.F. 1963. Chemistry of the micronutrient elements in soils. *Adv. Agron.*, 15; 119-159.

Howarth, R.J. 1983. *Handbook of Exploration Geochemistry, vol.2 - Statistics and Data Analysis in Geochemical Prospecting*. Elsevier, Amsterdam.

Jenny, H. 1941. *Factors of Soil Formation*. McGraw-Hill, New York.

John, M.K. 1972. Cadmium adsorption maxima of soils as measured by the langmuir isotherm. *Can. J. Soil Sci.*, 52; 343-350.

John, M.K. & VanLaerhoven, C.J. 1976. Differential effects of cadmium on lettuce varieties. *Environ. Pollut.*, 10; 163-173.

Kabata-Pendias, A. & Pendias, H. 1984. *Trace Elements in Soils and Plants*. CRC Press, Florida.

Kim, K.W. & Thornton, I. 1993. Influence of Ordovician uraniferous black shales on the trace element composition of soils and food crops, Korea. *Appl. Geoche.*, Supplement 2; 249-255.

Kim, K.W. 1993. Influence of uraniferous black shales on trace elements in soils and crops in Korea. PhD thesis, University of London.

Kitagishi, K. & Yamane, I. 1981. *Heavy Metal Pollution in Soils of Japan*. Japan Sci. Soc. Press, Tokyo.

Korea Meteorological Office 1991. *Climatological Standard, Normals of Korea, vol. 2*. Meterological Office, Seoul (in Korean).

Korea Soil Survey. 1971. *Reconnaissance Soil Map - Chung Cheong Bug Do*. Office of Rural Development, Suweon (in Korean).

Krauskopf, K.B. 1956. Sedimentary deposits of rare metals. *Econ. Geol.*, 50th Anniv. Vol.; 411-463.

Krauskopf, K.B. 1979. *Introduction to Geochemistry (2nd ed.)*. Mc-Graw Hill, New York.

Lakin, H.W. 1972. Selenium accumulation in soils and its absorption by plants and animals. *Geol. Soc. Am. Bull.*, 83; 181-190.

Levesque, M. 1974. Selenium distribution in Canadian soil profiles. *Can. J. Soil Sci.*, 54; 63-68.

Levinson, A.A. 1974. *Introduction to Exploration Geochemistry*. Applied Publishing Ltd., Calgary.

Lindberg, P. & Bingefors, S. 1970. Selenium levels in forages and soils in different regions of Sweden. *Acta Agric. Scand.*, 20; 133-136.

Lindsay, W.L. 1972. Inorganic phase equilibria of micronutrients in soils. In: *Micronutrients in Agriculture*, J.J. Mortvedt, P.M. Giordano & W.L. Lindsay (eds.), Soil Sci Soc Am., Madison; 41-57.

Lindsay, W.L. 1979. *Chemical Equilibria in Soils.* Wiley, New York.

Mahler, R.J., Bingham, F.T. & Page, A.L. 1978. Cadmium-enriched sewage sludge application to acid and calcareous soils ; Effects on yield cadmium uptake by lettuce and chard. *J. Environ. Qual.*, 7; 274-281.

Miltimore, J.E. & Mason, J.L. 1971. Copper to molybdenum ratio and molybdenum and copper concentrations in ruminant feeds. *Can. J. Anim. Sci.*, 51; 193-200.

Moon, C.H., Lee, Y.S. and Yoon, T.H. 1991. Seasonal variation of heavy metal contamination of topsoils in the Taejun-industrial complex (II). *Environ. Tech.*, 12; 413-419.

Pettersson, O. 1977. Differences in cadmium uptake between some plant species and cultivars. *Swedish J. Agric. Res.*, 7; 21-24.

Ramsey, M.H., Thompson, M. & Banerjee, E.K. 1987. Realistic assessment of analytical data quality from inductively coupled plasma atomic emission spectrometry. *Anal. Proc.*, 24; 260-265.

Reisenbauer, H.M., Tabilch, A.A. & Stout, P.R. 1962. Molybdenum reactions with soils and the hydrous oxides of iron, aluminum and titanium. *Soil Sci. Soc. Am. Proc.*, 26; 23-27.

Rose, A.W., Hawkes, H.E. & Webb, J.S. 1979. *Geochemistry in Mineral Exploration.* Academic Press, London.

Rosenfeld, I. & Beath, O.A. 1964. *Selenium ; Geobotany, Biochemistry, Toxicity, and Nutrition.* Academic Press, London.

Singh, B.R. & Steenberg, K. 1975. Interactions of micronutrients in barley grown on zinc-polluted soils. *Soil Sci. Soc. Am. Proc.*, 39; 674-679.

Street, J.J., Sabey, B.R. & Lindsay, W.L. 1978. Influence of pH, phosphorus, cadmium, sewage sludge, and incubation time on the solubility and plant uptake of cadmium. *J. Environ. Qual.*, 7; 286-290.

Thornton, I. 1983. Geochemistry applied to agriculture. In: *Applied Environmental Geochemistry*, I. Thornton (ed.), Academic Press, London; 231-266.

West, T.S. 1981. Soil as the source of trace elements. *Phil. Trans. R. Soc. Lond.*, B294; 19-39.

Section 3 :

WATER RESOURCES MANAGEMENT AND GROUNDWATER HYDROLOGY IN FRACTURED ROCKS

GROUND WATER ABSTRACTION FROM SHALLOW UNCONFINED DECCAN BASALTIC AQUIFERS OF MAHARASHTRA, INDIA

H. KULKARNI & S.B. DEOLANKAR
Department of Geology, University of Poona,
Pune - 411 007, India

ABSTRACT. Shallow unconfined Deccan basaltic aquifers tapped through large diameter dug wells, constitute an important source of water supply in Maharashtra State, India. Lithological variation, coupled with varied weathering and jointing patterns attribute a high degree of inhomogeneity to the Deccan basalts. This inhomogeneous character causes yields of wells tapping the Deccan basaltic aquifer(s) to vary over a contiguous area. Well yields influence ground water abstraction and hence control the agricultural support of different wells (area irrigated and the type of crops sustained). Well hydrographs, supported by lithology, can help to understand the relationship between the yields of different wells and their agricultural support. The regulation of ground water abstraction in light of the hydrogeological factors controls the agricultural sustenance of a well, particularly under drought conditions. This regulation of crops grown on a well.

INTRODUCTION

The Deccan basalts of west-central India cover an area of over 500,000 km^2. These basalts from an important source of water supply as shallow unconfined aquifers. The erratic rainfall pattern, along with the low ground water recharge - from 7 to 12 % (Lerner et al., 1990; Athavale et al., 1992) - subjects the Deccan basaltic region to frequent droughts.

In addition to the vagaries of the monsoon, the Deccan basalts exhibit a complex geometry, especially in context to ground water occurrence. This uneven and complex geometry of Deccan basalt units contributes to hindrances in ground water exploration in this region (Kale et al., 1992). A variation in their weathering and jointing properties causes a high degree of inhomogeneity in the hydrogeological characteristics of different Deccan basaltic units. However, in spite of such highly inhomogeneous conditions, the shallow Deccan basaltic aquifers constitute the only source of water in many areas, both, for agricultural and domestic purposes.

The agricultural patterns in many contiguous tracts from the Deccan basaltic province are completely influenced by ground water potentials (yields) of wells tapping the shallow Deccan basaltic aquifers. The present paper attempts to highlight how the variation in hydrogeological factors influences the ground water abstraction for agriculture, from a shallow unconfined Deccan basaltic aquifer. The aquifer forms a part of a typical lithological setup with a recurrence pattern over the Deccan basaltic terrain of Maharashtra State, India.

TYPICAL LITHOLOGICAL PATTERN

The Deccan basalts, on the basis of their physical character, can be broadly classified into :-

i) the vesicular-amygdaloidal type

ii) the finer grained dense-compact type

The vesicular-amygdaloidal basalts are typically characterized by the presence of vesicles and/or amygdales. Generally, the top and (very often) the bottom portions of these basalt units are vesicular. A vesicular-amygdaloidal basalt unit is strewn with a single basalt unit vary in size and number (both laterally and vertically). Another noteworthy feature of the vesicular-amygdaloidal basalts is the presence of varying amounts of tuffaceous material within these units. The vesicular-amygdaloidal basalts are capped by red tuffaceous material within these units. The vesicular-amygdaloidal basalts are capped by red tuffaceous layers which act as reliable marker horizons. The vesicular-amygdaloidal basalts are prone to sub-horizontal sheet jointing. These sheet joints are apparent as isolated joints as well as a network of interconnected joints.

The fine grained dense-compact basalts are very low in amygdale content, except at the base which is marked by pipe shaped amygdales. Their top portions are jointed, the joints being essentially subvertical in disposition. These top jointed portions grade downward into a fairly unjointed dense basalt.

An fine sequence of vesicular-amygdaloidal basalts (capped by red tuffaceous layers) and dense-compact basalts is widely observed over the Deccan basaltic province, especially around Pune, Ahmednagar and Solapur (Kulkarni, 1987). The degree of development of sheet jointing, subvertical jointing and the complex jointing pattern at the contacts between different basalt units governs the accumulation and movement of ground water in the Deccan basalts.

A typical lithological setup is constituted within the above sequence when a vesicular-amygdaloidal basalt (capped by a red tuffaceous layer) is underlain by a dense-compact basalt. Such a lithological setup was studied to ascertain how hydrogeological factors influence ground water abstraction and agricultural support.

HYDROGEOLOGY OF STUDY AREA

The study area lies about 50 km NNE of Pune city (Figure 1). The main occupation of the people from Pabal and the nearby inhabitations is farming. The area receives an average annual rainfall of 550 mm. Pabal village lies in the Vel river, a tributary of the Bhima.

The Vel river basin shows an alternating sequence of vesicular-amygdaloidal and dense-compact basalt types, the former being capped by red tuffaceous horizons (Figure 1). In the study area (Pabal area), this alternating sequence is represented by five mappable basaltic units (Figure 2). The vesicular-amygdaloidal basalts (unit 1,3 and 5) are comparatively more inhomogeneous and coarser grained than the dense-compact basalts (units 2 and 4).

The amygdaloidal basaltic unit 3 (referred to henceforth as the "amygdaloidal basalt unit") and the jointed upper portion of the underlying compact basaltic unit 2 (referred to henceforth as "jointed basalt unit") constitute the shallow unconfined aquifer in the Pabal area. This aquifer is tapped through over 200 dug wells (Figure 2). Many of these dug wells tap only the amygdaloidal basalt unit as the unconfined aquifer as they are not deep enough to have penetrated the underlying jointed basalt unit, e.g. wells numbered 72, 73, 99 and 112. In portions of lower elevations (lower than 670 m above msl) - where the jointed basalt is exposed at the surface - wells tap only the jointed basalt unit as the unconfined aquifer, e.g. wells numbered 125, 126 and 127. Only a few wells in the area penetrate and therefore, tap both the amygdaloidal and jointed basalt units together as the unconfined aquifer, e.g. well numbered 29, 85 and 146.

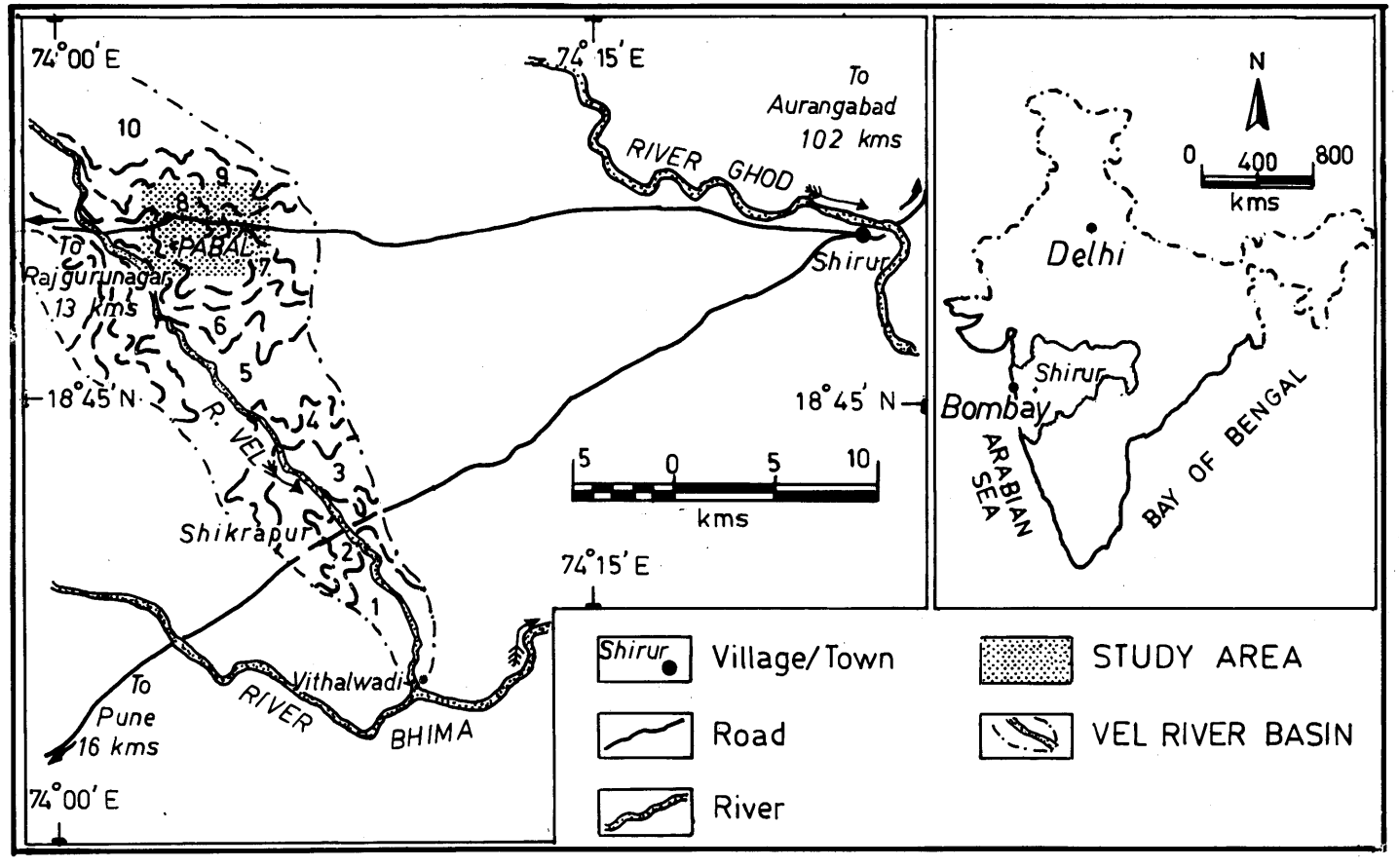

Figure 1: Location map of study area. The Vel river basin shows 10 Deccan basaltic units. Units 1,3,5,7 and 9 are dense compact basalts and 2,4,6,8 and 10 are vesicular-amygdaloidal basalts. The vesicular-amygdaloidal basalts are capped by red tuffaceous layers.

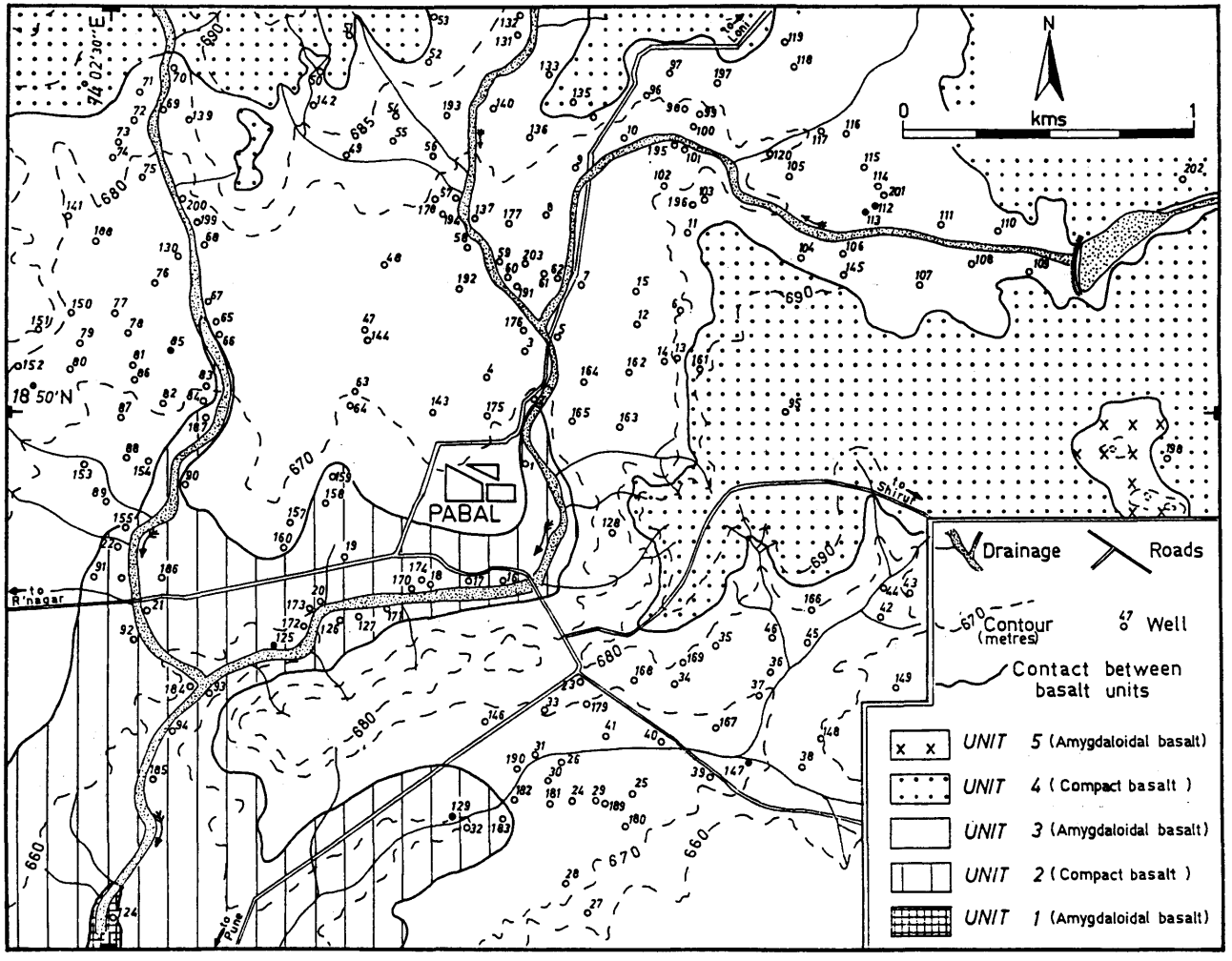

Figure 2: Hydrogeological map of Pabal area. Unit 1 and 3 are capped by red tuffaceous layers. Shaded circles represent wells discussed as type cases in text.

The accumulation and movement of ground water in this shallow basaltic aquifer is subject to the degree of development of the following openings:

a) the sub-horizontal sheet joints of the amygdaloidal basalt unit;

b) the sub-vertical sheet joints of the amygdaloidal basalt unit;

c) the contact zone between the amygdaloidal and jointed basalt units.

These three types of openings represent the "inflow zones" in different wells (Kulkarni and Deolankar, 1990). Inflow zones openings through which water enters a well. The degree of development of these inflow zones in wells depends upon the lithological conditions prevailing in different parts of the area and hence the degree of development of inflow zones in dug wells from the Pabal area is variable. For instance, wherever the thickness of the amygdaloidal basalt unit is substantial (and shows an increased amount of associated tuffaceous material), sheet joints are prolifically developed along the well face (wells numbered 99, 112, 113 and 195). In areas where the thickness of the amygdaloidal basalt unit is reduced due to its undulating contact with the underlying jointed basalt unit, there is a restricted sheet joint development in wells (wells numbered 11, 72 and 73). Further, sheet joints get accentuated due to the interaction between the rock matrix and circulating ground water. the accentuation may result in the widening of the sheet joints along the well face (Kulkarni, 1987 and Kulkarni and Deolankar, 1990).

WELL YIELDS

Inhomogeneity in the hydrogeological properties of the Deccan basalts (such as the varied inflow zone development in wells) causes a variation in well yields in an area. Well yields depend upon the number of inflow zones tapped by the well, their aperture and the quantum of inflow through them. Further, this variation is bound to affect the agricultural output in the area (each well will have an agricultural output that is dependent upon its capacity to yield water).

In order to quantify well yields to obtain an index for correlation, a parameter called "Infiltration index" was adopted. Infiltration index denotes the Specific capacity of a dug well per unit aquifer surface area tapped (Deolankar, 1979). this parameter takes care of large diameter of well and the saturated thickness tapped saturated thickness tapped by the well.

Infiltration index values were calculated for 65 dug wells from the area using well-test data. A few values for representative dug wells have been listed in Table 1. The table also gives a summary of the draught for these wells, representing the ground water abstraction.

AGRICULTURAL SUPPORT

Variable agricultural support over the Deccan basaltic terrain can be correlated to the varied well potentials (Deolankar and Kulkarni, 1985). The agricultural support of a well is the area irrigated (in hectares) along with the number and type of crops (cropping pattern) that it can sustain during the course of a single year. Three crops are usually cultivated over a period of one year (beginning at the onset of the monsoon). The monsoon crop (June-September/October), called the "Kharif", is only marginally supported by ground water. The winter crop (November-February), called the "Rabi" and the summer crop (March-May) are fully supported by ground water obtained from pumping different wells.

Singhal et al.(1987) have studied the effects of draught and ground water draught on a ground water regime from a hard rock terrain of south India. Their study indicates that the Kharif crop requirement (for about 1 hectare) of ground water in this area is 51 pumping hours per week whereas the Rabi crop requirement (for about 1 hectare) is 81 pumping hours per week at a pumping rate of 4.5 m^3/hour.

The relationship between well yields (as a response to the hydrogeological properties), ground water abstraction and the agricultural support can be well illustrated over a two year cycle. Pabal receives an (average) normal annual rainfall of 550 mm. In Pabal, the first year (1984), which showed a more than average annual rainfall (717 mm) was followed by a low annual rainfall year (1985), showing average annual rainfall of 308 mm. The well hydrographs for a few representative wells, over this two year period are illustrated in Figure 3 (a,b,c,d,e and f). The plots also illustrate the lithology of each well, with the disposition of inflow zones along the vertical section of the well.

The plots (Figure 3) show the response of wells to ground water recharge and ground water abstraction. Each plot shows how ground water recharge from more than average rainfall (during 1984) raised water levels in most wells to within 2 m of the ground level (just after the rainy season). Subsequently, during the winter period of 1984 and the following summer period of 1985, ground water abstraction from the wells, for agricultural support, resulted in the water levels falling in these wells. The plots further show that the average rainfall during 1985 was less than normal and therefore, the ground water recharge was limited. Each well, as a consequence, recorded a water level rise of only a couple of meters (decipherable after the rainy season). Ground water abstraction (under the limited ground water recharge), during the following winter (1985), and summer (1986) caused water levels in wells to fall further, even drying up many wells during the course of the year.

Table 1 and Table 2 give details regarding Infiltration index, weekly ground water abstraction and agricultural support (both winter and summer) for representative dug wells from the study area. The degree of saturation and the operativeness of inflow zones that a well maintains at the end of summer (end May) each year can form a measure of its ground water abstraction and well yield. Well from the Pabal area exhibit a fair amount of variation (Table 1) insofar as ground water abstraction is concerned (130-2500 m^3/week). This variation is particularly significant in light of the cropping pattern during the two year period of study. Abstraction of ground water for agriculture causes a depletion of saturation in wells during summer, thereby rendering some or all inflow zones in many wells inoperative (e.g. well numbered 129 and 85). On the other hand, there are wells (e.g. wells numbered 147 and 113) which, even in summer, maintain some saturation with at least some inflow zones remaining operative.

The variable cultivation patterns in the study area a direct consequence of the hydrogeological variations in different wells (the inflow zone configuration being the most important). In order to study the ground water abstraction in response to these hydrogeological conditions, three comparisons are presented below.

a) Wells numbered 112 and 113

Located very near each other (Figure 2), both these wells tap the amygdaloidal basalt unit dominantly as the aquifer [refer lithological section in Figure 3(a) and 3(b)]. Table 1 indicates a high ground water draught for both these wells (more than 2000 m^3/week). Both wells, on the whole, support high water requirement crops like corn, potatoes and sugarcane (Table 2).

Table 1: Ground water abstraction for typical dug wells from Pabal area (ascertained during summer of 1985).

Well No.	Pumping hours/week	Ave. pumping rate (m^3/hour)	Ave weekly abstraction (m^3/week)	Aquifer units (Inflow zones)
112	49	42	2058	Ab (S)
99	42	35	1486	Ab (S)
115	8	39	312	Ab (S) + C
113	60	42	2520	Ab (S) + C
103	8	40	321	Ab (S) + C
193	25	32	810	Ab (S) + C
180	5	27	135	Jb (J)
125	6	33	198	Jb (J)
129	4	33	132	Jb (J)
85	28	43	1192	Ab (S) + C + Jb (J)
147	7	41	290	Ab (S) + C + Jb (J)

Ab = Amygdaloidal basalt unit
Jb = Jointed basalt unit
S = Sheet joint
C = Contact zone
J = Joints (in Jb)

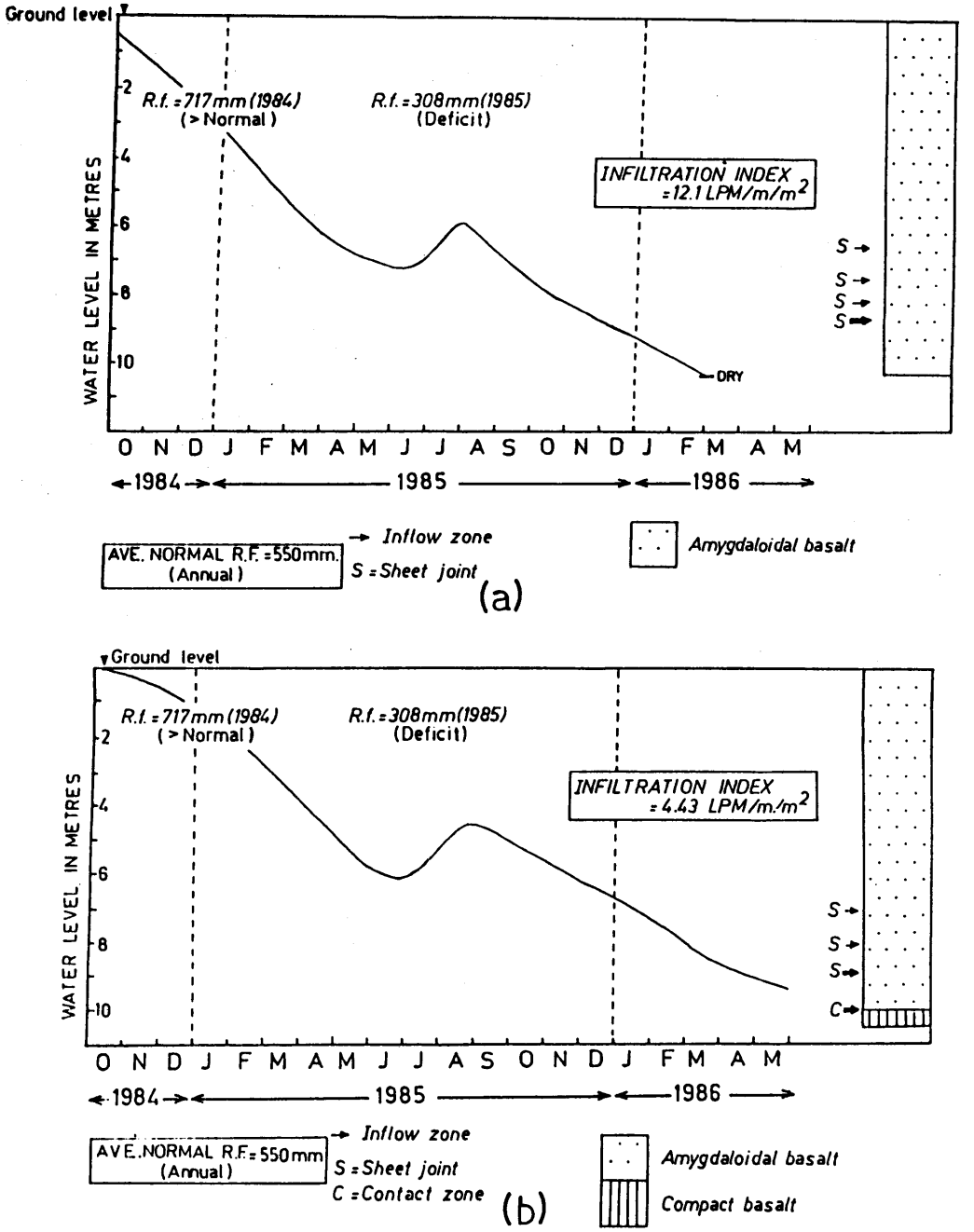

Figure 3: (a) Well numbered 112 and (b) Well numbered 113.

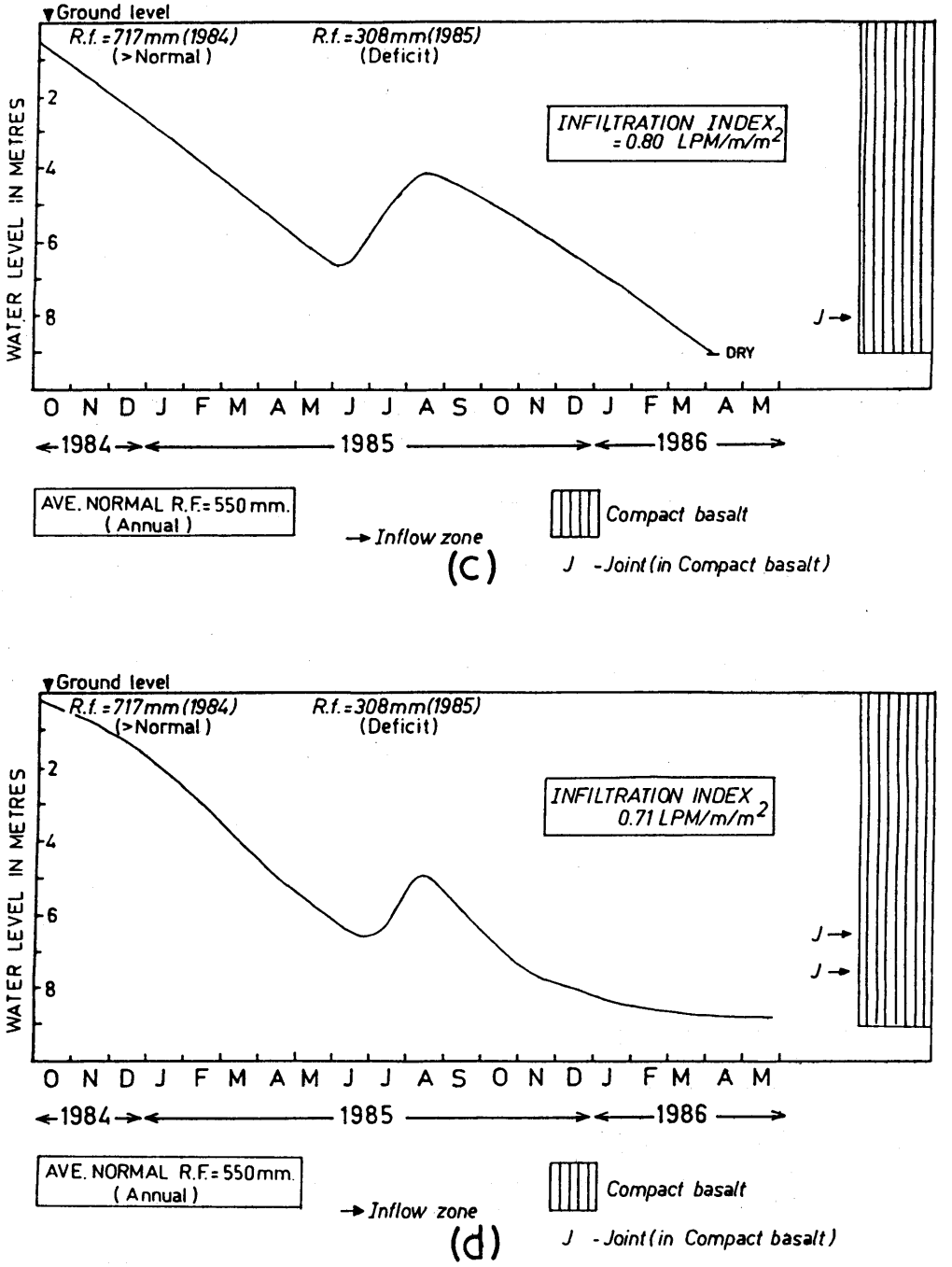

Figure 3: (c) Well numbered 125 and (d) Well numbered 129.

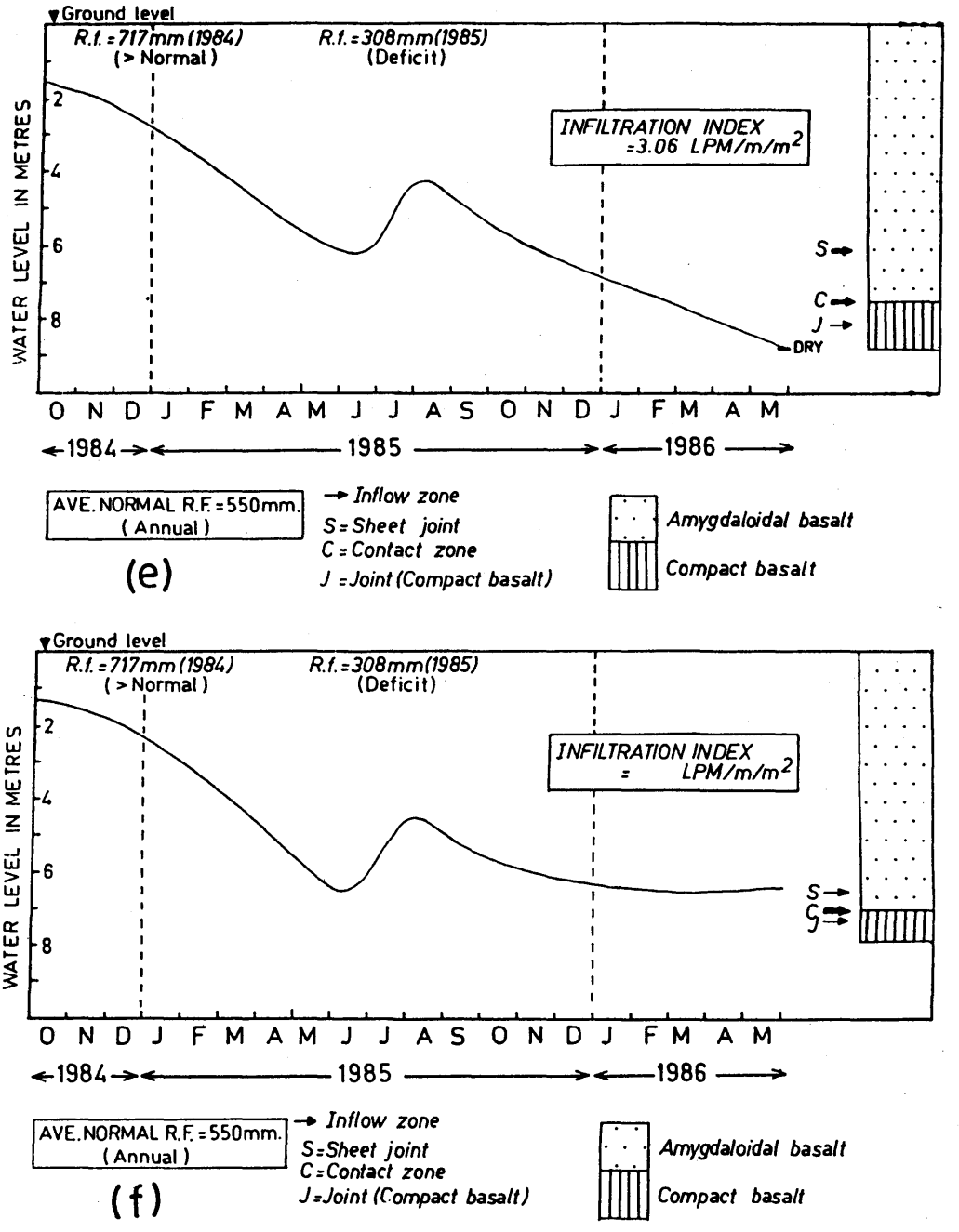

Figure 3: (e) Well numbered 85 and (f) Well numbered 147.

Table 2: Agricultural support for typical dug wells from Pabal area.

Well No.	Aquifer Units (inflow zones)	Infiltration Index ($LPM/m/m^2$)	1984 - 85 Winter CU	1984 - 85 Winter Crop	1984 - 85 Summer CU	1984 - 85 Summer Crop	1985 -86 Winter CU	1985 -86 Winter Crop	1985 -86 Summer CU	1985 -86 Summer Crop
112	Ab (S)	12.10	10.0	C,P,O, G,V	4.0	P,O,F	4.0	C,O, V,Fg	-	-
99	Ab (S)	4.43	3.0	C,O,F,	2.0	Ch,F, Fg	1.5	C,O,F,	0.5	V,F,Fg
115	Ab (S),C	1.23	1.5	C	1.0	Ch,F, Fg	0.5	V,Fg	0.02	Fg
113	Ab (S),C	3.26	2.5	C,V,S	2.0	O,Ch,S	1.0	C,V,S	0.8	C,V,Fg
103	Ab (S),C	0.65	0.5	C,P,O	0.25	O,Ch	0.25	Ch,Fg	-	-
193	Ab (S),C	3.17	1.0	C,P,O	0.5	O,Ch,F	0.5	V,Fg	-	-
180	Jb (J)	0.35	1.0	C,P,O	-	-	-	-	-	-
125	Jb (J)	0.78	1.5	C,P,O,V	-	-	0.25	Fg	-	-
129	Jb (J)	0.71	0.5	C,P,O	0.25	Ch, Fg	0.25	C	-	-
85	Ab(S),C, Jb (J)	3.06	2.5	C	1.0	C,O	1.0	C	-	-
147	Ab(S),C, Jb (J)	1.00	1.0	C,O,G	0.5	V,Ch, Fg	0.5	C,Ch,F	0.25	V,Fg

CU = Cultivation in hectares
C = Corn; P = Potato; O = Onion; G = Groundnut; V = Vegetables; S= Sugarcane; F = Fruit;
Ch = Chilly; Fg = Fodder grass.
Ab = Amygdaloidal basalt unit
Jb = Jointed basalt unit
S = Sheet joints; C = Contact zone; J = Joints (Jointed basalt unit)

Well numbered 112 shows a higher Infiltration index value (12.10 LPM/m/m^2) than well numbered 113 (3.26 LPM/m/m^2) and also irrigated larger areas during the winter and summer of 1984-85 and the winter of 1985-86 (Table 2). This is due to large inflows observed through widened sheet joints of the amygdaloidal basalt unit in well numbered 112. However, as is evident from Table 2 and Figure 3 (a and b), well numbered 112 had run dry during the summer of 1985-86 (drought period), whereas well numbered 113 maintained some saturation at the end of this period. It is interesting to note from Figure 3 (a and b) that all the inflow zones (sheet joints of the amygdaloidal basalt unit) where even at the end of the summer of the drought year (1986), showed that the lowermost sheet joint and the contact zone the amygdaloidal and jointed basalt units were still yielding water and supporting 0.8 hectares of crops (Table 2).

In spite of both wells having the same number of inflow zones (4), well numbered 112 ran dry during the drought period (summer of 1986) with all its inflow zones becoming inoperative. This is due to the fact that well numbered 112 only partially penetrates the aquifer thickness (the contact zone between the two basalt units is not encountered in the well), as against which well numbered 113 penetrates into the jointed basalt unit shows some inflow through the contact zone between the amygdaloidal and jointed basalt unit.

b) Wells numbered 125 and 129

Wells numbered 125 and 129 are situated in low lying portions of the area (Figure 2) and therefore, tap only the jointed basalt unit as the confined aquifer [Figure 3(c) and 3(d)]. Table 1 shows that these two wells show a low ground water draught (less than 200 m^3/ week) and their agricultural support during all the seasons is low (Table 2).

The wells show comparable Infiltration index values (0.71 LPM/m/m^2 for well numbered 129 and 0.78 LPM/m/m^2 for well numbered 125). Figure 3 (c and d) indicates that well numbered 125 ran day during the drought summer period of 1986, whereas well numbered 129 still held some water (which was essentially used for drinking). Although the joint(s) of the jointed basalt unit, that acted as inflow zone(s) in the period proceeding the drought summer (of 1986) had dried up in both these wells, the slightly lesser pumping by well numbered 129 (e.g. 132 m^3/week) during the summer of 1985 has helped it to retain some water during the drought summer. Well numbered 125 has dried up due to a slightly greater ground water draught (e.g. 198 m^3/week during the summer of 1985).

c) Well numbered 85 and 147

Wells numbered 85 and 147 tap, both, the amygdaloidal and jointed basalt units together, as the unconfined aquifer [Figures 3(e) and 3(f)]. The figure shows that inflow into both these wells occurs through the sheet jointed of the amygdaloidal basalt unit, the joints of the jointed basalt unit and the contact zone between the two units. Well numbered 85 shows a higher Infiltration index (3.00 LPM/m/m^2) than well numbered 147 (1.00 LPM/m/m^2), due to a greater inflow through the sheet joints. The ground water draught for well numbered 85 is also higher as compared to that for well numbered 147 (Table 1). Well numbered 85 irrigated (during the first three seasons) twice the irrigated by well numbered 147 (Table 2). The cropping pattern for wells is markedly different, with well numbered 85 always supporting a corn crop (requiring a large quantity of water). Well numbered 147, on the other hand, irrigated two or three crops, in such a way, so as to regulate its water requirement (combining groundnut with onion and corn, or combining fodder grass with vegetables, chilly or fruit), as evident from Table 2.

The cropping pattern, inducing a variation in ground water abstraction, caused differential responses of these two wells to the drought of 1986. The relentless ground water draught from well numbered 85 (for the corn crops) during the drought winter (1985) gradually rendered all three inflow zones inoperative leaving the well totally dry by summer of 1986 [Figure 3(e)]. As against this, in spite of its lower potential, well numbered 147 could retain a fair amount of water at the end of the drought summer of 1986 [Figure 3(f)], with all its three inflow zones remaining operative. Most importantly, a controlled abstraction of ground water by well numbered 147 (Table 2) has permitted it to sustain at least 0.5 hectares of vegetables and fodder grass during the peak period of the drought year (i.e. summer of 1986).

The three cases described above bring out the relationship between hydrogeological conditions, well yields and ground water abstraction from a typical shallow Deccan basaltic aquifer, clearly indicating how these conditions are reflected in the agricultural support of different dug wells.

SUMMARY AND CONCLUSIONS

Sallow unconfined Deccan basaltic aquifers almost entirely support agriculture (except during the monsoon period) in many rural parts of the state of Maharashtra in India. These aquifers exhibit a high degree of variation in hydrogeological factors over a contiguous area. It is, therefore, essential to correctly decipher their aquifer geometry and delineate their hydrogeological controls over the well performance or yields. This is especially important since well yields eventually determine the amount and nature of agriculture that a well can sustain during any cropping season. With this background the present study for a typical shallow unconfined Deccan basaltic aquifer (from Pabal area) yielded the following results.

Variable hydrogeological conditions (particularly the non-homogeneity in the development of inflow zones) in different well causes well yields over the area to vary considerably (as indicated by the Infiltration index values). Higher well yields (Infiltration index values) influence farmers to cultivate larger areas of high water requirement crops like corn on their wells. Sufficient ground water recharge under normal rainfall can help these wells to sustain such agriculture throughout the year. This means that the abstraction from the high yielding wells of a higher magnitude, resulting in water levels in these wells dropping during the course of the year following the rainy season.

Whenever the rainfall is deficient, the operativeness of inflow zones during any season (winter and summer) influences the agriculture that is sustained by a well. This sustenance is also related to the regulated ground water draught from such wells. This regulation can actually be controlled by rotating the crops grown during different seasons of the year. The combination of crops grown during a particular season also forms an important aspect of such a regulation. Hence, wells that may be potentially high yielding may run dry under stress (low rainfall drought periods) due to an excessive ground water draught. On the other hand, some low yielding wells retain some water during stress periods only because of a regulated and controlled ground water draught (with a systematically supported cropping pattern).

ACKNOWLEDGEMENTS

This work was undertaken during the tenures of research fellowships and the research associateship of the first author for which the C.S.I.R. is gratefully acknowledged. The authors are grateful to Drs. A.V. Phadeke, V.V. Peshwa, V.G. Phansalkar and Vivek Kale and to Mr. Anil Lalwani for valuable discussions and encouragement during the course of this study.

REFERENCES

Athavale, R.N., Rangarajan, R. and Muralidharan,D. 1985. Measurement of natural recharge in India. *J. Geol. Soc. India,* 39; 235-244.

Deolankar, S.B. 1989. Infiltration index - a parameter for comparison between dug wells in the Deccan Trap area. *Bull. Earth Science,* 7; 33-36.

Deolanker, S.B. and Kulkarni, H. 1985. Impact of hydrogeology on agriculture in the Deccan basaltic terrain of Maharashtra, *India. Mem. IAH 18th Int. Cong. on Hydrogeology in the Service Man,* 18; 212-213.

Kale, V.S. Kulkarni, H. and Peshwa, V.V. 1992. Discussion on, 'A geological map of the southern Deccan traps, India and its structural implications by Widdowson, M. and C. Mitchell (J. Geol. Soc. London, 148 (1991); 495-505)'. *J. Geol. Soc. London,* 149; 473-478.

Kulkarni. H.C. 1987. *A study of the Deccan basaltic unconfined ground water system in the Pabal area of Shirur taluka, Pune district, Maharashtra state.* Unpubl. Ph.D. thesis, University of Poona, Pune; 285.

Kulkarni. H. and Deolankar, S.B. 1990. Calibration of permeability for the conceptual hydrogeological model of a Deccan basaltic unconfined ground water system from Maharashtra, *India. ModelCARE - 90, Int. Symp. on Calibration and Reliability in Ground Water Modeling,* 199-209.

Lerner, D.N. Issar, A. S. and Simmers, I. 1990. Groundwater Recharge (A guide to understanding and estimating natural recharge) *IAH,* 8; 345.

Sighal, B.B.S. Singhal, D.C. and Awasthi, A.K. 1987. A study of bore wells and dug wells in the state of Karnataka, India. *Tech. Rep. for NABARD,* Consultancy Proj. No. GG-6/85-86; 223.

STATISTICAL ANALYSIS OF GEOHYDROLOGICAL DATA IN FIVE CRYSTALLINE ROCK SITES IN SOUTHERN AND EASTERN FINLAND

A. NIEMI & K. KONTIO
Technical Research Centre of Finland
VTT/TGL/BK1, Betonimiehenkuja 1,
SF-02150 Espoo, Finland

ABSTRACT. The treatment of in-situ measured hydraulic conductivity data as samples of a random variable that can be represented through their statistical properties and modeled stochastically is a relatively new concept in the case of fractured media. It was first proposed by Neuman (1987) and was inspired by conceptual problems in fracture network modeling and in upscaling and downscaling the highly discontinuous and connectivity dependent hydraulic conductivity data into model parameters. When determining the geostatistical properties of hydraulic conductivity data from realistic site scale investigations, a major problem is the scarcity of data bases. This article presents statistical analyses of geohydrological single borehole data from five crystalline rock sites investigated for final disposal for high level nuclear waste in Finland. The data are analyzed for statistical moments and distributional assumptions as well as confidence bounds of the distribution parameters, for spatial trends and autocorrelation structures, with special consideration given to the proportion of data close to the detection limit of the measuring equipment. Data from various sites are compared by means of statistical testing and the effect of combining data from statistically similar sites is considered. Furthermore, topics investigated include distinction between stochastic and deterministic data at the scale of interest and role of 'fracture zones' in stochastic analysis. Application of these kinds of data to actual site scale modeling with the Monte Carlo technique is also briefly discussed.

INTRODUCTION

During 1987-1992 the Industrial Power Company of Finland (TVO) has carried out site investigations for the final disposal of high level nuclear waste at five crystalline rock sites, namely Romuvaara (Kuhmo district), Veitsivaara (Hyrynsalmi district), Kivetty (Konginkangas district), Olkiluoto (Eurajoki district) and Syyry (Sievi

district). The objective of the investigations has been the preliminary characterization of the five sites, as well as the selection of three of them for further, more detailed investigations. The field investigations program included systematic hydraulic testing with a fixed-interval two-packer system. Results from these studies have been used together with geophysical and geological data for structural characterization of the sites as well as for deterministic finite element type of modeling of the five sites.

The objective of the present work is to examine the hydraulic conductivity data through their geostatistical properties. Areas of interest include the representativeness of various data, statistical similarities and differences between various data sets and spatial variability i.e. autocorrelation structures and trends observed within various data sets.

In the case of fractured media it is a relatively new concept to consider the in-situ hydraulic packer test data as samples of a random variable that can be described through its statistical properties and modeled stochastically. This stochastic continuum approach was first proposed by Neuman (1987) and has been inspired by the fact that upscaling and downscaling hydraulic data for deterministic flow models is presently an unresolved question due to the highly discontinuous and connectivity dependent nature of hydraulic conductivity in fractured rock.

Furthermore, application of fracture network modeling (for example Long *et al.* 1982, Herbert & Gale 1990, Cacas *et al.* 1990) in determining the support scale of stochastic analysis also has conceptual problems in incorporating the important parameters of conductive fracture connectivity and conductivity. Even if these conceptual difficulties are resolved, the amount of data required in order to obtain statistically representative continuum permeabilities for site scale models using fracture network approach would become prohibitively large.

Our interest in studying the geostatistical properties of the data is two-fold: 1) to look at the statistical properties themselves as indicators of the field conditions for site characterization purposes and 2) to provide a basis for stochastic modeling. Detailed statistical analyses of the geohydrological data from the five sites have already been presented in progress reports (Niemi and Kontio 1991, 1992 and 1993). Here the pertinent findings of these studies are summarized and some representative example results discussed. Application of this type of data to an actual stochastic Monte Carlo simulation of groundwater flow has been undertaken by Niemi (1993), and this work will be briefly discussed as well.

DATA BASE

In each investigation area, systematic testing has been carried out in five subvertical boreholes, one of which is about 1000 m deep and the others approximately 500 m deep. Horizontal distances between the boreholes are of the order of 500 m. Measurements have been carried out systematically with a 31 m test interval starting from a depth of 70-100 m. The constant pressure method of testing has been used, with a one hour injection period followed by a one hour recovery period. Three different methods have been used for interpreting the data: the Moye method (Moye 1967) based on the steady state behaviour of the injection phase, the Jacob-Lohman method (Jacob & Lohman 1952) based on the transient behaviour of the injection-phase and the Horner method (Uraiet & Raghavan 1980) based on the transient behaviour of the fall-off phase (see for example Pingoud *et al.* 1988, Kuusela-Lahtinen & Front 1990).

Most of the geostatistical analyses were carried out using the data interpreted with Moye formulae as this data base contains the largest number of observations. For the sake of comparison some sensitivity studies were carried out using the other two data bases as well.

All three methods assume continuum behavior of the flow from the test interval. This is the underlying assumption in the stochastic continuum approach as suggested by Neuman (1987) as well. The scale of the measurement should be large enough in comparison to the scale of individual fractures to allow the continuum presentation, but small in comparison to the problem itself to justify a stochastic analysis.

A review of recent studies shows that continuum scales applied have varied from 3 m to 10 m. Herbert & Gale (1990) used the fracture network simulation to determine a 8 m continuum scale for their stochastic model representing the Stripa mine in Sweden. Cacas *et al.* (1990) used 5 m and 10 m continuum scales when modeling the Fanay-Augeres mine in France. Neuman (1987) discussed data obtained at a 3.8 m scale and Follin (1992) applied the stochastic continuum approach to data obtained with a 3 m test interval. With increasing dimension the continuum behavior is better satisfied and therefore the 31 m scale should satisfy the continuum condition even better. On the other hand, the referred studies took place in the upper hundreds of meters of the rock. In deeper portions, which are of primary interest in the present study, the fracture networks are likely to be less connected. Then the continuum scale probably also should be larger than in the previous studies and the 31 interval appears to be a justified choice. Also the dimension of the sites investigated here is larger than in the previous studies. Therefore the criterion concerning the stochastic nature of the data in the scale of the problem of interest should be met as well.

In order to make the data sets from all boreholes comparable only measurements above approximately 500 m borehole depths were considered. In accordance with standard geohydrological practice all the analyses were carried out with the base ten logarithms of the hydraulic conductivity values, even though in geostatistical literature the natural logarithm is more commonly used.

SAMPLE STATISTICS

Summary sample statistics of the 31 m hydraulic conductivity data from all five investigation areas are shown in Table 1a. Inspection of Table 1a shows that the statistics for Romuvaara, Veitsivaara, Kivetty and Olkiluoto are very similar, but for Syyry the mean, median and standard deviation are higher.

Table 1: Summary statistics of the 31 m hydraulic conductivity measurements (log m/s) in the five investigation sites: a) original data and b) data from which fracture zones have been excluded.

Site	n	Mean	Median	Standard deviation
Romuvaara	66	-8.9	-9.2	1.3
Veitsivaara	71	-8.7	-9.0	1.3
Kivetty	66	-8.7	-9.0	1.3
Olkiluoto	67	-8.7	-9.0	1.4
Syyry	67	-8.2	-8.5	1.9

Site	n	Mean	Median	Standard deviation
Romuvaara	47	-9.2	-9.8	1.0
Veitsivaara	46	-9.2	-9.5	0.9
Kivetty	58	-8.9	-9.1	1.2
Olkiluoto	46	-9.2	-9.7	1.0
Syyry	39	-9.1	-10.0	1.4

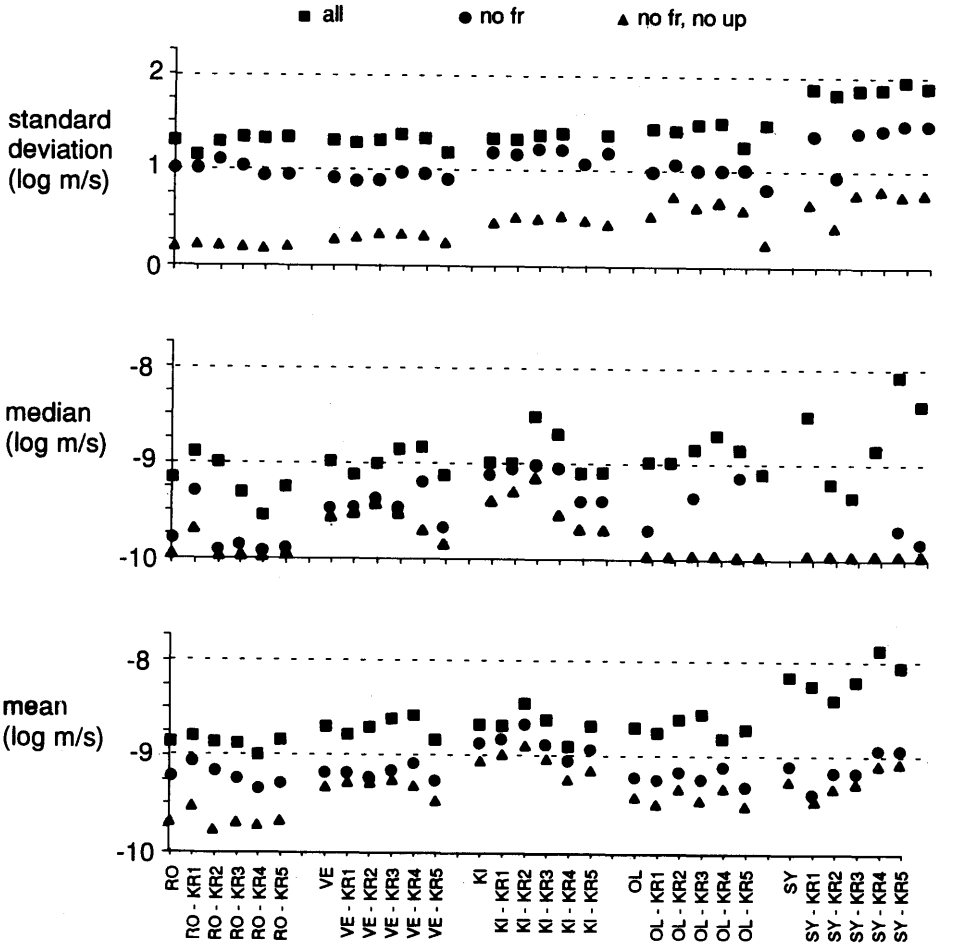

Example of symbols: RO = Romuvaara, all data; RO-KR1 = Romuvaara, borehole KR1 not included

Figure 1: Means, medians and standard deviations for site data for all five boreholes and with the removal of one borehole at a time, 1) original data (square symbols), 2) data with no fracture zones (circular symbols) and 3) data for borehole depths > 200 m, with no fracture zones (triangular symbols).

The data sets available are relatively scarce. Therefore it is of interest to estimate how statistically representative they are. The robustness of these statistics was evaluated by removing one borehole at a time from the data and by computing the statistics for the remaining four boreholes. The objective was to assess whether the

statistics observed are caused by individual boreholes or indicative of more general behavior of the site data. The results for both the original data and for the four-borehole subsets of the data are shown in Figure 1 with square symbols. They indicate that the variations within each site are of the same order as the differences between various sites. Mean values are usually from -9. to -8.5 log m/s and median values from -9.5 to -8.5 log m/s. Again the data from Syyry differ from the others in having a higher mean and a median that is more sensitive to the borehole combination used than the other sites.

EFFECT OF FRACTURE ZONES

The above data sets contain measurements that might not be fully comparable. According to the investigators carrying out the exploratory program (Teollisuuden Voima 1992) some of the boreholes have been aimed at locating so-called fracture zones i.e. zones, that based on prior geophysical or geological information were believed to be significant hydrological features. In different sites the number of measurements related to such zones may vary, thus making the comparison of data sets in previous tables difficult. In terms of modeling, the distinction between 'fracture zones' and 'average rock' could be seen as the difference between stochastic and deterministic conductors at the scale of the problem of interest (Niemi 1993). If a fracture zone is prominent enough to appear in several boreholes or as a dominant reflector in geophysical profiles, it is best modeled as a deterministic feature.

With this concept in mind we can look at the data in terms of which hydraulic conductivity measurements can be seen to be related to deterministic zones at the scale of the present problem and at the present scale of measurement. Such fracture zones have been sought to facilitate modeling of the five sites using the traditional deterministic finite element approach (for example Taivassalo & Meszaros 1992). Methods from surface and borehole geophysics have been combined with geological information as well as information from the hydraulic packer tests themselves. Expert opinion has been used to combine all this information and to identify such significant zones. The structures and the methodology used as well as the uncertainties associated with identifying them are presented in Saksa et al. (1991, 1992a, b, c and d). The distinction between fracture zones and sound rock is, however, not clear and there is always some subjective bias in this type of data selection. These interpretations nevertheless provide the best available estimate of what could be considered 'deterministic features'.

The hydraulic conductivity measurements associated with these zones were excluded from the original data and the basic statistics were computed for the remaining data. The statistics are shown in Table 1 b and the results are shown graphically in

Figure 1 with circular symbols, computed for both the entire site data and for subsets of data from which one borehole at a time is again removed.

Comparison with the corresponding results for the original data in Figure 1 shows that all parameter values are smaller. The mean values are about half a log-cycle smaller than for the original data and the median values vary from -10. to -9. log m/s. Inspection of the results in Figure 1 also shows that the median value, which is a good measure of statistical behavior, is as dependent on the borehole combination used as in the case of the original data. Thus this type of removal of measurements related to 'deterministic fracture zones' was not sufficient to make the rest of the data entirely stochastic and statistically representative. A possible explanation for this is the nonstationary character of the hydraulic conductivity with depth.

DEPTH TREND

Evidence from earlier investigations elsewhere supports the assumption that hydraulic conductivity in crystalline rock decreases with increasing depth. This is due to increasing lithostatic pressure which tends to close fractures, thus increasing resistance to flow. A good supply of field data allowing examination of depth vs. hydraulic conductivity in fractured rock has been obtained in the Swedish KSB 3 program, for example, and these data do in fact show vertically decreasing trends (Carlsson & Winberg 1983).

According to Freeze *et al.* (1987), the three basic approaches available for modeling data with trends are a) zonation, b) trend analysis, and c) non-stationary geostatistics. De Marsily (1986) gives a good description of the third of these. Delfiner (1973) and Kitanidis (1983) give examples of trend removal through the use of Intrinsic Random Functions (Silliman 1986). An approximate iterative solution for the simultaneous determination of drift and variogram is given by Matheron (1969). Neuman (1984) also employs iterative techniques to determine spatial trends (de Marsily 1986).

The data sets analyzed here are relatively scarce. In addition, a large portion of the data is below the detection limit of the measuring equipment. The actual values of these data must therefore be estimated or otherwise biased trend models are obtained. Some kind of iterative approach could be used in which the values below the detection limit are estimated during each iteration, based on the current best estimate for the depth trend model. As the iteration proceeds the number of values predicted by the model as being below the device detection limit approaches the number actually observed. However, where there are a large number of data to be estimated, the effect of model assumptions becomes significant and the result less reliable, regardless of the elegance of the model.

For this reason the depth dependency was evaluated simply by classifying the data into two groups according to the depth interval. The division was done by assigning a measurement to the upper depth interval, if the center of the test interval was above 200 meters depth in borehole depths. The approximate vertical depths from ground level thus included in the upper section varied from 173 m to 201 m depending on the borehole. This division resulted in the upper data sets being distinctly smaller than the lower ones, and was used in order to keep the number of data in lower sets reasonable large, for the purpose of further studies.

Comparison of the median values gave the best estimate of the depth trend as it was not affected by the measuring device detection limit. The median values in the upper depth interval were usually above -8.0 log m/s whereas in the lower intervals they were usually below -9.0 log m/s (Niemi & Kontio 1992).

To study the effect of depth trend on the type statistics shown in Figure 1, one more set of statistics was computed for the data from which both the fracture zones and the data of the upper section of the rock - as specified above - are filtered out. These results are shown in Figure 1 with triangular symbols. Inspection of these results shows that variations within each site are at least in some cases smaller than the differences between sites. Based on the mean values the data from Kivetty appear most conductive and the data from Romuvaara least conductive. On the basis of median values Kivetty and Veitsivaara are more conductive than the other three sites.

PARAMETERS OF GAUSSIAN DISTRIBUTION

Recognition of the underlying mathematical distribution provides tools for modeling the data and for estimating the confidence limits of parameters describing the data. Assumption of a normal distribution of the log K or ln K is commonly used in stochastic geohydrology. For example according to Dagan (1989), application of the normal distribution is, however, more often based on the convenience of the mathematical formulation than on thorough analysis of the data.

Example histograms of the original data, data without fracture zones and data for lower part without fracture zones are shown in Figures 2 a,b and c for the Veitsivaara site. The appearance of the histogram is rather typical among those observed for the five sites. Only the histogram based on the data from Syyry showed a distinctly different, more homogeneous appearance, with more high conductivity zones than at the other four sites and also showing different statistical properties in Table 1. The large number of data points at the device detection limit can be seen in Figure 2. The amount of data at the device detection limit varied from 30% to nearly 40%

depending on the site in question. The true values of these data is smaller than that shown in the histograms.

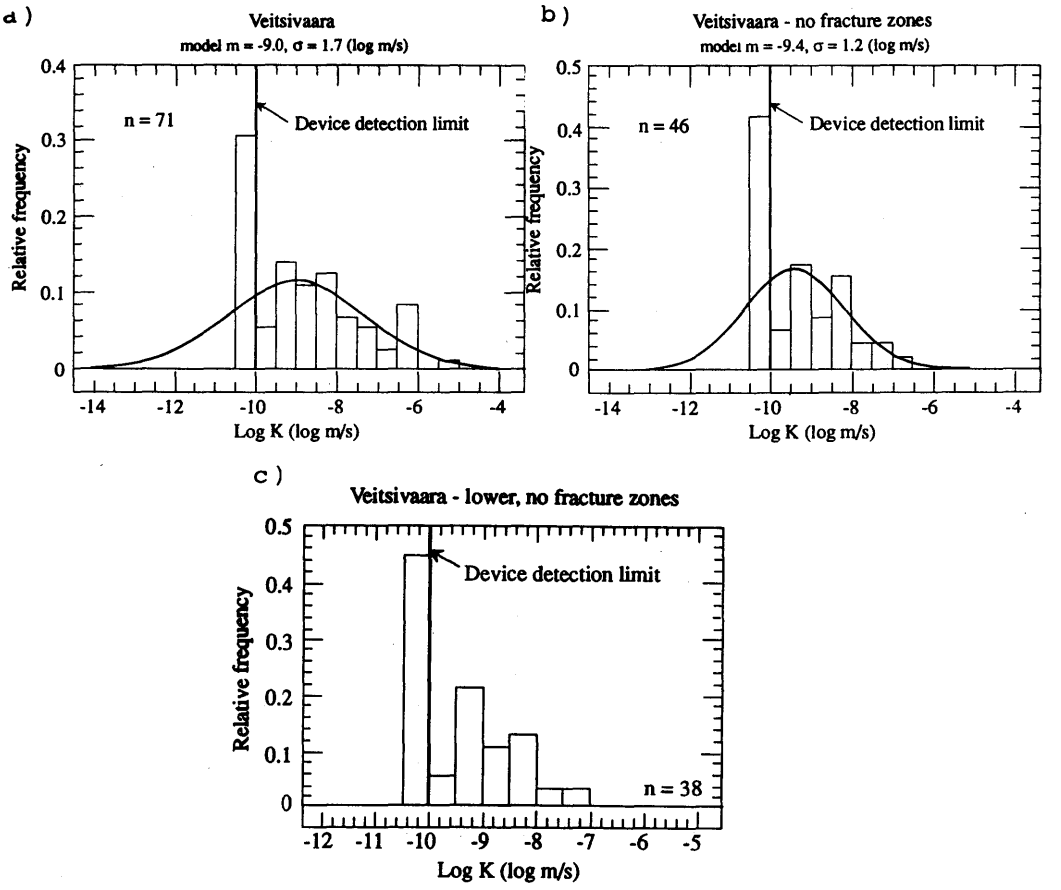

Figure 2: Example histograms and fitted Gaussian models for Veitsivaara data a) original data, b) data from which the fracture zones are excluded and c) data from which fracture zones and data above 200 m borehole depth are excluded

With a large number of measurements at the detection limit of the measuring device, the mean and variance of normal distribution do not coincide with sample mean and variance even if the data are normally distributed. Therefore, the model parameters

were determined using two approaches specially suited for truncated normally distributed data. One method employs iteration by always using the current best estimate of the Gaussian model parameters for estimating the values of data at device detection limit. First the sample mean and standard deviation are determined from the n observations. Next, using a random number generator, n normally distributed values are generated with these sample parameters. The small values of this generated sample (log K< -10. log m/s) are used to replace an equal number of values at the detection limit (log K= -10. log m/s) of the original sample. Next the mean and standard deviation of the new sample are determined and the previous steps repeated with the new parameter values. Iteration is continued until the parameter values do not change. Then, in the case where the original data did have an adequately Gaussian appearance, the model mean is approximately equal to the sample median and the number of values predicted with the model to be less than the detection limit is approximately equal to the number of corresponding data measurements.

In the second approach the parameters were determined by simple regression to the normal probability plot. Using these two approaches the parameter values were predicted for the five sites, both for the original data sets and for data from which the fracture zones were excluded. In most cases the predictions with the two models were within one decimal unit (in log m/s), which is a good agreement considering the reporting accuracy of the data. The Gaussian fit obtained with the iterative model is shown in Figures 2a and b together with the data histograms. Comparison of the parameters in Figures 2 and sample statistics in Table 1 shows the magnitude of error that would be introduced if the Gaussian parameters were determined directly from sample statistics. A typical standard deviation of 1.7 log m/s would be interpreted as 1.3 log m/s.

TESTING FOR DISTRIBUTIONAL ASSUMPTIONS

Niemi (1993) tested the hypotheses of two different distributional assumptions with a chi-squared test. The hypotheses of normal and, for the sake of comparison, of homogeneous distribution were used. Using the 10% risk as a limit, for both the original data, and the data from which the fracture zones had been excluded, the assumption of a normal distribution could not be rejected in the case of Romuvaara, Veitsivaara, Kivetty and Syyry. For Olkiluoto it had to be rejected for all the cell spacing used. The reason for this rejection was the discontinuity in data just above the device detection limit. Otherwise, based on the general appearance of the histogram the Olkiluoto data did not appear less Gaussian than the other four data sets. The standard deviation for the Syyry data was high.

For the original unfiltered data the assumption of a homogeneous distribution could be rejected for all other data sets except the Syyry data. For data from which fracture zones were excluded the homogeneous assumption could be rejected for all data sets with less than 10% risk. For Syyry the P-value was however between 10 and 5%. Visual inspection of the histograms supported these test results.

For the data sets with both fracture zone data and data from the upper part excluded no chi-squared test was carried out as the small number of observations would make the test unreliable. Visual inspection of for example the histogram in Figure 2 c still shows some Gaussian appearance.

STATISTICAL TESTING FOR DATA SET COMPARISON

Inspection of the statistical properties like those shown in Table 1 as well as data histograms and cumulative density functions allows a preliminary comparison of various data sets. Whether the differences and similarities observed are significant given the amount of observations they are based on, can be estimated by means of statistical testing.

Three different statistical tests were used for comparing the data from the five sites:

1) Kolmogorov-Smirnov test based on the comparison of the cumulative density functions of two data sets. The maximum difference between the two curves is computed and the probability determined based on this difference and the degrees of freedom, the latter being a function of sample size.

2) Wilcoxon rank sum test. In this test the data from the two samples are combined and ranked in ascending order of magnitude. Each observation is assigned a rank based on its position in the ordered sample and the ranks of observations of both original samples are summed up. The test is based on comparison of the two rank sums.

3) The Kruskal-Wallis test. This test is similar to the Wilcoxon test, but is used for comparing several samples simultaneously.

These tests are described in more detail in most statistical texts such as Freund (1992). The statistical comparison with the aforementioned tests was carried out for the site data divided into two depth classes as described earlier. The analysis was carried out for both the original data and the data from which the fracture zones had been excluded. An example test result is shown in Figure 3, for data sets from which the fracture zones have been excluded and data interpreted with Moye formulae. The

values shown are P-values in permils (o/oo). Number 50 (5%) indicates that the assumption of the samples coming from the same distribution can be rejected with 5% risk. A 10 % risk level has been used as a criterion and P-values below that have been shaded. The shaded test results indicate that the assumption of same underlying distribution between the two samples can be rejected with less than 10 % risk.

a)

	KIU	KIL	OLU	OLL	SYU	SYL	ROU	ROL	VEU	VEL
KIU		5	575	0	92	1	680	0	723	0
KIL			14	233	519	292	4	73	245	644
OLU				3	95	2	794	0	817	8
OLL					210	482	1	612	14	728
SYU						97	113	45	637	482
SYL							0	173	225	449
ROU								0	833	2
ROL									7	151
VEU										49
VEL										

b)

	KIU	KIL	OLU	OLL	SYU	SYL	ROU	ROL	VEU	VEL
KIU		9	435	0	355	5	639	0	593	1
KIL			94	80	358	156	7	17	211	435
OLU				1	515	13	659	0	1000	6
OLL					114	863	0	576	17	323
SYU						68	457	31	795	280
SYL							4	630	80	433
ROU								0	584	1
ROL									9	79
VEU										58
VEL										

U = upper depth interval
L = lower depth interval

Figure 3: P-values (in per mil) of a two-sided a) Kolmogorov-Smirnov test and b) Wilcoxon-test, when data from various sites classified in depth intervals are compared; data sets from which the fracture zone data are excluded.

A clear trend could be observed in the results, both in the original data and in the data from which the fracture zones have been excluded. In general, data from the lower part of the bedrock at any given site differ from the data from the upper part of any site, but does not differ from the data from the lower part of any of the other sites. Neither do the data from the upper parts differ from each other. Some exceptions to this general rule were nevertheless observed also. In the case of the results for 'average rock' in Figure 3, the Kolmogorov-Smirnov test classifies the lower data from Kivetty and Romuvaara as different, while according to the Wilcoxon test the lower data from Kivetty and Olkiluoto and Romuvaara and Veitsivaara are different as well. Inspection of the cumulative density functions in Figure 4 shows that the function for Romuvaara is located towards lower and Kivetty towards higher conductivity values in comparison to the other sites. The data from Olkiluoto and Veitsivaara do not show such clear differences, but the former appear to be toward the lower end of the hydraulic conductivity region and the latter towards the higher values.

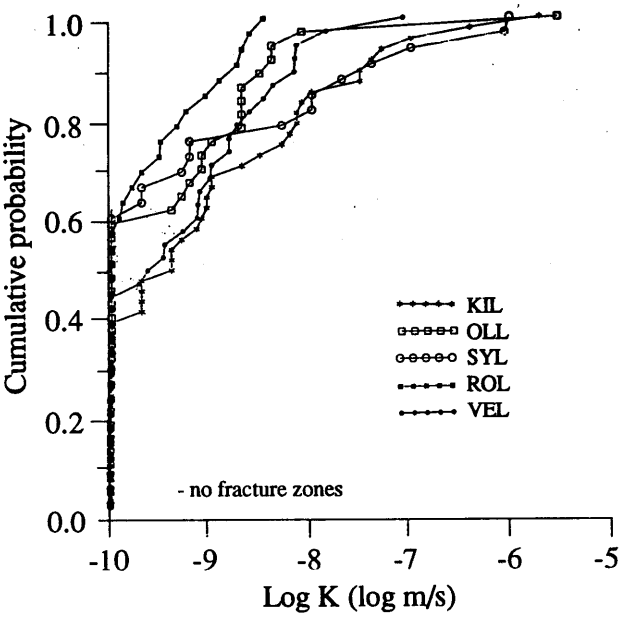

Figure 4: Cumulative density functions of hydraulic conductivity data from which fracture zone data and data in the upper section (borehole depths < 200 m) are excluded.

According to the Kruskal-Wallis test, the P-values for original data in the lower depth interval was P=0.48, while in the upper depth interval P=0.73. For data from which the fracture zone data had been filtered out, the corresponding values were P=0.13 and P=0.87. Thus, according to this test the assumption of the same underlying distribution for all sites cannot be rejected with less than 10% risk. For the data in the lower part with no fracture zones the probability is, however, very low and close to the 10% risk level.

For statistical comparison tests also data bases interpreted with the transient Jacob-Lohman and Horner formulae were used, the purpose being to confirm the results obtained with the Moye formula, or else to conclude that the observations, especially regarding the differences between the sites, were not significant if they could not be observed with all data bases.

Detailed results for all these tests are given in Niemi and Kontio (1992, 1993). In general the test results using data obtained with the two transient formulae agreed with those obtained with the Moye formulae. The differences observed were caused more by the difference in the size of the data bases - less data was included into transient data sets - than differences in the actual values.

CONFIDENCE BOUNDS OF MODEL PARAMETERS

In order to estimate the total uncertainty related to a modeling process, we need to know the uncertainties related to the statistical properties of our input data. The 100 x (1-α) % confidence bounds of the mean and variance of a normal distribution can be estimated exactly (Freund, 1992) with:

$$m = \overline{x} \pm t_{\alpha/2,n-1} \frac{s}{\sqrt{n}} \qquad (1)$$

where m = mean
$\overline{x}$ = sample mean
s = sample standard deviation
n = sample size
$t_{\alpha/2,n-1}$ value of t-distribution with n-1 degrees of freedom

$$\frac{(n-1)s^2}{\chi^2_{\alpha/2,n-1}} < \sigma^2 < \frac{(n-1)s^2}{\chi^2_{(1-\alpha/2),n-1}} \qquad (2)$$

where σ^2 = variance
$\chi^2_{\alpha/2,n-1}$, $\chi^2_{(1-\alpha/2),n-1}$ are values of chi-squared distribution

Using these equations the confidence bounds for mean and standard deviations were determined for various site data (Niemi and Kontio 1992). Example results are shown in Figure 5 for data divided into two depth intervals, with and without fracture zones. The Gaussian parameters in this case were determined with regression to normal probability plot for the data from the lower section of the rock and from sample statistics for the upper sections. The data in the latter group are not affected by the device detection limit enough to justify an other type of determination of the Gaussian parameters.

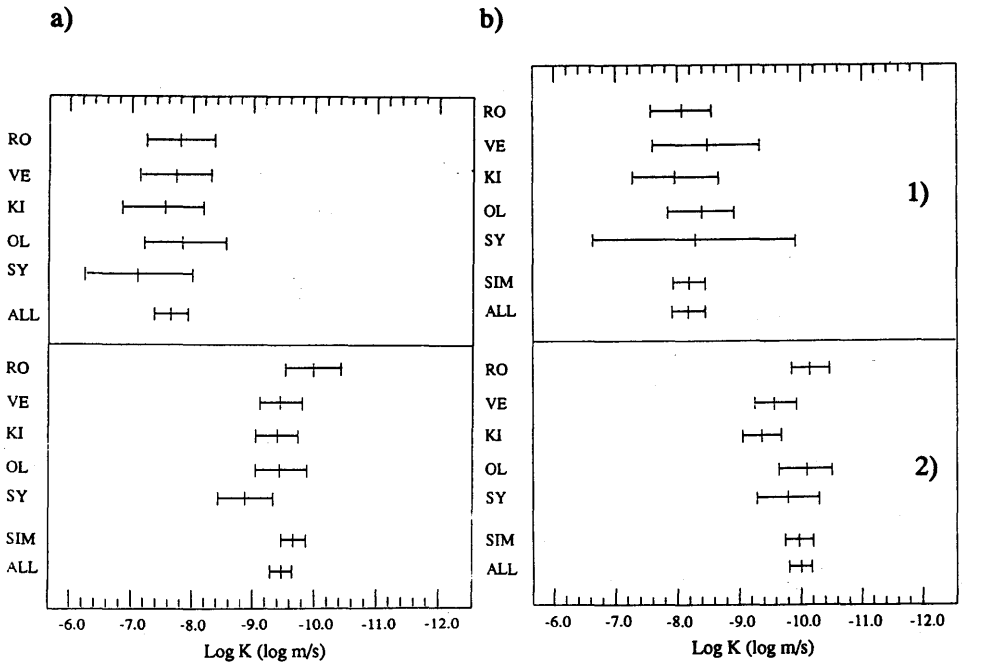

ALL = all five sites combined, SIM = statistically similar sites combined

Figure 5: 90% confidence bounds for estimated means of normal distribution with data divided into depth classes 1) borehole depth <200 m and 2) borehole depth >200 m: a) for the original data and b) data from which fracture zones have been removed (Niemi 1993).

Due to the small sample size the confidence intervals in the upper section are wide, as can be expected. A clear difference can still be observed between the upper and lower data, with the 90% confidence intervals in the upper section usually ranging

from -9. to -7. log m/s and in the lower section from -10.5 to -9. log m/s. A difference can also be observed between original data and data without fracture zones, the latter being systematically smaller.

For the sake of comparison the corresponding confidence bounds were also determined for data sets in which measurements from various sites were combined. This was done in order to gain an insight into how much the confidence bounds are influenced by increasing or decreasing the data base. The results are also shown in Figure 5.

The data were combined in two ways by 1) combining data that, on the basis of which based on the statistical comparison on a site-to-site basis, were not statistically different and 2) by combining data from all five sites together, based on the results of the Kruskal-Wallis test. The abbreviation SIM refers to data sets into which all statistically similar data are included - based on the type of testing discussed above while the abbreviation ALL refers to the data set which contains data from all five sites.

VARIOGRAPHY

Stochastic variability in space was studied with variography, which characterizes the correlation between two points as a function of the distance between them.

A variogram is determined by

$$\gamma(h) = 1/2E((Z(x+h)-Z(x))^2) \qquad (3)$$

where

$\gamma(h)$ = variogram
E = expected value
Z(x) = value of the variable at point x
h = distance between the two points to be compared (lag)

The data analyzed were relatively scarce so that it was of interest to see whether they are numerous enough to allow site specific spatial properties to be observed. Variograms based on too few data typically lack obvious structures and appear scattered.

The variograms were determined as 'omnidirectional' variograms combining data of all orientations along the borehole depth and by combining all five boreholes within each site into one data set. The horizontal distances between the boreholes were too

large to allow variography in horizontal directions or anisotropic properties to be studied. Omnidirectional variograms do yield the smoothest variograms and are good first estimates of the spatial variability within a site (Englund and Sparks, 1988).

Sensitivity studies were carried out by determining the variograms for subsets of the site data by removing one borehole at a time and determining the variograms for the remaining four boreholes. This was to assess whether the structures observed are caused by individual boreholes or indicative of a more general behavior of the data.

Most of the variograms showed an increase with distance, usually indicative of a decreasing trend in permeability with depth. The possible depth trend effect was studied with a simple zonation concept, so that the data were divided into two depth intervals as described earlier. After this division, two methods were used for filtering out the possible depth trend effect: 1) The two data sets were made 'compatible' by subtracting the difference in median values of log K from the log K-values of the upper data sets. After this transformation the variograms were determined normally. 2) The two data sets were studied separately and the values in the upper class were not compared to those in the lower. The two approaches are conceptually close to one another and the resultant variograms also showed similar behavior for all practical interpretation purposes; the latter is perhaps more correct however, as no assumptions are made in this approach.

Example variograms for the original data and data with the latter trend correction are shown in Figures 6 for one site. The figure also shows a variogram with four boreholes that for this particular site was most different from the original five-borehole variogram. As we can see the difference in this particular case is negligible.

In summary, some conclusions could be made based on these variograms. Very distinctive features in individual boreholes could dominate the entire site variogram, and examples of this were seen in case of two sites. In other cases the variograms were not very sensitive to the borehole combination used and the variograms in Figures 6 represent this type behavior. After the distinctive boreholes were removed, most of the site variograms showed similar behavior. Transitional type correlation structures in the variograms were not prominent, but they could be identified. Autocorrelation distances observed were of the order of 100 to 200 m i.e. similar to those observed by Winberg (1989) with similar data in Sweden. Trend removal with simple classification by depth appeared to be a worthwhile procedure in order to gain insights into the system behavior.

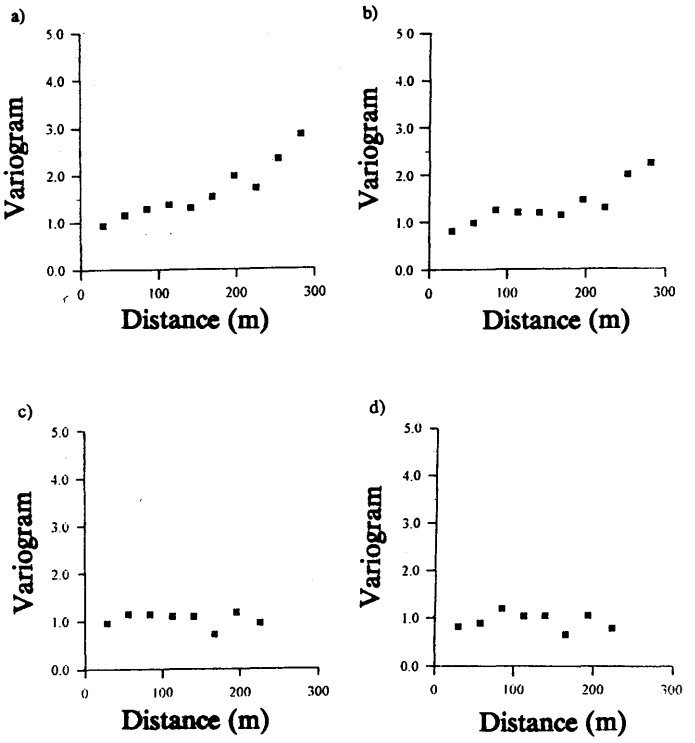

Figure 6: Omnidirectional variograms in direction of borehole depth (subvertical) for Veitsivaara: a) original data, b) data from which borehole KR5 excluded, c) original data after trend removal and d) data with borehole KR5 excluded after trend removal.

DISCUSSION AND APPLICATIONS FOR MONTE CARLO SIMULATIONS

When combined with a stochastic Monte Carlo simulation in the support scale of hydrological measurements, the type of data analysis discussed here can be used for estimating the total uncertainty in the modeling prediction, given the amount, location and measurement scale of the data available. The confidence limits of the data parameters like those shown in Figure 5 can be related to simulated flow distributions. Niemi (1992 and 1993) has carried out such analyses. In the simulations the dependency of permeability with depth was taken into account with zonation by assigning different statistical properties to different depth classes.

The fracture zones were usually treated as deterministic boundary conditions to the stochastic 'average rock', the statistical properties of the latter being based on data from which fracture zone data had been excluded. Gaussian type permeability distribution was used for the average rock. While with the chi-squared test the assumption of a Gaussian distribution could often not be rejected with the original data either, the appearance is less Gaussian and the possible inaccuracies in model prediction more critical if the high conductivity values are not reproduced with the theoretical model (compare Figures 2a and 2b). Secondly, at higher conductivity values, to which the fracture zones usually are related, the radius of influence of the test becomes large in comparison to the length of the test interval and the underlying assumptions of hydraulic conductivity values as local samples may no longer hold.

Most of the previous analyses were carried out with data interpreted with the Moye method as this data contained by far the largest number of observations in comparison to the data bases interpreted with the Horner and Jacob-Lohman methods. The biggest reason for the difference was that with the other two methods no numerical value was assigned to measurements at the equipment detection limit. According to both Andersson & Persson (1985) with this type of data in Sweden and Niemi (1993) with the present data, the steady state Moye solution yields somewhat higher conductivity values than the other two transient solutions. Also the transient solutions were different from one another. On the other hand, also the effective hydraulic conductivity describing a larger section of a porous medium has been determined to be a function of the flow condition being less for transient than steady flow situations (Gomez-Hernandez & Gorelick 1989). To go into the details of steady state versus transient well test analysis and subsequent modeling is outside the scope of the present work.

The Moye solution assumes a radial flow geometry up to a distance L/2, where L is the measurement interval and spherical flow beyond this distance. The other two methods assume radial flow during the entire test period. The actual flow dimension between radial and spherical is difficult to determine uniquely from this type of a well test data (Dr. T.Doe, oral communication). This could also be observed when analyzing the flow dimensions of the present data (Kuusela-Lahtinen 1992). Both geometries were observed. Conceptually a radial flow geometry would be more attractive for this type of analysis where values are averaged and partial spherical geometry migh mean overlapping at higher conductivities. Again going into details of well test analysis, radius of influence of the test and flow geometries is beyond the scope of the present work.

Niemi (1993) compared the statistical properties of the three data bases and found that, for example, combining all data above the equipment detection limit from all five sites, the following mean values are obtained: for the Moye equation -8.2 log m/s, for the Jacob-Lohman equation -8.4 log m/s and for the Horner equation -8.65

log m/s. These values, even though not directly comparable to the statistics in the present work give an impression of the order of magnitude of the difference. The deviation did remain similar throughout the conductivity region of interest. Therefore, using the Moye data base is likely to yield conservative statistics in comparison to those that would be obtained with transient data, but should not otherwise affect the results. This could also be observed in the statistical comparison tests which were carried out with all three data bases.

ACKNOWLEDGMENTS. The statistical analyses of the site data discussed here were carried out with financing from the Industrial Power Company of Finland (TVO) and most of the related model development with financial support from the Ministry of Trade and Industry of Finland. The authors wish to express their thanks to the sponsoring organizations.

REFERENCES

Andersson, J-E. & Persson, O. 1985. Evaluation of single-hole hydraulic tests in fractured crystalline rock by steady state and transient methods. SKBF-KBS. Technical Report, 85-19. Svedish Geological Company, Uppsala, Sweden. 18 p.

Cacas, M.C., Ledoux, E., de Marsily, G., Tillie, B., Barbreau, A., Durand, E., Feuga, B. & Peaudecerf, P. 1990. Modeling Fracture Flow With a Stochastic Discrete Fracture network: Calibration and Validation; 1. The Flow Model. *Water Res. Res.* 26(3): 479 - 489.

Carlsson, L. & Winberg, A. 1983. 'Model calculations of the groundwater flow at Finnsjön, Fjällveden, Gideå and Kamlunge'.SKBF-KBS. Techn Report, 83-45.

Dagan, G. 1989. *Flow and Transport in Porous Formations*. Springer-Verlag, Berlin.

Delfiner, P. 1973. The intrisinc random functions and their applications. *Adv. Applied Physics*, 5: 439 - 444.

de Marsily, G. 1986. *Quantitative Hydrogeology - Groundwater Hydrology for Engineers*. Academic Press, San Diego.

Englund, E. and Sparks, S. 1988. GEO-EAS Users Guide. Version 1.2.1. EPA/600/4-88/033a. US Environmental Protection Agency, Las Vegas, NV.

Follin (1992). Numerical calculations on heterogeneity of groundwater flow. PhD. Thesis. Royal Institute of Technology, Stockholm. Dept of Land and Water Res.

Freeze, A.R., de Marsily, G., Smith, L. & Massmann, J. 1987. 'Some Uncertainties About Uncertainty'. In: *Geostatistical, Sensitivity and Uncertainty Methods for Ground-Water Flow and Radionuclide Transport Modeling*. San Fransisco, California, September 15-17, 1987.

Freund, J.E. 1992. *Mathematical Statistics*. Fifth Edition. Prentice-Hall International, Inc. Englewood Cliffs, New Jersey.

Gomez-Hernandez, J.J. & Gorelick, S.M. 1989. Effective groundwater model parameter values: Influence of spatial variability of hydraulic conductivity, leakance and recharge. *Water Res. Res.* 25(3); 405-420.

Herbert, A.W. & Gale, J. 1990. Fracture flow modeling of the site characterization and validation area in the Stripa mine. In: *Proceedings of the 3rd NEA/SKB Symposium on the International Stripa Project in Stockholm 3.-4.* October, 1989, pp. 223 - 235.

Jacob, C.E. & Lohman, S. 1952. Nonsteady flow to a well of constant drawdown in an extensive aquifer. *Trans. Am. Geophys. Union.* 10: 559-569.

Kitanidis, P. 1983. 'Statistical Estimation of polynomial Generalized Covariance Functions and Hydrologic applications'. *Water Res. Res.* 19(4): 909-941.

Kuusela-Lahtinen, A. & Front, K. 1990. Interpretation of hydraulic conductivity measurements in Sievi, Syyry: boreholes KR2 ja KR3. TVO/Site Investigations. Progress report 90-51, 45 p. (in Finnish, abstract in English)

Kuusela-Lahtinen. 1992. Interpretation of flow dimensions from the constant pressure well tests. TVO/Site Investigations. Progress report 92-50, 10 p. (in Finnish, abstract in English)

Long, J.S.Y., Remer, C.R., Wilson, C.R. & Witherspoon, P. 1982. 'Porous Medium equivalents for networks of discontinuous fractures.'*Water Res. Res.* 18: 645 -658.

Matheron, G., 1967. *Elements pour une Theorie de Milieux Poreux.* Masson, Paris.

Moye,D.G., 1967. Drilling for foundation exploration. *Civil Eng. Trans.*, Inst. Eng. Australia. April: 95-100.

Neuman, S. 1984. 'Role of Geostatistics in subsurface hydrology' In: *Geostatistics for nature resources characterization.* Proc. NATO-ASI, (Verly, G., David, M., Journel, A.G. and Marechal, A. eds.) Part 1, pp. 787 - 816. Reidel, Dordrecht, the Netherlands.

Neuman, S. 1987. 'Stochastic continuum reperesentation of fractured rock permeability as an alternative to the REV and fractwork concepts'. In *28th US Symposium on Rock Mechanics*/Tuscon/29 June - 1 July 1987.

Niemi, A & Kontio, K. 1991. Geostatistical analysis of hydrological data from Romuvaara and Veitsivaara. TVO/Site Investigations. Progress report 91-12, 42 p. (in Finnish, abstract in English)

Niemi, A & Kontio, K. 1992. Geostatistical analysis of hydrological data from Konginkangas, Olkiluoto and Syyry and additional studies for Romuvaara and Veitsivaará. TVO/Site Investigations. Progress report 92-62, 79 p. (in Finnish, abstract in English)

Niemi, A. 1992. Modeling of large scale flow in fractured medium with Monte Carlo simulation. *Am. Geophys. Union / Can. Geophys. Union Meeting* 1992 Spring Meeting. May 12-16, 1992, Montreal. pp. 118.

Niemi, A & Kontio, K. 1993. Geostatistical analysis of hydrological data from five crystalline rock sites in Finland. *Report YJT-93.* Publication of Nuclear Waste Commission of Finnish Power Companies. 42p.

Niemi, A. 1993. Uncertainty in modeling flow in fractured media - analysis with stochastic continuum concept. To be published as Technical Research Centre of Finland / VTT-Publications. Technical Research Centre of Finland. Helsinki, Finland.

Pingoud, K., Pitkänen, P. & Kuusela, A. 1988. Interpretation of hydraulic conductivity measurements in Kuhmo, Romuvaara: boreholes KR1 and KR2. TVO/Site Investigations. Progress report 88-20. Industrial Power Company of Finland, Helsinki. (in Finnish, abstract in English)

Saksa, P., Paananen, M., Paulamäki, S., Anttila, P., Ahokas, H., Pitkänen, P. Front, K. & Vaittinen, T. 1992a. Bedrock model of Romuvaara area. Report YJT-92-06. Publication of Nuclear Waste Commission of Finnish Power Companies. Industrial Power Company of Finland, Helsinki.

Saksa, P., Kuivamäki, S., Kurimo, M., Anttila, P., Ahokas, H., Front, K., Pitkänen, P., Korkealaakso, J. & Vaittinen, T. 1992b. Bedrock model of Veitsivaara area. TVO/Site Investigations. Progress report 92-37. Industrial Power Company of Finland, Helsinki.(in Finnish, to be translated into English)

Saksa, P., Paulamäki, S., Paananen, M., Anttila, P., Ahokas, H., Front, K., Pitkänen, P., Korkealaakso, J. & Okko, O. 1992c. Bedrock model of Kivetty area. TVO/Site Investigations. Progress report 92-61. Industrial Power Company of Finland, Helsinki.(in Finnish, to be translated into English)

Saksa, P., Paulamäki, S., Paananen, M., Anttila, P., Ahokas, H., Front, K., Pitkänen, P., Hassinen, P. & Ylinen, A. 1992d. Bedrock model of Olkiluoto area. TVO/Site Investigations. Progress report 92-84. Industrial Power Company of Finland, Helsinki. (in Finnish, to be translated into English)

Saksa, P., Kuivamäki, S., Kurimo, M., Paananen, M., Anttila, P., Ahokas H., Front, K., Hassinen, P. & Ylinen, A. 1992e. Bedrock model of Syyry area. TVO/Site Investigations. Progress report 92-85. Industrial Power Company of Finland, Helsinki. (in Finnish, to be translated into English)

Taivassalo, V., ja Meszaros,F. 1992. Simulation of groundwater flow in Konginkangas, Kivetty - flow model and element meshes. TVO/Site Investigations. Progress report 92-76. Industrial Power Company of Finland, Helsinki. (in Finnish, abstract in English)

Teollisuuden Voima Oy. 1992. Final disposal of spent nuclear fuel in the Finnish bedrock. Preliminary site investigations. Nuclear Waste Commission of Finnish Power Companies. Report YJT-92-32. December 1992. 322 p. Helsinki. (In Finnish with English abstract. To be translated into English).

Uraiet, A.A. & Raghavan, R., 1980. Unsteady flow to a well producing at constant pressure. *J. Pet. Tech.* Oct: 1813-1824.

Winberg, A. 1989. Analysis of spatial variability of hydraulic conductivity data in the SKB database GEOTAB. Technical report IRap 89405. SKI TR 89:12. Swedish Geological Co, Goteborg, Sweden.

GROUNDWATER BALANCE IN A PRECAMBRIAN FRACTURED AREA: PALMOTTU, SW FINLAND

H. NIINI & M. VESTERINEN
Laboratory of Engineering Geology and Geophysics
Helsinki University of Technology
TKK-V, FIN-02150, Espoo, Finland
A. KUIVAMÄKI & R. BLOMQVIST
Geological Survey of Finland, FIN-02150, Espoo, Finland

ABSTRACT. Observations, measurements, and calculations aimed at determining the groundwater flow regime at deeper levels were carried out in the Lake Palmottu drainage basin. These water movements affect the migration of radionuclides from the Palmottu U-Th deposit. The deep water flow is essentially restricted to bedrock fractures. Determination of the detailed water flow variations was based on fracture-tectonic modelling of the 12 most significant underground water-flow pathways that cross the surficial water divide of the Palmottu area. According to the direction of the hydraulic gradient, the deep water flow is mostly outwards from the Palmottu catchment but in the westernmost section it is partly towards the centre. Estimation of the water flow through the U-Th deposit by the water-balance method is still only approximate and needs continued observation series and improved field measurements.

INTRODUCTION

The deep groundwater-flow studies of the Palmottu project aim at determining the water flow that affects the migration of radionuclides from the Palmottu U-Th deposit. Specific problems include determining (1) the quantity of water flowing through the deposit proper, (2) variations in the distribution of flow with depth, and (3) the sources and pathways of this flow.

We report our findings in the three sections below, namely (1) description of the relevant features of the Palmottu U-Th deposit study area and its surroundings, (2) estimation of water-balance components, and (3) interpretation of the underground flow pathway analysis.

THE STUDY AREA

The Palmottu deposit

The study area comprises the surficial drainage basin of Lake Palmottu and its immediate vicinity including the area of the Palmottu U-Th deposit (Figure 1). The deposit is an irregular

body, about 300 m long and 1—15 m thick (Figure 2). It is associated with granitic veins in migmatitic mica-gneiss host rocks. The deposit contains 1 Mt of rock with an average grade of 0.1 % uranium.

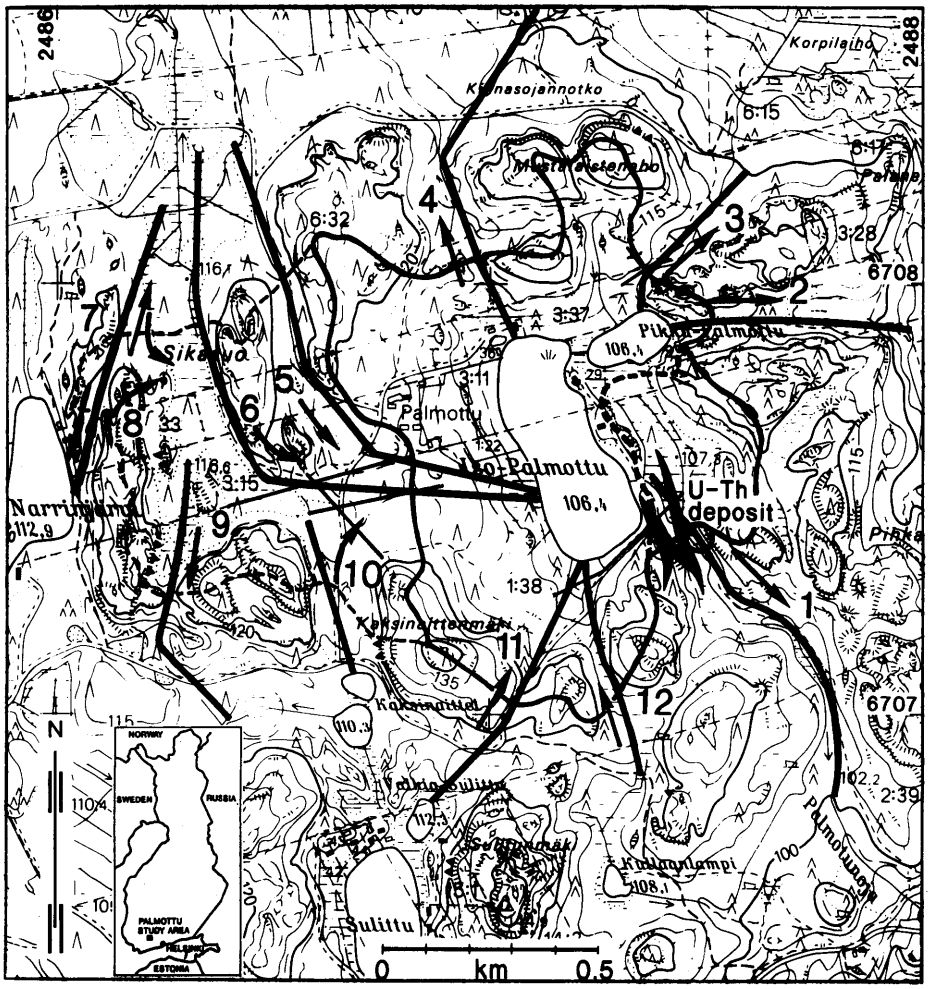

Figure 1: The Palmottu study area. The surficial drainage basin is shown with a continuous line; the areas shown with a broken line are areas of special interest. A circle close to the U-Th deposit shows the location of the measuring weir. The probable groundwater flow pathways formed by the prominent fracture zones are marked with broad black lines and numbered (1—12). Arrows indicate underground flow directions. Straight narrow lines represent seismic soundings.

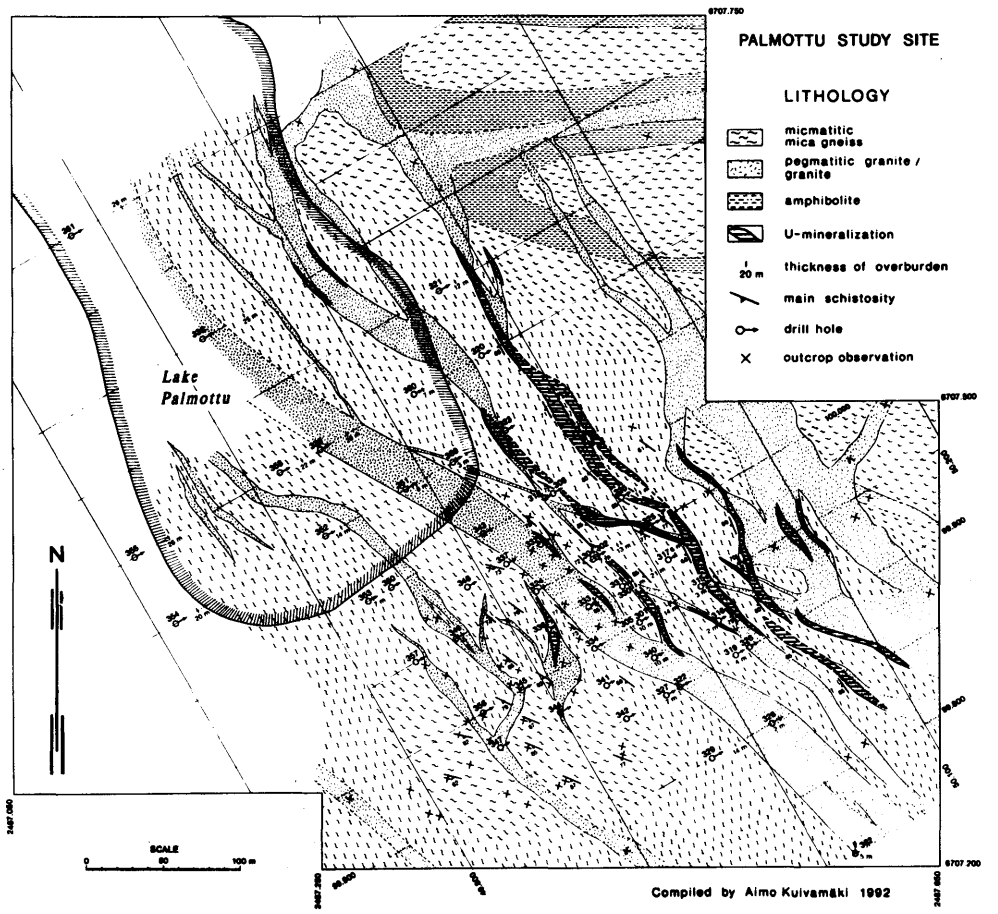

Figure 2: Lithological map of the Palmottu U-Th deposit. The local drill-hole grid has been determined by the general strike of the deposit.

The petrological as well as fracture-tectonic features of the study have been summarized recently (Suksi *et al.* 1992, pp. 10—12) and presented in detail earlier (Vuorela *et al.* 1991, pp. 17—20; Kuivamäki *et al.* 1991, pp. 21—45; Ruskeeniemi & Vesterinen 1991). These studies also describe in detail — based on 30 drill-holes — how the variable fracture and fault zones irregularly dissect the rocks.

The drainage area

The Palmottu drainage basin as deduced from surface contours is about 0.85 km^2 in area. A small swamp east of Lake Palmottu is included; it discharges into the outlet stream of Lake

Palmottu just above the measuring weir and almost on the same level as the lake (see Figure 1).

On the basis of geological observations about the thickness of the Quarternary deposits and the abundance of deep fracture zones (explained later) it seems likely that the surficial drainage basin essentially differs from the groundwater drainage area in the western section of the water divide. This area is particularly interesting from the point of view of underground water flow. When this western area is included in the Palmottu drainage area, the total area rises to 1.25 km^2 (see Figure 1).

The deposit, or the drillhole area, southeast of Lake Palmottu, lies partly in the Palmottu drainage basin, and partly outside the basin, around the outlet of Lake Palmottu. Topographically, the study area is undulating with altitudes varying between 100 and 145 m above sea level; these topographical features, including the general inclination towards SE, are well seen from the computer-based relief model of the area (Figure 3).

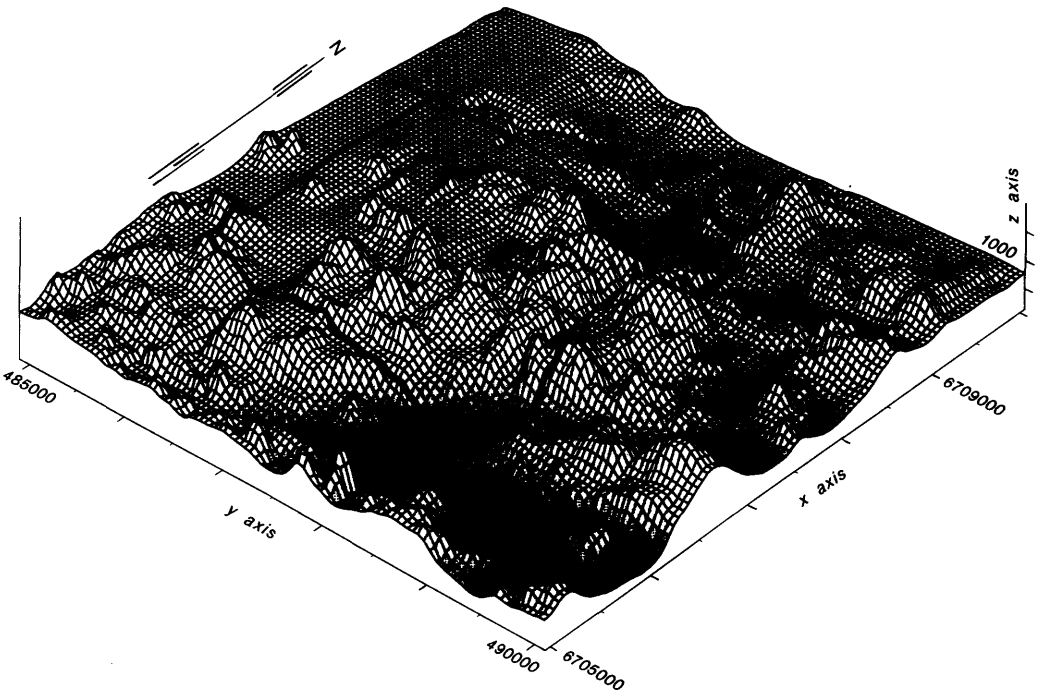

Figure 3: The relief of the study area showing the drainage basin of Lake Palmottu. The rectangular area of Figure 4 is indicated. Computer processing by Maija Kurimo, Geological Survey of Finland, from digitized data of the Finnish National Board of Survey.

Surficial geology

The Quaternary deposits overlying bedrock (Figure 4), consist of a thin till horizon throughout much of the area. The abundance of outcrops indicates that the till layers, except in certain valleys, are relatively thin (few metres at the most). The larger valleys are covered by peat whose thickness may be up to 5 metres.

The hydrogeologically interesting area west of Lake Palmottu consists of glaciofluvial deposits and peat. The area represents the foreland to a large delta formation (Salpausselkä III) consisting of washed till and glasiofluvial sand, with a maximum thickness of about 25 m.

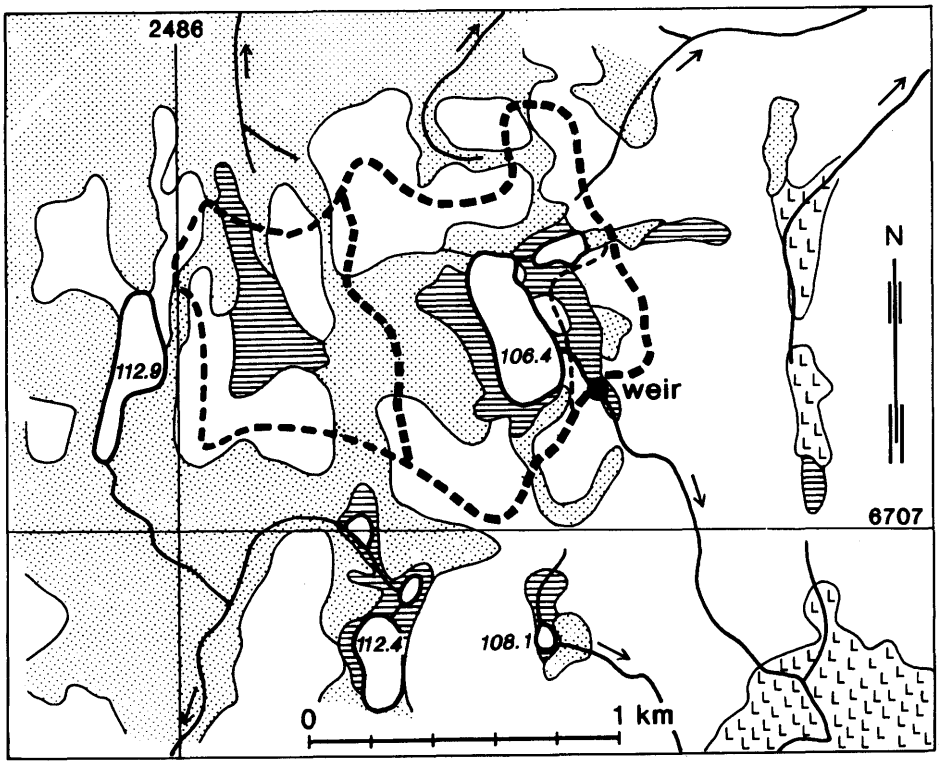

Figure 4: The Quaternary layers of the Palmottu area generalized from the 1:20,000 scale Quaternary deposits Map, sheet 2023 09, Johannislund. Dotted areas represent glasiofluvial deposits and horizontally ruled areas peat. White areas comprise outcropped terrain partly covered by a thin layer of till. Water courses are shown by bold lines and the areas considered by broken lines. Lake level indicated in metres above sea level.

WATER-BALANCE ESTIMATION

Principles

To determine the groundwater movements affecting the migration of uranium and thorium in the drillhole area, it was deemed important to locate and estimate all potential water-flow pathways to and from the drainage basin. Excluding precipitation and evapotranspiration, there are three basic options for water to escape or enter the basin (Figure 5).

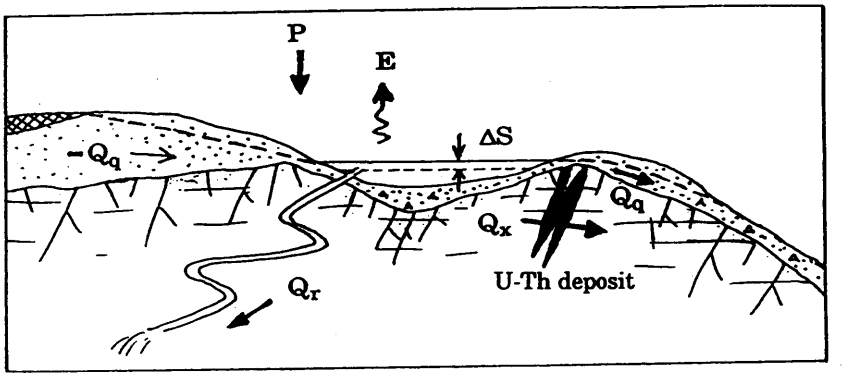

Figure 5: Schematic representation of water balance components. Key: Qx is the groundwater flow through bedrock, P precipitation, E evapotranspiration, Qr surface runoff from the basin, Qq the groundwater flow through the Quaternary layer, and ΔS the seasonal change in water storage.

(a) Southeastwards runoff via the Palmotunoja outlet brook; to measure this by normal hydrological discharge measurements, a Thompson weir was installed in the outlet.

(b) Groundwater flow in Quaternary layers, especially in the thick, permeable sandy sediments west of Lake Palmottu. Geophysical measurements carried out in this delta area showed that the thickness of the sand layers is more than 15 m and the groundwater table is about 3—4 m below the ground surface.

(c) Groundwater flow along bedrock fracture zones in all directions; this presumably very slow movement cannot be directly measured but may be assessed from hydraulic gradients and transmissivities of the fracture zones, if evapotranspiration, surface discharge, and the flow through the loose Quaternary layers are first subtracted. The underground flow through bedrock is most probably outflow, but in principle inflow is also possible.

The connection between the mentioned factors in the Palmottu drainage basin can be described by the water balance equation:

$$P - E - Qr \pm Qq \pm Qx \pm \Delta S = 0 \quad (1)$$

where P is precipitation, E evapotranspiration, Qr surface runoff from the basin, Qq the underground flow through the Quaternary layer, Qx the underground flow through the bedrock, and ΔS the seasonal change in water storage.

An estimation of the water-balance components (Table 1) was obtained by using the annual precipitation value and the mean annual evapotranspiration of the region (Lemmelä 1976), by measuring the outflow from the outlet stream, and neglecting the seasonal storage changes, since a bottom dam at the outlet of Lake Palmottu prevents considerable changes of the water table. The most uncertain component Qq was obtained by observing the soils and measuring the hydraulic gradient at the 12 passes (fracture zones) cutting the water divide. A numeric model was used in which the aquifer-property values (cross section and hydraulic conductivity) of the soils were taken from similar nearby areas using physiographic analogies (Niini 1989). This procedure implies that (a) the hydraulic conductivity of the soils varied being 10—1000 times that of the bedrock fracture zones beneath them, (b) the total cross-sectional area of the soil pathways leading water through the surficial water divide was of the same order as that of the bedrock aquifers, and (c) the hydraulic gradient in the Quaternary layers was directed clearly outwards from the area in only five fracture zone profiles: pathways numbers 1, 3, 7, 8 and 9 (see Figures 1 and 6).

Table 1: A summary calculation of the water balance at Palmottu.

Component	P	E	Qr	Qq	ΔS	Qx
in mm/year	750	—430	—130	+35	±0	= 225
in 100 m^3/year	550	—315	—95	+25	±0	= 165
assessed inaccuracy %	±15	±20	±20	±500	±5	±30

Subterranean flow pathways

The results of 12 seismic-sounding and ground-penetrating-radar profiles were projected on 12 longitudinal fracture-zone profiles, of which four examples are shown in Figure 6. The variations in water flow are dependent on two basic factor groups: the hydraulic gradient and the hydrological properties of the fracture zones, both of which generally show considerable areal and depth variability. The hydrological properties of each fracture zone were not measured but assumed to be "known" in the sense that the analogical numerical values were obtained from the Palmottu drill-hole data (Ahonen & Paananen 1991, Ruskeeniemi & Vesterinen 1991) and from correlations established by studies of other similar areas in southern

Finland (Niini 1968, Ehlers 1970, Niini & Ekholm 1976; Brusila 1983). These analogies imply assumed similarities in the three-dimensional occurrence of the fracture zones and their materials, representing the crucial hydraulic conductivities and pathway dimensions. The hydraulic gradient was measured from the heights and inclinations of the water table along the fracture-zone profiles.

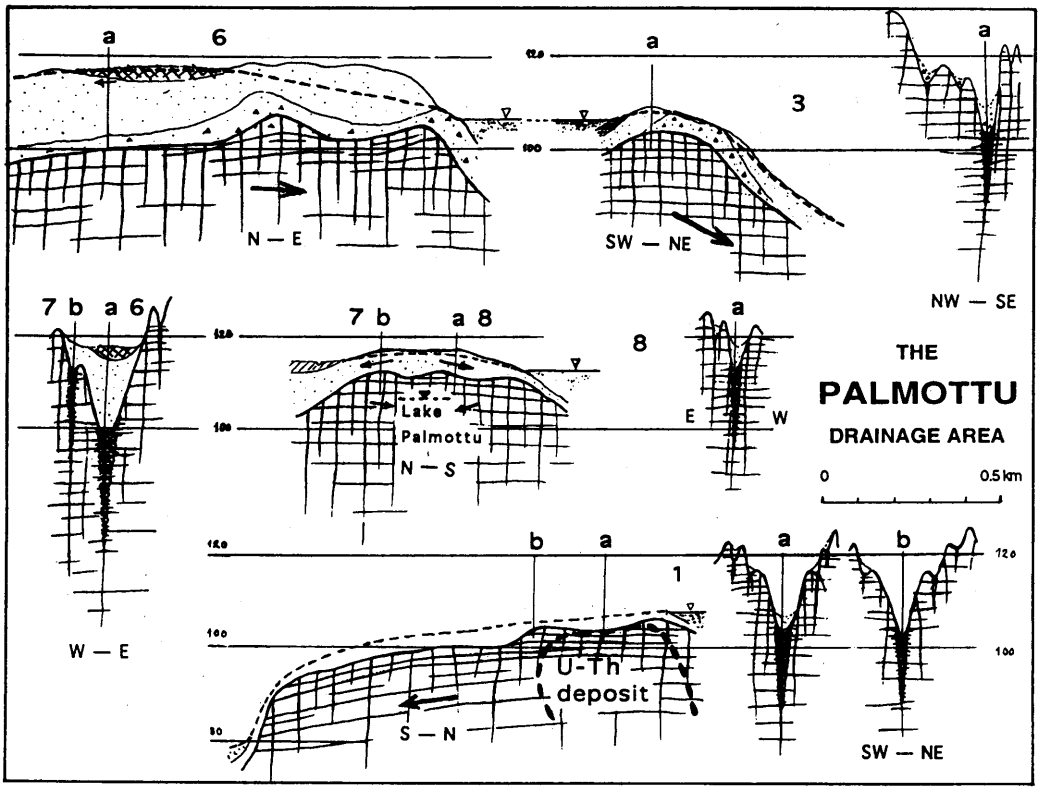

Figure 6: Longitudinal fracture-zone profiles as measured from the 1:10,000 topographic maps and interpreted geologically on the basis of observations, seismic and radar measurements, and earlier analogues from corresponding areas. Sharp broken line indicates water table, and arrows indicate the direction of groundwater flow.

Without going into the details of this 3-stage calculation procedure we present a summary grouping of the water flow pathways according to the direction of the flow through the water divide (Table 2).

Table 2: Underground flow (positive Qx outwards) along the fracture zones through the surficial water divide of the drainage area of Lake Palmottu, grouped according to flow direction.

Fracture-zone group	Qx(1000 m^3/year)
a. Pathway number 1 through the U-Th deposit	15
b. Other pathways with outwards flow (numbers 2, 3, 4, and 9)	240
c. Pathways with inwards flow (numbers 5, 6, 10, 11, and 12)	—430
d. Outflow in upper part, inflow parts (numbers 7 and 8)	340
Total drainge area	165

Conclusions

The main purpose of this case study was to assess the underground water movement controlling the migration of radionuclides from one specific U-Th deposit (see Table 2; 15,000 m^3/year). In addition, the study also yields three more general considerations:

(a) The use of the water-balance method implies that the sizeable inaccuracies originating from the directly measured or "known" terms (precipitation, evapotranspiration, surface runoff, storage change and groundwater flow in the soils) culminate in the rest term, the target, *i.e.*, flow in bedrock. Naturally, follow-up work requires a more accurate determination of both the common water-balance components and the hydraulic properties of the individual pathways. This method may then give quite realistic limits. However, to reach a reasonable accuracy use of other methods are inevitable, *eg.*, hydraulic testing of drill-holes (Andersson *et. al.* 1991), temperature measurements in drill-holes (see Drury *et al.* 1984) and/or tracer methods (see Freeze and Cherry 1979).

(b) The deep groundwater flow is essentially concentrated in the large bedrock fractures that in many places transect the water divides. Because such fractures form a structural feature typical of the Fennoscandian shield area, it seems important to emphasize, more than hitherto, the deviation between the surface drainage area and the deep groundwater drainage area.

(c) The horizontal extension, depth, and timely variations of the waterflow in the bedrock are essentially dependent on the material properties, hydraulic conductivity of particular, in the fracture zones. These have been developed in, and are still affected by, complicated geological processes (see Munier 1993). Therefore, we think that the study and the calculation procedure presented clearly emphasizes the importance of the accurate three demensional observations of the geological variations.

ACKNOWLEDGEMENTS

The study is part of a broader nuclear-waste analogue project financed by the Finnish Centre for Radiation and Nuclear Safety and the Ministry of Trade and Industry of Finland. The English text was corrected by Dr. Peter Sorjonen-Ward.

REFERENCES

GSFR = Geological Survey of Finland, Report YST.

Ahonen, Lasse & Paananen, Markku, 1991. The Palmottu Analogue Project, Drill hole hydrogeology. *GSFR* 73, 75—88.

Andersson, J.-E., Ekman, C., Nordqvist, R. & Winberg, A., 1991. Hydraulic testing and modelling of a low-angle fracture zone at Finnsjön, Sweden. J. Hydrol. 126, 45—77.

Brusila, Jukka, 1983. Bedrock permeability investigations (in Finnish), *GSFR* 34 G.

Drury, M.J. & Jessop, A.M. & Lewis, T.J., 1984. The detection of groundwater flow by precise temperature measurements in boreholes. Geothermics 13, 163-174.

Ehlers (von Knorring), Mary, 1970. Use of airphoto interpretation in estimating bedrock fracture zones (in Swedish). Master thesis, Åbo Akademi (The Swedish University of Turku).

Freeze, R. Allan & Cherry, John A., 1979. Groundwater. Prentice-Hall, Inc. Englewood Cliffs, N.J., 588 pp.

Kuivamäki, Aimo & Paananen, Markku & Kurimo, Maija, 1991. The Palmottu Analogue Project, Bedrock structures, *GSFR* 73, 21—45.

Lemmelä, Risto, 1976. Maps of water balance elements of Finland. *Aqua Fennica* 6, 10—17.

Munier, Raymond, 1993. Segmentation, Fragmentation and Jostling of the Baltic Shield with Time. Acta Universitatis Upsaliensis. Uppsala Dissertations from the Faculty of Science 37, 96 pp. Uppsala.

Niini, Heikki, 1968. A study of rock fracturing in valleys of Precambrian bedrock. *Fennia* 97:6.

Niini, Heikki, 1989. Glacial sculpture in bedrock valleys differing in orientation. *Geological Survey of Finland, Special Paper* 7, 19—24.

Niini, Heikki & Ekholm, Matti, 1976. Assessing the macroporosity of bedrock using physiographic measurements in order to evaluate ground-water damage caused by tunnel construction. *Nordic Hydrological Conference, Reykjavik 1976, Proceedings* III-52-60.

Ruskeeniemi, T. & Vesterinen, M., 1991. The Palmottu Analogue Project, Fractures and fracture minerals in drill core 346. *GSFR* 73, 47—58.

Suksi, Juhani & Ahonen, Lasse & Niini, Heikki (ed.), 1992. The Palmottu Analogue Project, Progress Report 1991. *GSFR* 78.

Vuorela, Paavo & Lindberg, Antero & Räisänen, Esko, 1991. The Palmottu Analogue Project, geological framework. *GSFR* 73, 17–20.

ESTIMATION OF SCALE EFFECT ON EFFECTIVE POROSITY AND LONGITUDINAL DISPERSIVITY OF A TERTIARY SEDIMENTARY ROCK BY LABORATORY TRACER TESTS AND A FIELD TRACER TEST

H. II
Research Institute, Shimizu Corporation
4-17, Etchujima 3-Chome, Koto-ku, Tokyo 135, Japan
K. SUGIHARA
Chubu Works, Power Reactor & Nuclear Fuel Development Corporation
959-31, Jyorinji, Izumi, Toki, Gifu 509-51, Japan
Y. ISHIKAWA
Dowa Engineering Co. Ltd.
19-22, Chikkosakaemachi, Okayama, Okayama 702, Japan
Y. UTSUGIDA
Nuclear Power Division, Shimizu Corporation
2-3, Shibaura 1-chome, Minato-ku, Tokyo 105-07, Japan

ABSTRACT. We have performed a field tracer test in a Neogene sedimentary rock and have also performed laboratory tests using core samples of the sedimentary rock. We have estimated effective porosity and longitudinal dispersivity which are essential to evaluate mass transport in groundwater. The results of these tests indicate that test scale should be considered to evaluate effective porosity and longitudinal dispersivity. As test scale increases, effective porosity decreases and longitudinal dispersivity increases. The following empirical relationship has been found for the sedimentary rock: longitudinal dispersivity equals one tenth of test scale. This is in agreement with the relationship presented in the paper by Leonhart *et al.* (1985). The decrease of effective porosity is probably due to loss of connectivity of continuous pores.

INTRODUCTION

Porosity is defined as the total pore proportion and includes closed pores, branches and continuous pores. Effective porosity is defined as the proportion of pores through which water flows and consists of continuous pores. Therefore, in most cases, porosity is lager than effective porosity (Ii & Sugiyama, 1991). Effective porosity should be determined in order to calculate actual velocity of groundwater, but porosity is sometimes used as effective porosity because of some difficulties in the measurement of effective porosity. As actual velocity of groundwater is an essential parameter for the estimation of mass transport in groundwater, accurate estimation of effective porosity is particularly important.

Dispersion is also an essential phenomenon for estimating mass transport in groundwater. In this study, longitudinal dispersivity is used as the parameter which represents dispersion. Longitudinal dispersivity is defined as dispersion coefficient per actual velocity.

We discuss effective porosity and longitudinal dispersivity estimated by laboratory tests and a field test. In this paper, a field tracer test was performed in a Neogene sedimentary rock and laboratory tests were performed using core samples of the rock. We can compare values of effective porosity and longitudinal dispersivity from laboratory tests with those from field tracer test and study the effect of test scale on these two parameters.

The field test site is located in the south part of Gifu prefecture, central Japan. In this area, several kinds of sedimentary rocks unconformably cover granite basement. There is a permeable zone which is composed of Neogene coarse sandstone and weathered granite above and below the unconformity (Ishikawa & Sugihara, 1991).

TRACER

Conservative tracers are suitable for the tracer test which is carried out to estimate effective porosity and longitudinal dispersivity as it is not necessary to consider adsorption of tracers to rocks. We selected Br^- and Cl^- as tracers, and performed batch experiments to confirm that Br^- and Cl^- would not be adsorbed by rock samples. Distribution coefficients (Kd) of the tracers can be calculated, according to the following formula in batch experiments:

$$Kd(ml\ g^{-1}) = \frac{q(g\ g^{-1})}{Cq(g\ ml^{-1})} \quad (1)$$

The quantity q, representing mass of tracer on the rock sample per unit mass of the rock sample, is calculated by comparing the initial concentration (C_0) of Br^- or Cl^- in the solution with the equilibrium concentration (Cq) of Br^- or Cl^- in the solution with the addition of rock sample after several days. q can be calculated as follows:

$$q = \frac{(C_0 - C_q) \times V_s}{W_b} \quad (2)$$

Vs:Volume of tracer solution Wb:Weight of rock sample

The initial concentration of solution was 13 ppm for Cl^- and 21 ppm for Br^-. The weight ratio of sample to solution ranges from 3.1 to 4.4 per 100. In this experiment at all cases, q was calculated to be about 0. The results suggested that Br^- and Cl^- could be regarded as conservative tracers in the tracer tests.

Method

Figure 1 shows a schematic figure of the field tracer test. There were two bore holes, each about 90m in depth and 7m apart. There were permeable layers of mainly weathered granite and coarse sandstone, which was formed in the Neogene period, from 80 to 90m in depth. These layers were sandwiched between impermeable layers of siltstone and fresh granite. The bore holes were fully lined from 0 to 80 m in depth and perforated in the zone of permeable coarse sandstone. Before the tracer was injected, groundwater was pumped out at the recovery bore hole and injected at the injection bore hole.

Groundwater was kept circulating until a steady state groundwater regime was obtained. When steady state was obtained and the circulation flow rate was maintained at 7800 $cm^3\ min^{-1}$, Br^- tracer solution was injected at the injection bore hole. The original volume of tracer solution which contained 2 kg NaBr was 180000 cm^3. Br^- was selected because of its low background concentration in the groundwater. During the test, groundwater was sampled regularly at the recovery bore hole to measure the concentration of Br^- by ion exchange chromatography.

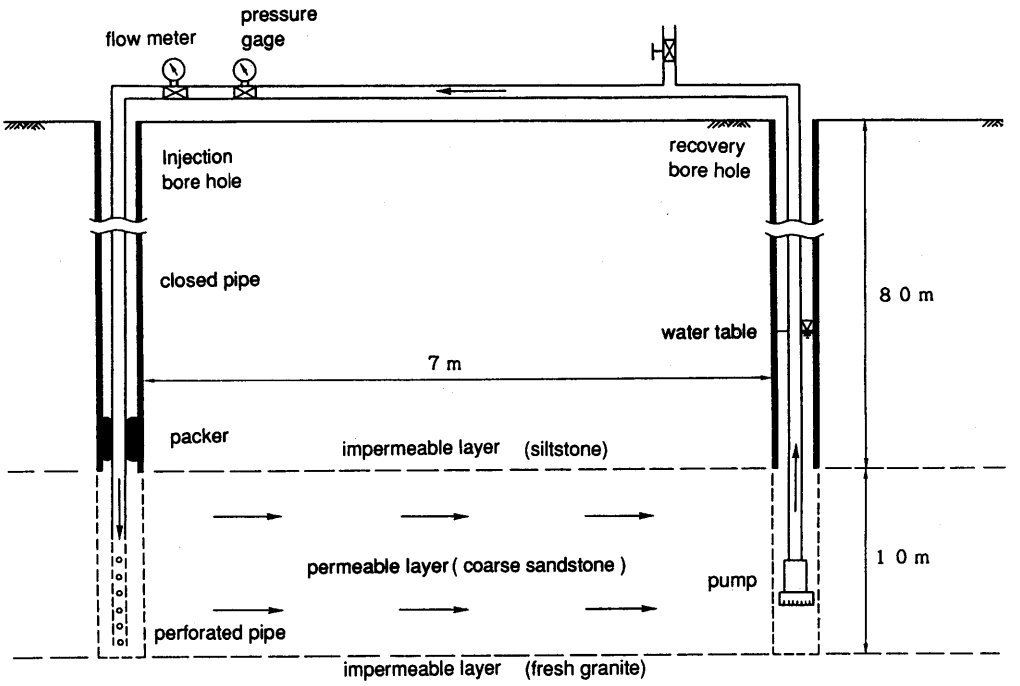

Figure 1:Schematic figure of field tracer test.

Analysis

From the breakthrough curve for Br^- in the field tracer test, the actual velocity and longitudinal dispersivity were calculated based on the following analytical solution of the two dimensional diffusion equation for a two-well (pumping-injection) flow system (L.W.Gelhar, 1982):

$$Cw = \frac{Q}{M}\int_0^{\infty} \frac{Q\exp[-a(-T)^2/4eb]}{\varepsilon h L^2 (4\pi eb)^{\frac{1}{2}}} d\hat{\varphi}$$

$$T = \frac{QT}{\varepsilon h L^2} \qquad e = \frac{\alpha}{L}$$

$$a(\varphi) = \pi(\sin\phi - \phi\cos\phi)/\sin\phi^3 \qquad :\phi = \pi\varphi$$

$$b(\gamma,\phi) = \pi^2[(\gamma+\phi)/2+(\sin\gamma\cos\gamma)/2+(\sin\phi\cos\phi)/2-2\cos\phi(\sin\gamma+\sin\phi)+(\gamma+\phi)\cos^2\phi]/2\sin^5\phi \quad (3)$$

where

Cw : concentration at recovery bore hole, t : time,

ε : effective porosity Q : flow rate, h : thickness of layer,

M : mass of tracer, γ : position of the tracer pulse

φ : stream function $\hat{\varphi}=2h\varphi/Q$, L : distance between bore holes,

α : longitudinal dispersivity

Table 1 shows the conditions which were used for analysis of the field tracer test.

Table 1:Conditions of two dimensional analysis for field tracer test.

Distance (m)	7
Flow rate ($cm^3\ min^{-1}$)	7800
Thickness of permeable layer (m)	10
Mass of tracer (g)	3000 (NaBr)
Effective porosity (%)	2～30
Longitudinal dispersivity (m)	0.014 ～ 7

Results

Figure 2 shows the relationships, which were obtained by the two dimensional analysis and in the field test (Ii *et al.*, 1993), between the concentration of Br^- at the recovery bore hole and elapsed time after the start of tracer injection. Effective porosity and longitudinal dispersivity were analyzed to be 4.5% and 3.5m respectively.

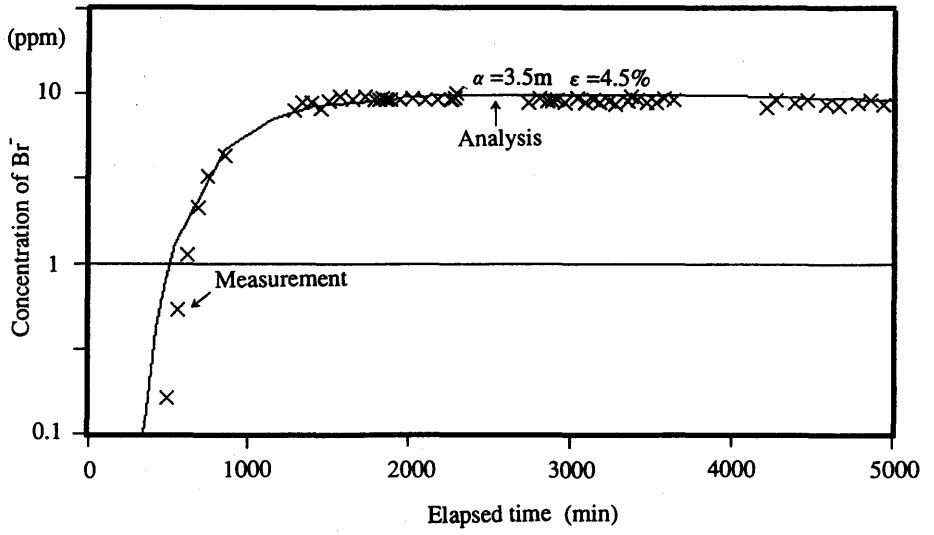

Figure 2:Relationship between concentration of Br^- and elapsed time.

LABORATORY TRACER TEST

Method

Porosities of core samples of the permeable layer were measured from weights of the samples in both water saturated and dry conditions. The porosity values ranged from 6～47% and were mainly concentrated in the range of 25～30% (Ii *et al.*, 1993). Three samples of different porosities were used in laboratory tracer tests. Figure 3 shows the apparatus for the laboratory tests. To determine effective porosity, solutions containing Br^- or Cl^- as tracers with concentrations of 100 to 300 ppm were pumped into the column under constant flow rates maintained through manual adjustments of the nitrogen cylinder valve. Volume of effluent solution was measured to determine the flow rate. The Br^- or Cl^- concentration of the effluent solution was analyzed with ion exchange chromatography.

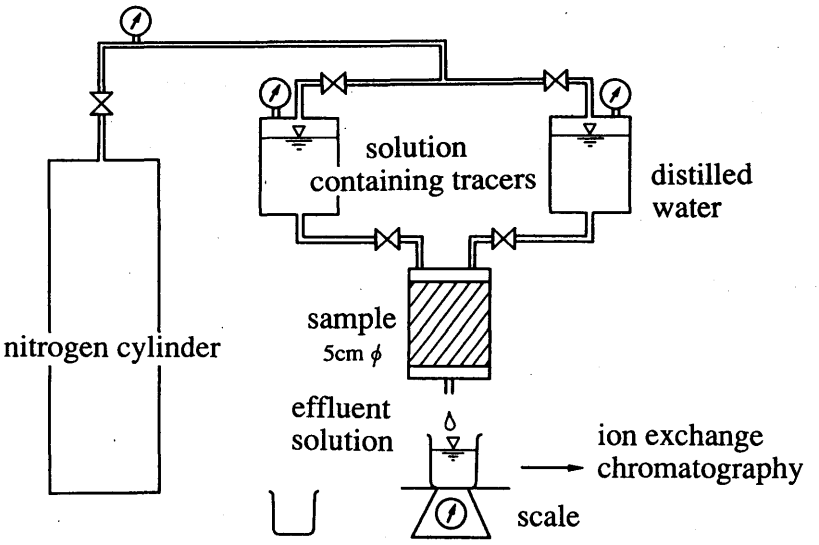

Figure 3:Apparatus for laboratory tracer test.

Analysis

From the breakthrough curves of Br^- or Cl^- under several constant-head conditions at the laboratory tests, the actual velocity and dispersion coefficient were calculated based on the following analytical solution of the one dimensional diffusion equation:

$$\frac{C}{C_0} = \frac{1}{2}\{\mathrm{erfc}(\frac{L-Vt}{2\sqrt{Dt}}) + \mathrm{erfc}(\frac{L+Vt}{2\sqrt{Dt}}) \times \exp(\frac{VL}{D})\} \quad (4)$$

where

C:concentration, C_0:initial concentration, L:length of sample,
D:dispersion coefficient, t:time, V:actual velocity

The initial and boundary conditions are:

C_0=constant, V=constant
C=0, X=∞, at all times
C=0, X>0, at t=0.

From the actual velocity (V) and the monitored constant flow rate (Q), the cross-sectional area of void which the pore water passes through (A) was calculated, based on the equation $A=Q V^{-1}$. The effective porosity (ϵ) was then calculated, based on the equation $\epsilon = A A'^{-1}$ on the assumption of Depuit-Forchheimer. A' represents the total area of the cross section of a sample.

Results

Figure 4 shows an example of a breakthrough curve obtained in the laboratory tests. The line represents the regression curve using the analytical solution. Based on equation (4), the actual velocity and the dispersion coefficient for the Br^- or Cl^- were calculated according to the relationship between elapsed time and the Br^- or Cl^- concentration normalized by initial concentration. Table 2 gives the conditions and results of the laboratory tests. When the length of sample was 1.0 cm, effective porosity equaled porosity. As the length of samples increased from 1.0 cm to 6.0 cm, effective porosity decreased.

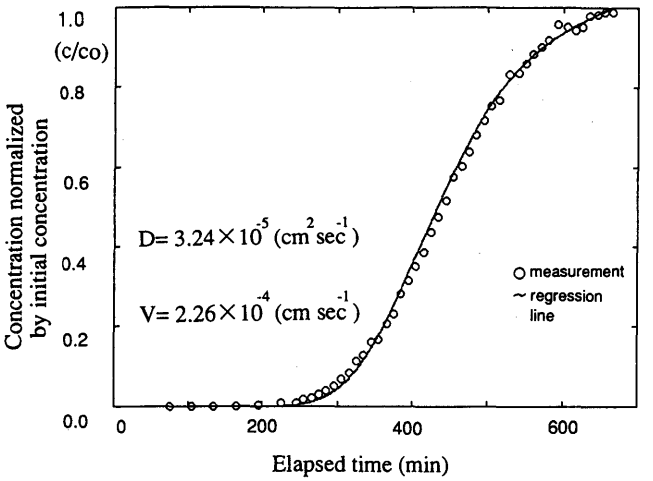

Figure 4:Example of breakthrough curve in laboratory test.

DISCUSSION

Figure 5 shows the relationship between effective porosity per porosity and test scale. Test scale is a length of sample in a laboratory test and a distance between bore holes in a field test. The ratio of effective porosity to porosity indicates the proportion of volume of the pores where solution flows actually to volume of all kinds of pores. Porosities of 3 samples used in the laboratory test were 27, 29 and 31%. The porosity value of the field can be estimated to be about 30%. As the test scale increased from 1.0 cm to 7 m, effective porosity decreased from 30% to 4.5%. The decrease of effective porosity is probably due to loss of connectivity of continuous pores.

The results of field permeability test between the two bore holes used for the field tracer test (Ii *et al.*, 1993) shows the hydraulic conductivity of the permeable layer was 2×10^{-5} cm sec^{-1}. This value is much larger than those estimated in the laboratory tests, which were $2 \times 10^{-8} \sim 3 \times 10^{-6}$ cm sec^{-1}. Ishikawa & Sugihara (1991) indicates no remarkable permeable zone which consists of faults or fracture zones. But if cracks or fissures which are smaller than faults or

fracture zones exist, the hydraulic conductivity can become lager. For example, if there is a fracture with a width of 0.1～0.2mm, the mean hydraulic conductivity of a 10m zone can be 2 $\times 10^{-5}$ cm sec^{-1} based on Hele-Shaw model. The fracture will not change effective porosity of the zone so much. Therefore, we consider that permeable cracks or fissures possibly exist at this field scale.

Table 2:Conditions and results of laboratory tests.

Rock Type	Porosity (%)	Hydraulic conductivity (cm sec^{-1})	Length of sample (cm)	Effective porosity (%)	Flow rate (cm^3 sec^{-1})	Dispersion coefficient (cm^2 sec^{-1})
Sandstone	27	2.6×10^{-7}	1.10	24	1.9×10^{-3}	9.2×10^{-5}
				27	5.5×10^{-4}	3.5×10^{-5}
				28	1.2×10^{-3}	8.5×10^{-5}
		4.2×10^{-7}	2.01	22	3.2×10^{-3}	2.5×10^{-4}
				24	4.6×10^{-4}	3.8×10^{-5}
				25	7.4×10^{-3}	9.4×10^{-4}
	31	2.4×10^{-8}	1.99	25	1.1×10^{-3}	4.5×10^{-5}
				26	2.6×10^{-4}	8.8×10^{-6}
				27	7.1×10^{-4}	2.3×10^{-5}
				27	1.5×10^{-3}	3.8×10^{-5}
				27	2.8×10^{-4}	8.2×10^{-6}
		3.1×10^{-8}	5.01	21	2.7×10^{-4}	1.4×10^{-5}
				21	1.5×10^{-4}	7.6×10^{-6}
				22	7.3×10^{-4}	3.5×10^{-5}
				23	6.8×10^{-4}	2.7×10^{-5}
				24	6.1×10^{-4}	2.5×10^{-5}
		4.7×10^{-8}	6.05	22	1.4×10^{-3}	6.9×10^{-5}
				24	8.1×10^{-4}	3.2×10^{-5}
	29	8.3×10^{-8}	2.37	21	1.7×10^{-3}	2.3×10^{-4}
		4.2×10^{-8}	6.14	19	9.8×10^{-4}	7.5×10^{-5}

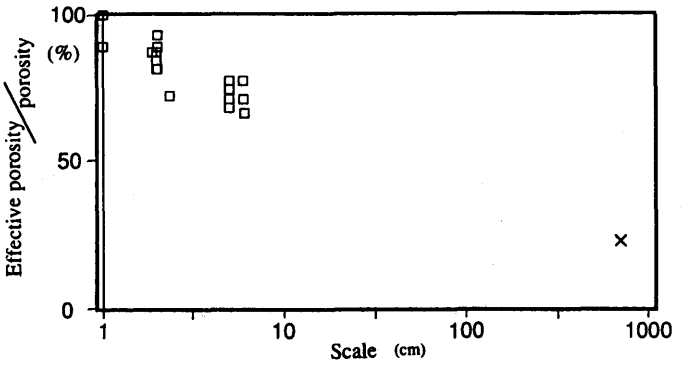

Figure 5:Relationship between effective porosity per porosity and test scale.

□ : in laboratory × : in field

Figure 6 shows the relationship estimated in laboratory tests between dispersion coefficient and actual velocity. As the actual velocity increases, the dispersion coefficient increases. Figure 7 shows the relationship between the test scale and longitudinal dispersivity in sedimentary rocks. Longitudinal dispersivity is the dispersion coefficient per actual velocity. Originally Leonhart *et al.* (1985) showed that as the scale of field tests increased, longitudinal dispersivity increased. Our results and the Leonhart *et al.* (1985) results indicate that as the test scale increased from several centimeters to several thousand meters, longitudinal dispersivity increased proportionally. The following empirical relationship has been found from these results: longitudinal dispersivity equals one tenth of test scale.

At the sample scale, the increase of longitudinal dispersivity has not been detected. According to the effective porosity discussion, selective flow paths such as cracks and fissures may exist. The existence of selective flow paths possibly affects the increase of longitudinal dispersivity, but quantitative estimation of the influence has been impossible because of lack of information on geometry and character of the selective flow path.

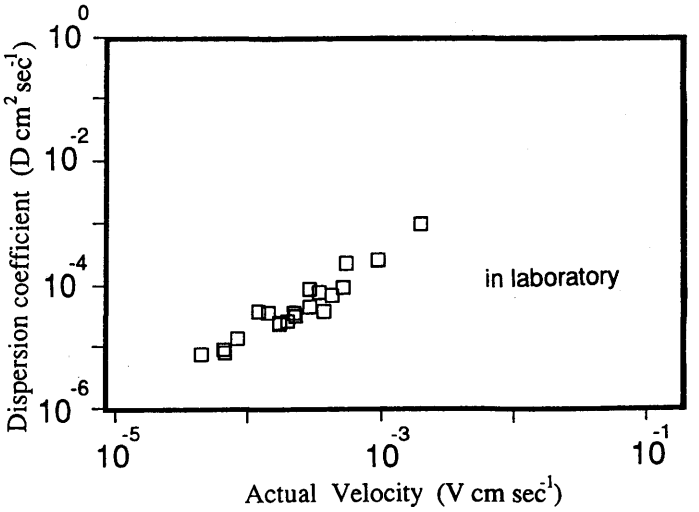

Figure 6:Relationship estimated in laboratory tests between dispersion coefficient and actual velocity.

CONCLUSION

We have performed both laboratory and field tracer tests using the conservative tracers in order to estimate effective porosity and longitudinal dispersivity of a sedimentary rock. Both the laboratory and field tracer test results indicate that as the test scale increases from 1.0 cm to 7 m, the effective porosity decreases and longitudinal dispersivity increases. The following empirical relationship has been found for the sedimentary rock: longitudinal dispersivity equals one tenth of scale.

The decrease of effective porosity may be attributed to the loss of connectivity of continuous pores. The existence of selective flow path such as cracks and fissures has been suggested based on the results of field permeability test, but the effect of selective flow path on the increase of longitudinal dispersivity has not been quantified because of the lack of information on geometry and character of the selective flow path.

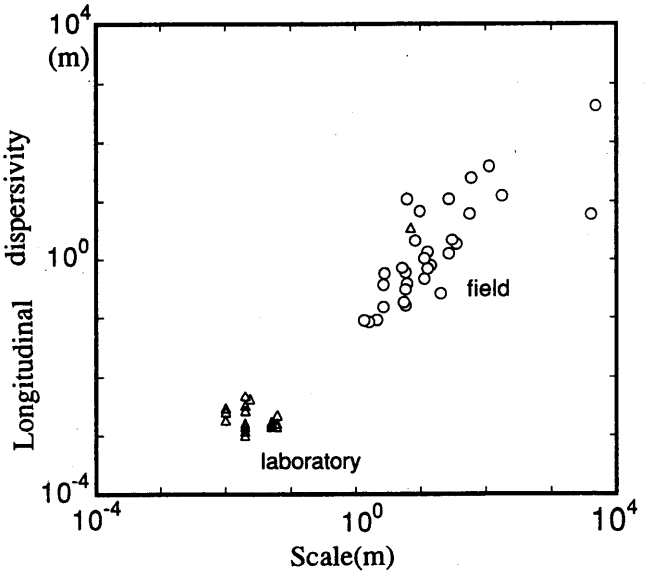

Figure 7:Relationship between longitudinal dispersivity and test scale.

△: this study
○: (Leo S.Leonhart et al,1985)

REFERENCE

Ii, H. & Sugiyama, H. 1991. Physical properties, especially effective porosity, of a bentonite and quartz sand mixture as backfill and buffer material for disposal of high-level radioactive waste. *Proceeding of the 1991 Joint International Waste Management Conference*, 2; 243-248.

Ii, H., Ishikawa, Y., Sugihara, K. & Utsugida, Y. 1993. Dispersion coefficient and effective porosity of a sedimentary rock by a field tracer test. *J,Groundwater Hydrology.*, 35,1.23-36. (in Japanese).

Ishikawa, Y. & Sugihara, K. 1991. Data acquisition in order to estimate the operating conditions of Uranium mine developed by the in-place leaching method. *PNC TN*, 78; 59 -66. (in Japanese).

Leonhart, L.S., Jackson, R.L., Graham, D.L., Gelhar, L.W., Thompson, G.M., Kanehiro, B.Y. & Wilson, C.R 1985. Analysis and interpretation of a recirculating tracer experiment performed on a deep basalt flow top, *Bulletin of the Association of Engineering Geologists*, Vol.XXII, 3; 259-274.

Gelhar, L W. 1982. Analysis of two-well tracer tests with a pulse input, *RHO-B W-CR*, 131P.

Section 4 :

HYDROLOGY AND GEOCHEMISTRY OF VOLCANIC REGIONS

HYDROGEOLOGY OF VOLCANIC OCEANIC ISLANDS

FRANK L. PETERSON
Dept. Geology & Geophysics
University of Hawaii
Honolulu, Hawaii, USA

ABSTRACT. Volcanic oceanic islands fall into two major provinces, the andesitic and the basaltic or oceanic. Islands of the andesitic province are associated with island arc volcanism and lie on the continental side of deep ocean trenches within the zone of lithospheric plate subduction. As such, they have typically continental affinities, thus, the term andesitic province. Examples of Pacific Ocean island groups within the andesitic province are the Northern Marianas, Guam, Palau, the Solomons, Vanuatu, Tonga, Fiji, and parts of the Cook Islands. Volcanic rocks in the andesitic province occur as lava flows and pyroclastics, and range in composition from basaltic to trachytic; however, submarine pyroclastics predominate. The permeability and water-bearing properties of volcanic rocks in the andesitic province are generally poor, and little usable groundwater can be developed from them. Instead, most groundwater is developed from limestone and raised coral reefs that are often associated with these islands. Islands of the oceanic province are typically basaltic, although composition may range to andesitic, and lava flows rather than pyroclastics predominate. The islands occur on the ocean side of trench/subduction systems and are associated with intraplate volcanism, thus, the name basaltic or oceanic province. Islands in this province are generally comprised of large, gently-dipping shield volcanoes. The lavas, if young and basaltic, such as those found typically in the Hawaiian Islands, French Polynesia, and parts of Samoa, are extremely permeable and make up the principal aquifers. Conversely, on islands where the lavas are older and contain more pyroclastic material, such as on Yap, Truk, and Pohnpei in Pacific Micronesia, the volcanics are poorly permeable and the most productive aquifers are sedimentary alluvial deposits and weathered lavas. Hence, depending on which volcanic province an island occurs within, the strategy for groundwater exploration and development may differ considerably.

INTRODUCTION

Freshwater development on small oceanic islands is one of the most challenging problems facing hydrogeologists today. The task is made especially difficult by adverse geologic conditions and the ever-present threat of salt water intrusion. To better understand the problems of occurrence and development of fresh water in this environment, knowledge of the geology of small oceanic islands is a necessity.

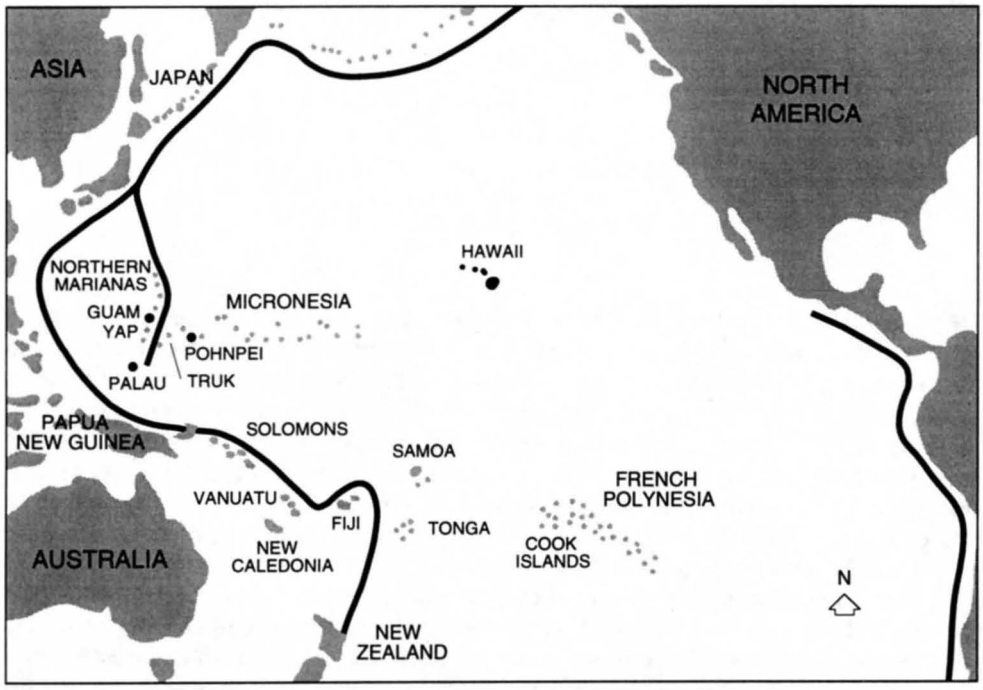

Figure 1: Location map of Pacific Ocean Basin with oceanic trench/subduction zones shown by heavy lines.

Islands are often conveniently separated into two broad groups: "low" islands and "high" islands. The high islands are primarily comprised of volcanic rocks, but also often contain substantial quantities of sedimentary materials, including raised coralline limestone and reef debris. The high islands are older and much larger than the low islands, and generally contain developable quantities of surface water and groundwater. The low islands, which are mainly comprised of coralline atolls and reef material, are very small and usually stand only a few meters above sea level. They have little if any surface water, thus users must rely on direct rainfall catchment and a thin, often brackish, groundwater lens. This paper will describe the geology and water-bearing characteristics of the high volcanic islands.

Volcanic oceanic islands fall into two major provinces, the andesitic or arc and the basaltic or oceanic. As described by Mink (in United Nations, 1983, p. 260) islands of the andesitic province are associated with island arc volcanism and lie on the continental side of deep ocean trenches within the zone of lithospheric plate subduction (Fig. 1). As such, they have typically continental affinities, thus, the term andesitic or arc province. Typical examples of Pacific Ocean island groups within the andesitic province are the Northern Marianas, Guam, Palau, the Solomons, Vanuatu, Tonga, Fiji, and parts of the Cook Islands. Volcanic rocks in the andesitic province occur as lava flows and pyroclastics, and range in composition from basaltic to trachytic; however, submarine pyroclastics predominate. The permeability and water-bearing

properties of volcanic rocks in the andesitic province are generally poor, and little usable groundwater can be developed from them. Instead, most groundwater is developed from limestone and raised coral reefs that are often associated with these islands.

Islands in the oceanic province are typically basaltic, although composition may range to andesitic, and lava flows rather than pyroclastics predominate. The islands occur on the ocean side of trench/subduction systems (Fig. 1) and are associated with intraplate volcanism, thus, the name basaltic or oceanic province. Islands in this province are generally comprised of large, gently-dipping shield volcanoes. The lavas, if young and basaltic, such as those found typically in the Hawaiian Islands, French Polynesia, and Samoa, are extremely permeable and make up the principal aquifers. Conversely, on islands where the lavas are older and contain more pyroclastic material, such as on Yap, Truk, and Pohnpei in Pacific Micronesia, the volcanics are poorly permeable and the most productive aquifers are sedimentary alluvial deposits and weathered lavas.

Thus, the hydrogeology of a volcanic island depends on which volcanic province the island occurs within, and is also profoundly affected by whether the island is emergent or submergent. After volcanic activity has ceased, generally arc islands rise and oceanic islands sink. Coral reef limestones are deposited on arc islands whose surface lay below sea level, as well as along the coasts of oceanic islands and arc islands whose surfaces lay above sea level. As arc islands rise, the coral reef limestones become exposed and new reefs grow along the expanded margin of the islands. Some arc islands are entirely covered with several hundred meters of limestone, while others exhibit both raised limestone and exposed volcanics. Conversely, the coral reefs around the margin of the oceanic islands subside with the sinking volcanic mass. Fossil reefs generated during high sea stands may fringe oceanic islands, but do not form dominant subaerial limestone deposits often found on arc islands.

The hydrogeology of three different volcanic island provinces are described for: (1) the Hawaiian Islands, an example of young, highly permeable oceanic volcanic islands; (2) Pohnpei, an example of an older, poorly permeable oceanic volcanic island; and (3) Guam, an example of a poorly permeable andesitic arc island containing extensive raised reef limestone deposits.

HAWAIIAN ISLANDS

The Hawaiian Islands consist of six major populated islands and numerous other smaller island (Fig. 1). They were formed by extrusion of basaltic lavas as the Pacific plate moved northwestward over the Hawaiian hotspot. Although the islands vary considerably in size, all but Hawaii Island are less than 1,000 km^2 in area. Annual precipitation over the Hawaiian islands averages about 200 cm, and because the surface materials are so permeable nearly one-third of this recharges the groundwater. Flow in most streams tends to be flashy and undependable for domestic and municipal use, thus groundwater is the principal source of potable water supplies.

All the major Hawaiian islands consist of one or more shield volcanoes which are primarily composed of thin basaltic lava flows. These basalts are especially permeable due to their very young age and the thinness of individual lava flows, which averages only 2-3 meters. The lavas

which stand above sea level range in age from about five million years to only a few years. The high permeability results from primary flow structures such as clinker layers, lava tubes, irregular openings associated with the surface between flows, vertical contraction joints formed by the cooling of lavas, and gas vesicles (Peterson, 1972). The horizontal component of permeability certainly exceeds the vertical, however, permeability in both directions is so great and so subject to local deviations that any difference between them is difficult to assess.

The lava flows were erupted from central calderas and from fissures in linear rift zones along the volcano flanks. As a result, the summit calderas and rift zones contain many nearly vertical dikes which cut through the gently sloping lava flows. In the calderas and central portions of the rift zones the dikes are closely spaced and almost completely replace the lava flows. Toward the outer edges of the calderas and rifts the dikes are more widely spaced and form large compartments which enclose permeable lavas. Because the dikes are relatively impermeable, groundwater may be impounded within these compartments.

On most of the older islands, the margins of the volcanic mountains are overlapped by coastal plain sediments of alluvial and marine origin which were deposited during periods of volcanic quiescence. Although the permeability of the sediments varies widely, the overall effect is one of low permeability compared to the basalts, and the sediments act as a caprock retarding the seaward movement of fresh groundwater from the more permeable underlying basaltic aquifers.

Two principal types of groundwater bodies occur (Peterson, 1972): (1) basal water bodies floating on and displacing salt water, and (2) high-level bodies impounded within compartments formed by impermeable dikes that have intruded the lava flows, and to a lesser extent, high-level bodies perched on impermeable layers of ash, soil, or dense flows. The occurrence and development of these groundwater bodies are illustrated in Figure 2.

Owing to their relatively small volumes, development of high-level groundwater sources in Hawaii is limited. Dike-confined groundwater bodies are often identified by natural spring discharges. The compartments formed by dikes may be saturated with fresh groundwater to levels a few hundred meters above sea level. Dike water has been primarily developed by horizontal or inclined tunnels which penetrate one or more dike compartments and, to a lesser extent, by vertical wells drilled into individual dike compartments. Although the volume of water stored in dike-confined aquifers is small compared to fresh basal groundwater, it is large compared to other sources of high-level water. Natural storage in perched aquifers is generally small and the flow of perched water springs tends to be relatively unstable. As a result, perched water is important primarily because of its high elevation and is only a very small part of all high-level groundwater developed.

The principal source of fresh groundwater in the Hawaiian Islands, as it is for most young basaltic islands, is the roughly lens-shaped basal water body floating on and displacing denser sea water. Recharge of the basal water body results directly from percolating rainwater or by underground leakage from perched-water bodies and bodies impounded by dikes. Where the permeable lava flows containing basal water extend to the coast without a cover of sediments, the head above sea level is generally small. Where the basaltic aquifers are directly overlain by the less permeable sedimentary caprock along some of the coastal margins, artesian heads of a

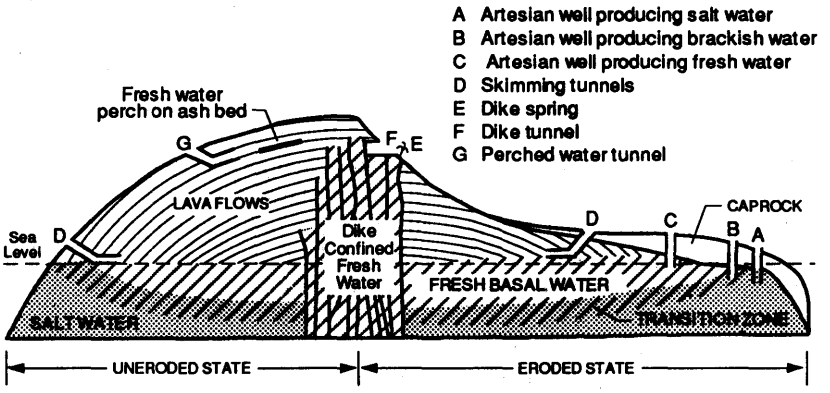

Figure 2: Cross section of typical Hawaiian volcanic dome showing occurrence and recovery of groundwater (modified after Peterson, 1972).

few meters to over 10 meters above sea level may occur. The depth to the bottom of fresh water is normally a few tens of meters to several hundred meters. In some of the drier coastal areas where heads may be less than one meter above sea level, tidal fluctuations very rapidly mix all the fresh rainwater with the underlying sea water so that only brackish groundwater occurs.

In Hawaii basal groundwater has been developed by drilled wells in artesian and unconfined aquifers and by skimming tunnels in unconfined aquifers (Fig. 2). The skimming tunnels consist usually of a vertical or inclined shaft constructed from the ground surface down to just below the water table, and one or more horizontal tunnels constructed laterally just below the water level to collect water. The fundamental advantage of skimming tunnels is their capability to collect large quantities of fresh water from lenses so thin that vertical wells would recover only brackish water. However, in the highly permeable basaltic lavas even vertical wells routinely produce 4,000-5,000 m^3/day or more. The sustainable yield of the island of Oahu, on which most of the population resides, is estimated at nearly 7 x 10^8 m^3/year.

To summarize, the basic strategy for developing groundwater from the highly permeable Hawaiian basaltic lavas is to locate poorly permeable confining and retarding layers which keep the fresh groundwater from rapidly escaping into the surrounding ocean.

POHNPEI

The Pohnpei Group, located in the Eastern Caroline Islands (Fig. 1), consists of the main volcanic island of Pohnpei and several small satellite atolls capping submerged volcanoes. In this paper only the large island of Pohnpei (land area of approximately 340 km^2) will be discussed. Like the Hawaiian Islands, the Pohnpei Group, together with Truk to the west and Kosrae to the

east, is thought to have formed by extrusion of basaltic lavas as the Pacific plate moved northwestward over a hotspot.

In contrast to the Hawaiian Islands, however, the volcanic rocks which comprise Pohnpei are older (up to about 8.5 Ma; Keating *et al.*, 1984; Dixon *et al.*, 1984) and much less permeable. They consist of moderate to poorly permeable shield-building basaltic lavas which are covered by a thick cap of low permeability post-shield-building lavas (Spengler *et al.*, 1992). Due to extensive regional subsidence and sea-level rise Pohnpei lacks coastal plains of sedimentary materials and raised coral reefs around its perimeter, and instead is covered by volcanic rock and fringing mangrove swamps along its coastline around much of the island.

Rainfall is abundant year-round and ranges from about 400 cm/year along the coastline to nearly 900 cm/year in the island's interior. Owing to the low-permeability capping volcanic rocks about two-thirds of the total precipitation is returned as surface runoff, with the remainder divided between evapotranspiration and infiltration (Spengler *et al.*, 1992).

Because of the general availability of abundant surface water supplies, groundwater development on Pohnpei has been quite minimal, and hence quantitative information on its occurrence and development is very limited. Nonetheless, during prolonged periods of drought surface water supplies decline substantially and in recent years some groundwater development has been undertaken. Unlike in the Hawaiian Islands, however, where voluminous groundwater supplies can readily be developed from the shield-building lavas, on Pohnpei groundwater development from this source is much more difficult, and only moderate amounts of groundwater can be developed from the upper relatively unweathered shield-building lavas and the weathered zone that overlies them. A second source of developable groundwater on Pohnpei is the sediments within local unconformities between flow units of the post-shield-building volcanics and the unconformity between these volcanics and the underlying shield-building lavas (Spengler *et al.*, 1992). Groundwater production rates from wells on Pohnpei typically range from about 100-500 m^3/day per well, only a fraction of typical pumping rates from wells in the Hawaiian Islands.

GUAM

Guam, with an area of approximately 550 km^2 is the largest and southernmost of the Mariana Islands (Fig. 1). It is a typical example of an andesitic arc province volcanic island capped by raised limestone deposits.

The entire island was initially formed by island arc andesitic volcanism during Eocene-Miocene time (probably about 20-60 Ma). Subsequently, a thick sequence of marine limestone was deposited on the volcanic rocks, and uplift of the entire island mass has resulted in raised limestone deposits covering large portions of the original volcano. Guam is divided into two distinct geologic and hydrologic provinces. The northern half of the island is composed of an extremely permeable raised limestone platform overlying deeper volcanic rocks, and the southern half of the island is composed predominantly of poorly permeable andesitic volcanic rocks (Fig. 3).

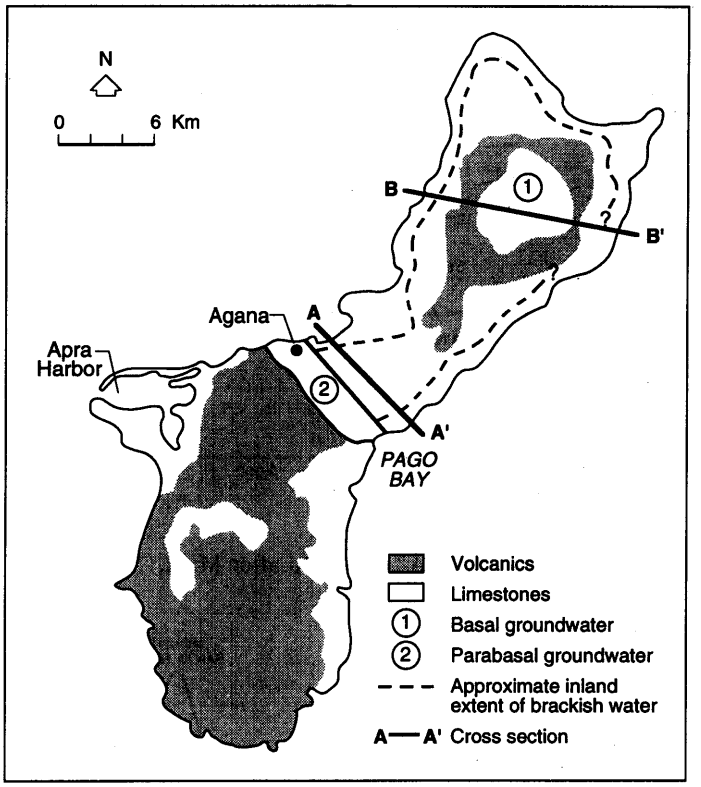

Figure 3: Hydrogeologic map of Guam (modified after Mink, 1976)

Rainfall on Guam is similar to Hawaii, and averages about 250 cm/year. Surface runoff is virtually non-existent from the extremely permeable limestones in the north where much of the rainfall recharges the groundwater body. Conversely, the poorly permeable volcanic surface of the south is drained by more than 40 streams, and surface runoff accounts for well over half of the annual rainfall.

Virtually all the exploitable groundwater occurs in the permeable limestone aquifers of the north, which provide more than 95% of the total island groundwater supply (United Nations, 1983). The fresh groundwater occurs there as basal lenses floating on and displacing salt water, and less commonly, as parabasal water which is continuous with the basal lens but is not underlain by sea water because it rests directly on the impermeable volcanic basement (Mink, 1976). Figures 4 and 5 show hydrogeologic sections through AA' and BB', respectively. Groundwater production rates for wells in the limestone aquifers typically range from 500 to as high as 10,000 m^3/day per well. Pumping rates from the few wells developed in the southern volcanic rocks generally are less than 250 m^3/day per well (United Nations, 1983). Groundwater sustainable yield from the island as a whole is estimated to be just under 7×10^7 m^3/year, about one-tenth that of Oahu, Hawaii which is about twice the size of Guam.

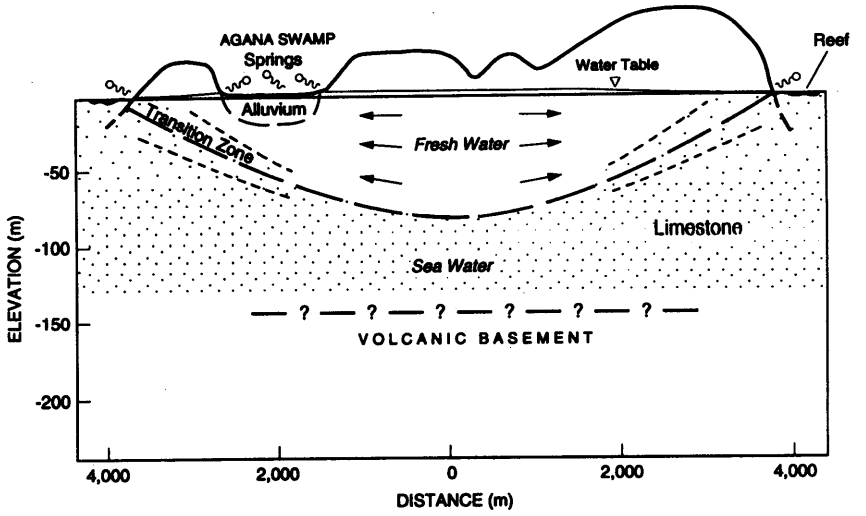

Figure 4. Hydrogeologic cross-section AA' (modified after Mink, 1976).

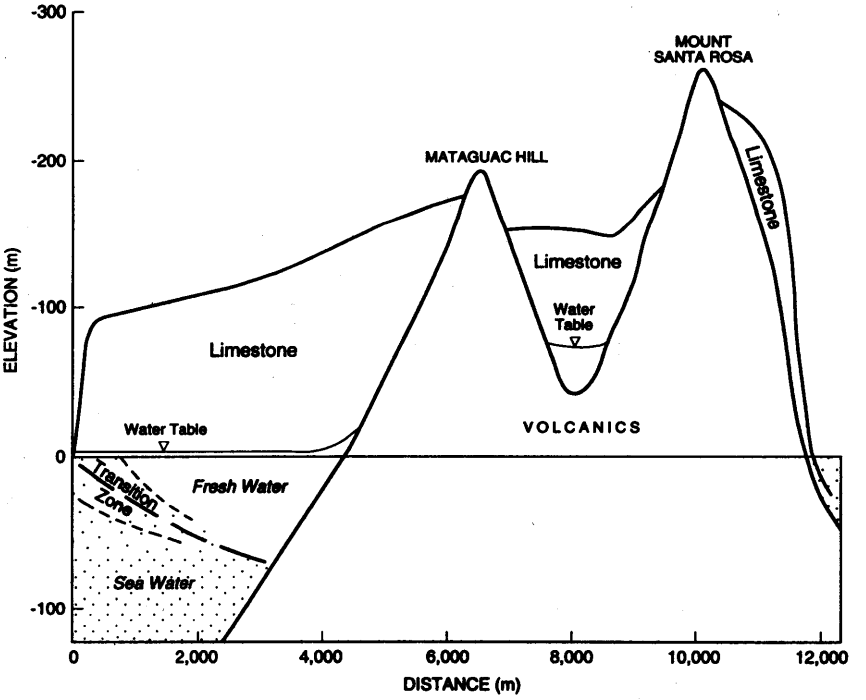

Figure 5. Hydrogeologic cross-section BB' (modified after Mink, 1976).

CONCLUSIONS

The geology, including volcanic province, age, and sea-level history, of volcanic oceanic islands exerts critical control on groundwater recharge, occurrence, and aquifer properties, and hence greatly influences strategies for groundwater exploration and development. For example, in young basaltic province islands such as Hawaii, groundwater development strategy generally concentrates on the highly permeable unweathered shield volcanics and gives only secondary consideration to sedimentary aquifers. Conversely, in andesitic arc province islands such as Guam, raised limestone deposits usually are the primary target for groundwater development, as the low-permeability volcanic rocks generally make poor aquifers. In older, less permeable oceanic province islands such as Pohnpei, prospects for development of significant groundwater supplies are less favorable, and weathered basalts and sediments within unconformities between volcanic flows are often the best groundwater development targets.

REFERENCES CITED

Dixon, T.H., Batiza, R., Futa, K. & Martin, D. 1984. Petrochemistry, age and isotopic composition of alkali basalts from Ponope Island, Western Pacific. *Chem. Geol.*, 43; 1-28.

Keating, B.H., Mattey, D.P., Helsley, C.E., Naughton, J.J., Lazarweicz, A., Schwank, D. & Epp, D. 1984. Evidence for a hot spot origin of the Caroline Islands. *Jour. Geophys. Res.*, 89; 9937-48.

Mink, J.F. 1976. *Groundwater resources of Guam: occurrence and development.* Tech. Rpt. No. 1. Water Resources Research Center. Univ. of Guam.

Peterson, F.L. 1972. Water development on tropic volcanic islands-type example: Hawaii. *Ground Water.* 10, 5; 18-23.

Spengler, S.R., Peterson, F.L. & Mink, J.F. 1992. *Geology and hydrogeology of the island of Pohnpei, Federated States of Micronesia.* Univ. Hawaii Water Resources Research Center Tech. Rpt. No. 189.

United Nations. 1983. *Ground Water in the Pacific Region.* Natural Resources/Water Series No. 12. Dept. Tech. Co-operation for Development. ST/ESA/121, New York.

SURVEY OF GROUNDWATER FLOW IN A VOLCANIC AQUIFER BY THE $^{3}H+^{3}He$ DATING METHOD

Y. MAHARA & T. IGARASHI
Abiko Laboratory, Central Research
Institute of Electric Power Industry,
1646 Abiko, Abiko City, Chiba, 270-11, Japan

ABSTRACT. This study investigates a tritium and helium-3 ($^{3}H+^{3}He$) dating method to survey the groundwater flow in a large groundwater basin. The dating method is based on calculating the residence time in a radioactive decay formula by substituting the tritum concentration and the tritiogenic ^{3}He measured in the groundwater sample. Since it is very difficult to detect trace amounts of tritiogenic ^{3}He in a 15 ml groundwater sample, tritiogenic ^{3}He is determined from the ratio of ^{3}He to ^{4}He and the dissolved total He measured by a high resolution mass spectrometer.

We applied this dating method to a confined aquifer formed by the deposition of the Aso pyroclastic flow in the Kumamoto plains on the west side of Mt. Aso volcano. The measured ages of groundwater under the Kumamoto plains range from 7 to 74 years old and are aligned from young to old along the major path of groundwater flow in the Togawa lava area. Analytical data on dissolved noble gases (Ne and He) in groundwater samples are available to determine the geohydrologic formation of the volcanic aquifer.

INTRODUCTION

In Japan, volcanic areas are known to hold rich reservoirs of groundwater which collect due to lava flows or pyroclastic flow deposit layers. Recently, many high technology industries are rapidly setting up manufacturing plants near sources of abundant groundwater. Consequently, the groundwater is being polluted by the organic solvents used to clean high technology products, and local residents are concerned that drinking this groundwater may damage their health. It is important to understand the origin of groundwater and the residence time of groundwater in water circulation in order to prevent the pollution from spreading and to decontaminate the groundwater. There are many methods for investigating the flow of groundwater. We have been developing techniques for determing the origin of groundwater and dating groundwater in the macrocirculation of groundwater in a large geohydrologic catchment area.

In this study, we have focused on demonstrating the viability of a $^{3}H+^{3}He$ dating method

(Mahara. et al. 1991) to measure the residence time of groundwater, to identify the origin of groundwater and to separate the regions of groundwater flow. Since the $^3H+^3He$ dating method measures the natural tritium and the natural dissolved helium isotopes, this method has the great advantage of tracing the groundwater flow without further contamination.

STUDY AREA

The Kumamoto plains are located on the west side of Mt. Aso volcano, outside the caldera. The profile of a longitudinal geological formation of the Kumamoto plains is shown in Fig.1.

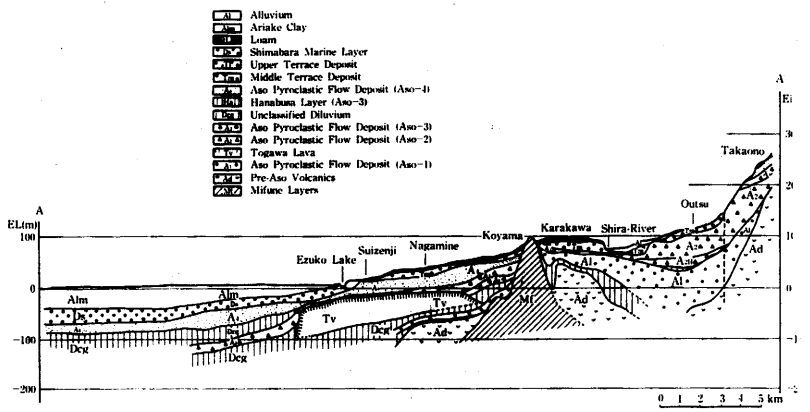

Figure 1 : The profile of a longitudinal geological formation of the Kumamoto Plains.

The basic rocks, which are nonpermeable, consist of Mifune layers which are metamorphic rocks, Pre-Aso volcanic rock and unclassified Diluvium. Four pyroclastic flow deposits, called Aso-1, Aso-2, Aso-3 and Aso-4 in chronological order from the bottom to ground level, and a cracked lava layer, which is called Togawa lava, cover the basic rocks. The pyroclastic flow deposit and cracked lava layers form a major groundwater reservoir, because the rocks are very permeable. The four pyroclastic flow layers and the Togawa lava were produced by eruptions of Mt. Aso volcano from 8×10^4 to 3.6×10^5 years ago.

The Shira river flows a cross the Kumamoto plains from east to west, and is one of the sources of groundwater under the plains. There are many springs, ponds and lakes. All the water of Ezuko lake is supplied from groundwater, which is about 4×10^5 to $9\times10^5 m^3$/day. There are groundwater flow paths under the Kumamoto plains ; the main path is along the old Kase river valley, which is buried with the Aso pyroclastic flow deposits, as shown by the groundwater reservoir to the north of the Shira river. The groundwater flows north-east to south-west along the old Kase river valley, therefore the ages of groundwater determined by the $^3H+^3He$ dating method are likely to range from young to old along the direction of groundwater flow. We collected 13 samples from wells and 9 samples from springs and spouting ponds, the location of sampling sites are shown in Fig.2.

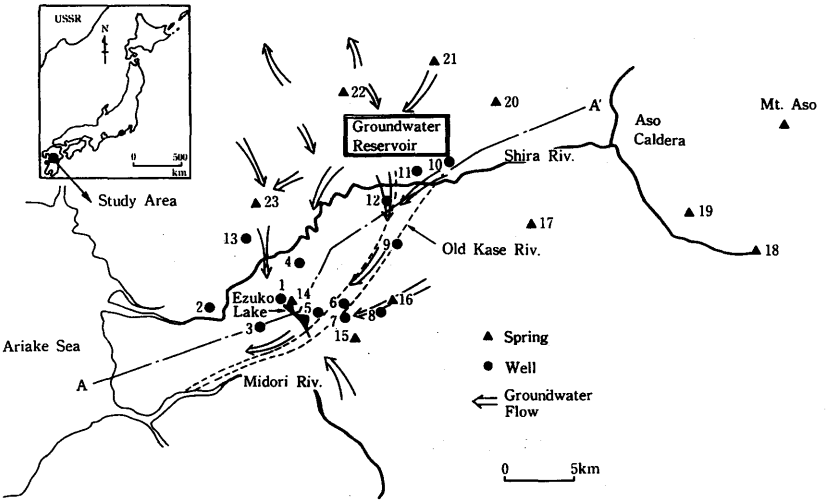

No.	Sampling Site (Well) / Sampling Date 1990. 5/21~5/24	No.		No.	
1	Suizenji (GL-40m)	9	Fukasako (GL-77m)	18	Shirakawa Suigen
2	Rendaiji (GL-45m)	10	Outsu (GL-103m)	19	Shioisha Suigen
3	Tamukae (GL-45m)	11	Kubota (GL-90m)	20	Maki Yusui
4	Shinnabe GL-50m)	12	Kikuyo (GL-110m)	21	Kusubaru Yusui
5	Kengun (Spout)	13	Tsuboi (GL-40m)	22	Kikouji Yusui
6	Akitsu (GL-45m)		Spring	23	Tsuboi Kawa
7	Numayamatsu (GL-70~140)	No.	Sampling Date 1989. 12/5~12/8		
8	Togawa (Spout)	14	Kamiezuko		
		15	Ukishima		
		16	Akai		
		17	Hakamano		

Figure 2 : Location of the sampling sites of groundwater in the Kumamoto Plains.

MATERIALS AND METHODS

Method of sampling groundwater

Groundwater samples for dating by the $^3H+^3He$ method were collected from 13 wells and 9 springs. To measure the tritium concentration and the dissolved cations and anions, a 2000-ml sample was taken at each sampling site. The sample for measuring dissolved ^3He must be collected in such a way to prevent direct contact with the atmosphere, and to prevent gassing and degassing. To ensure this, a new groundwater sampler was designed and built (Fig.3). This sampler has two special mechanisms : (a) The water stoppers are closed by oil pressure under remote control when the sampler reaches a predetermined depth in the well. (b) The water contained in the annealed copper tube was exchanged easily by heating for 20 minutes by a small heater above the top water stopper. Water inside the annealed copper tube is endosed by the top and bottom water stoppers and is sealed completely by two steel clamps. All the sealed water samples were protected against leakage of dissolved gases or intrusion of atmospheric air for long-term storage (10000 years) (Weiss, 1968). As 10 g

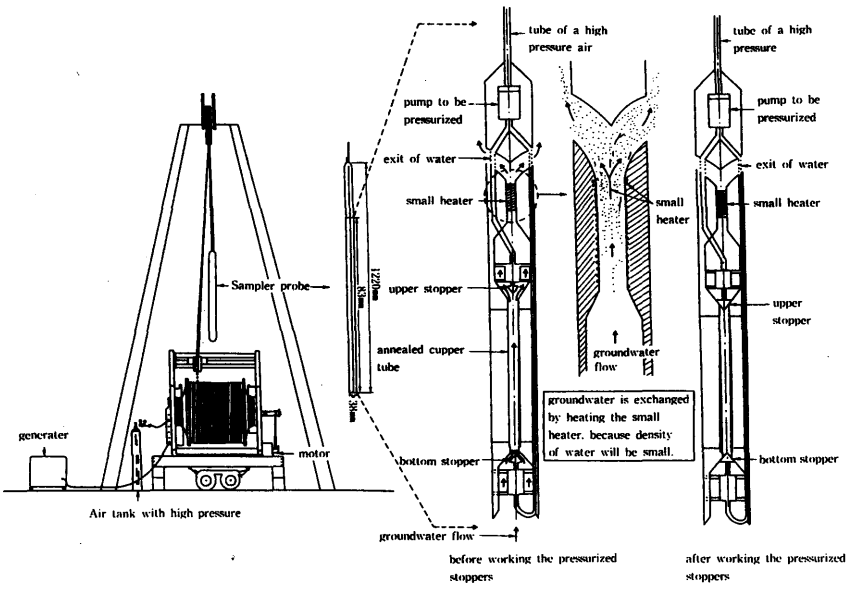

Figure 3 : The whole view of sampler and the mechanism of sampler probe.

water is required to measure the dissolved He-3, 15 to 17 g of water were collected using this sampler.

Analytical methods

Tritium : The concentration of tritium in the groundwater was measured by beta-ray counting after enrichment. 100 ml of groundwater was reduced to about 40 ml by electrolysis using Ni/Fe electrodes. Forty milliliters of distillate and 60 ml of scintillation cocktail Aquasol-2 (New England Nuclear Ltd.) were mixed in a 100 ml teflon vial and the mixture was measured for 1000 minutes by a low-background liquid-scintillation counter.

Helium isotopes (^3He and ^4He) and ratio of ^{20}Ne to ^4He : The dissolved gases were separated from the water in a stainless-steel extraction line at ultra-high vacuum (1×10^{-9} Torr) using an oil-diffusion pump and an ion pump. Ultrasonic vibration for 15 minutes was used to extract dissolved gases from the water sample. Water vapor and condensable gases were removed by a liquid-nitrogen cold trap. Active gases were trapped by a titanium-zirconium getter. The heavy noble gases Ar, Kr and Xe were removed by an activated-charcoal trap cooled in liquid nitrogen. The residual He and Ne left in the extraction line were introduced to a VG-5400 mass spectrometer (VG Isotope Ltd.). The concentration of ^3He was determined by measuring the ^4He concentration, and the ratio of ^3He to ^4He ($^3He/^4He$) was compared with that of standard air 1.4×10^{-6}. The ratio of ^{20}Ne to ^4He was measured by a quadruple polar mass using the purified residual helium and neon sample in the extraction line.

Hydrogen and oxygen isotope ratios : The ratio of deuterium to hydrogen (D/H) was measured with a mass spectrometer after reducing the water sample of 1 or 2 ml to the hydrogen gas using metal uranium heating at 600℃. The ratio of oxygen-18 to oxygen-16 ($^{18}O/^{16}O$) was measured with a mass spectrometer after establishing the isotopic exchange equilibrium between the water sample of 1 or 2 ml and gaseous CO_2. Both ratios of (D/H) and ($^{18}O/^{16}O$) were expressed as a deviation from SMOW. The measurement errors are ±1% for (D/H) and ±0.1% for ($^{18}O/^{16}O$).

RESULTS AND DISCUSSION

Concentration of cations and anions

The concentration of cations (Na^+, K^+, Ca^{2+}, Mg^{2+}) and anions (Cl^-, SO^{2-}, HCO^-) of groundwater samples collected in the Kumamoto plains were analyzed by the conventional technique using ion chromatography. The results are shown on the Key-diagram in Fig.4. Most groundwater samples are distributed in the region of the groundwater type $Ca(HCO_3)_2$ which is characteristic of shallow groundwater, but some samples (Kengun and Tamukae) show the geochemical properties of the deep groundwater type $NaHCO_3$, and other samples (Togawa, Ukishima and Akai) show the geochemical properties of volcanic groundwater $CaSO_4$. We cannot determine anything from only the concentrations of cations and anions,

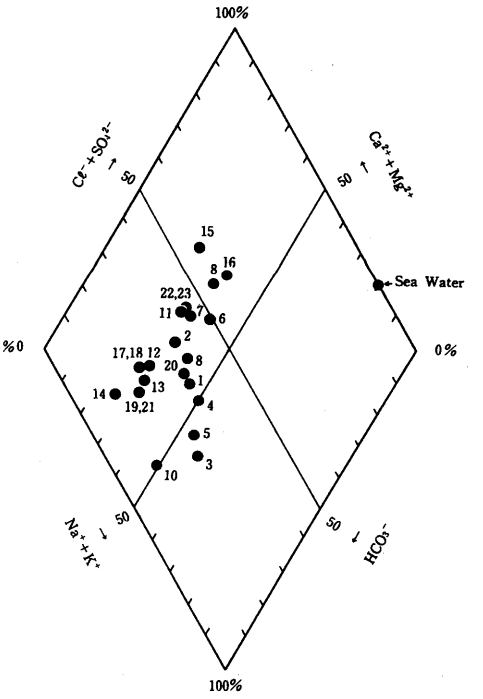

Figure 4 : Key-diagram of groundwater in the Kumamoto Plains.

but we could probably guess that groundwater of Togawa (No.8), Ukishima (No.15) and Akai (No.16) have the same origin of groundwater, judging from previous investigations (Kimura, 1986).

Distribution of hydrogen and oxygen isotope ratios

Hydrogen and oxygen isotope ratios of groundwater samples are distributed in the region between the global meteoric water line $\delta D=8 \cdot \delta^{18}O+10$ and the line of $\delta D=8 \cdot \delta^{18}O+4$ in Fig.5. Furthermore, ^{18}O and D of most samples are concentrated in the narrow ranges of -6.5 to -7.3 ‰ and of -41 and -51 ‰ respectively. On the other hand, only four samples (Nos.7, 17, 18 and 19) have obvious differences from the others in Fig.5. However, No.17 to No.19 were collected from high altitude areas inside the Aso caldera and from the slope of the outer rim of the volcanic crater of Mt. Aso, at a height of about 1000 m above sea level.

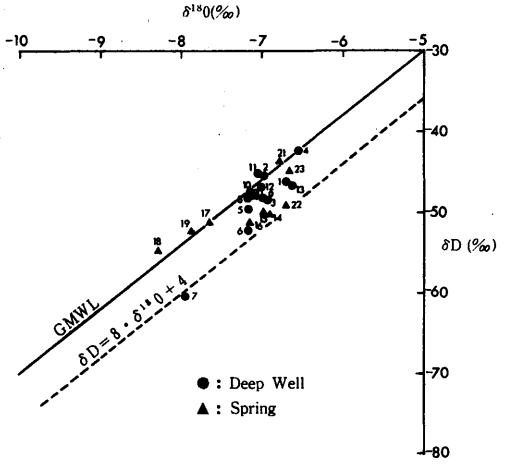

Figure 5 : The relationship between the global meteoric water line (GMWL) and the correlated plots of $\delta^{18}O$ and δD of groundwater in the Kumamoto Plains.

Consequently, their greater shift the negative direction of ^{18}O and D indicates the effect of altitude on the separation of deuterium (D) and heavy oxygen (^{18}O) in the process of evaporation and condensation of water. However, the groundwater of Numayamatsu (No.7) occupies a strange position in Fig.5. The deviations of deuterium and heavy oxygen from SMOW are plotted independently in Fig.5 compared to the other 22 samples. This discrepancy suggests that the Numayamatsu groundwater possibly consists of very old groundwater caused by rainwater infiltrating during the glacial period when the average climatic temperature was about 4 or 5 degrees lower than at present.

Tritium concentration

The tritium concentrations of groundwater, except for the two samples Shinnabe (No.4) and Tsuboi (No.13), lie in the range of 6.6 T.U. to 18.2 T.U., which is similar to recent observations of shallow groundwater at only 100 meters depth in Japan. Most of the tritium

in groundwater is distributed in the range of 6 T.U. to 10 T.U., and there are few groundwater samples in which tritium concentrations are more than 10 T.U.. In contrast, the Shinnabe and Tuboi samples have very low concentrations around the limit of detection using the scintillation counting method after electrolysis enrichment.

In past surveys conducted by Kimura (1986) from 1977 to 1978, groundwater with lower tritium concentrations than the limit of detection was confirmed near Tsuboi. Furthermore, he reported that the tritium concentrations at Suizenji, Kengun and Numayamatsu were on average 24, 20 and 23 T.U. in 1977, respectively. We measured the tritium concentrations at Suizenji, Kengun and Numayamatsu to be 18.2, 9.2 and 8.8 T.U. respectively in 1990, at 13 years after Kimura's measurements. Tritium concentrations at Kengun and Numayamatsu decreased by half during the 13 years, which is approximately equivalent to one half life of tritium. If the tirtium concentration in groundwater from Kengun and Numaymatsu decreased by half during one half life of tritium (12.3 years), then the tritium concentration must have been more than 50 T.U. in the early 1960's, when precipitation with a tritium content of more than 1000 T.U. was observed throughout the world and the tritium level of shallow groundwater rose sharply. Yet the tritium concentration of groundwater at Suizenji decreased by only one fourth in 13 years, suggesting that there may be a lot of groundwater with high tritium content resident under the Suizenji area.

Dissolved noble gases

The results of analyzing the dissolved helium content and helium isotope ratio of ^{3}He to ^{4}He of groundwater in the Kumamoto plains is shown in Fig.6. Most samples except Rendaiji (No.2) and Tsuboigawa (No.23) contained 5.0×10^{-7} to 1.1×10^{-8} ccSTP/g of total dissolved helium, with helium isotope ratios in the range of $1.38\text{-}3.6\times10^{-6}$. This suggests that the helium generated by the alpha decay of alpha radionuclides into uranium and thorium in rock accumulates in groundwater. This accumulated helium in groundwater, the excess helium, is

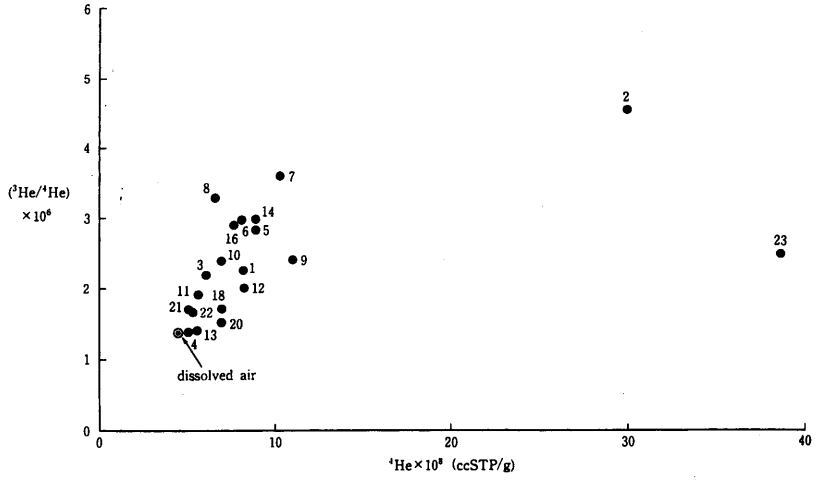

Figure 6 : A correlation plot between ($^{3}He/^{4}He$) and ^{4}He of groundwater in the Kumamoto Plains.

referred to as the component of crustal helium which has the characteristically low ratio of neon to helium and a low ratio of ^{3}He to ^{4}He. The increase of crustal helium component in the dissolved helium decreases with the ratio of neon to helium. However, the correlation between the decreasing ratio of neon to helium and the decreasing ratio of ^{3}He to ^{4}He are not evident in Fig.7. On the contrary, the ratio of ^{3}He to ^{4}He increases with the increasing content of the excess helium. This implies that the excess helium contains a not insignificant amount of mantle helium, which has a characteristically low ratio of neon to helium 10^{-3} and a high ratio of ^{3}He to ^{4}He 1.1×10^{-5} . On the other hand, the Rendaiji and Tsuboigawa samples have 7 to 9 times more helium than dissolved helium (4.5×10^{-8} ccSTP/g) in water at equilibrium with helium in the atmosphere at 15℃. The huge excess of helium samples in No.2 and No.23 shows a high helium isotope ratio compared to air 1.4×10^{-6}. Moreover, the ratio of neon to helium is extremely low compared to that in dissolved atmospheric air (4.3, at 15℃). This result suggests the Rendaiji and Tsuboigawa samples contain large amounts of a mixture of crustal helium and mantle helium, because the measured ratios of ^{3}He to ^{4}He are very low compared to that of only mantle helium at 1.1×10^{-5}.

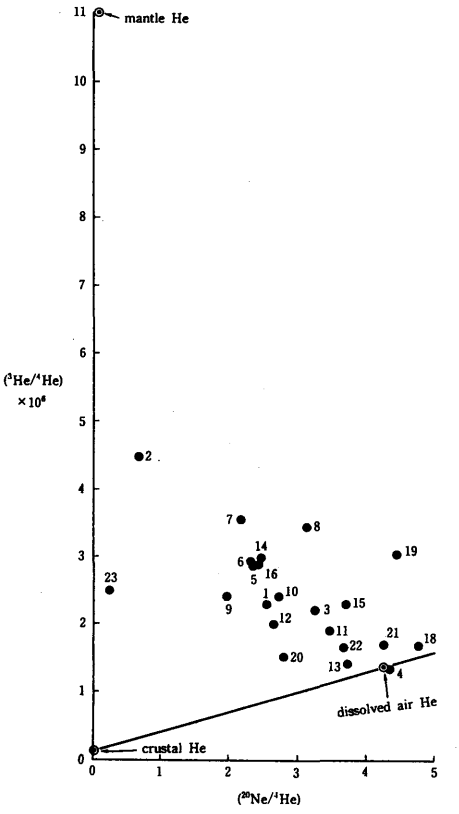

Figure 7 : A correlation plot between (^{3}He/ ^{4}He) and (^{20}Ne/ ^{4}He) of groundwater in the Kumamoto Plains.

A contour map of the ratio of ^{3}He to ^{4}He is shown in Fig.8. This figure shows that the high ratio area ($>2\times10^{-6}$) and the low ratio area ($<2\times10^{-6}$) are probably divided with the Shira river. The high ratios are concentrated in the Togawa lava area. There seems to be correlation between the Togawa lava area and the high ratio area of ^{3}He to ^{4}He. The area with the highest ratio of ^{3}He to ^{4}He ($>3\times10^{-6}$) coincides with the area with the thickest lava layer. Judging from the measured ratio of ^{3}He to ^{4}He, the Togawa lava is distributed in the direction from southeast to northwest corresponding to the direction of decreasing thickness of lava layer. Furthermore, the Togawa lava is not likely to be distributed beyond the northern side of the Shira river judging from the low ratio of ^{3}He to ^{4}He measured at Shinnabe and Tsuboi. The hot spots with the high ratio of ^{3}He to ^{4}He, however, are also found in the area with the low ratio of ^{3}He to ^{4}He. This suggests that some spots actively release the helium mixture of the mantle component and the crustal component through faults.

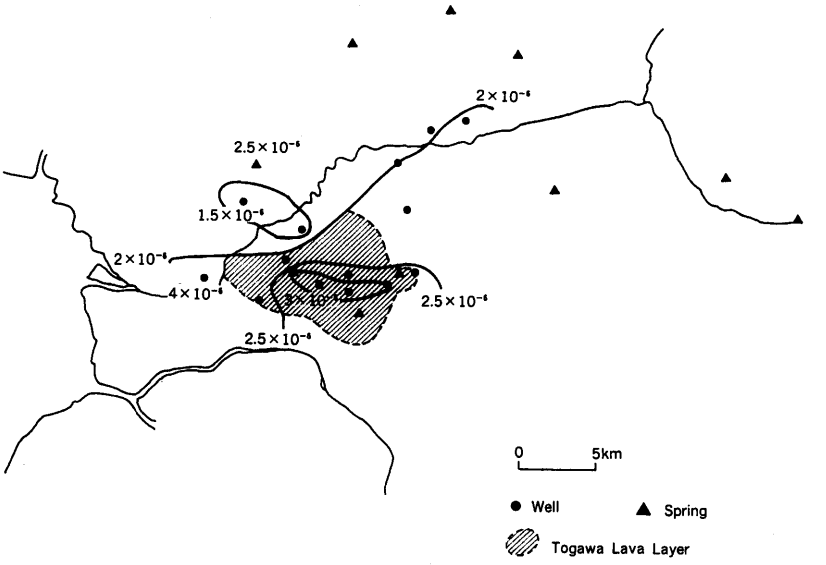

Figure 8 : Distribution of Togawa lava and contour map of ($^{3}He/^{4}He$).

A correlation plot between the ratio of ^{3}He to ^{4}He and the tritium concentration of groundwater samples collected in the Togawa lava area is shown in Fig.9. Tritium concentration decreases with increasing ratio of ^{3}He to ^{4}He. In other words, there is an inverse correlation between the tritium concentration and the ratio of ^{3}He to ^{4}He. The tritiogenic ^{3}He, which is produced by the beta decay of tritium in groundwater, helps to increase the ratio of ^{3}He to ^{4}He. The old groundwater has a lower tritium content as well as a higher ratio of ^{3}He to ^{4}He than the younger groundwater. Based on the evidence of an inverse correlation between the tritium concentration and the ratio of ^{3}He to ^{4}He, we tried to estimate the ages of the groundwater using the $^{3}H+ {}^{3}He$ dating method. The results are tabulated in Table 1.

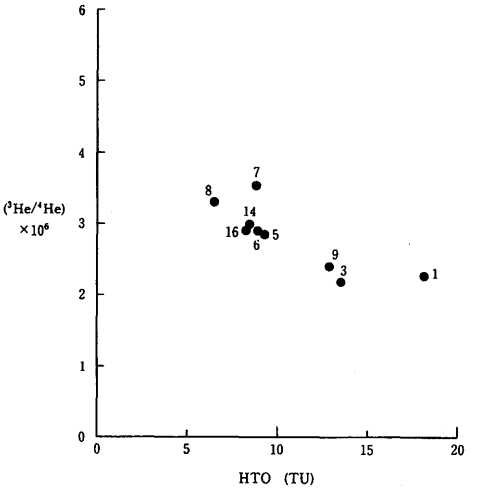

Figure 9 : A correlation plot between ($^{3}He/^{4}He$) and HTO of groundwater in the Togawa lava area.

The ages of groundwater in the Kumamoto plains, except Rendaiji and Tsuboigawa, range from 7.3 to 47.7 years old. The groundwater

Table 1 : Analytical results of ^4He, ($^3He/^4He$), ($^{20}Ne/^4He$) and tritium in groundwater and dating results.

Sampling Site	$4He \times 10^8$ (ccSTP/g)	$(^3He/^4He) \times 10^6$	$(^{20}Ne/^4He)$	HTO (TU)	Age (y)
Shirakawa suigen	6.87	1.70	4.76	7.2	2.7
Oustu	6.95	2.41	2.72	8.1	32.3
Kubota	5.64	1.93	3.46	8.3	12.8
Kikuyo	8.20	2.00	2.63	7.2	33.0
Fukasako	10.95	2.39	1.93	12.9	34.6
Akistu	8.06	2.93	2.31	8.9	38.6
Kengun	8.90	2.85	2.34	9.2	39.3
Togawa	6.24	3.39	3.13	6.6	40.5
Numayamazu	10.30	3.59	2.17	8.8	47.7
Kamiezuko	8.64	3.00	2.44	8.4	41.2
Tamukae	6.05	2.20	3.23	13.5	19.9
Tsuboi	5.83	1.42	3.70	0.5	47.0
Rendaiji*	30.22	4.50	0.71	8.0	74.1
Suizenji	8.18	2.27	2.53	18.2	23.0
Shinnabe	5.03	1.37	4.35	0.4	18.4
Akai	7.63	2.90	2.40	8.3	38.3
Maki Yusui	6.94	1.52	2.78	11.0	15.8
Kusubaru Yusui	5.02	1.73	4.22	16.8	7.3
Kikouji Yusui	5.26	1.69	3.67	7.5	15.4
Tsuboi Kawa*	38.6	2.50	0.50	7.9	68.0

* The dissolved He in this sample is suspected to be a mixture of mantle He component.

in the Togawa lava basin is generally more than 30 years old. The ages of groundwater along the old Kase river buried by the Aso pyroclastic flow deposit do go from young to old in the direction of groundwater flow : in the upstream area of the old Kase river, groundwater is 12.3 to 33 years old, and in the downstream area, 38.6 to 47.7 years old. The ages of groundwater of fountains on the fringes of the mountains range from 7.3 to 15.8 years old, which is relatively young. At Shinnabe and Tsuboi where tritium concentrations were down to the limit of detection, groundwater was 18.4 and 47 years old, respectively. Groundwater in the Tsuboi area was expected to be very old from past surveys and, our results were consistent with past results. The groundwater from Rendaiji and Tsuboigawa was over 68 years old, because groundwater samples contained excess helium with a mixture of mantle and crustal helium, therefore the ages were overestimated.

The $^3H+ {}^3He$ dating model should be applied to groundwater containing excess helium after separating the mantle helium component and the crustal component from the total dissolved helium. We used the following model to separate the mantle helium component and the crustal component from the total dissolved helium,

$$[RHe]s = [RHe]a \cdot A + [RHe]m \cdot M + [RHe]r \cdot R \quad (1)$$

$$[RNe]s = [RNe]a \cdot A + [RNe]m \cdot M + [RNe]r \cdot R \quad (2)$$

$$A + M + R = 1 \quad (3)$$

where [RHe] is the ratio of ^3He to ^4He, [RNe] is the ratio of neon to helium, s means samples, a is the atomospheric component, m is the mantle component, r is the radiogenic (crustal) component, A is the ratio of the atmospheric component to the total, M is the ratio

of the mantle component to the total, and R is the ratio of the crustal component to the total. We used 1.1×10^{-5} for [RHe]m, 1×10^{-7} for [RHe]r, 4.24 for [RNe]a, 10^{-3} for [RNe]m and [RNe]r in the estimation. Rendaiji groundwater was estimated to consist of a mixture of 25% young groundwater (32 years old) and 75% old groundwater (20000 years old). The detailed results have been reported elsewhere (Mahara, 1992).

Finally, we conlude that the major groundwater flow is along the old underground Kase river from the groundwater reservoir on the northern side of the Shira river. This was confirmed to exist in the Togawa lava basin in the Kumamoto plains by the $^{3}H+ {}^{3}He$ dating method. We also reconfirmed that old groundwater is resident in the area surrounding Tsuboi and Rendaiji.

CONCLUSION

The $^{3}H+ {}^{3}He$ dating method was used in combination with other survey techniques for a groundwater survey in the Kumamoto plain basin, which is a representative volcanic aquifer in Japan. The dating results suggest that there was a major groundwater flow along the valley of the old Kase river formed by the Aso pyroclastic flow during the Aso volcanic explosion 40000 - 100000 years ago. Old groundwater still exists in the Kumamoto groundwater basin. The results of analyzing noble gases dissolved in the groundwater revealed that there are hot spots which release large quantities of helium with a high ratio of $^{3}H+ {}^{4}He$ along the fault, and that the groundwater flow region is probably divided by the Shira river. The data on the ratio of ^{3}H to ^{4}He indicates the range of the Togawa lava. Thus, the $^{3}H+ {}^{3}He$ dating results can be used to reveal the groundwater flow regions, the groundwater flow paths and the geohydraulic formation of groundwater basins.

REFERENCES

Mahara, Y., Igarashi, T. & Tanaka, Y. 1991. Survey of groundwater using $^{3}H+ {}^{3}He$ dating method. In : proceeding of the 3rd International Symposium on Advanced Nuclear Energy Research−Global Environment and Nuclear Energy. *The Japan Atomic Energy Research Institute*, Mito (March, 1991). 85-89.

Weiss, R. F. 1968. Piggyback sampler for dissolved gas studies on sealed water samples. *Deep-Sea Research.*, 15 ; 695-699.

Kimura, S. 1986. Behavior analysis of subsurface water using radioisotopes contained in it. *Bulletin of the Notional Research Institute of Agricultural Engineering*, No.25. 1-91. (in Japanese)

Mahara, Y. 1992. Dating results of groundwater in the Kumamoto plains using analysis of the dissolved noble gases. *Proceedings of the 47th Annual Conference of the Japan Society of Civil Engineers*, Vol. 2. 582-583. (in Japanese)

A STUDY OF GROUNDWATER FLOW SYSTEMS IN VOLCANIC MEDIA: ISOTOPIC EVIDENCE FOR WHEN RECHARGE OCCURS IN MT. YATSUGATAKE, CENTRAL JAPAN

M. YASUHARA, A. MARUI & K. KAZAHAYA
Geological Survey of Japan, 1-1-3 Higashi,
Tsukuba, Ibaraki 305, Japan
Y. SUZUKI & S. TAKAYAMA
Institute of Geoscience, University of Tsukuba,
1-1-1 Tennoudai, Tsukuba, Ibaraki 305, Japan

ABSTRACT. An isotopic study of groundwater flow systems in volcanic media has been carried out at Mt. Yatsugatake, a dormant volcano in central Japan. Water samples from more than 60 low-temperature, ephemeral and perennial springs were analyzed for hydrogen isotopic compositions to determine when groundwater recharge occurs in Mt Yatsugatake. Springs on the western slope of the mountain were found to be isotopically more depleted than those of the same elevations on the eastern slope. Taking account of the dominant wind directions in the study area, it is concluded that groundwater recharge takes place primarily from summer precipitation from June to September when the western slope is on the leeward side with respect to the winds, whereas the eastern slope is on the windward side. Winter precipitation, which generally occurs as snow, is assumed to be a less important component of groundwater recharge in Mt. Yatsugatake.

INTRODUCTION

Mt. Yatsugatake, a 2900-m high dormant volcano, is about 130 km northwest of Tokyo, Japan (Fig. 1). Although groundwater is now in great demand for agricultural, industrial, and domestic use, little is known about the nature of the groundwater resources in the region. Characterization of the groundwater resources has been impeded by the lack of reliable hydrogeologic information, especially for the high areas of the mountain.

Isotope hydrology using environmental isotopes as tracers permits an accurate and inexpensive determination of where, when and how recharge occurs in vast, mountainous areas where there is otherwise a scarcity of hydrogeologic information (e.g. Basmaci & Al-Kabir, 1988; Sklash & Mwangi, 1991). Therefore, we have investigated the nature of groundwater recharge and flow processes in the southern portion of Mt. Yatsugatake through the application of environmental isotope techniques to spring waters. As a part of the study, the recharge elevations of the springs have already been determined by using deuterium as a tracer (Yasuhara *et al.*, 1993). The purpose

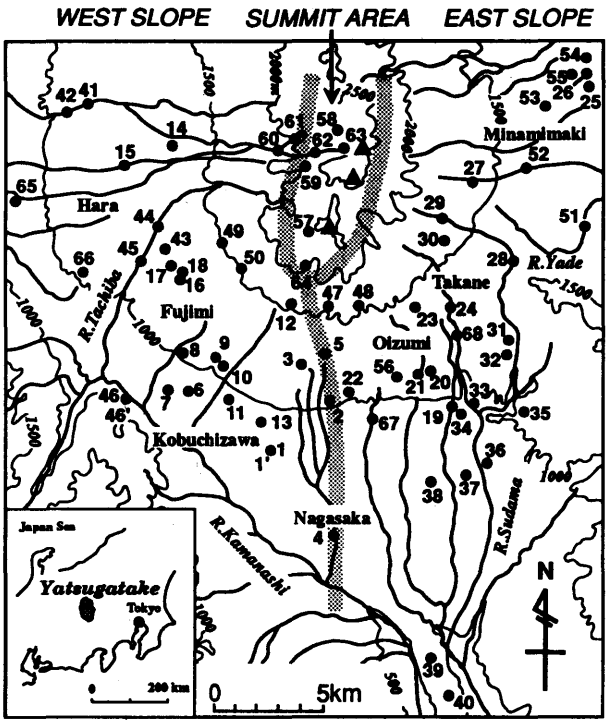

Figure 1: Location map of springs, showing also the three physiographic areas of the southern portion of Mt. Yatsugatake.

of this paper is to identify the season most responsible for the groundwater recharge in Mt. Yatsugatake.

THE STUDY AREA

Mt. Yatsugatake is characterized by many volcanic cones and domes, and consists of lava flows, volcanic ash, lake sediments, and volcanic-fan deposits of Pleistocene age. In general, the Upper Minamisaku Formation, composed of Middle Pleistocene lake sediments up to about 100 m thick, forms major aquifers in the southern portion of Mt. Yatsugatake. These aquifers have hydraulic conductivities that are relatively high, with values typically in the range 10^{-5} to 10^{-6} m sec^{-1} (Kanno & Groundwater Research Group for Yatsugatake, 1988).

The study area experiences humid climatic conditions and is influenced by summer and winter precipitation periods. Summer precipitation consists primarily of 'long rains' due to the so-called Baiu in June and July, and rains accompanying typhoons in August and September (Fig. 2). Rainfall amounts from June to September, mainly brought by large rainfall events, account for nearly half of the annual precipitation. Winter precipitation generally occurs as snow. The high

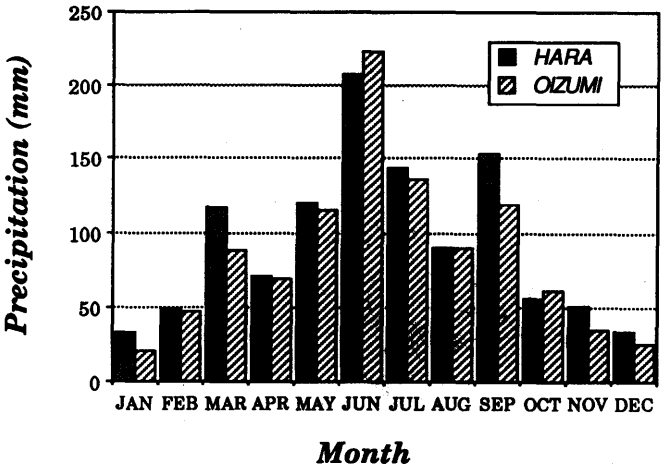

Figure 2: Monthly mean precipitation at Hara and Oizumi from 1984 to 1988 (Japan Meteorological Agency, 1985, 1986, 1987, 1988, 1989).

areas of Mt. Yatsugatake are covered with snow of about 1-2 m thickness from late November to mid-April. Average annual precipitation between 1984 and 1988 was 1125, 1031 and 1320 mm at Hara, Oizumi and Minamimaki (Nobeyama), respectively (Japan Meteorological Agency, 1985, 1986, 1987, 1988, 1989).

Mt. Yatsugatake has a radial surface drainage network of low density (Fig. 1). River Tachiba and River Sudama, originating in the high areas of the mountain, are two important perennial rivers with large flows. Highest flows generally occur from June to September due to rains associated with the Baiu and typhoons. April and May are also high-flow months due to snowmelt. Lowest flows occur in January and February.

Three physiographic areas are defined on Mt. Yatsugatake (Fig. 1). A chain of summits above an elevation of 2000 m is referred to as the summit area. The western and eastern slopes are divided by a low ridge running from north to south. More than 60 low-temperature, ephemeral and perennial springs are in the study area. Six perennial springs are at the summit area. Other springs are distributed almost evenly on the western and eastern slopes. The total range in elevation of the springs is 1800 m.

SPRING DISCHARGE RATES AND RECHARGE ELEVATIONS

Figure 3 shows the distribution of daily spring discharge rates in August 1988 (Marui *et al.*, 1993). Springs above the 1500 m elevation have low discharge rates except for springs nos. 47 and 60. Springs with high discharge rates are found at elevations of approximately 1000 m. The maximum discharge rate was measured to be 15 000 m^3 day^{-1} for spring no. 22. Springs in the summit area and at elevations below 700-800 m have low discharge rates.

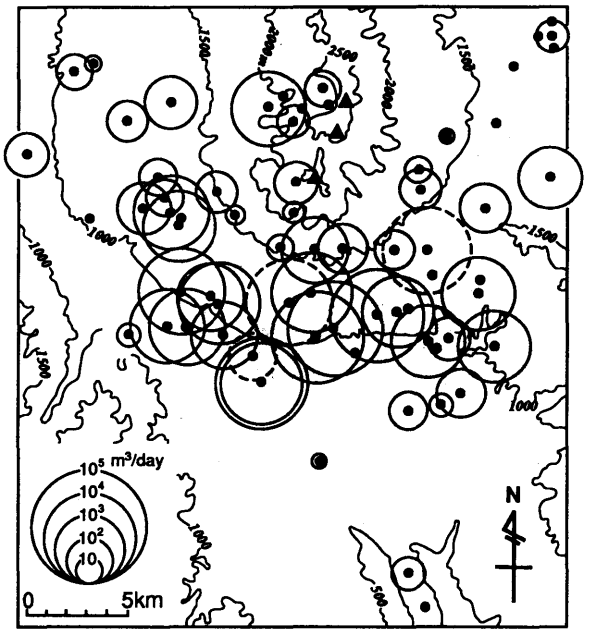

Figure 3: Distribution of spring discharge rates for measurements taken in August 1988. Reproduced from Marui *et al.* (1993).

Taking account of the geochemical and hydrological observations as well as the isotopic results, the groundwater flow system is shown schematically for the summit area and eastern slope of Mt. Yatsugatake (Fig.4). According to Yasuhara *et al.* (1993), the 1000-m elevation springs are fed by a large groundwater reservoir with a long flow path within the mountain. Many of the 1000-m elevation springs are recharged from precipitation at elevations of around 1900-2100 m. In contrast, the groundwater flow feeding the 1500-m elevation springs is smaller in size and has a shorter and shallower flow path than that feeding the 1000-m elevation springs. These 1500-m elevation springs are considered to be recharged primarily from precipitation occurring at 1700-1900 m elevations. Groundwater in the summit area involves a localized flow which is isolated from flow systems associated with spring discharges at lower elevations.

WATER SAMPLING AND ANALYSIS

Sample collection

The field investigation was carried out in August 1988 and January 1989. These two investigation periods were chosen because they coincide with the maximum discharge after the Baiu and the minimum discharge in mid-winter. Water samples were collected from the springs and kept in rigid plastic bottles. Attention was paid not to entrap air in the bottles. The bottles were sealed

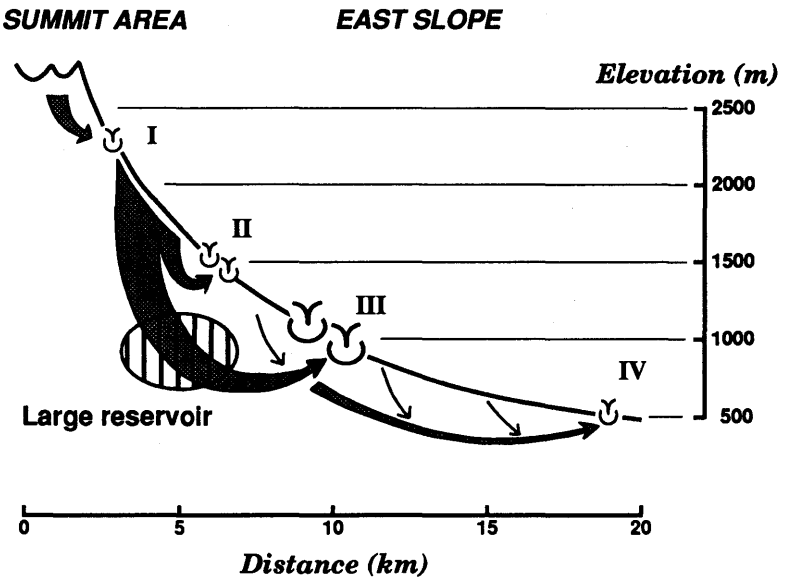

Figure 4: Schematic representation of groundwater flow system in the summit area and eastern slope of Mt. Yatsugatake (Yasuhara *et al.*, 1993).

with plastic tape to prevent leakage and evaporation. For January 1989, the number of sampled springs was restricted by the inaccessibility of many springs located in the high areas of the mountain.

Sample analysis

Water samples were analyzed for hydrogen isotopic compositions. The hydrogen isotopic compositions, δD, are expressed as the per mil difference relative to standard mean ocean water (SMOW). The sampled water was converted to hydrogen gas by an oxidation reaction with zinc. The resulting hydrogen gas was then analyzed using a Finnigan-matt 251 mass spectrometer. Duplicate analyses were carried out for each sample to improve the reproducibility of the δD values. All isotopic analyses were completed at Geological Survey of Japan and the reproducibility of the δD values are within ±1.5‰.

RESULTS AND DISCUSSION

Hydrogen isotopic compositions

The δD values of spring waters for August 1988 are depicted in Fig. 5. Spring waters with the greatest depletion in δD (lighter than -90 ‰) occur at springs nos. 59 and 63 in the summit area and at spring no. 60 on the upper flank of the western slope. These depleted values are consistent

with the higher elevation and cooler climate of the summit area. The most enriched δD values of heavier than -70 ‰ are observed at springs nos. 39 and 40, probably reflecting their lower recharge elevations and warmer temperatures.

In Fig.5, it should be noted that the spring waters on the western slope of Mt. Yatsugatake are more isotopically depleted when compared with those of the same elevations on the eastern slope. The springs on the western slope have δD values between -90 and -80 ‰, whereas those on the eastern slope generally range between -80 and -70 ‰.

Figure 6 shows a plot of δD vs. elevation for spring waters sampled in August 1988. There is a marked off-set in the δD values between the western and eastern slopes of Mt. Yatsugatake. About 10 ‰ difference in the mean δD values is apparent for the springs of the same elevations. This is also the case for spring waters sampled in January 1989 (Fig. 7). This striking contrast of the δD values between the western and eastern slopes throughout the year provides us with useful information for the identification of when significant groundwater recharge takes place in Mt. Yatsugatake.

Identification of recharge periods

It is reasonable to assume that the distribution of δD values of spring waters should reflect the isotopic composition of precipitation which occurs during the periods most responsible for infiltration and groundwater recharge in the study area. Figure 8 shows the wind directions with maximum frequency for January and August 1988. In the summer period between June and

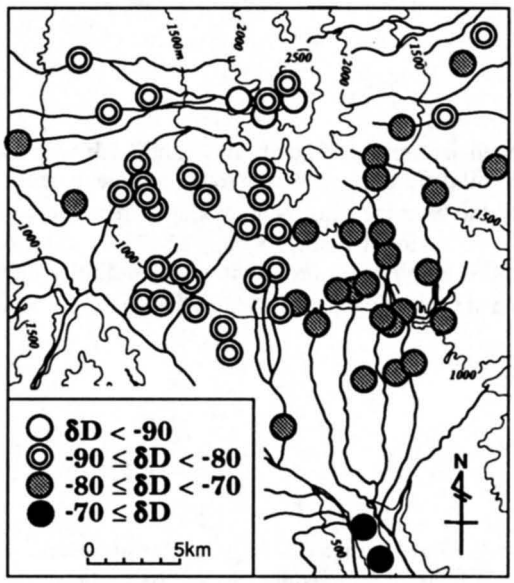

Figure 5: Distribution of δD values (‰) of spring waters for August 1988.

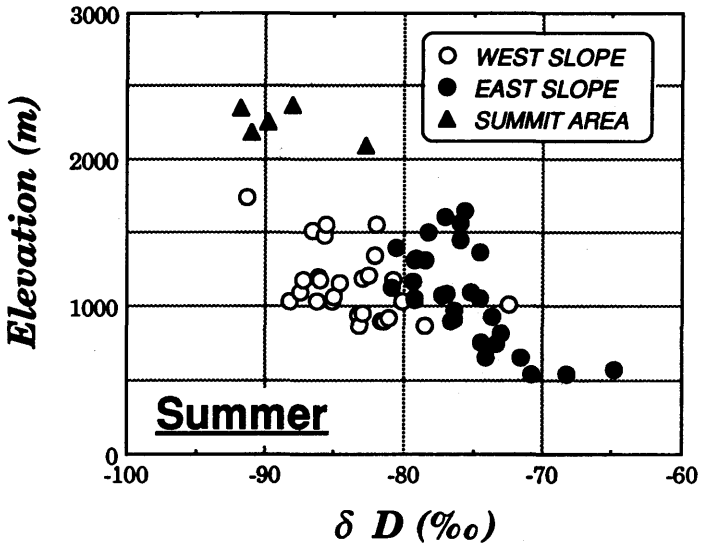

Figure 6: Plot of δD vs. elevation for spring waters on the western and eastern slopes of Mt. Yatsugatake (August 1988).

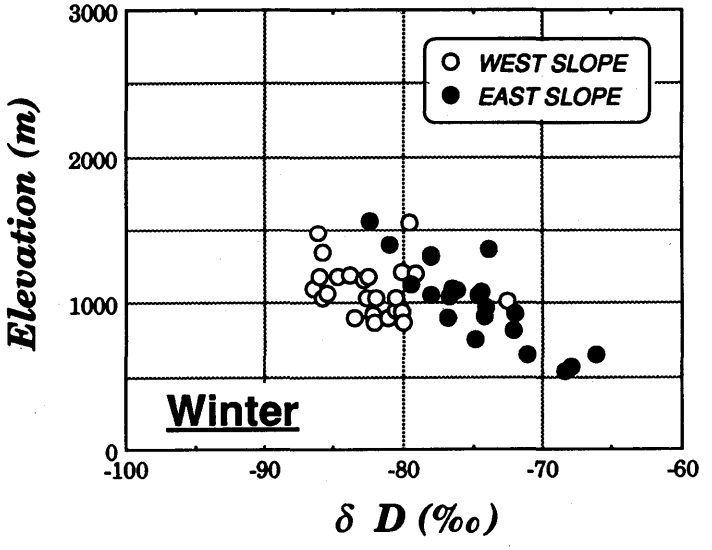

Figure 7: Same as Fig. 6, but for January 1989.

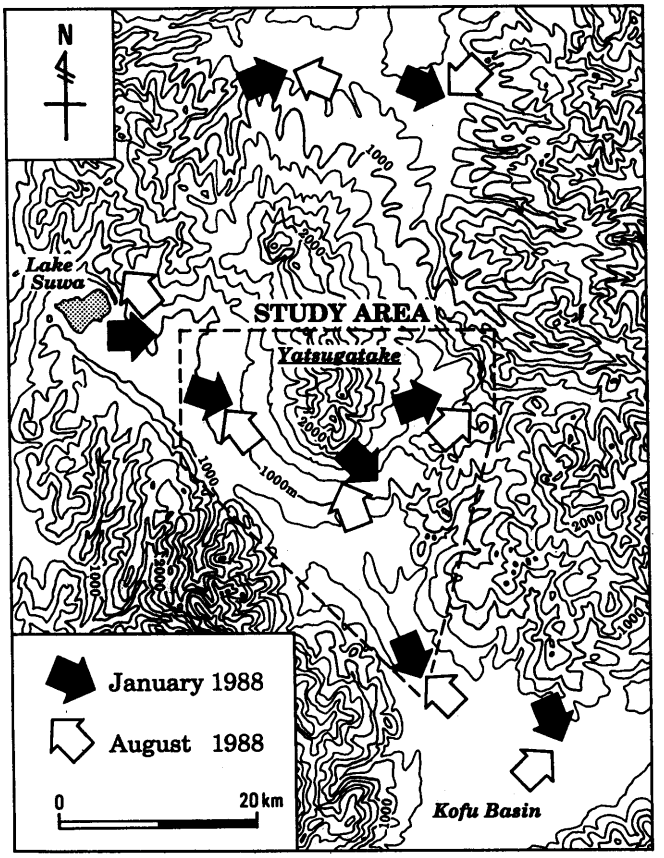

Figure 8: Dominant wind directions for January 1988 and August 1988 (Japan Meteorological Agency, 1989).

September, as typically represented by that for August, the southeast wind is dominant and is accompanied by large rainfall events. In contrast, during the winter period from November to April, the northwest or west wind with a long fetch over the Japan Sea becomes dominant (as shown for January in Fig. 8), bringing much snow to the study area .

In general, precipitation air masses are drifted by the wind. As wind-drifted air masses rise up the mountains, rain is gradually precipitated by condensation, accompanied by more efficient condensation of water molecules with heavier isotopes. The residual moisture in the air masses thus becomes isotopically lighter, and more depleted rain or snow is progressively formed (Mazor, 1991). As a result, precipitation is expected to become more depleted with higher elevations, and become more depleted on the leeward side of the wind than that on the windward side.

The springs on the western slope of Mt. Yatsugatake have depleted δD values throughout the year when compared with those of the same elevations on the eastern slope (Figs. 6 & 7). Therefore, we can conclude that groundwater recharge to Mt. Yatsugatake occurs primarily from summer precipitation between June and September when the western slope is on the leeward side with respect to the dominant southeast wind, whereas the eastern slope is on the windward side. Reflecting the depleted δD values of precipitation, the spring waters on the western slope tend to have more depleted δD values than those on the eastern slope.

It is plausible that winter precipitation, which generally occurs as snow, is a less important component of groundwater recharge in Mt. Yatsugatake. One explanation for this is that a large part of meltwater derived from snow may be promptly directed into the rivers by lateral flow in the snowpack. Consequently, meltwater can contribute little to vertical infiltration and groundwater recharge. The generation of lateral flow during snowmelt is considered to be attributable to a combined effect of the presence of frozen soils below the snowpack and the steep slope of the high areas of Mt. Yatsugatake. These processes are supported by the study of Cooper *et al.* (1991), who showed the low degree of mixing between snow (meltwater) and underlying soil water when frozen soils are present below the snowpack.

SUMMARY

Distribution of the hydrogen isotopic compositions strongly suggests that summer precipitation between June and September is responsible for recharging the groundwater in Mt. Yatsugatake. Recharge is concluded to be accomplished by large rainfall events associated with the Baiu and typhoons. It is likely that winter precipitation contribution to groundwater recharge is either rare or masked by higher contribution of summer precipitation. These results would have important implications for the groundwater development and long-term planning for water supplies in Mt. Yatsugatake and its vicinity.

The authors are analyzing stable isotopic compositions of groundwaters from a number of shallow and deep wells in the study area. In addition, groundwater samples from springs and wells are being analyzed for tritium concentrations for estimating residence times. More detailed clarification of the nature of the groundwater resources in Mt. Yatsugatake based on these isotopic data is an objective for our future research.

Acknowledgments The authors gratefully acknowledge James M. Wilkinson, U.S. Geological Survey, for his thoughtful criticism and improvement of the manuscript. Special thanks are also due to Dr. Yukihiro Matsuhisa, Geological Survey of Japan, for his useful comments on the stable isotope analyses.

REFERENCES

Basmaci, Y. & Al-Kabir, M. 1988. Recharge characteristics of aquifers of Jeddah-Makkah-Taif Region. In: *Estimation of Natural Groundwater Recharge,* I. Simmers, (ed.), Reidel, Dordrecht; 367-375.

Cooper, L.W., Olsen, C.R., Solomon, D.K., Larsen, I.L., Cook, R.B. & Grebmeier, J.M. 1991. Stable isotopes of oxygen and natural and fallout radionuclides used for tracing runoff during snowmelt in an arctic watershed. *Water Resour. Res.,* 27; 2171-2179.

Japan Meteorological Agency. 1985. Kannsokusyo Kisyo Nennpo 1984 (Annual Report of Climatological Stations, 1984), Tokyo.

Japan Meteorological Agency. 1986. Kannsokusyo Kisyo Nennpo 1985 (Annual Report of Climatological Stations, 1985), Tokyo.

Japan Meteorological Agency. 1987. Kannsokusyo Kisyo Nennpo 1986 (Annual Report of Climatological Stations, 1986), Tokyo.

Japan Meteorological Agency. 1988. Kannsokusyo Kisyo Nennpo 1987 (Annual Report of Climatological Stations, 1987), Tokyo.

Japan Meteorological Agency. 1989. Kannsokusyo Kisyo Nennpo 1988 (Annual Report of Climatological Stations 1988), Tokyo.

Kanno, T. & Groundwater Research Group for Yatsugatake. 1988. Yatsugatake sannroku no chikasui (Groundwater of Yatsugatake volcanic terrain). In: *Quaternary System around Mts. Yatsugatake,* Assoc. Geol. Collab. Japan, Monograph no. 34, Tokyo; 233-241.

Marui, A., Yasuhara, M., Kazahaya, K., Suzuki, Y., Shimanao, Y. & Takayama, S. 1993. Minami-Yatsugatake no suimon kannkyo (Hydrological environment in southern parts of Mts. Yatsugatake). *Hydrology,* 23(2) ; 91-103.

Mazor, E. 1991. *Applied Chemical and Isotopic Groundwater Hydrology.* Halsted Press, New York.

Sklash, M.G. & Mwangi, M.P. 1991. An isotopic study of groundwater supplies in the Eastern Province of Kenya. *J. Hydrol.,* 128; 257-275.

Yasuhara, M., Marui, A., Kazahaya, K. & Suzuki, Y. 1993. An isotopic study of groundwater flow in a volcano under humid climatic conditions. In: *Tracers in Hydrology,* Proceedings of the IAHS Yokohama Symposium (in press).

ON THE RELATIONSHIPS BETWEEN SUBSURFACE AND SPRING WATER TEMPERATURES IN VOLCANIC ISLAND OF BALI, INDONESIA

Y. SAKURA
Department of Earth Sciences,
Chiba University, Chiba 263, Japan
K. ITADERA
Hot spring Research Institute,
Kanagawa Prefecture, Kanagawa 250-03, Japan

ABSTRACT. Seasonal variation in air temperature was less than 3 °C and diurnal one was about 15 °C from the meteorological data in Bali. Heat conduction theory suggests that diurnal variation does not affect more than 50 cm deep and the isothermal layer where seasonal variation is less than one tenth of the range of surface temperature, locates at 5 to 6 m below the surface. Therefore the information of subsurface thermal regime in the tropical region is more important than those in the other regions. The objectives of this paper are to make clear the relations between subsurface and spring water temperature, and to estimate where the recharge area of the spring water at the southern slope of the central part of Bali locates. As a result of investigating many data, it was found that springs could be classified into three different types.

INTRODUCTION

There are many studies to deal with subsurface temperature in prospecting for groundwater and in related problems (Fukutomi,1951; Kappelmeyer,1957; Cartwright,1968; Birman,1969; Krcmar and Masin,1970; Birman et al.,1971). Some studies have been using the distribution of groundwater temperatures as an environmental tracer to estimate the groundwater flow (Mink,1964; Shneider,1964; Arai and Sakura,1980; Taniguchi,1987). Mathematical analyses have been made of the relationship of temperature and groundwater flow by Suzuki(1960), Stallman(1963,1965), Bredehoeft and Papadopulos(1965), Parsons(1970), Domenico and Palciauskas(1973) and Andrews and Anderson(1979). Furthermore, Sakura(1984) and Taniguchi et al.(1991) have reviewed the research method by using thermal data for determining the groundwater flow. Although Yamamoto(1960) and Shimano(1988) have reported qualitatively on the relation between spring water temperature and its altitude, in the volcanic mountain area, Japan, there have been few studies dealing with the subsurface and groundwater thermal regime in the tropical and volcanic mountain slope except of the study on the island of Oahu, Hawaii by Mink(1964).

THERMAL CONDITIONS IN BALI

Annual and daily variations of air temperature

There are three meteorological stations in Bali, which locate in Candikuning at 1247 m altitude, Besakih at 900 m and Ngura Rai at 3 m, respectively. These locations are shown in

Figure 1. We could not recognize that such air temperatures for a year of 1987 showed the seasonal variation clearly. Figure 2 shows the changes of monthly maximum, average and minimum temperatures based on the daily mean temperature. Then, we removed high frequency components less than one month from the changes of air temperature by using Fourier transformation technique following to Nogami and Sugiura(1985). After the processing of the inverse Fourier transformation, we can see the seasonal variations as in Figure 3. From Figure 3, it was found that the difference of the seasonal variations depends on the topographical conditions and an annual amplitude based on the monthly mean air temperature is less than 3 °C.

Altitude effect of the thermal regime

we calculated the linear regression relations between spring water and subsurface temperatures, and those altitude by the method of least square approximation. Figure 4a shows the relation between spring water temperature and altitude. The relations between altitude and subsurface temperature at the depth of 1 m and 2 m are shown in Figure 4b and 4c, respectively.

The decreasing ratios of subsurface temperature at the depth of 1 and 2 m to altitude were almost the same of about 5.9 °C/1000 m, but less than that of spring water temperature which is about 6.7 °C/1000 m. At the same altitudes, spring water temperature was lower than subsurface one by 0.7 °C at 0 m altitude, and by 1.5 °C at 1000 m altitude. These differences indicate generally that an altitude of recharge area locates at 100 m to 250 m higher than that of spring. The standard deviation of 2 m deep is less than that of 1 m, because the scattering range of subsurface temperature decreases with the depth mentioned above. The standard deviation of spring water was intermediate between those of 1 m and 2 m.

As for the altitude effect on the temperatures of spring water and air, Shimano(1988) suggested that spring water temperature is generally 2 °C higher than the annual mean air temperature, around Mt. Aso, Japan, however, spring water temperature was not so different to the annual mean air temperature in this study area. It may be not sure because there are only three meteorological stations in Bali.

DISTRIBUTION OF TEMPERATURES

Subsurface temperature

The distribution of subsurface temperature at 1 m deep is shown in Figure 5. All of measuring points are 100 at 1 m deep and 82 at 2 m deep. Reliable and uncertain isothermal lines show the solid and dotted ones, respectively. This is due to the lack of the observation density.

The zone where temperature is less than 20 °C locates in the mountain region over 1000 m altitude. It is clear that the relative cool zone extends from the west part of Batur caldera rim along the River Petanu and Pekerisan, while the relative warm zone extends southeastward from Penelokan at the caldera rim along the Rivers Melangi and Unda. An isothermal line of 27 °C extends narrowly from Bangli to the northeast part of Denpasar. At the coastal area, subsurface temperature at 1 m deep reaches 28 °C and higher.

Spring water temperature

We could find 51 springs in this study area. From the measurement of three times from 1988 to 1990, it is found that spring water temperature does not change very much daily and seasonally.

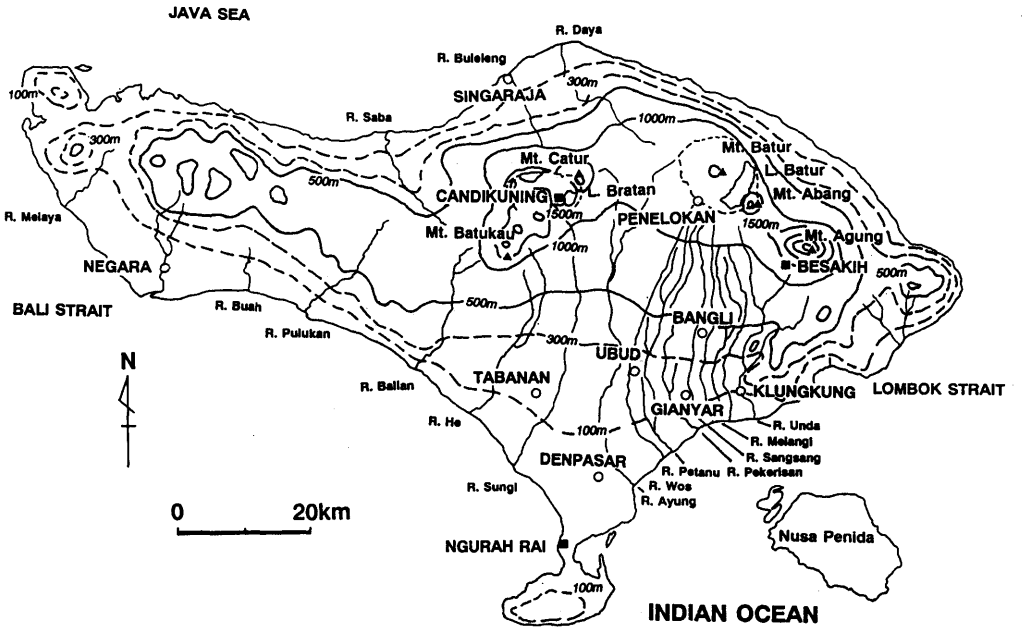

Figure 1 : Location map of the meteorological stations shown as solid squares and main cities as open circles.

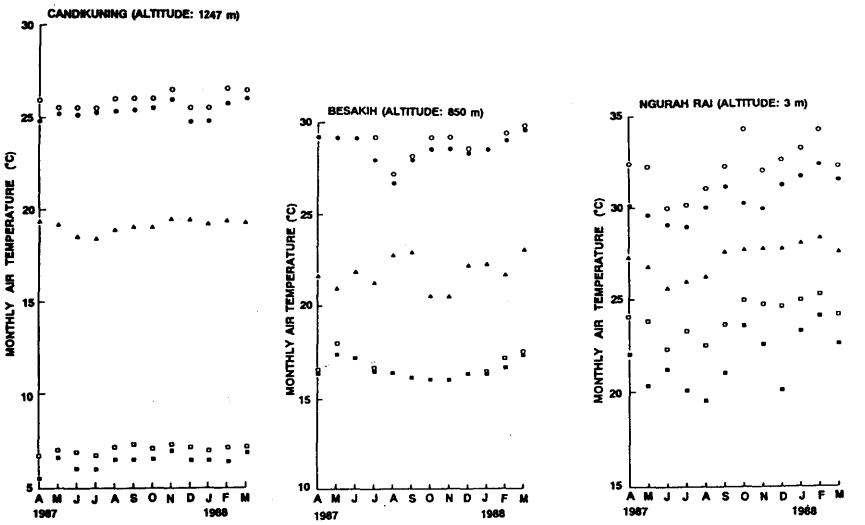

Figure 2 : Changes of monthly air temperature .Open circles show the maximum temperature based on the daily maximum temperature. Solid circles show the mean maximum temperature based on the daily maximum temperature. Open triangles the mean temperature based on the daily mean temperature. Open squares show the mean minimum temperature. Solid squares show the minimum temperature.)

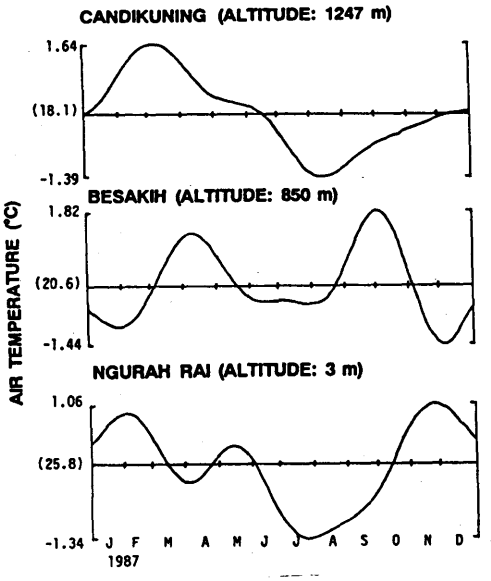

Figure 3 : Changes of air temperature removed high frequency components less than one month by using Fourier transformation technique.

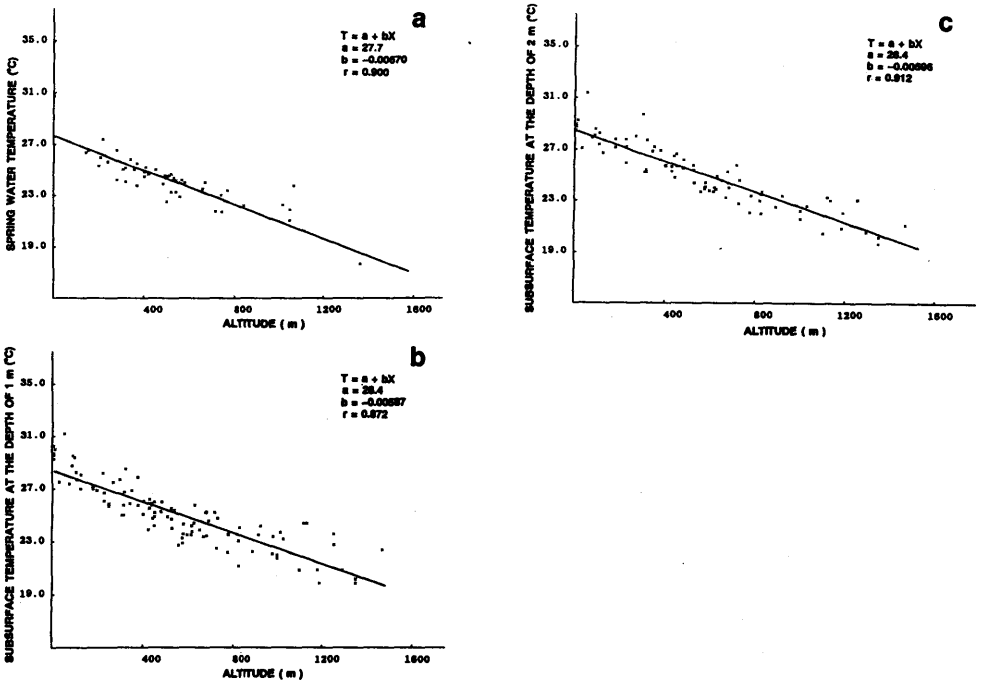

Figure 4 : Linear regression relations between spring water temperature (a), subsurface temperature at 1 m deep (b), subsurface temperature at 2 m deep (c) and altitude.

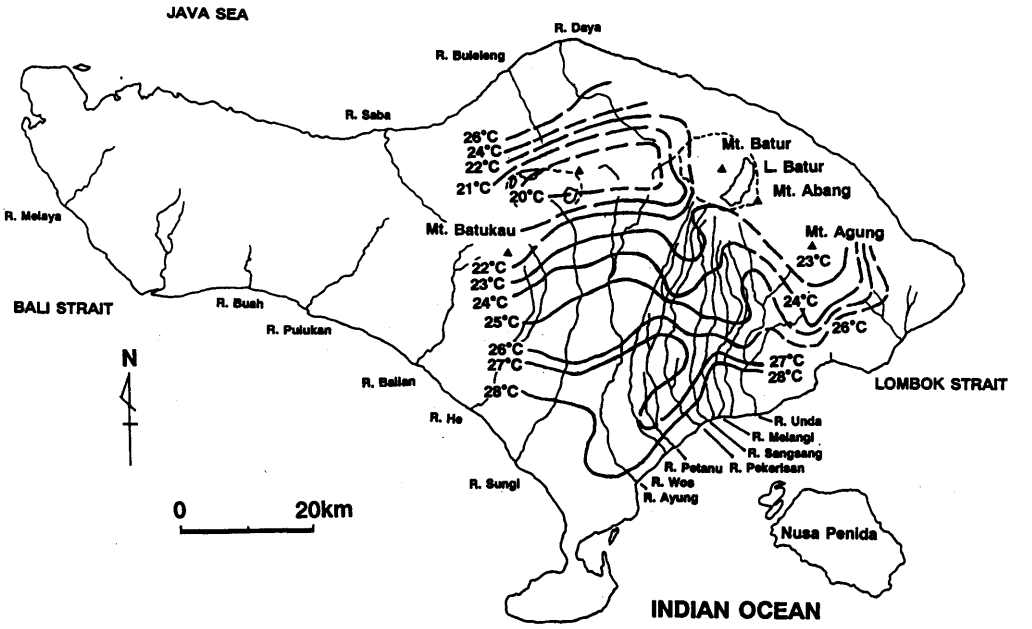

Figure 5: Distribution of subsurface temperature at 1 m deep.

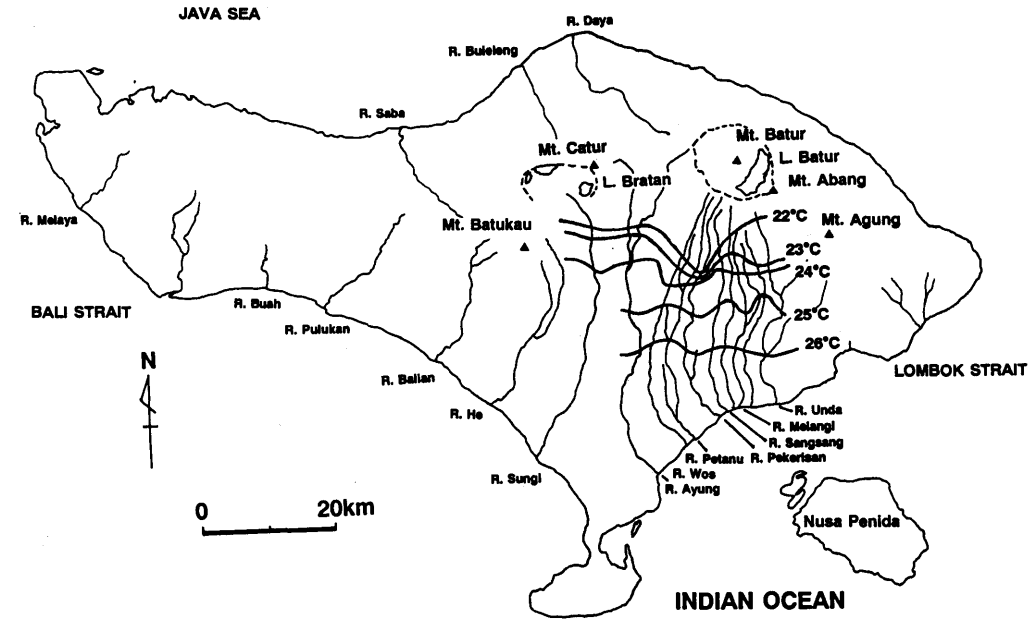

Figure 6: Distribution of spring water temperature.

The distribution of spring water temperature is shown in Figure 6 and indicates that the zone with relative lower temperature extends southward from the middle point between Penelokan and Bangli, along River Petanu and Pekerisan. On the contrary, the relative warm zones exist both in the east and west side of the cool zone mentioned above. This waving phenomena of isothermal lines maintain in the lower area. It was found that the warm zones of spring water locate between River Ayung and Wos at the altitude of more than 500 m, between River Wos and Petanu at that of less than 500 m and between River Sangsang and Melangi.

Relation between subsurface and spring water temperature

Both distributions of subsurface temperature at the depth of 1 m and spring water temperature show the same tendency. That is, the cool zone extends from the mountain region to the south downward along the River Petanu and Pekerisan up to the altitude of about 500 m. This tendency also is recognized along the River Sungi. This is due to the existence of the groundwater which have high fluidity and low temperature compared to groundwater in the surrounding area. This temperature difference of 2 °C indicates that the springs in this area are recharged in the mountain region at altitude of about 300 m higher than that of spring.

As for the distribution of subsurface temperature at 1 m deep, the cool zone within an isothermal line of 27 °C extends narrowly from Gianyar to the north part of Denpasar and the isothermal line of 28 °C also extends in the same direction. This tendency was not recognized from the spring water temperature, because there are few springs in the relative low land within an altitude of 200 m. The disturbance of subsurface temperature in this area is probably influenced by the heavy pumping at the North Denpasar well field for the municipal water supply (Min. of Public Work, 1986).

DISCUSSION AND CONCLUSION

This study area is constructed geologically by Quaternary volcanic material dipping southward from the volcanic ranges in the north and classified roughly into three zones (Nielsen and Widjaya, 1989). First is the zone of Volcanic Cones and Calderas, which located in the mountain ranges over 1000 m altitude. Second is the zone of Buyan-Bratan and Batur Volcanics situating under about 300 m altitude. Third is the zone of Lava Flows located intermediate between the first and second zones.

Nielsen and Widjaya(1989) suggested that many of the south flowing rivers have their origin in major springs. Those springs which locate over 1000 m altitude are classified into Type 1 and locate in the zone of Volcanic Cones and Calderas, however it is not so easy to reach such springs which are generally discharging from the valley wall as waterfalls. In the zones of Lava Flow, and Buyan-Bratan and Batur Volcanics, almost all springs are classified into Type 2. Those are discharging from the valley side walls as waterfalls, but some of them are flowing from the valley floor. Furthermore, at the altitude of about 500 m and between the River of Petanu and Pekerisan, we can find only two unique springs and classify them into Type 3. These springs are discharging from the bottom of spring pond and the discharging water spouts sand in the pond just like mud volcano. We could classified discharging processes of spring water into three types illustrated as Figure 7 schematically.

To estimate the recharge area and the flow path of the spring water, we compared the types of spring discharge with the distributions of temperature and electric conductivity of the spring water. From Figure 4, it became clear that spring water temperature is generally lower than the subsurface temperature.

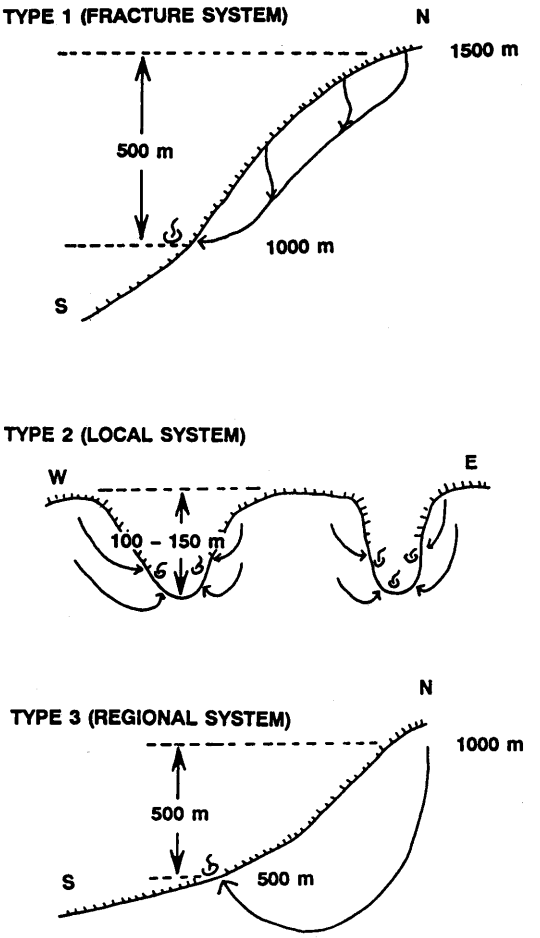

Figure 7: Schematic discharging process of spring water in the island of Bali .

Table 1: Relations between discharging type, temperature and electric conductivity of springs.

Discharging type	Temperature*	Electric conductivity**
1 Fracture flow system	low (< 20° C)	low (= 150 μS/cm)
2 Local flow system	equivalent	medium
3 Intermediate or regional flow system	equivalent or high (24° -25° C)	high (500 - 600 μS/cm)

*shows the comparison with subsurface temperature at the same altitude.

**shows the comparison with the mean value of the spring water.

The springs classified into Type 1 exist geologically in the zone of Volcanic Cones and Calderas over the altitude of 1000 m, and its temperature is lower than the subsurface temperature by more than 3 °C and a value of electric conductivity shows about 150 μS/cm. These data indicate that rainwater infiltrates in the upstream area whose altitude is about 500 m higher than that of the spring, and flows through the relative shallow layer with fractures.

Almost all springs of Type 2 locate in the zones of Lava Flow, and Buyan-Bratan and Batur Volcanics. As rivers dissect the week consolidated parts in the zone of Lava Flow and make a gorge whose maximum relative height reaches 150 m, springs discharge from side walls of valleys as waterfalls, but some of them discharge from the valley floor. The temperature of these springs scattered around the linear regression line within the range of ± 1°C (Figure 4a). Therefore, many of springs are assumed to be recharged on the upland near the spring. In the concept of groundwater flow systems introduced by Toth(1963), groundwater flow discharging as Type 2 is equivalent to local flow system.

We could find two springs classified into Type 3, which locate at the altitude of about 500 m. Those locations coincide with the geological boundary between Lava Flow and Buyan-Bratan and Batur Volcanics. The temperatures range from 24 °C to 24.5 °C and are equal to or more than the average temperature of springs as in Figure 7a. While, the values of electric conductivity show from 500 to 600 μS/cm and seem to be high remarkably compared to the other type of springs. Those springs have the ability to spout sand from the bottom of spring pond. Judging from these evidences, it is clear that this spring water is recharged in the mountain range and discharging as intermediate or regional groundwater flow system defined by Toth(1963).

On the other hand, Lake Batur locates at the altitude of 1031 m, southeast part in the Batur caldera rim and have a length of 7.5 km, a maximum width of 2.5 km and a depth of 65 to 70 m. From Table D, we can find temperature distribution of lake water show about 23 °C except of the surface layer of lake water. This temperature seems to be relatively high compared to the spring water temperature at the same altitude as Lake Batur. And electric conductivity is about 2100 μS/cm, extremely high. Following to the concept of water balance on closed lake (Nakao et al, 1970), we can expect not a few leakage from the lake. This water have to discharge from the surrounding springs outside the caldera rim. If we can find such springs whose temperature and electric conductivity are relatively high, in the valley below the altitude of Lake Batur, the hypothesis mentioned above will be verified. It may be considered that the springs classified into Type 3 are originated partially from Lake Batur. The relations between the discharging type, temperature and electric conductivity of the springs are summarized in Table 1.

ACKOWLEGEMENTS

The authors would like to acknowledge the encouragement of Professor Isamu Kayane, the Institute of Tsukuba, who was our team leader of the research project " Water Cycle and Water Use in the Volcanic Area in the Tropics", financially supported by Ministry of Education, Science and Culture in Japan (Nos 63041023 and 01041011).

REFERENCES

Andrews,C.B. & Anderson,M.P. 1979. Thermal alternation of groundwater caused by seepage from a cooling lake. *Water Resour. Res..*, 15; 595-602.

Arai,T. & Sakura,Y. 1980. Recent trend of phenomenal water temperature of Ye-Gawa, Tokushima Prefecture, *Hydrology*, 10; 2-11.

Birman,J.H. 1969. Geothermal exploration for groundwater. *Geol. Soc. Amer. Bull..*, 80; 617-630.
Birman,J.H., Esmilla,A.B. & Indreland,J.B. 1971. Thermal Monitoring of leakage through dams. *Geol. Soc. Amer. Bull..*, 82; 2261-2284.
Bredehoeft,J.D. & Papadopulos,I.S. 1965. Rates of vertical groundwater movement estimated from earth's thermal profile. *Water Resour. Res..*, 1; 325-328.
Cartwright,K. 1968a. Temperature prospecting for shallow glacial and alluvial aquifers in Illinois. *Illinois State Geol. Survey Circular* 433; 41.
Cartwright,K. 1968b.Thermal prospecting for ground water. *Water Resour. Res..*, 4; 395-401.
Cartwright,K. 1971. Redistribution of geothermal heat by a shallow aquifer. *Geol. Soc. Amer. Bull.*, 82; 3197-3200.
Domenico,P.A. & Palciauskas,V.V. 1973. Theoretical analysis of forced convective heat transfer in regional ground-water flow. *Geol. Soc. Amer. Bull..*, 84; 3803-3813.
Fukutomi,T. 1951. On the possibility of the prospecting of hot-springs by the geographical distribution of underground temperature in 1 m depth. *Geophys. Bull. Hokkaido Univ.*, 1; 1-14.
Kappermeyer,O. 1957. The use of near surface temperature measurements for discovering anomalies due to causes at depths. *Geophys. Prospecting*, 5; 239-258.
Kayane,I. 1991. Studies of water cycle and water use in the volcanic area in the tropics. *Gakujyutsu Geppo.*
Krcmar,B. & Masin,J. 1970. Prospecting by the geothermic method. *Geophys. Prospecting*, 18; 255-260.
Mink,J.F. 1964. Groundwater temperature in a tropical island environment. *Jour. Geophys. Res.*, 69; 5225-5230.
Nakao,K., Otsuki, S., Tanoue, R. & Naruse, R. 1967. Watershed leakage from the closed lake - Lake Kuttara-. *Geophys. Bull. Hokkaido Univ.*, 17; 47-64.
Nielsen,G.L. & Widjaya,J.M. 1989. Modeling of ground-water recharge in Southern Bali, Indonesia. *Ground Water*, 27; 473-480.
Nogami,M. & Sugiura,Y. 1985. *Suuri Chirigaku Ensyuu.* Kokon Syoin, Tokyo.
Parsons,M.L. 1970. Groundwater thermal regime in a glacial complex. *Water Resour. Res..*, 6; 1701-1720.
Sakura,Y. 1984. Methods of temperature prospecting for groundwater flow. *Jour. Groundwater Hydrology*, 26; 193-197.
Schneider,R. 1964.Relation of temperature distribution to ground-water movement in carbonate rocks of central Israel. *Geol. Soc. Amer. Bull.*, 75; 209-216.
Shimano,Y. 1988. Characteristics of the spring distribution and the spring water temperature in the Aso caldera and its surrounding areas. *Ann. Rep., Inst. Geosci., Univ. Tsukuba*, 14; 12-16.
Stallman,R.W. 1963. Computation of ground-water velocity from temperature data. *U. S. Geol. Surv. Water-Supply Pap..*, 1544-H; H36-H46.
Stallman,R.W. 1965. Steady one-dimensional fluid flow in a semi-infinite porous medium with sinusoidal surface temperature. *Jour. Geophys. Res..*, 70; 2821-2829.
Suzuki,S. 1960. Percolation measurements based on heat flow through soil with special reference to paddy fields. *Jour. Geophys. Res.*, 65; 2883-2885.
Toth,J. 1963. A theoretical analysis of groundwater flow in small drainage basins. *Jour. Geophys. Res..*, 68; 4795-4812.
Yamamoto,S. 1957. Spring water temperature on the foot of volcanic mountain slope in Japan., *Research on Water Temperature*, 1; 135-139.

Section 5 :

TECHNOLOGY AND SUBSURFACE RESERVOIRS

ARTIFICIAL RECHARGE OF GROUNDWATER IN DUNE SAND FOR THE USE OF THERMAL ENERGY

S. ISHIDA & A. INAMOTO
Hokuriku Regional Agricultural Administration Office, MAFF
2-2-60 Hirosaka, Kanazawa, Ishikawa 920, Japan
I. KOBAYASHI
Ministry of Agriculture, Forestry and Fisheries (MAFF)
1-2-1 Kasumigaseki, Chiyodaku, Tokyo 100, Japan
K. NAKAGAWA
Consulting Engineer, 3-13-5 Nagadohei, Kanazawa, Ishikawa 920, Japan
K. FUJINAWA
Department of Environmental Science, Shinshu University
3-1-1 Asahi, Matsumoto, Nagano 390, Japan
T. YOKOYAMA
Faculty of Engineering, Yamagata University
4-3-16 Jyounan, Yonezawa, Yamagata 992, Japan

ABSTRACT. Some experiments of aquifer thermal energy storage were conducted by Ministry of Agriculture, Forestry and Fisheries (MAFF), Japan. The system of these experiments is characterized as follows; (a) Using natural energy source (river water), (b) Simple recharge method (water spreading method), (c) Storage in an unconfined aquifer (figure 1). Energy recovery ratio was 43.0% (111 days after recharge), 31.6% (161 days after recharge).

INTRODUCTION

In Japan, there is little utilization of Aquifer Thermal Energy Storage (ATES). For most experiments of ATES, hot water was recharged into deep confined aquifer through a well (Yokoyama et al.,1980). But the cost of ATES is too expensive to operate economically and a simple method is required.

In order to save the cost of agricultural energy, such as energy to heat or cool greenhouses or to melt snow in winter, experiments on Aquifer Thermal Energy Storage had been carried out by MAFF at Sanrihama dune on the coast of Japan Sea, between 1978 to 1992. For these experiments, energy source was natural river water and the reservoir was a shallow unconfined aquifer. The results of these experiments are reported in this paper.

EXPERIMENT FIELD

The experiment field is in a dune, called "Sanrihama dune", on the coast of Japan Sea (Figure 2). The height from sea level in this area is about 10m and the distance between recharge ponds and Japan Sea is about 200m. The reservoir for the thermal energy was a shallow unconfined aquifer composed of medium dune sand. The thickness of the sand layer is 15 meters, and an impermeable basement of muddy conglomerate is under the sand layer (Figure 3).

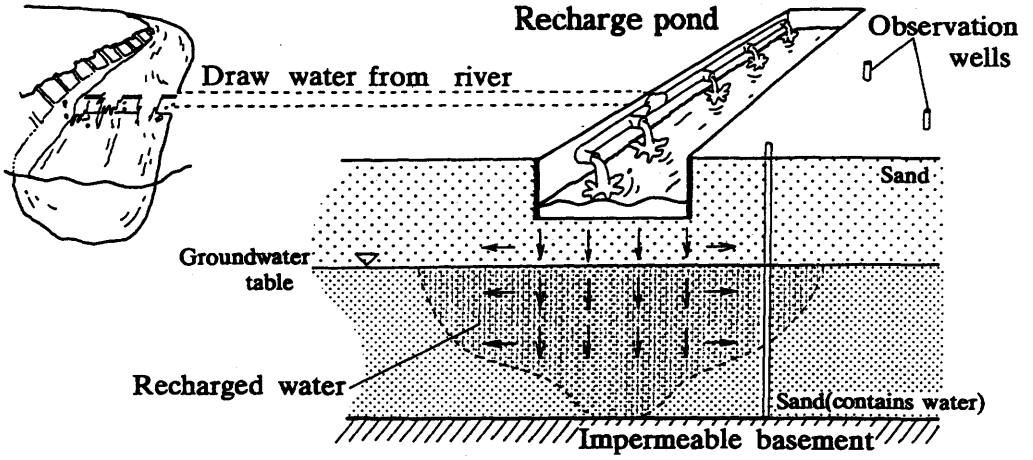

Figure 1: Model of recharge system.

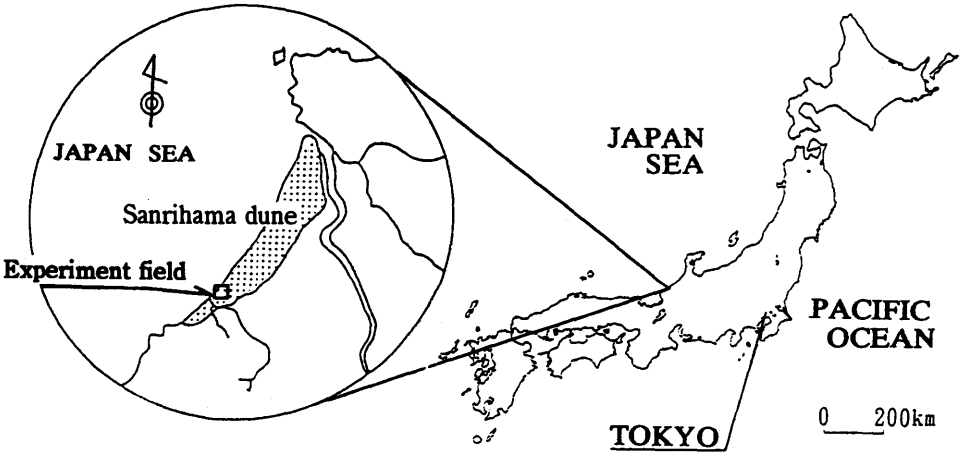

Figure 2: Location map of the experiment field.

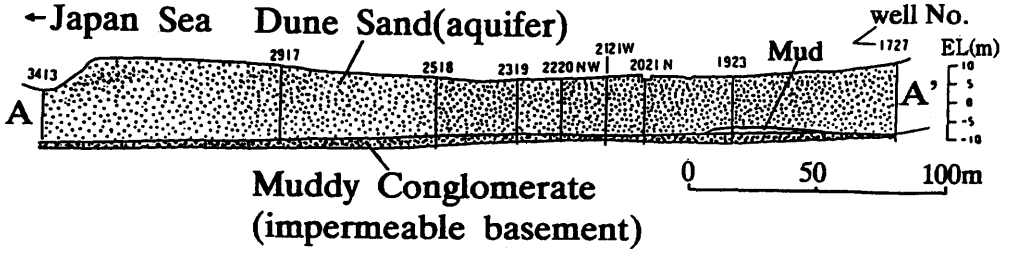

Figure 3: Geologic profile.

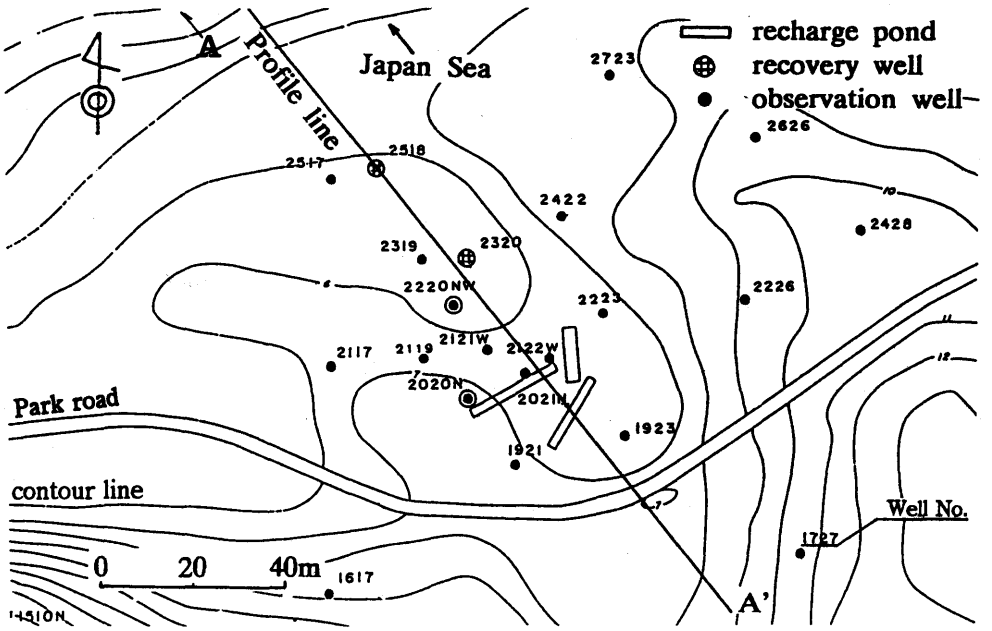

Figure 4: Distribution of the recharge ponds, recovery wells, observation wells.

Table 1: Result of cold-water recharge experiment in 1990.

Recharge period	399.2 hours (16.63 days)
Total recharge volume	27,444.6 m^3
Bottom area of recharge ponds	62.0 m^2
Velocity of recharging	0.019 m^3/sec
Highest water temperature Lowest water temperature Average water temperature	10.8 ℃ 4.4 ℃ 7.17 ℃

The medium diameter of the dune sand is 0.65mm at well No.2020 GL-4.3m and that of the matrix of muddy conglomerate is 0.092mm at GL-18.3m. According to Creager method, the permeability of the former is 5.54 x 10^{-2}cm/sec and that of the later is 6.25 x 10^{-5}cm/sec. The groundwater flows toward Japan Sea and its velocity is about 4 x 10^{-6}m/s. The mean annual temperature of the groundwater is about 15 °C and the difference between maximum and minimum temperature is 2 °C. The experiment system has 3 recharge ponds, 30 observation wells, and 2 water recovery wells around the recharge ponds in the dune (Figure 4).

EXPERIMENT

Recharge experiment

The recharge experiment has been done five times (in 1985, 1986, 1987, 1990, and 1991). In these experiments, the energy source was river water. It had been pumped up and drawn from Takasu river that flows through Sanrihama dune to the experiment field during the recharging. In 1990's cold-water recharge experiment, the water had been infiltrated in dune sand through recharge ponds from 3 February to 21 February. The river water had not been cooled artificially and its average temperature through recharge period was 7.17 °C. Total volume of water recharged was 27,444.6m^3. Table 1 shows the result of recharge experiment in 1990.

During the experiment, the river water often became muddy and the bottom of recharge ponds was clogged by fine mud. When clogging occurred recharging was stopped to remove these mud films.

Observation

During and after recharging, temperature of groundwater was taken every 1 meter depth in all observation wells every ten days. From these observations, the volume of recharged water and its thermal energy calculated.

Figure 5 shows the distribution of recharge water during the recharge experiment. At first the water penetrated vertically as far as the impermeable basement, then spreaded horizontally.

Movement of recharged water

After the end of recharging, the recharged water remained as an identifiable mass for 161 days. During this time, it was found that recharged water moved slowly to the Japan Sea as a mass and thermal energy had been decreased gradually. Figure 6 (a), (b), (c), (d), (e) show the distribution of the groundwater temperature after recharging.

Recovery

When 161 days passed from the end of recharging, a recovery experiment began. Recharged water was pumped for 1,440 hours (60 days) through recovery wells. In this experiment, two wells were used as recovery wells (No.2518 and 2320). In this experiment, clogging had not occurred. Figure 6 (f), (g) show the distribution of recharged water during recovery.

Table 2 shows the result of recovery experiment. Total volume of recovery water is 22,320.02m^3 recovery water was 9.8 °C at first and had been rising gradually until 13.3 °C. The average temperature is 12.3 °C.

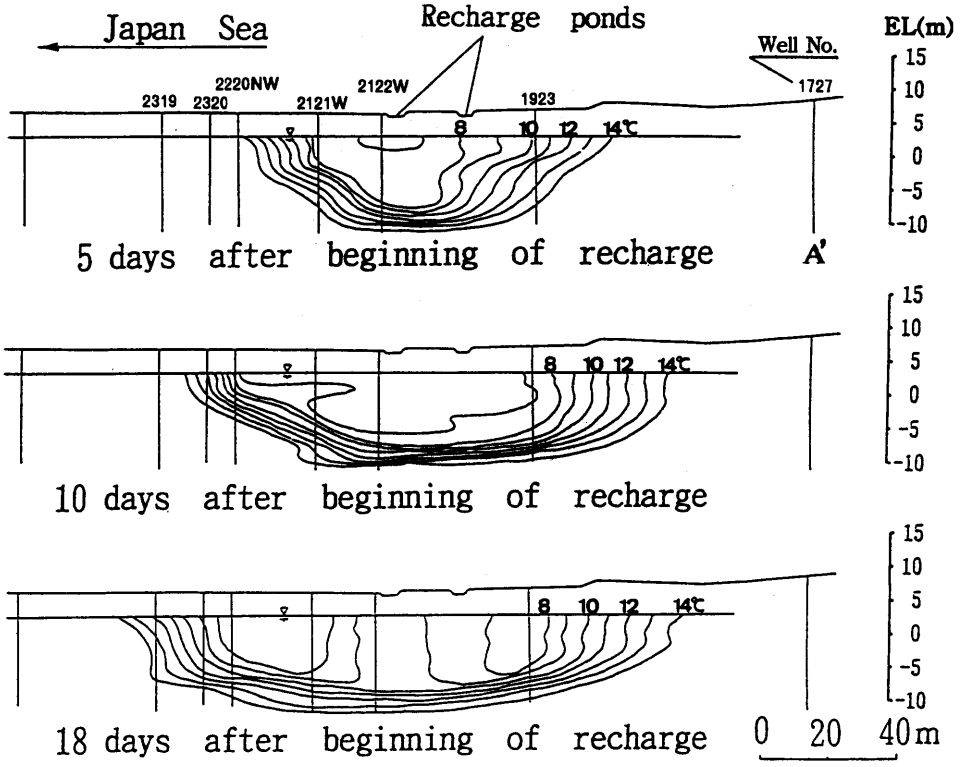

Figure 5: Profile of recharged water during recharging (1990).

Table 2: Result of cold-water recovery experiment in 1990.

	No.2518	No.2320	Total(average)
Recovery time	1,440hours (60days)	840 hours (35 days)	
Recovery volume	7,771.28 m^3	4,548.7 m^3	22,320 m^3
Lowest temperature	9.8 ℃	11.9 ℃	
Highest temperature	13.3 ℃	14.5 ℃	
Average temperature	12.04 ℃	13.45 ℃	12.3 ℃

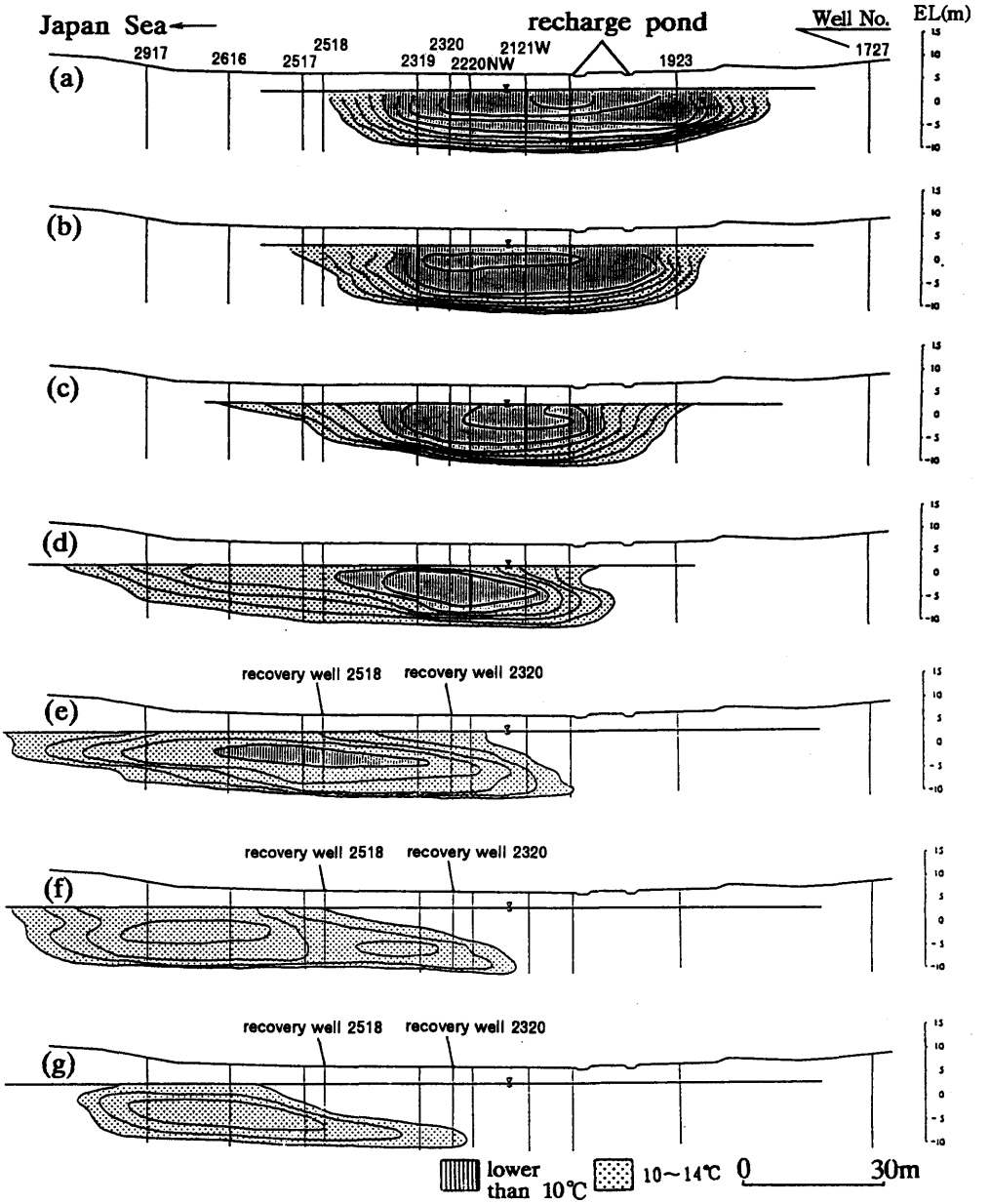

Figure 6: Profile of recharged water after recharging.
(a), (b), (c), (d), (e): 11, 30, 62, 98, 157 days after the end of recharging
(f), (g): 31, 61 days after beginning of recovery (at the end of recovery)
Equal temperature lines are 1 ℃ (≤14 ℃).
No.2581 and No.2320 are recovery wells.

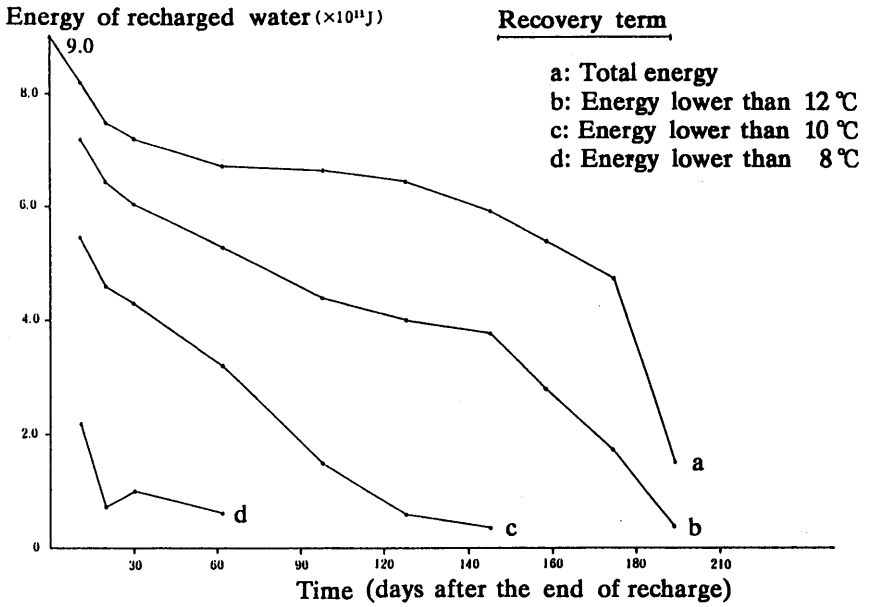

Figure 7: Alteration of recharged energy.

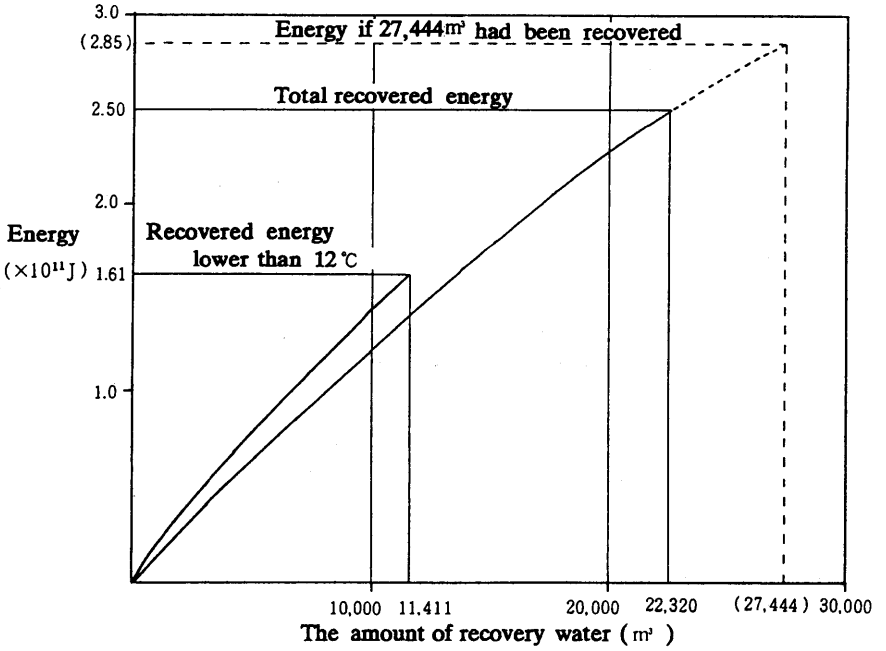

Figure 8: Relation between recovery volume and recovery energy.

Table 3: Comparison between cold water recharge and warm water recharge

Recharge material	Cold water	Warm water
Volume of recharge water	27,444 m^3	30,121 m^3
Recharge period	399.2hours (16.6days)	365.4hours (15.2days)
Average recharged temperature	7.17 ℃	25.5 ℃
Recharged energy ($\times 10^{10}$ J)	90.14	132.46
Time between the end of recharge and the beginning of recovery	161 days	111 days
Volume of recovery water	22,320 m^3	23,390 m^3
Average recovery temperature	12.3 ℃	20.2 ℃
Recovery energy ($\times 10^{10}$ J)	25.0	50.4
Expectable energy ($\times 10^{10}$ J)	28.5	57.0
Energy recovery ratio	31.6 %	43.0 %

ENERGY RECOVERY RATIO

The result of 1990's experiment

The background of groundwater temperature is 15 ℃ in the experiment field. In this paper, energy of recharged water is defined as difference from energy of water which temperature is 15 ℃. In this definition, total energy that recharged in 1990 was 90.14 x 10^{10}J.

Figure 6 shows the alteration of recharged energy. In this figure, the total energy had decreased to 80.0% for first 30 days. After that, the energy decreased gradually and its ratio was 5.0% per 30 days. After the beginning of recovery, the energy decreased rapidly.

The total energy of recovered water was 24.99 x 10^{10}J which is 27.7% of recharged energy. Figure 7 shows the relation between volume of water and its energy during recovery experiment. From this figure, if the same volume of recharging water (27,444m^3) had been recovered, thermal energy of 28.50 x 10^{10}J would have been recovered. The expectable energy recovery ratio is 31.6%.

Comparison with other experiment

Table 3 shows comparison between cold water recharge in 1990 and warm water recharge in 1987. In 1987's experiment, energy recovery ratio is higher than that of 1990's because the time between recharging and recovery of 1990's was 50 days shorter than that of 1987's and 1990's recharged energy was about two third of 1987's.

CONCLUSION

An unconfined aquifer well preserves thermal energy, and more than 30% of recharge energy can be recovered 161 days after recharging. At first recharged water is isolated from surrounding groundwater, then mixed gradually. In this field, energy recovery ratio of ATES was more than 30% whether recharge material is cold water or warm water. Thermal energy storage in unconfined aquifer has capabilities to save agricultural energy.

REFERENCES

Yokoyama, T., Umemiya, H. & Abiko, H. 1975. Heat exchange of storage through underground strata by artificial recharge. *J.Groundwater Hydrol.*,17-2.

Yokoyama, T. et al. 1977. Model experiment and numerical analysis for the purpose of the cyclic heat generative through underground strata. *Refrigeration.*, 52

Yokoyama, T. et al. 1977. Artificial recharge & utilization of aquifer for thermal energy storage. *Symp. of water resources.*, p.557-563.

Werner, D & Kley, W. 1977 Problems of heat storage in aquifers. *J. Hydrol.*,34;35-43.

Fujinawa, K. & Mitsuta, M. 1984. Review of theoretical and practical aspect for aquifer thermal energy storage techniques. *J.Agicultural engineering.* 160; pp. 121-144.

Kobayashi, I. & Hashida, T. 1989. A study on temperature field formed by artificial groundwater recharge in an unconfined aquifer. *J. Groundwater Hydrol.*, 31-4.

Kobayashi, I., Inamoto, A., Nakagawa, K. et al. 1990 Thermal energy storage in an unconfined aquifer at Sanrihama dune. *EOS.*, 71; 28.

Inamoto, A., Ishida, S. et al. 1992. Artificial recharge of groundwater in dune sand. *Symp. on Geo-Environment 1992.*; pp.147-152.

GEOTECHNICAL DEVELOPMENT OF SUBSURFACE DAM PROJECT IN JAPAN

S. KAWASAKI, T. SUGAHARA, J. MIYAKITA & M. KOTOKU
Ministry of Agriculture, Forestry and Fisheries,
1-2-1 Kasumigaseki, Chiyodaku, Tokyo m., Japan
J. NAGATA
Okinawa General Bureau, Japan
S. NAGATA & N. ENAMI
Kyusyu Regional Agricultural Administration Office, Japan
T. NISHIJIMA & K. AZUMA
Chugoku-Shikoku Regional Agricultural Administration Office, Japan

ABSTRACT. The agriculture in Ryukyu Islands in the southwest of Japan is deeply dependent upon the stochastic rainfall and quite unstable. The annual amount of rainfall in the islands is dependent on the passage typhoons. When no typhoon passes through the islands, a severe drought may hit the area. Though the mean annual rainfall in the Ryukyu Islands reaches to 2,000 mm, it is very stochastic year by year varying from 1,000 to 3,000 mm. The geology of the most part of the islands consists of an elevated reef-coral limestone called as Ryukyu Limestone (Hanzawa, 1935) which is, in general, under karstism and highly pervious. The major part of rainfall infiltrates into the ground due to high permeability of the limestone. The fluvial system in the islands is, therefore, less developed and characterized by small catchment area and short river length. The groundwater runs off into the sea without use through the permeable Ryukyu Limestone and sea-water intrudes into the coastal aquifer of Ryukyu Limestone by pumping up the groundwater excessively.

The development of water storage for agriculture has, therefore, been required for years in those islands. In consideration with the said situation in the islands, a water storage project on the ground has been deemed to the hardly realized.

The Ministry of Agriculture, Forestry, and Fisheries, the Government of Japan (MAFF) has conducted since 1974 to date the subsurface dam development program in the islands to develop the groundwater resource by subsurface dam which can dam up groundwater flow into an aquifer and reserve groundwater which is wasted into the sea without use (MAFF, 1986). An irrigation project with subsurface dams in a consideration size is now under implementation based on the know-how obtained through the program. A historical background of survey, some salient features of subsurface dam for irrigation purpose and the current technology related to the program, study and construction of subsurface dam are presented in this paper.

BACKGROUND

In the 1940s, Prof.Dr.K.Kachi formulated a plan for a subsurface dam in a moderate size for irrigation at an alluvial fan area in Nasunogahara, Tochigi Prefecture (Kachi, 1943). His plan is not realized yet, but still deemed to be attractive.

Kabashima Subsurface Dam with a storage capacity of some 20,000 m^3 and daily yield of 300 m^3 was constructed in 1973 to be the first subsurface dam in Japan for the water supply to Nomozaki town, Nagasaki Pref. In 1974, MAFF commenced the subsurface dam development program in Ryukyu and Amami Islands in the southwestern Japan to initially focus the potential for subsurface dam construction in Ryukyu Limestone.

Since then a systematic investigation and study on the subsurface water storage scheme for irrigation have been conducted up to the date.

In 1979, MAFF, in collaboration with Okinawa General Bureau, completed Minafuku Subsurface Dam with a storage capacity of 700,000 m^3 for an experimental purpose in Ryukyu Limestone on Miyakojima Island, Okinawa Pref. Minafuku Subsurface Dam was the largest subsurface dam in Japan in term of storage capacity at that date.

On the basis of successful results of Minafuku Subsurface Dam, MAFF initiated an irrigation project in a national level with subsurface dams in considerable size in Miyakojima Island to cover the beneficial area of some 8,400 hectares. The project was planned to develop the groundwater resource by the construction of two subsurface dams, Sunagawa (9,500,000 m^3 capacity) and Fukusato (10,500,000 m^3 capacity) Subsurface Dam in addition to the existing Minafuku Subsurface Dam.

Sunagawa Subsurface Dam is about completion at present. Fukusato Subsurface Dam is now ready to commencement of construction. In 1992, MAFF started irrigation projects with subsurface dam(s) in Ryukyu Limestone region in the southern area of Okinawa-Honto Island, Okinawa Pref. and Kikaijima Island, Kagoshima Pref. The outline of projects is shown in Table 1.

Since 1981, MAFF has also conducted another survey program for other types of aquifer such as alluvial sand and gravel deposits and volcanic pyroclastics. As a link of the program, an experimental construction of cutoff wall into a valley-fill alluvial deposits has been under way since 1989 in Nakajima Island, Ehime Pref.

The technology and know-how on the subsurface dam in Japan have been steadily progressed since MAFF initiated the subsurface dam development program in 1974. For instance, the curtain grouting method was adopted for the cutoff wall construction of Minafuku Subsurface Dam. But, at present, new methods as a slurry wall in various methods were tested and evaluated to select an appropriate quality and method in accordance with the nature of aquifers. In addition to subsurface dams in large size mentioned above, the dams in small size were completed to prevent sea-water intrusion into coastal aquifer and to develop the fresh water resource for supply. Those are Tunegami Subsurface Dam in Mikata town, Fukui Pref. (1983), Tengakuma Subsurface Dam in Umi town, Fukuoka Pref. (1988) and Waita Subsurface Dam in Nii town, Nagasaki Pref.(1992)(Aiba, 1983, Wada et al, 1989).

The major dimensions and location of subsurface dams in Japan are shown in Table 1 and Figure 1 respectively.

Table 1: List of subsurface dam in Japan.

No	Name of Dam	Locality	Use	Cutoff wall		Strage Capacity *1000m³	Reservor Rock	Remarks
				Hight (m)	Length (m)			
1	Tunegami	Fukui	T.W.	18.5	202	73.5	Alluvial dep.	1983 Complete
2	Nakajima	Ehime	Irr.	24.8	88	27.0	Alluvial dep.	Under Construction
12	Waita	Nagasaki	T.W		105	12.0	Alluvial dep.	1992 Complete
3	Tengakuma	Fukuoka	T.W.	12.5	129	17.5	Alluvial dep.	1988 Complete
4	Nomozaki	Nagasaki	T.W.	25.0	60	20.0	Alluvial dep.	1974 Complete
5	Kikai	Kagoshima	Irr.	36.0	2190	1681.0	Limestone	Under Planning
6	Komesu	Okinawa	Irr.	81.0	2489	2062.0	Limestone	Under Planning
7	Nashiro	Okinawa	Irr,	25.0	906	388.0	Limestone	Under Planning
8	Giiza	Okinawa	Irr.	51.0	955	389.0	Limestone	Under Planning
9	Sunagawa	Okinawa	Irr.	49.0	1835	9500.0	Limestone	Under Construction
10	Fukusato	Okinawa	Irr,	52.0	1720	10500.0	Limestone	Under Planning
11	Minafuku	Okinawa	Irr,	16.5	500	700.0	Limestone	1979 Complete

T.W./ Town Water
Irr/ Irrigation

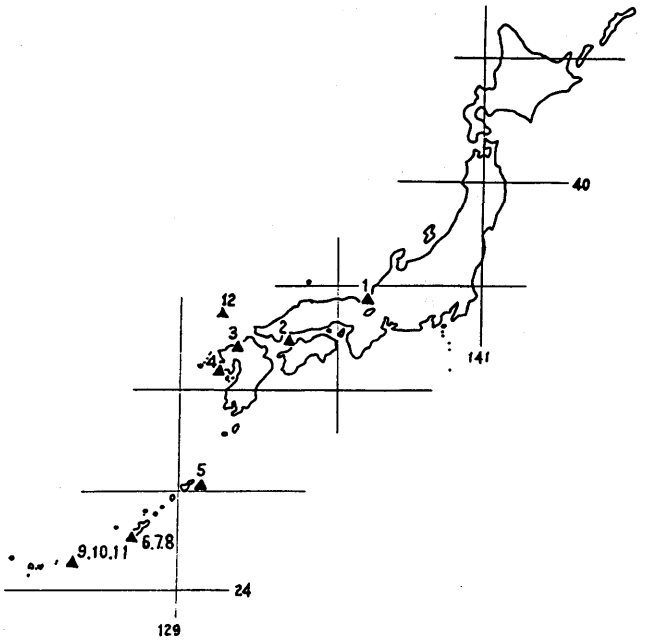

Figure 1: The location map of subsurface dam in Japan.

OUTLINE OF IRRIGATION PROJECTS WITH SUBSURFACE DAM

Through the subsurface dam development program, MAFF selected some 40 potential sites for subsurface dam development in Ryukyu Islands. Taking both the technical possibility and magnitude of demand of irrigation water into consideration, MAFF took up three irrigation projects with subsurface dam(s) in national level. The outline of projects are summarized in Table 2 below:

Miyako Irrigation Project

Miyakojima Island consists of Shimajiri formation of mudstone and siltstone (Shimajiri Mudstone) in Tertiary age as the bed rock and overlaid Ryukyu Limestone in Quaternary age (Hanzawa, 1935).

In the uplifting process of the island, both formation were inclined and thrusted. The unconformable contact between the impervious Shimajiri Mudstone and Ryukyu Limestone inclines around 10 degrees toward west and divided into several blocks by major faults dipping toward the northeast. Thus, valley-shaped groundwater basins were formed in the island as shown in Figure 10.

The limestone of Miyakojima Island is under a moderate karstism showing high permeability and storativity, and forms an excellent aquifer. The mean values of permeability coefficient and specific yield of the limestone estimated through a number of aquifer tests conducted at Minafuku Subsurface Dam are 0.35 cm S^{-1} and 0.1 respectively. The coefficient permeability of limestone were concentrated within a range of 0.15 to 0.7 cm S^{-1} exceeding 1 cm S^{-1} in some places.

The hydrogeological setting mentioned above is not permit the development of fluvial system in Miyakojima Island. The surface runoff is generated only when a heavy rain fall. The coefficient of surface runoff to annual rainfall is to be 5% or less.

While, annual groundwater recharge in the island is estimated to reach some 150 million m^3 or some 45% of annual rainfall. The groundwater thus recharge is once stored in the aquifer, and runs off into the sea. A number of coastal and off-shore springs are seen around the island. The total discharge from those springs is estimated to reach some 200,000 m^3 in the day. Although the inhabitant in Miyakojima Island uses groundwater to some extent through springs and wells for domestic and irrigation purposes, the most of groundwater is wasted into the sea without use because groundwater runs off into the sea immediately and groundwater level is too low to easily pumping up.

The aim of groundwater resource development by means of subsurface dam is to increase both the storage capacity and water depth in the aquifer and to secure the groundwater resource for irrigation.

Miyako Irrigation Project aims to improve farm economy of the island introducing the irrigation farming and land improvement for some 8,400 hectares of beneficial area. The general plan of the project is shown in Figure 2. It is expected the project improves the existing monoculture farming by rainfed sugar-cane cultivation into the irrigated multiculture farming, and the farm economy to a high income type. To achieve the aim, two subsurface dams were planned to secure the groundwater resource for irrigation. The gross storage capacities of dams are 9,500,000 m^3 in Sunagawa Subsurface Dam and 10,500,000 m^3 in Fukusato Subsurface Dam respectively.

The construction of Sunagawa Subsurface Dam was commenced in 1988, and will be completed in early 1994. The construction of Fukusato Subsurface Dam is expected to be started in 1994. The

Table 2: List of Irrigation Project with subsurface dam in national level.

Name of Project	Benefit Area (ha)	Name of Dam	Main Irrigation Facilities	Cost (million us$) Project total (Subsurface dam)
Miyako	8400	Sunagawa Fukusato Minafuku	Main pipe line 135km Booster pump station 8 Regulator tank 7	391 (217)
Okinawa-Honto-Nanbu	1382	Komesu Giiza Nashiro	Main pipe line 40km Booster pump station 2 Regulator tank 3	224 (151)
Kikai	1642	Kikai	Main pipe line 40 Booster pump station 3 Regulator tank 2	160 (85)

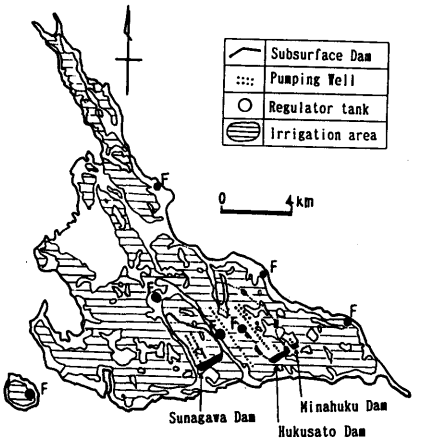

Figure 2: Miyako Irrigation Project.

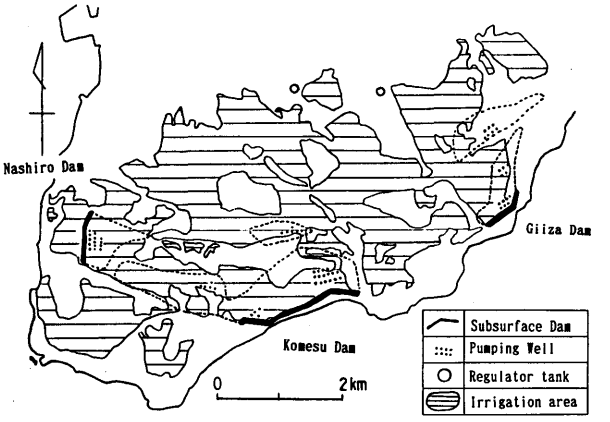

Figure 3: Okinawa-Honto-Nanbu Irrigation Project.

major dimensions of dams are shown in Table 2. The cutoff wall of dams is to be constructed by the mixed-in-place slurry wall method.

Okinawa-Honto-Nanbu Irrigation Project

The southern-most area of Okinawa-Honto Island stands upon the same environment as Miyakojima Island in the geological setting in Ryukyu Limestone overlying Shimajiri Mudstone, the poor fluvial system and predominate drought-hit.

Rainfed sugar-cane has been mere cultivable crop in the area due with its nature in the drought resistance and strong stem against typhoon. A lot of groundwater runs off into the sea without use through the valley- shaped groundwater basins which were formed by faults. MAFF formulated the same agriculture development plan to the area as in Miyakojima Island (Okinawa-Honto-Nanbu Irrigation Project). Fortunately the area situates a hinterland of a major crop consumptive zone.

The project is to construct three subsurface dams and other facilities and to cover some 1,400 hectares of irrigable area. The major dimension and general plan are as shown in Table 2 and Figure 3 respectively. The project was commenced in 1992.

Figure 4 shows a contour map of top of impervious basement in Komesu Basin wherein the largest Komesu Subsurface Dam is planned. The geological profile along the dam axis is shown in Figure 5. The length and maximum depth of Komesu Subsurface Dam are 2,500 m and 80 m respectively.

Since Komesu Basin situates at the southern coast of Okinawa-Honto Island and the aquifer in the basin extends below the sea level, the sea-water intrudes into the inland aquifer at present as shown in Figure 6.

It is remarkable that the mode of interface between fresh and saline waters varies in places in accordance with the hydraulic features in aquifer. The subsurface dam makes possible to increase storage capacity and to prevent sea-water intrusion into the reservoir basin even when the water level in the reservoir lowered below the sea level by pumping groundwater.

The leakage analysis made so far indicated the permeability of cutoff wall is to be 1×10^{-7} cm S^{-1} or under to prevent the sea-water intrusion through the cutoff wall.

Kikai Irrigation Project

Kikaijima Island situated at 30 km east of Amami-Oshima Island and occupies an area of some 56 km^2. The pervious Ryukyu Limestone overlies impervious Shimajiri Mudstone. Only the rainfed sugar-cane cultivation is major farming due with the poor water resource in the island.

MAFF commenced the implementation of irrigation project (Kikai Irrigation Project) in 1992 to cover an irrigable area of some 1,700 hectares by the groundwater secured by Kikai Subsurface Dam (refer to Figure 7).

The dam is located in a valley-shaped groundwater basin in the southwest of island. The sea-water intrusion takes place at the dam since the lowest top of impervious basement at the dam axis is 12 m below the sea level as shown in Figure 8.

Test construction of cutoff wall by several methods were carried out at the dam site to testify the availability of designed permeability of cutoff wall by construction method.

Nakajima Experimental Subsurface Dam

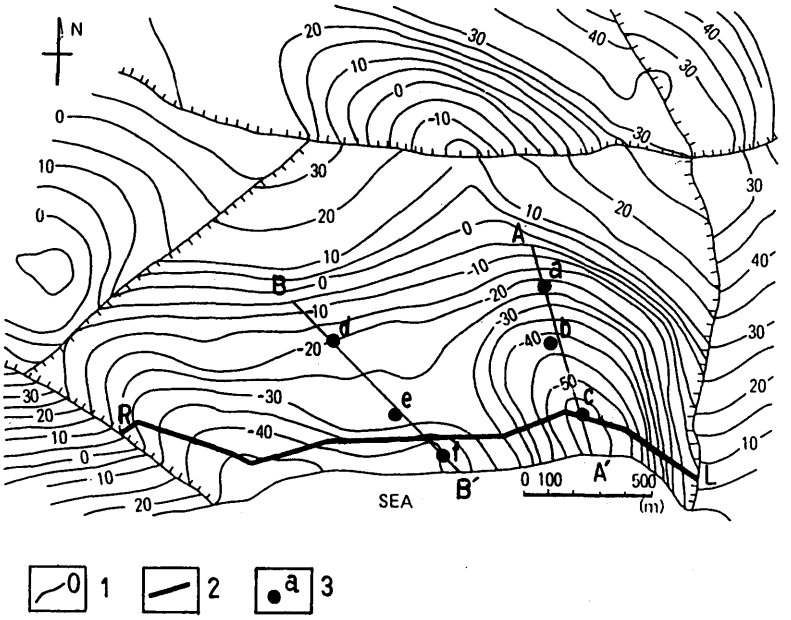

1 : Contour of upper plane of impermeable basement(Shimajiri Mudstone or Chinen Sandstone) 2 : Dam axis 3 : Water quality observation point

Figure 4: Hydrogeological map of Komesu Subsurface Dam.

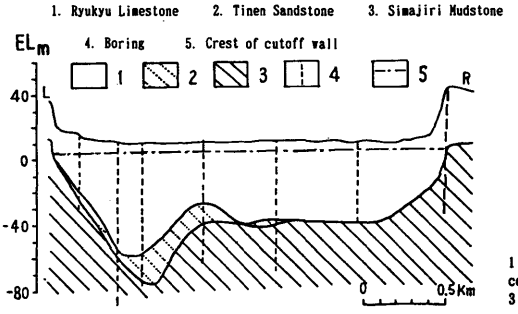

Figure 5: Hydrogeological profile of Komesu Subsurface Dam.

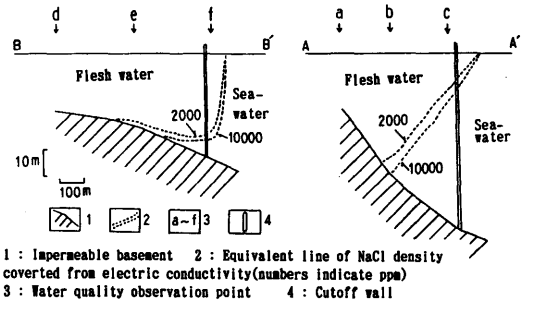

Figure 6: Actual sea-water intrusion of Komesu Subsurface Dam (1987.6.20).

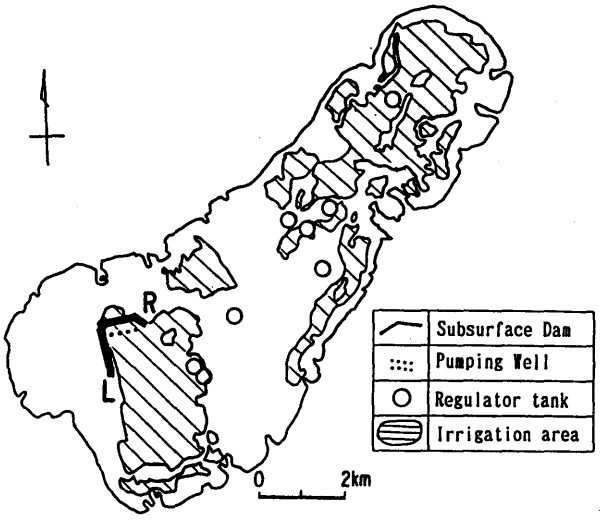

Figure 7: Kikai Irrigation Project.

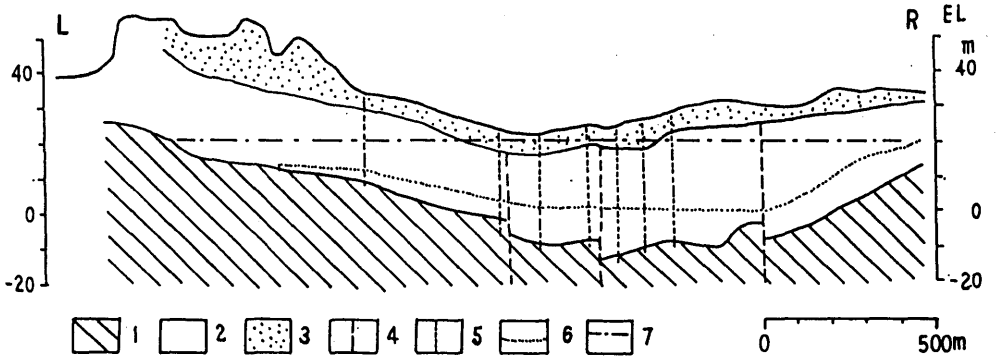

1. Simajiri F. 2. Ryukyu Limestone 3. Calcarious sand 4. Fault 5. Boring
6. Groundwater level 7. Crest line

Figure 8: Hydrogeological profile of Kikai Subsurface Dam.

MAFF has been constructing an experimental subsurface dam (Nakajima subsurface dam) at the coastal valley plain in Nakajima Island in Seto-Naikai Sea (Ehime Pref.) in order to establish a technology to construct the cutoff wall into the soft alluvial deposits and to prevent the sea-water intrusion.

Nakajima Subsurface Dam is located some 200 m from the sea-shore. The alluvial deposits filling valley is 25 m thick at the maximum at the dam site overlying andesite bed rock as shown in Figure 9. A clay layer divides the deposits into an unconfined upper aquifer and a confined lower aquifer. The permeabilities of upper and lower aquifers are ranges within 10^{-4} cm S^{-1} and 10^{-3} cm S^{-1} respectively. That of bed rock is in a range in 10^{-4} to 10^{-5} cm S^{-1}. The electric conductivity of groundwater is 400 μS cm^{-1} or less in the upper aquifer and 4,000 μS cm^{-1} or more in the lower aquifer. Chemical analysis shows the lower groundwater is contaminated sea-water. Cutoff wall was made by slurry wall method of series mixed-in-place soil-cement pile in 550 mm diameter. The storage capacity of the dam is most 27,000 m^3 (Nishijima et al, 1992).

TECHNOLOGICAL REVIEW ON SUBSURFACE DAM

The technology and know-how obtained so far through the MAFF's subsurface dam development program are summarized as follows;

Hydrogeological conditions

The most sites for subsurface dam in a large size were selected at areas where consist of Ryukyu Limestone in Ryukyu and Amami Islands. The limestone is composed of reef-coral and under a moderate karstism; and forms an excellent aquifer with a high specific yield ranging 0.07 to 0.13 and a high permeability within an order of 10^{-1} cm S^{-1}. Shimajiri Mudstone composed of mudstone and siltstone overlaid by the limestone may act to be the impervious basement. The uplifting, tilting and a number of faulting have been taken place by the significant tectonic movement in Ryukyu and Amami region. The movement formed an ideal hydrogeological structure for the construction of subsurface dam in such narrow and long valley-shaped groundwater basins as illustrated in Figure 10 (Momikura et al, 1989).

Besides Ryukyu and Amami Islands, a number of plans on subsurface dam project are formulated in remote islands and peninsulas where are an alluvial lowland facing with the sea-water intrusion.

Methodology of cutoff wall construction

The cutoff wall of Minafuku Subsurface Dam was made by the curtain grouting of cement and clay. The width of cutoff wall was designed to be 5 m with grout-hole in 7 rows in 0.57 m interval. The permeability in 60 % of cutoff wall thus constructed reached to 5 x 10^{-5} cm S^{-1} or less. The maximum depth of cutoff wall was 35 m below the ground. The groundwater hydrograph in the reservoir basin after the cutoff wall construction is shown in Figure 14.

The cutoff wall of Sunagawa Subsurface Dam was planned to reach up to 65 m depth and to attain the mean permeability of 5 x 10^{-5} cm S^{-1} or less.

After the trial construction, the cutoff wall construction since 1988 (refer to Figure 11) shifted to the mixed-in-place slurry wall method, and the improved permeability was attained to an order of 1 x 10^{-6} to 10^{-7} cm S^{-1}.

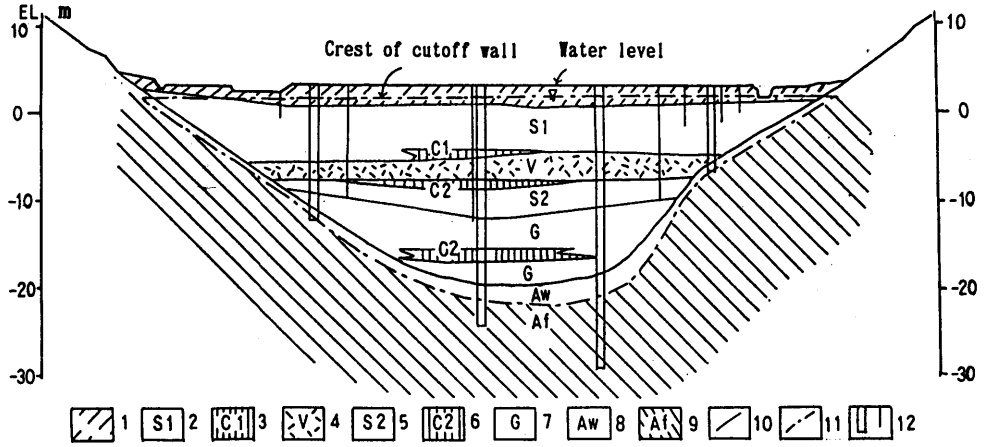

Figure 9: Hydrogeological profile of Nakajima Subsurface Dam.

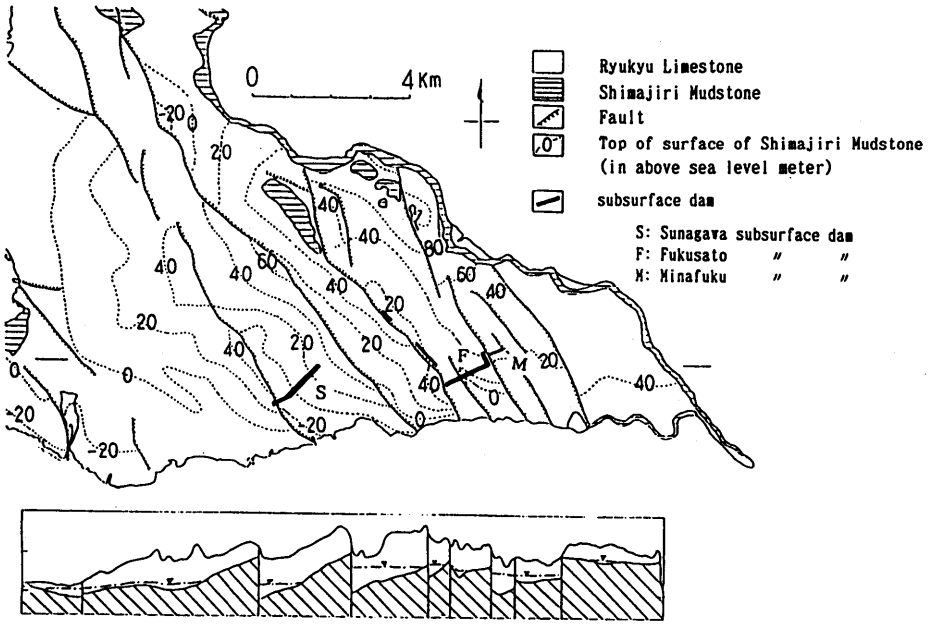

Figure 10: Hydrogeological map of Miyakojima Island.

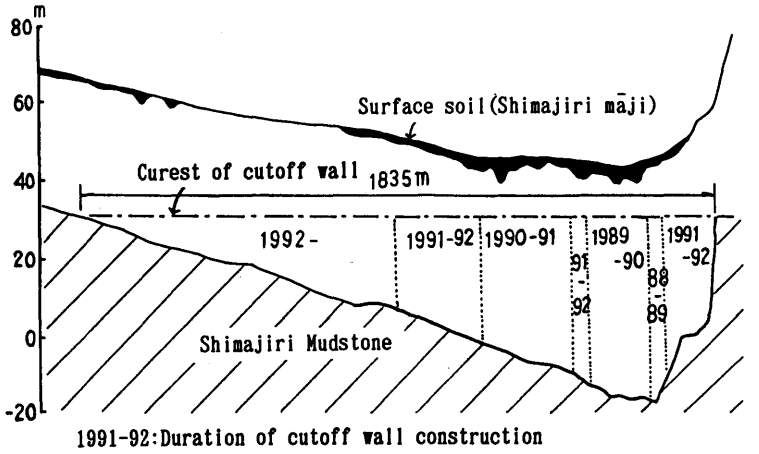

Figure 11: Cutoff wall construction of Sunagawa Subsurface Dam.

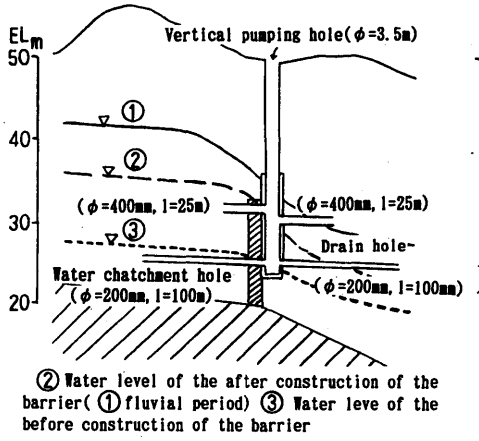

Figure 12: Intake facility of Minafuku Subsurface Dam.

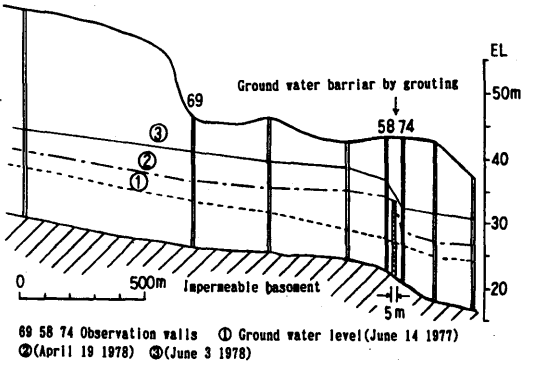

Figure 13: Fluctuation of groundwater level in the Minafuku Subsurface Dam area.

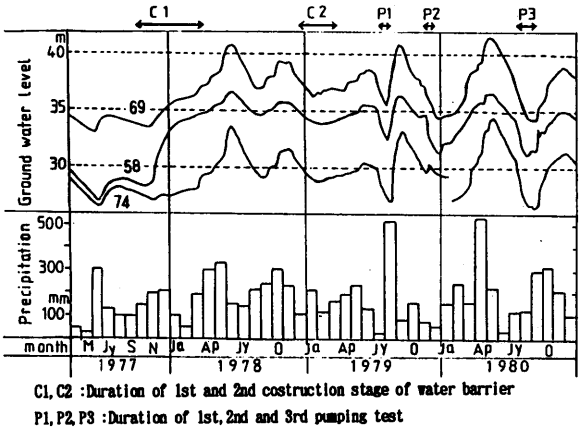

Figure 14: Fluctuations of groundwater level on Minafuku Subsurface Dam.
(See elevation of water level after construction of cutoff wall)

The trials construction for cutoff wall in other methods were made in Kikai Subsurface Dam site to obtain the best-adapted method of cutoff wall construction in order to prevent sea-water intrusion into fresh reserved water near sea coast. A paper on results of trials will be published shortly by S. Nagata et al.

Analytical methods for water balance and flood

Water balance analysis : The best-adapted irrigation plan and design for irrigation system and appurtenant facilities are to be formulated by the aid of a mathematical model which could simulate a long-term groundwater behavior in the study basin. The model is to be that which treat both unsaturated and saturated phases of groundwater system. The former is to deal the mechanism of groundwater recharge taking the precipitation, evapo-transpiration, surface runoff, infiltration (unsaturated seepage) and soil retention into account. The latter is to handle the storage and flow of groundwater in an aquifer.

To deal with the groundwater system, various models (the synthetic storage model, the tank model, the finite difference model, the finite element model and so forth) are used.

A model, so-called the synthetic storage model was developed to deal both phases simultaneously (Aiba et al, 1983). The model is useful to clarify the specific mechanism of stochastic groundwater recharge in connection with the surface hydrology, the groundwater behavior in the reservoir basin and the stochastic reservoir yield. In the case of Minafuku Subsurface Dam, the groundwater level calculated by the method was fine fitting to observed groundwater level. Water balances of Okinawa-Honto-Nanbu Irrigation Project and Kikai Irrigation Project were analyzed by the synthetic storage model.

Flood analysis : The design criteria is firmly designated for the large surface storage dam. For instance, the design flood for spillway of a high dam is to be return period in 200-year. While, the destruction due to flood overtopping on a subsurface dam is hardly taken place since the cutoff wall is hold by the ground from the both sides. The damage of cutoff wall may be made by seepage in high velocity generated by a high water head in the reservoir area. Another negative effect generated by groundwater flood is an inundation of surface area above the reservoir area due to the rise of groundwater table. As per the reasons mentioned above, a flood analysis in the following manner is required in the planning stage for the decision of crest height of cutoff wall and the design of surface drainage system;

(a) delineation of an area within the reservoir area where is to be inundated by the groundwater rise after the construction of cutoff wall,
(b) decision of the crest height of cutoff wall which permit a high groundwater level (critical high groundwater level) staying below the ground in the reservoir area in consideration of environment factor,
(c) determination of the highest groundwater level in the reservoir area in the design flood year after the construction of cutoff wall in a crest height through the model simulation.

The simulation for flood analysis is used to apply the finite-element model or the finite-difference model.

The surface drainage system (spillway) and/or subsurface outlet work may be considered in case that the crest height of cutoff wall has to be set at a level which generate the high groundwater level beyond the critical high groundwater level due with the requirement of storage capacity in irrigation plan.

Design of intake facility

A collector well in 3.5 m diameter with two horizontal boreholes (Diameter: 200 mm x Length: 100 m, Diameter: 400 mm x Length: 25m) and four tubewells were made as the water-intake facilities of Minafuku Subsurface Dam (Figure 12). The water-intake test in Minafuku reservoir were made four times through the facilities since 1979. Daily maximum discharge of 10,300 m^3 and total water of 290,600 m^3 was discharged within 52-days continuous pumping. The specific yield of reservoir basin was evaluated to be 0.10 through the test. The groundwater hydrograph in Minafuku reservoir after the completion of cutoff wall and during the intake tests is as shown in Figure 14 (Okinawa General Bureau, 1983).

The same type of collector wells were initially planned for intake facilities for Sunagawa and Fukusato Subsurface Dam. Tubewells in 400 mm diameter were, however, finally designed to discharge 2,000 m^3 day^{-1} each. The wells have been constructed and tested at present.

Management of storage and quality of groundwater

Since the groundwater is one of limited and precious resources in Ryukyu Islands, the municipalities in the Ryukyu Islands established regulations on development priority in public use, ie. water-supply, irrigation, industry and so forth; the rule for quality preservation; and the development control for private use.

The pollution on the groundwater stored in a man-made subsurface reservoir is hardly predicted under the natural condition. However, if the contamination with any pollutant took place, it may take a considerable time and cost to recover the groundwater quality as before since the

replenishment of groundwater under the hydrologic cycle is very slow comparing with that of surface system.

In consideration of above, the preventing measure for conservation of groundwater quality has to be taken by mean of the regulation of total load of pollutant from human and industrial wastes over the whole catchment basin of subsurface reservoir.

CONCLUSION

A number of subsurface dams in large size for irrigation purpose is realized within next few years in Japan. And some more progress for the technology and know-how on this specific water storage scheme would be attained through confirmation on the hydrologic balance, reservoir yield, subsurface flood, sea-water intrusion and so forth.

Besides the Ryukyu Limestone region, other subsurface dams in small size are required for such in coastal valley plains, peninsulas and remote islands where are difficult to develop surface water resource, limited to use groundwater by sea-water intrusion, and hazardless to the existing groundwater right in the lower reach.

New technology and experience of subsurface water storage in Japan could be applied for other nations under various conditions in the same nature.

REFERENCES

Aiba,M. 1983. Irrigation Water Resources Development Project by Groundwater Storage Dam. Civil Engineering in Japan, *Japan Society of Civil Engineers,* 22; 152-163. (in Japanese)

Aiba,M.,Kurokawa,M.,Nagata,S.,Hosotani,H. & Yoshikawa,M. 1983. The hydrologic behavior of underground reservoir in the Miyakojima Island. *The Japanese Society of Soil Mechanics and Foundation Engineering,* vol.31, No.3; 17-23.

Hanzawa,S. 1935. Topography and geology of Riukiu Island. *Sci. Rep. Tohoku Univ.,2nd. Ser,* 17; 1-61.

Kachi,k. 1943. *Groundwater recharge and agricultural water use.* Chijinsyokan. (in Japanese)

Ministry Of Agriculture, Forestry And Fisheries & Okinawa General Bureau. 1986. *Subsurface Dam: A new technology for water resource development.* (in Japanese with English summary)

Momikura,K.,Kunihiro,M. & Subsurface Dam Research Group. 1989. Management and control of the groundwater stored by subsurface dam at Miyako-jima island, *the Ryukyu Japan. International commission on irrigation and drainage. 7th Afro-Asian conference Tokyo, 1989.*

Nagata,S.,Enami,N.,Nagata,J.,Katoh,T. & Okamoto,M. 1993. Design and construction of cutoff walls for subsurface dams on Amami and Ryukyu islands most southeastern part of Japan. *IAH Selected paper* vol. 4, (on contribution).

Nishijima,T.,Azuma,K. & Asano,M. 1992. A construction of subsurface dam at Nakajima island. *Proceeding of the Regional conference International rainwater catchment system association.*

Okinawa General Bureau. 1983. *An experimental underground dam project in Miyako-jima island.* (in Japanese)

Wada,M.,Aiba,M.,Enami,N.,Fukushima,K.,Sayama,M. & Subsurface Dam Study Group. 1989. New technology for the construction of subsurface dam for irrigation water resource development. *International commission on irrigation and drainage. 7th Afro-Asian conference Tokyo, 1989.*

DESIGN AND CONSTRUCTION OF CUTOFF WALLS FOR SUBSURFACE DAMS ON AMAMI AND RYUKYU ISLANDS IN THE MOST SOUTHWESTERN PART OF JAPAN

S. NAGATA
Chugoku-Shikoku Regional Agricultural Administration Office,
9-24, Tenjin-cho, Okayama, Japan
N. ENAMI
Kyusyu Regional Agricultural Administration Office, Japan
J. NAGATA
Okinawa General Bureau, Japan
T. KATOH
Kinki Regional Agricultural Administration Office, Japan

ABSTRACT. Subsurface dams under construction in Ryukyu and Amami Islands, in the most southwestern part of Japan, have main two purposes. First is to dam up and store groundwater which quickly runs off to the sea by constructing cutoff walls, and to use it effectively for agricultural use. Second is to prevent saltwater intrusion into fresh reserved water near sea coast and to separate saltwater and inland groundwater by cutoff walls. In any case, cutoff walls for subsurface dams must have high impermeability. Suitable methods for the construction of cutoff walls, according to the topographical and hydrogeological conditions of each dam site,will be adopted. On Miyakojima, Okinawajima (Okinawa Pref.), and Kikaijima (Kagoshima Pref.) Islands, experimental continuous subsurface cutoff walls were constructed into the coral reef limestone called Ryukyu Limestone. The new technologies for subsurface dams preventing saltwater intrusion were established with several methods between 1986 and 1990. Satisfactory coefficients of permeability between $1x10^{-7}$ and 10^{-6} cm/sec. were obtained from the results of these test constructions.

SUMMARY

This paper summarizes outline of test constructions of subsurface continuous cutoff walls for subsurface dams executed on Kikaijima, Okinawajima, and Miyakojima Islands.

Kikaijima Island is located about 30km east of Amamioshima Island, Kagoshima Prefecture, and has an area of 55.7km^2. Okinawajima Island is located about 300km south of Amamioshima and Miyakojima Island is located about 300km southwest of Okinawajima (Figure 1).

The Wantobaru Subsurface Dam in Kikaijima is to be constructed under the gently-sloping plateau in the southwestern part of the island. The cutoff wall exists in the subsurface valley, which are bordered by parallel faults running from south to north on the land. It has the dam depth of 35m, the crest length of 2,400m and the storage capacity of 1,700,000m^3. It is used as a water resource of the National Irrigation Project which was started in 1992. This project aims to provide irrigation water for 1,700 hectares of farmland. Most parts of Kikaijima are covered with elevated coral reef

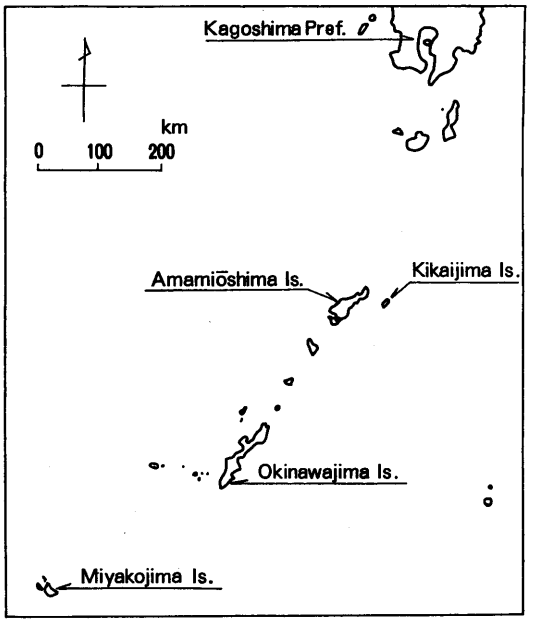

Figure 1: The location map.

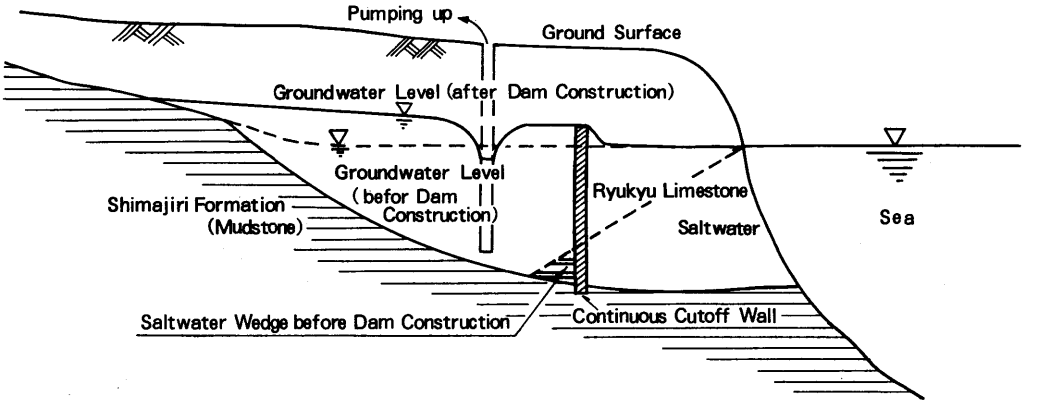

Figure 2: Saltwater cutoff type subsurface dam.

limestone called the Ryukyu Limestone of the Pleistocene age, and the Shimajiri Formation composed of mudstone and siltstone of the Pliocene age which forms the foundation for the Ryukyu Limestone. The Ryukyu Limestone acts as a excellent aquifer due to its high porosity. Because of an aquifer which is lying below sea level, a saltwater wedge is formed in the coastal area. If groundwater is excessively pumped up, the sea water may penetrate into the groundwater basin (Figure 2). Construction of subsurface dams will store groundwater in those aquifers and prevent sea water penetration. New impermeable cutoff wall construction methods for prevention of saltwater penetration have been tested at the Wantobaru site in Kikaijima. Five construction methods of continuous cutoff walls have been examined. Total crest length of cutoff walls was 90m with 10 ~ 20m length respectively, and the depth of each wall was about 35m.

The Komesu Subsurface Dam on Okinawajima will be constructed along the coral reef-dotted coast line. This dam is a saltwater cutoff type subsurface dam which seals off saltwater infiltration caused by pumping up groundwater. The scale of the test construction was the excavation length of 7m, the depth of 75m and the wall thickness of 1m.

The Sunagawa Subsurface Dam is under construction along the southern coast line of Miyakojima. The scale of dam is the depth of 65m, the crest length of 1,800m and the storage capacity of about 9,500,000m^3.

The Ryukyu Limestone mainly consists of clastic limestone and its thickness is 30 ~ 40m at the Wantobaru Dam site, 40 ~ 80m at the Komesu Dam site and 40 ~ 60m at the Sunagawa Dam site respectively. The Shimajiri Formation which is an impervious basement of the Ryukyu Limestone consists of mudstone and siltstone.

An excellent condition for subsurface dams need to have narrow outlets of underground valleys. These islands are divided by parallel-laying faults (Figure 3).

The facies of the Ryukyu Limestone can be classified into several geological layers which have clastic limestone, large foraminifera limestone, calcareous algae limestone and coralline limestone at Kikaijima (Figure 4).

The hydrogeological characteristics of the Ryukyu Limestone are as follows,
(a) The effective porosity obtained through the pumping tests and the boring core tests ranges from 7%to 15%.
(b) The coefficients of permeability concentrated within a range from $1x10^{-2}$ to 10^{-1} cm/sec. and caves are often formed in the limestone.
(c) The average unconfined compressive strength ranged between 80 to 250 kgf/cm^2 (max: approx. 580kgf/cm^2).

OUTLINE OF TEST CONSTRUCTIONS

The Ryukyu Limestone has high permeability and considerably various in hardness. The tests were conducted to study whether the various methods of continuous subsurface cutoff walls could be applied to those properties of the Ryukyu Limestone. The construction tests executed are shown in Table 1.

Slot Vertical Drilling Method (SDV Machine)

Outline of Slot Vertical Drilling Method : This is a drilling method where the SDV machine of middle-scale rock drill equipped with plural bits drills vertical continuous wall in the underground

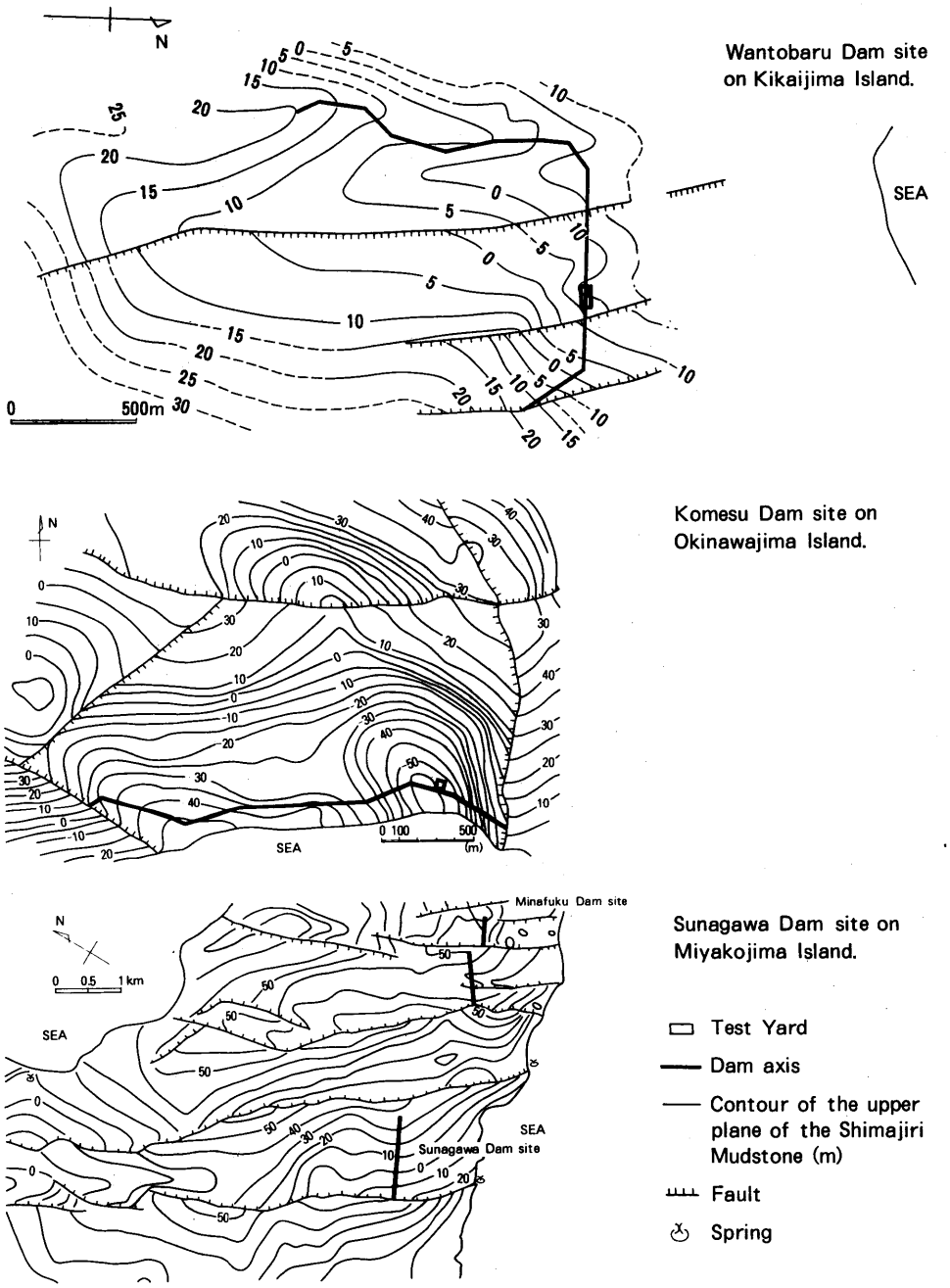

Figure 3: Contour maps of the upper plane of Shimajiri Mudstone.

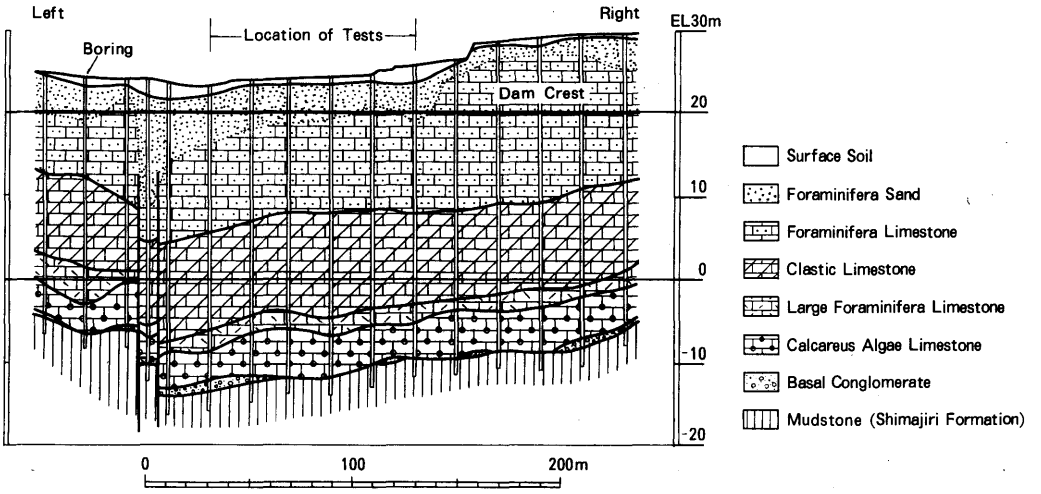

Figure 4: Geological closs-section of the Wantobaru Sbsurface Dam site.

Table 1: Construction methods of continuous subsurface cutoff walls.

Names of construction methods	Location of tests
(1) Slot vertical drilling method	Wantobaru, Kikaijima
(2) Large-diameter drilling method	Wantobaru, Kikaijima
(3) Chain-saw type narrow-trench excavation method	Wantobaru, Kikaijima
(4) Steel sheet piling method	Wantobaru, Kikaijima
(5) Bucket excavation method	Wantobaru, Kikaijima
(6) Horizontal multi-axis rotary excavator method	Komesu, Okinawajima
(7) In-situ churning method	Sunagawa, Miyakojima

(Figure 5). Thus, subsurface continuous piling is constructed by pouring mortar or solidifying agent into trenches. This method has the following.
(a) The SDV machine is equipped with a drilling mechanism which provides simultaneous impact and rotation to the rod, allowing the slot to be operated at a high drilling speed even for relatively hard limestone, having unconfined compressive strength of 1,500 kgf/cm^2 or greater.
(b) This method enables construction of the subsurface cutoff walls with thicknesses as thin as 20 to 35 cm, thus construction cost can be reduced.
(c) As the water-intrusion preventive cutoff wall is constructed by the replacement method using mortar or the like, a continuous subsurface cutoff wall which is uniform and superior in water-intrusion resistance can be constructed.

Results of Test Construction: : (a) Drilling speed of 3-continuous holes varied from 1.9m to 2.8m per hour. Such variation was caused by bending or twisting of holes due to heterogeneous limestone. In spite of that the machine exhibited adequate drilling capacity.
(b) Insufficient discharge of slime which worsened the work efficiency was caused by insufficient mud circulation method due to large open cracks and caves. Such trouble was eliminated by adopting the air lift method.
(c) After completion of the work, a permeability test was carried out with bored hole on the cutoff wall. The test result showed satisfactory coefficient of permeability in the range of 5.6×10^{-7} ~ 4.3×10^{-6}cm/sec..

Large-diameter Drilling Method

Outline of Large-diameter Drilling Method: This machine utilizes an all-casing rotary method which has been developed for field drilling and piling. The cutter is provided on the whole circumference of the casing end. Hard basement is drilled by giving rotation to the casing and the rock pieces in the casing is excavated by the hammer grab. In this method, freshly mixed concrete or mortar is poured into the hole to construct field pile. Thus constructed field piles are arranged side by side to form a cutoff wall. This method has been executed based on the experience obtained through the Slot Vertical Drilling method. Work sequence of this method is as shown in Figure 7.

Results of Test Construction : The continuous subsurface cutoff wall was constructed by drilling 20 field piles of 1.2m in diameter with overlap of 200 mm in the width. Distance with adjacent drilled hole was 1,000mm at center and minimum wall thickness obtained was 663mm. Figure 8 shows completion of cutoff wall.
(a) Easy drilling of rather hard basement containing cobbles, boulders and hard rocks like limestone was insured and no mud circulation method was required (Figure 9).
(b) Highly accurate cutout was insured by the casing, which leads the way by cutting the boulders and rocks with its special cutting edge.
(c) The casing leading the way economized the drilling space, thus minimizing consumption of mortar.
(d) Construction by replacement with mortar allowed to form cutoff wall having uniform and superior water-sealing ability.
(e) One piling (depth:35m) was executed in two days. Continuity was assured by the piling accuracy of 1/710.
(f) After completion of the work, the cutoff wall was bored for a permeability test. The test indicated satisfactory coefficient of permeability in the range of 3.8×10^{-8} ~ 4.1×10^{-7}cm/sec..

Chain-saw Type Narrow-Trench Excavation Method (Using impermeable sheets)

Outline of Chain-saw Type Narrow-Trench Excavation Method : This method uses impermeable sheets as the cutoff materials so as to create thin, but highly impermeable continuous cutoff walls. The characteristics of the construction method are outlined below;

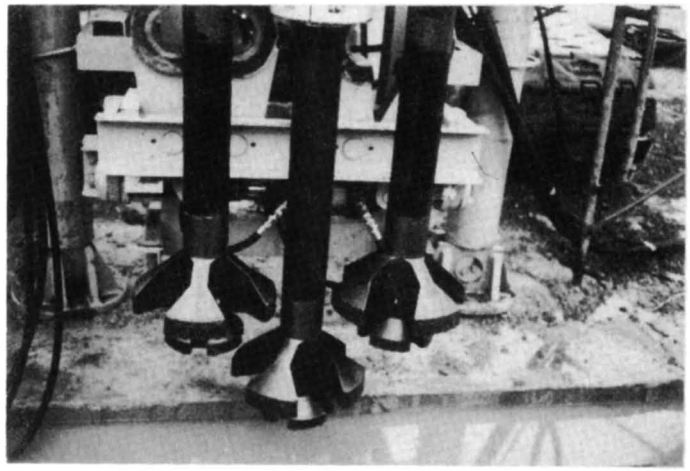

Figure 5: The SDV machine equipped with 3-continuous bits.

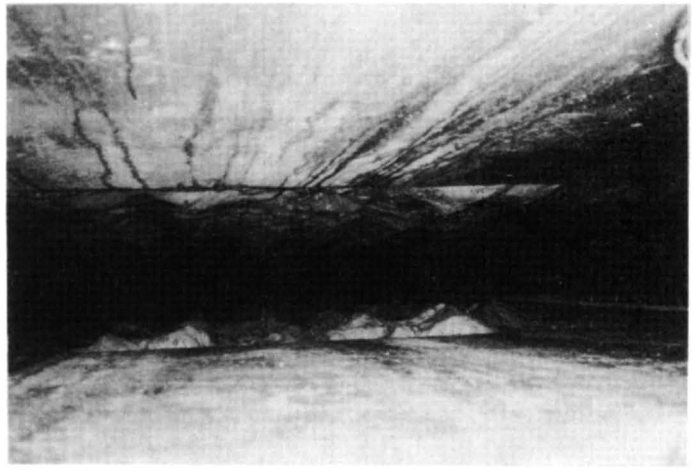

Figure 6: Wall of holes drilled by the SDV machine.

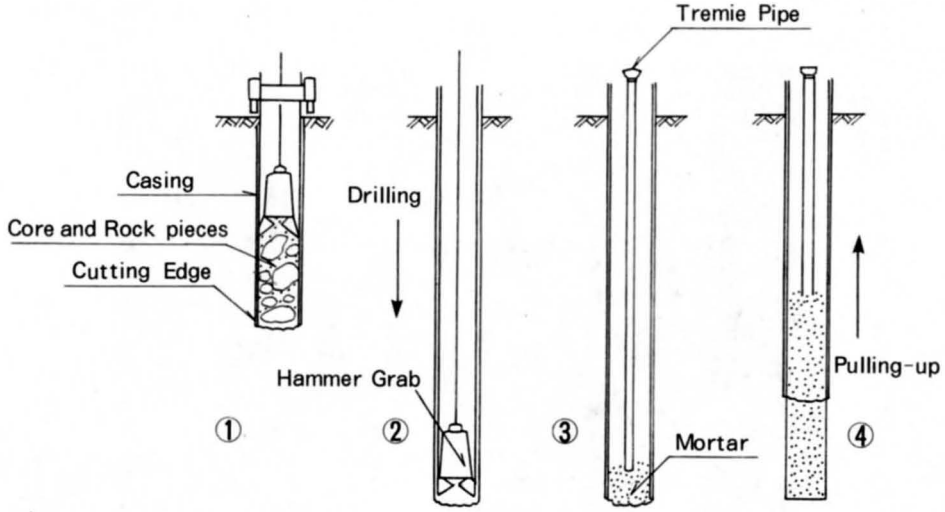

① After setting the drilling machine, the rotary casing attached with the cutting edge at its end started to drill. The casing was added as the drilling depth became deep.
② Drilling, crushing and discharge of core were carried out by the hammer grab.
③ After drilling the designed depth, the tremie pipe was set to pour mortar.
④ Mortar was poured to the designed depth while extracting the casing and tremie pipe.

Figure 7: Sequence of work execution by the Large-diameter Drilling Method.

Figure 8: Completion of the continuous subsurface cutoff wall.

Figure 9: Core and rock pieces being discharged by the hammer grab.

(a) Superior impermeability is obtained because of the use of rubberized asphalt sheets.
(b) The use of the impermeable sheets and chain-saw type narrow-trench excavator reduces the wall thickness and the quantities of the soil or rock excavation and mortar placement, thus leading to cost reduction.
(c) High adaptability to the deformation of the surrounding ground can be maintained without lowering the impermeability of the cutoff wall by ensuring that the fill materials have approximately the same rigidity as the surrounding ground.

As shown in Figure 10, the cutoff wall consists of columns (diameter: 81cm) at 2.3m intervals with thin wall sections (thickness: 15cm) in between. The impermeable sheets inserted in the reservoir side of the thin wall sections function as the cutoff materials, while the fill materials (mortar etc.) transfer the water pressure acting on the cutoff wall to the ground and improve the durability of the impermeable sheets (Figure 11, 12 and 13).

Results of Test Construction : The net excavation speed ranged between 0.07 and 0.11 m/min. (average: 0.09m/min.). The average speed including the time taken up in extending, lowering, and fixing the main body of the excavator, was 0.07m/min.. Success was achieved in creating narrow trenches approximately 18cm in width and with a smooth finish on the cut surface, except in some sections of the connections with the advance holes where partial collapse was observed. There was virtually no collapse of the trench surface as was originally anticipated.

Steel Sheet Piling Method

Outline of steel sheet piling method : This method uses vibratory pile drivers and water jets to drive steel piles into baserock. The piles act as the rockcutting bits and water jets clear the powdered rock from around the tip of the pile to prevent interference with its bits into the baserock. For this test construction, piles of H-shape steel were used (Figure 14).Work sequence of this method is shown in Figure 15, 16, 17, 18 and 19.

Bucket Excavation Method

Outline of Bucket Excavation Method : The test cutoff wall was constructed at the Wantobaru site of Kikaijima to check whether it could be constructed using a bucket excavation in the rather hard Ryukyu Limestone. It was found possible to construct the continuous subsurface cutoff wall. In constructing the cutoff wall, a deep trench was excavated using a clamshell type bucket and filled with mortar to form the cutoff wall. To facilitate bucket excavation, holes were drilled at both ends and at the center of the portion of excavation, in advance, using an auger. Figure 20 shows the dimensions of the holes by the auger and the trenches made by the bucket. The width (thickness) of the cutoff wall was determined by the width of the bucket, which was 0.8m in this case. The length of cutoff wall was equivalent to four elements of the width of the bucket opening. To insure that the continuous subsurface cutoff wall penetrated the impermeable Shimajiri Mudstone by about 1m, its total depth was set at 36.5m. Having excavated the full face of continuous subsurface cutoff wall, the trench was filled with mortar to form the body of the wall. Figure 21 ~ Figure 24 show the sequence of the construction test.

Results of Test Construction : It was confirmed that the bucket excavation of a trench in the Ryukyu Limestone was possible. It was also verified that the excavation was more effective if advance drilling is carried out at three locations at both sides and center of the bucket. By this method, the excavation rate was found to be about $1m^2$ per hour.

After completion of the work, this cutoff wall was bored for a permeability test. The test results indicated a coefficient of permeability of $7.4x10^{-6}$cm/sec..

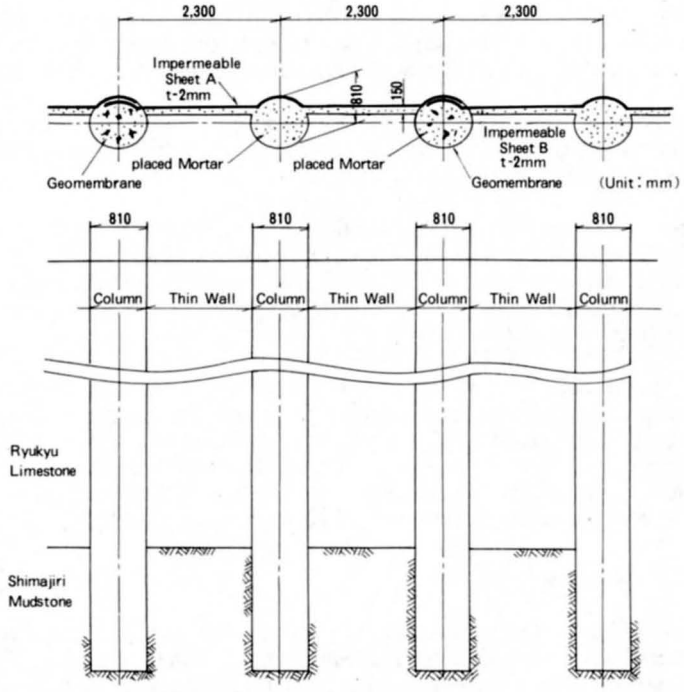

Figure 10: Structure of the cutoff wall.

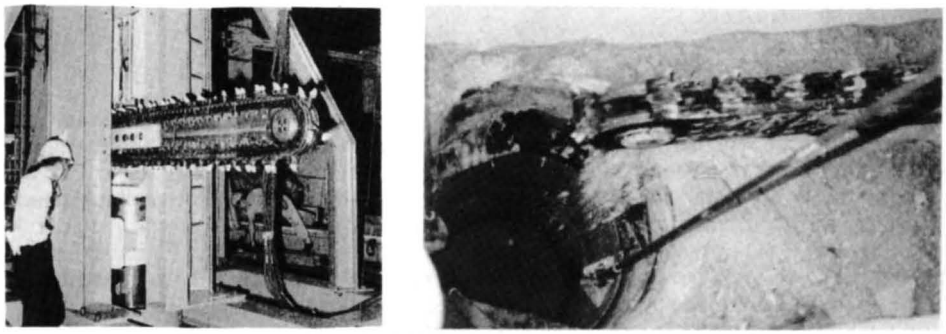

Figure 11: The chain-saw type narrow-trench excavator.

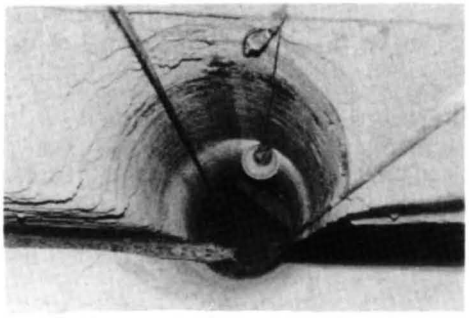

Figure 12: Finished thin wall.

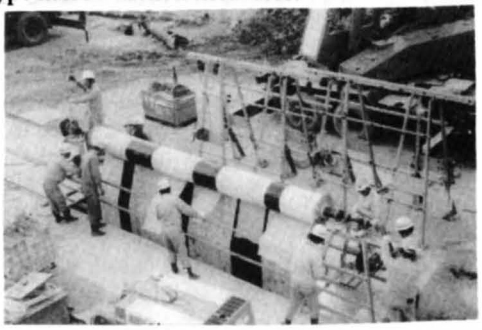

Figure 13: Sheet insertion.

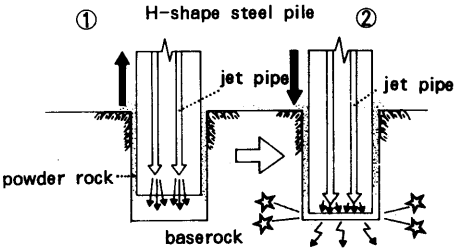

① Water jets remove powdered rock from the end of the steel pile as it bounces upward after striking baserock.
② Because the water jets remove the fragments of rock from beneath the pile, it always strikes directly on the baserock.

Figure 14: The principles of the steel sheet pilling method.

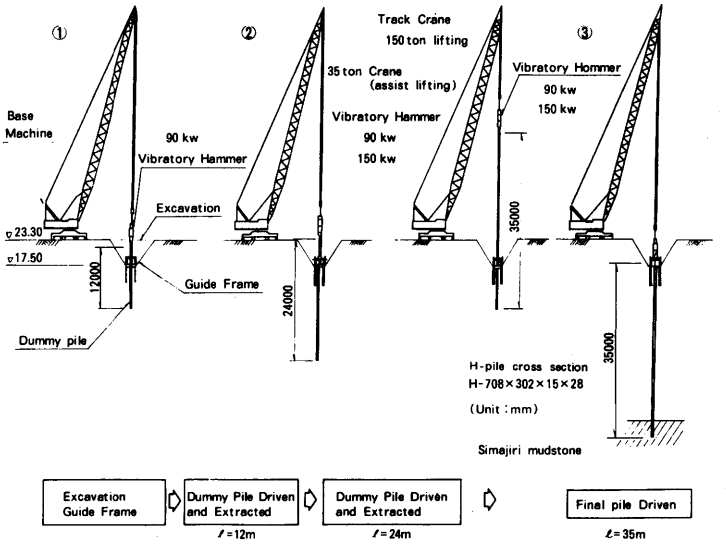

Figure 15: Constructions sequence of cutoff wall by the steel sheet piling method.

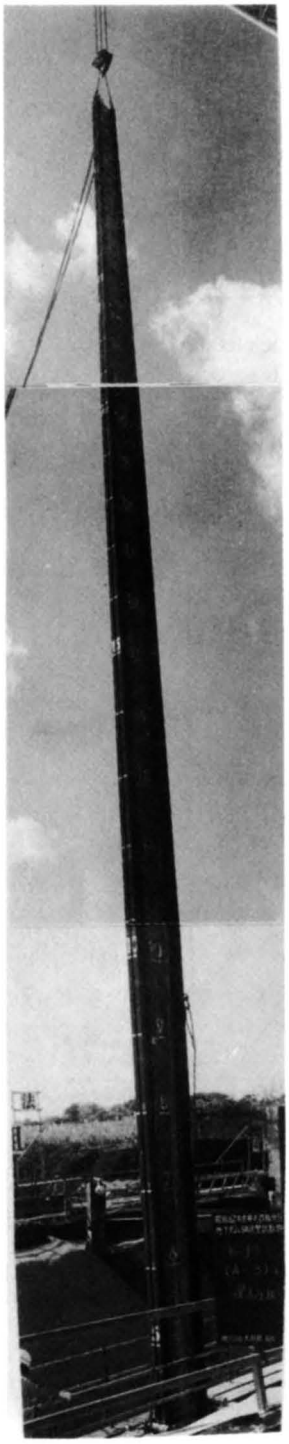

Figure 16: Overall view of the test construction. A crane raises a vibratory pile driver and vibrates the 35-meters H-pile directly into the baserock.

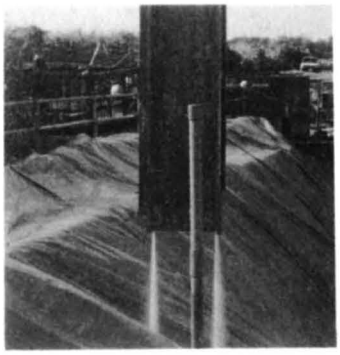

Figure 17:

Testing the water jets. The water is under about 40 kg/ cm^2 pressure. Jets are located at five places on the pile.

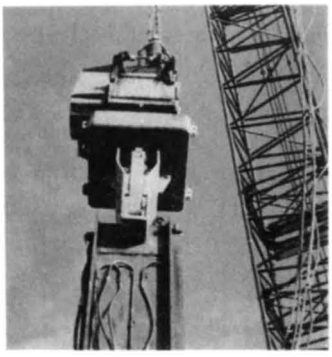

Figure 18:

The vibratory hammer and vibratory pile driver. The vibratory hammer is suspended from crane and cables vibrates the H-pile into the baserock.

Figure 19:

Completion of the subsurface cutoff wall.

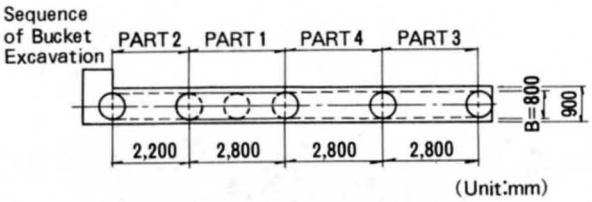

Figure 20: Dimensions of the bucket excavation.

Proceeding with drilling
Above the ground water level, drilling was done with the doughnut auger.
Below the groundwater level, drilling was carried out using the screw auger.

↓

Bucket excavation is carried out.

↓

Construction of cutoff wall (packing of mortar).

Figure 21: The sequence of the construction test.

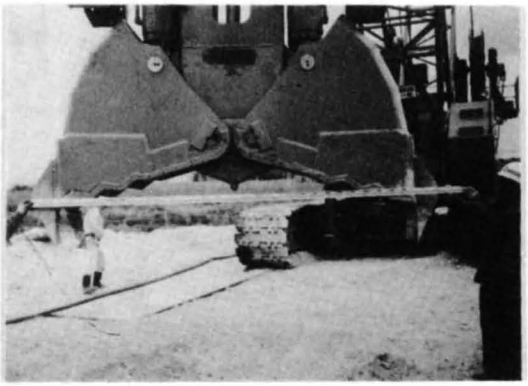

Figure 22: Tip of the bucket.

Figure 23: Situation of bucket excavation.

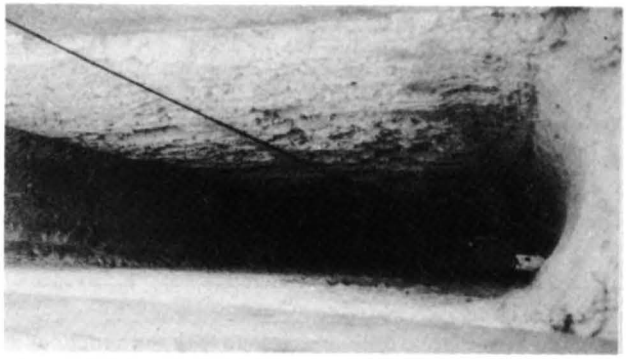

Figure 24: The wall of trench is excavating by the bucket.

Figure 25: Overall view of the horizontal multi-axis rotary excavator.

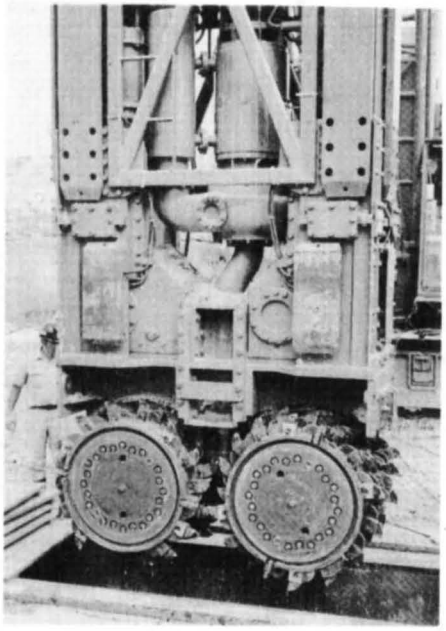

Figure 26: Top of the excavator.

Horizontal Multi-axis Rotary Excavator Method

Outline of Horizonta Multi-axis Rotary Excavator Method : A test construction by using a horizontal multi-axis rotary excavator was executed to check on the following points.
(a) Possibility of excavation by using underground water in lieu of bentonite slurry water.
(b) The continuous cutoff wall efficiency required for salt water cutoff type subsurface dam.
(c) Prevention of contamination of coral reef and underground water due to excavated circulating water.

The excavator (EMX-240) used is 7m in height, 1m in wall thickness, 2.4m in width, and about 30t in weight. The base machine is a 100 ton crane (Figure 25). For each of the large and small drums equipped with a number of tips at the apex rotate to excavate the Ryukyu Limestone (Figure 26). Sand thus excavated are fed to the ground together with circulating water through a submarine pump. The fed circulating water is separated into sand and circulating water and the circulating water is supplied again to the excavation ditch. The position and inclination of the excavator were indicated on the display by calculating the inclination of inclinometers mounted on the basic body by a computer and controlled by an operator in the operator room.

The test construction was executed on the three elements. First of all, the U-1 element was excavated up to GL -78m. After slime dischargment, concrete was poured. Then the U-3 element was excavated in the same way and the U-2 element was excavated last. Excavation of the U-2 element was executed while cutting the concrete of the U-1 and the U-3 elements by 12cm each. As a result, the excavation accuracy was as high as -40 ~ +50mm in the crosswise direction between the ground and GL -78m with the deviation of -50 ~ +60mm in the longitudinal directions. The excavation speed of the Ryukyu limestone was 1 ~ 2m/hour and the wall was stable. To prevent contamination of the underground water, the underground water (spring water) was used as the circulating water in place of bentonite slurry water. At this time, two observation wells were sunk to observe the PH, contamination and water level of the underground water. As a result, no contamination caused by the circulating water was detected on the underground water.

After completion of the subsurface cutoff wall construction, boring was performed at the center of the elements and the joints to carry out the on-site precision permeability test. The test result showed satisfactory coefficient of permeability in the range of 3.9×10^{-6} ~ 2.0×10^{-8}cm/sec..

In-situ Churning Method(Soil Mixing Wall Method)

Outline of In-situ Churning Method : In-situ Churing Method has been executed at the Sunagawa Dam site. The method consists of mixing soil with a cement emulsion in position to create the subsurface cutoff wall (Figure 27, 28). Overlapped multiple augers are drilled into the soil, mixing it with the cement milk injected from nozzles in the auger tips. The mixture hardens into a soil-cement to create a continuous subsurface cutoff wall. At the Sunagawa Subsurface Dam, both a single-shaft auger and a three-shaft auger were used. The single-shaft auger machine was used for predrilling. The three-shaft auger machine, equipped with a 550mm-diameter overlapping auger, was used for the cutoff wall construction.

The test construction of the cutoff walls using this method leads to the following conclusions:
(a) The soil churning wall proved to be a high quality reliable wall.
(b) A three-shaft auger machine was capable of drilling in many kinds of rocks, ranging from soft rocks to rather hard limestone.
(c) The In-situ churning method was effectively applied to highly permeable layers such as porous limestone of up to about 65m in the depth.

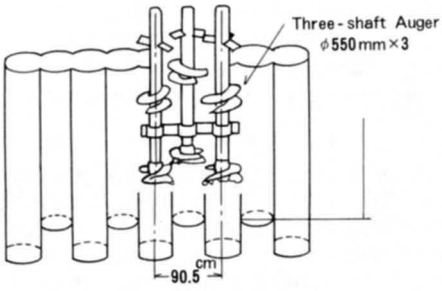

Figure 27: Illustrative description of forming the cutoff wall by in-situ churning method (Soil mixing wall method).

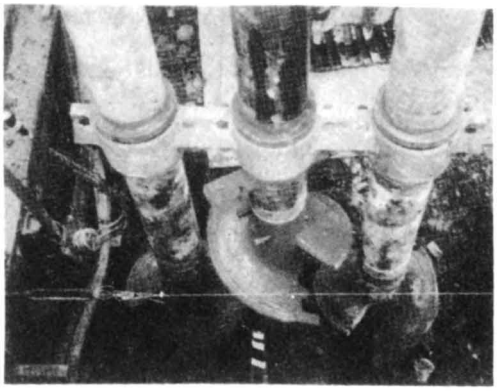

Figure 28: A photo of the three-shaft auger tips.

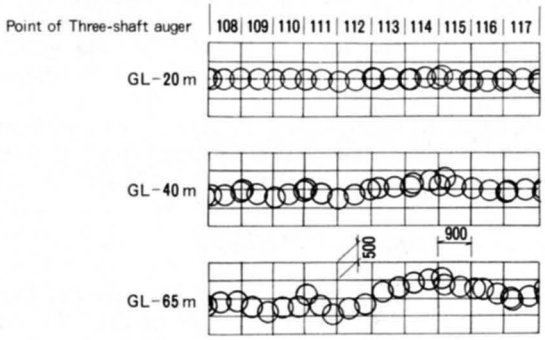

Figure 29: Configuration of constructed cutoff wall.

(d) As shown in Figure 29 the cross section of the cutoff wall becomes slightly irregular as the drilling depth increases. However, the continuity of the wall is maintained and the slight irregularity in geometry does not affect the soil function of the soil churning wall as a cutoff wall.
(e) The coefficient of permeability of the cutoff wall was measured in the range of $1x10^{-7}$ ~ 10^{-6}cm/sec.

CONCLUSION

The cutoff wall of the experimental Minafuku Dam on Miyakojima has been constructed using a cement and bentonite grouting method. In spite of this design, the coefficient value of permeability ($5x10^{-5}$ cm/s) has been obtained on only about 60%of the surface area of wall, while the water level of the storage basin has risen as planned.

However, for the proposed Sunagawa Dam, an examination of more reliable construction methods was requested in hopes of decreasing the $5x10^{-5}$ permeability of the experimental Minafuku Dam. These methods are thought to be necessary to accommodate the planned 65m of maximum construction depth which is greater than the 35m depth of the Minafuku Dam. Tests of grouting methods, including stage and double-packer techniques, at depths of 60m at the Komesu Dam site were conducted.

Satisfactory results could not be obtained due to problems including the influence of salt water mixing.Therefore, the methods using subsurface continuous walls were considered. As a result, some construction methods, which could excavate high permeability Ryukyu Limestone without the problem of mud water circulation, were examined. After test construction, the above-mentioned In-situ Churing Method was applied to the construction of the Sunagawa Dam. The coefficient of permeability for the cutoff wall at the Sunagawa Dam has been measured in order of 10^{-7} to 10^{-8} cm/s.. These figures are satisfactory given the design value of $1x10^{-6}$ cm/s..

Subsurface dams preventing saltwater intrusion which are located near the coast, which have great depths to their bases, such as the Komesu and Wantobaru Dam, have needed to utilize more reliable methods of construction.

Therefore, six construction methods were tested. These tests indicate that each method met the target for low cutoff wall permeability established at 10^{-6} cm/s.. However, with some of these methods, additional problems surfaced such as bending or twisting of holes, frequent collapse of excavated face, leaks of cement milk, and low excavation speed.

It is important that at each site, the advantages of each method must be considered given the various topographical and hydrogeological conditions created by various rock facies, along with the hardness and permeability of the Ryukyu Limestone.

REFERENCES

OKINAWA GENERAL BUREAU. 1983. An experimental underground dam project in Miyako-jima Island.
KAWASAKI, S. et. al. 1993. Geotechnological development of subsurface dam project in Japan. *IHA Selected paper* vol. 4, (on contribution)

Yasuo SAKURA

Associate Professor in the
Department of Earth Sciences,
Chiba University,
Chiba (Japan)

Secretary, Japanese N.C. of the
I.A.H.

This volume contains 19 papers from 10 countries, selected from the 154 articles presented at the **29th International Geological Congress (I.G.C.) held in Kyoto, Japan,** August 24 – September 3, 1992. The volume provides an overview of a wide spectrum of environmental hydrogeological studies and is grouped into five sections.

The first section deals with contaminant transport modelling and contains four papers. Two theoretical papers deal with solute transport based on pore-scale variations in the retardation factor and sorption of organic pollutants on natural solids. The remaining papers provide observational results of groundwater contaminants giving severe environmental problems.

The second section deals with environmental geochemistry of groundwater, soil and sediments and includes studies of groundwater pollution by nitrate in Japan, sulphur isotopes in a forested catchment in Sweden, sulphur removal from freshwater peat in the Czech Republic and toxic tracer elements in soils and crops in Korea.

The third section is devoted to water resources management and groundwater hydrology in fractured rocks. The first paper deals with the management of a shallow basaltic aquifer in India. The following two present statistical analyses of hydrogeological data and a groundwater balance in a fractured rock area of Finland, and the last discusses scale effects on the characteristics of mass transport for Tertiary sedimentary rocks in Japan.

The fourth section in concerned with volcanic regions. These papers describe the hydrogeology of volcanic islands in the Pacific and groundwater flow systems in volcanic mountains of Japan and Indonesia.

Finally, the fifth section contains three papers on technology and subsurface reservoirs. The first paper considers artificial recharge for thermal energy; the remaining two describe the concept and construction of subsurface dams in Japan.

ISSN 0938-6378
ISBN 3-922705-63-4

Verlag Heinz Heise GmbH & Co KG, P.O.B. 610407, D-30604 Hannover